Effect of FRP Anchors on the FRP Rehabilitation of Shear Critical RC Beams and Flexure Critical RC Slabs

by

Daniel Frank Baggio

A thesis
presented to the University of Waterloo
in fulfillment of the
thesis requirement for the degree of
Master of Applied Science
in
Civil Engineering

Waterloo, Ontario, Canada, 2013

Author's Declaration

I hereby declare that I am the sole author of this thesis. This is a true copy of the thesis, including any required final revisions, as accepted by my examiners.

I understand that my thesis may be made electronically available to the public.

Signature

Abstract

The use of fiber-reinforced polymer (FRP) composites as a repair and strengthening material for reinforced concrete (RC) members has increased over the past twenty years. The tendency for FRP sheets to debond at loads below their ultimate capacity has prompted researchers to investigate various approaches and designs to increase the efficiency of FRP strengthening systems. Various anchors, wrapping techniques and clamps have been explored to postpone and/or delay the debonding process which results in premature failure. FRP anchors are of particular interest because they can be selected to have the same material properties as the FRP sheets that are installed for strengthening or repair of the RC member and can be done so using the same adhesives and installation techniques.

This research study aimed to investigate the effectiveness of using commercially manufactured FRP anchors to secure FRP sheets installed to strengthen and repair RC beams in shear and RC slabs in flexure. Twenty one shear critical RC beams were strengthened in shear with u-wrapped FRP sheets and FRP anchors. Eight RC one-way slabs were strengthened in flexure with FRP sheets and FRP anchors. The test variables include the type of FRP sheets (GFRP,CFRP), type of FRP anchors (CFRP, GFRP) and the strengthening configuration.

The test results of the shear critical RC beams revealed that the installation of commercially manufactured FRP anchors to secure externally applied u-wrap FRP sheets improved the shear behaviour of the strengthened beam. The installation of FRP anchors to secure u-wrapped FRP sheets provided an average 15% increase in the shear strength over companion unanchored beams and improved the ductility of failure experienced with the typical shear failure in beams. The use of FRP anchors allowed the FRP sheets to develop their tensile capacity. Premature failure by FRP debonding was eradicated with the presence of FRP anchors and the failure modes of the strengthened beams with FRP anchors was altered when compared to the companion unanchored beam. Additionally, as the width of a u-wrapped FRP sheet was increased; larger increases in strength were obtained when FRP anchors were used.

The test results of the flexure critical RC slabs revealed that the installation of commercially manufactured FRP anchors to secure externally applied u-wrapped FRP sheets improved the behaviour of strengthened slabs. Installation of FRP anchors to secure flexural FRP sheets

provided an average 17% increase in strength over companion unanchored beams. The use of FRP anchors allowed the FRP sheets to develop their full tensile strength. Premature failure by CFRP debonding was not eliminated with the presence of FRP anchors; rather the critical failure zone was shifted from the bottom soffit of the slab to the concrete/steel rebar interface. The failure modes of slabs with FRP anchors were altered for all specimens when compared to the companion unanchored slab.

The effective strain in the FRP sheet was predicted and compared with the experimental results. The efficiency of FRP anchors defined as the ratio of effective strain in the FRP sheet with and without anchors was related to the increase in strength in beams and slabs. A good correlation was established between the FRP anchor efficiency and the increase in strength. A step-by-step FRP anchor installation procedure was developed and a model to predict the number of FRP anchors required to secure a FRP sheet was proposed.

This is the most comprehensive examination of beams and slabs strengthened with FRP sheets and FRP anchors conducted to date. This study provides an engineer with basic understanding of the mechanics, behaviour and failure modes of beams and slabs strengthened with FRP sheets and anchors.

Acknowledgements

Throughout my life I have been encouraged by my family to pursue my dreams, aspirations and ambitions. The path to continue my education and complete this thesis started long before I was a student at the University of Waterloo. I would like to express my deepest gratitude to my parents Frank and Doris Baggio. Thank-you for all the guidance and support you have provided me over the years and for pushing me to succeed. I am forever grateful for the sacrifices you have made and the opportunities you have provided me with.

In addition, I would like to thank several people who had a direct role in helping me complete my thesis. I want to express my sincere thanks to my supervisor, Dr. Khaled A. Soudki for his support, encouragement, guidance and valuable advice during my program of study. I would also like to thank fellow graduate students and friends Rizwan Azam, Ph.D. candidate and Martin Noel, Ph.D. candidate for their assistance and advice during the design, experimental testing and analysis of my research program.

Outside my academic colleagues, I would like to thank Joscelyn Noll. I am sincerely grateful for the unending support and friendship you have provided me. You have been there for me throughout my M.A.Sc. studies and I am truly grateful for everything you have done.

Finally, I would like to acknowledge the financial support received from: the Alexander Graham Bell Canada Graduate Scholarship provided by the Natural Sciences and Engineering Research Council of Canada (NSERC) and the federal government of Canada, the Ontario Graduate Scholarship (OGS) provided by the provincial government of Ontario and President's Graduate Scholarship (PGS) provided by the University of Waterloo.

Dedication

To Frank and Doris Baggio

and all those who travel, living life to the fullest

Table of Contents

Author's Declaration ii
Abstract iii
Acknowledgements v
Dedication vi
Table of Contents vii
List of Figures xi
List of Tables xx
Chapter 1 – Introduction 1
1.1 Research Significance 1
1.2 Research Objectives 2
1.3 Scope of the Work 3
1.4 Organization of Thesis 3
Chapter 2 – Background and Literature Review 5
2.1 General 5
2.1.1 Shear Failure Modes 5
2.1.2 Flexure Failure Modes 6
2.2 Techniques to Strengthen RC Members 7
2.3 Fiber Reinforced Polymers (FRP) 8
2.4 FRP Shear Strengthening/Repair of Reinforced Concrete Beams 10
2.4.1 Shear Strengthening Configuration 10
2.4.2 FRP Failure Modes in Shear Strengthening 11
2.4.2.1 FRP Debonding 11
2.4.2.2 FRP Rupture 17
2.4.3 Shear Strength Prediction of FRP Strengthened Slender Beams 18
2.5 Flexure Strengthening/Repair of Reinforced Concrete Beams & Slabs 22
2.5.1 FRP Flexural Strengthening Configuration 22
2.5.2 FRP Failure Modes in Flexural Strengthening 22
2.5.3 Flexural Strength Prediction of FRP Strengthened Slabs 25
2.6 Anchors for FRP Sheets 27
2.6.1 Types of Anchors 27

2.6.2 Load Transfer Mechanism for Anchors 34
2.6.3 Failure Modes of Anchors 35
2.6.4 Design of FRP Anchors 37
2.6.5 Construction of FRP Anchors 39
2.7 Gaps in Current Knowledge 41
2.8 Literature Review Summary 41
Chapter 3 – Experimental Program 42
3.1 Introduction 42
3.2 Test Program 42
3.3 Conceptual Design 44
3.4 Test Specimens 45
3.4.1 Pilot Study 45
3.4.2 Series I 48
3.4.3 Series II 52
3.4.4 Material Properties 53
3.4.4.1 Concrete 53
3.4.4.2 Reinforcing Steel 55
3.4.4.3 Fiber Reinforced Polymers (FRP) 56
3.5 Fabrication of Specimens 57
3.6 Strengthening of Specimens 60
3.6.1 FRP Sheet Installation 60
3.6.2 FRP Anchor Installation 63
3.7 Instrumentation 69
3.8 Test Setup and Procedure 74
Chapter 4 – Experimental Results 77
4.1 Introduction 77
4.1.1 Nomenclature 77
4.2 Shear Critical Beams – Series I 78
4.2.1 Control Beam 79
4.2.2 Beams Strengthened with Sikawrap 430G – 200 mm wide U-wraps 81
4.2.3 Beams Strengthened with Sikawrap 100G-200 mm wide U-wraps 87

4.2.4 Beams Strengthened with Sikawrap 430G-300 mm wide U-wraps 92
4.2.5 Pre-cracked Beams Repaired with Sikawrap 430G-800 mm wide U-wraps 97
4.2.6 Pre-cracked Beams Repaired with Sikawrap 100G-1100 mm wide U-wraps 105
4.3 Flexure Critical Slabs – Series II 111
4.3.1 Control Slab 112
4.3.2 Slabs Strengthened with Sikawrap 230C – Single Layer 113
4.3.3 Slabs Strengthened with Sikawrap 230C – Multi-layers 115
4.3.4 Slabs Strengthened with Sikawrap 600C – Single Layer 119
4.3.5 Slabs Strengthened with Sikawrap 600C – Multi-layers 121
Chapter 5 – Discussion of Shear Critical Beam Results 126
5.1 Introduction 126
5.2 Observed Behaviour of Shear Critical Beams 127
5.2.1 Beams with No Increases in Shear Capacity when FRP Anchors were Used 127
5.2.2 Beams with Increases in Shear Capacity when FRP Anchors were used 131
5.3 Failure Modes 136
5.4 FRP Strain Profiles 138
5.5 Effect of FRP Type 141
5.5.1 Intermittent Glass FRP - 430G vs. 100G 141
5.5.2 Continuous Glass FRP - 430G vs. 100G 147
5.6 Effect of FRP Configuration 152
5.6.1 Intermittent 200 mm wide vs. 300 mm wide GFRP 152
5.7 Effect of FRP Anchors 158
5.7.1 Presence of FRP anchors 158
5.7.2 FRP Anchors of U-Wrap vs. Full Wrap Beams 163
5.8 Shear Critical Beam Section Highlights 169
Chapter 6 – Discussion of Flexure Critical Slab Results 170
6.1 Introduction 170
6.2 Observed Behaviour of Flexure Critical Slabs 171
6.2.1 Slabs Strengthened with Sikawrap 230C Sheets 171
6.2.2 Slabs with 600C CFRP Strengthening 173
6.3 Failure Modes 176

6.4 Effect of Amount of FRP 178
6.5 Effect of FRP Anchors 185
6.5.1 Presence of FRP Anchors – 2 Layers of Sikawrap 230C 185
6.5.2 Presence of FRP Anchors – 2 Layers of 600C CFRP 190
6.6 Flexure Critical Slab Section Highlights 195
Chapter 7 – Efficiency of FRP Anchors 196
7.1 Introduction 196
7.2 FRP Anchor Installation Procedure 196
7.3 Efficiency of FRP Anchors in Shear Critical Beams 196
7.3.1 Shear Prediction Model 196
7.4 Efficiency of FRP Anchors in Flexure Critical Slabs 208
7.4.1 Flexure Prediction Model 208
7.5 Design Procedure: FRP Strengthening with FRP anchors 218
7.5.1 Sample Calculation for Proposed Design Procedure 219
Chapter 8 – Conclusions and Recommendations 221
8.1 Introduction 221
8.2 Experimental Conclusions 222
8.2.1 Effect of FRP Anchors 222
8.2.2 Effect of FRP Repair 223
8.3 Analytical Conclusions 224
8.4 Recommendations for Future work 225
References 226
Appendix A 233
Appendix B 270

List of Figures

Figure 2-1: Shear failure modes 6
Figure 2-2: Flexural failure modes 6
Figure 2-3: Shear & flexural strengthening techniques 7
Figure 2-4: Shear strengthening schemes 11
Figure 2-5: FRP wrapping configurations 11
Figure 2-6: FRP debonding in the concrete substrate: (a) shear (b) flexure 13
Figure 2-7: Debonding zones for side bonded & u-wrapped FRP strips 13
Figure 2-8: Shear crack crossing FRP sheets & debonding 14
Figure 2-9: Debonding of FRP after cracking 14
Figure 2-10: Ruptured GFRP u-wrapped sheet 17
Figure 2-11: Shear crack crossing FRP strips 18
Figure 2-12: Mechanisms of shear transfer 19
Figure 2-13: Flexural strengthened slab with CFRP sheets 22
Figure 2-14: Failure modes of RC beams with FRP flexural strengthening 23
Figure 2-15: Intermediate crack induced debonding 24
Figure 2-16: Plate end debonding 24
Figure 2-17: Interfacial shear stresses 24
Figure 2-18: Intermediate crack induced debonding 25
Figure 2-19: Stress & strain profile of beam strengthened in flexure with FRP 26
Figure 2-20: U-jacket anchor detail 28
Figure 2-21: Application examples for u-wrap anchors 28
Figure 2-22: U-anchor with Near Surface Mounted Rod Detail 29
Figure 2-23: Embedded metal thread configurations 30
Figure 2-24: The mechanical fastener system 30
Figure 2-25: Modified anchor bolt system detail 32
Figure 2-26: U-wrapped FRP sheet with FRP anchor 33
Figure 2-27: FRP anchor with 360 degree fan 34
Figure 2-28: FRP anchor load transfer mechanism 35
Figure 2-29: Force stress diagram of a 30 degree fan FRP anchor 35
Figure 2-30: FRP anchor pry-out with local concrete failure 36

Figure 2-31: FRP anchor pull-out failure 36
Figure 2-32: FRP anchor rupture 37
Figure 2-33: Commercially manufactured CFRP and GFRP anchors 39
Figure 2-34: Dry anchor construction 40
Figure 2-35: Wet anchor construction 40
Figure 3-1: Pilot study beam geometry and steel reinforcement details 46
Figure 3-2: Beam with full-depth FRP u-wraps 47
Figure 3-3: Beam with partial depth FRP u-wraps 47
Figure 3-4: Series I beam geometry and steel reinforcement details 48
Figure 3-5: Beams with 200 mm full depth FRP u-wraps 49
Figure 3-6: Beams with 300 mm full depth FRP u-wraps 50
Figure 3-7: Beams with 800 mm full depth FRP u-wraps 50
Figure 3-8: Beam with 1100 mm full depth FRP u-wraps 51
Figure 3-9: Beam with fully wrapped FRP sheets 51
Figure 3-10: Series II slab geometry and steel reinforcement details 52
Figure 3-11: Slab with FRP flexural strengthening 53
Figure 3-12: Pilot study casting 54
Figure 3-13: Concrete cylinder testing 55
Figure 3-14: Caging and fabrication of the beam specimens 57
Figure 3-15: Caging and fabrication of slab specimens 58
Figure 3-16: Lifting and transportation of a beam by overhead crane 58
Figure 3-17: Internal stirrup locations 59
Figure 3-18: Specimen grinding and sandblasting preparation 61
Figure 3-19: Specimen preparation and mixing of epoxy 61
Figure 3-20: Epoxy and FRP application 62
Figure 3-21: Intermittent vs. continuous FRP u-wrapped shear strengthened beam 62
Figure 3-22: Anchor hole drilling 64
Figure 3-23: FRP anchor preparation 64
Figure 3-24: FRP anchor installation 65
Figure 3-25: FRP anchor slab installation 67
Figure 3-26: Pilot study anchor locations 67

Figure 3-27: Series I anchor locations 68
Figure 3-28: Series II anchor locations 68
Figure 3-29: Anchor detail 68
Figure 3-30: Pilot study strain gauge detail 69
Figure 3-31: Series I strain gauge detail 70
Figure 3-32: Series II strain gauge detail 71
Figure 3-33: Strain gauge installation on the steel rebar & stirrups 72
Figure 3-34: FRP strain gauge application 73
Figure 3-35: LVDT setup during beam testing 73
Figure 3-36: Pilot study and Series I beam test setup 74
Figure 3-37: Series II slab test setup 75
Figure 3-38: Test setup 76
Figure 4-1: Experimental nomenclature used in this study 77
Figure 4-2: Load vs. deflection of control beam (series I) 79
Figure 4-3: Diagonal tension failure of control beam (series I) 80
Figure 4-4: Concrete and steel rebar strain response of control beam (series I) 81
Figure 4-5: Stirrup strain response of control beam (series I) 81
Figure 4-6: Failure mode of beam 430G-200-NA (a) aggregate interlock and FRP debonding and beam 430G-200-A (b) aggregate interlock and FRP rupture 82
Figure 4-7: Load vs. deflection of beams strengthened with Sikawrap 430G-200mm strips. 83
Figure 4-8: Concrete and steel rebar strain response of 430G-200 mm wide GFRP beams .. 83
Figure 4-9: Stirrup strain response of 430G-200 mm wide GFRP beams 83
Figure 4-10: Diagonal tension shear crack in 430G-200-NA 84
Figure 4-11: FRP strain response of beam 430G-200-NA 85
Figure 4-12: FRP strain response of beam 430G-200-A 86
Figure 4-13: Failure mode of beam 430G-100-NA (a) aggregate interlock and FRP debonding and beam 430G-100-A (b) aggregate interlock 87
Figure 4-14: Load vs. deflection of beams strengthened with Sikawrap 100G-200 mm strips 87
Figure 4-15: Concrete and steel rebar strain response of beams strengthened with Sikawrap 100G-200 mm wide strips 88

Figure 4-16: Stirrup strain response of beams strengthened with Sikawrap 100G-200 mm wide strips 89
Figure 4-17: FRP strain response of beam 100G-200-NA 90
Figure 4-18: FRP strain response of beam 100G-200-A 91
Figure 4-19: Load vs. deflection of beams strengthened with Sikawrap 430G-300 mm strips 92
Figure 4-20: Failure mode of beam 430G-300-NA (a) aggregate interlock and FRP debonding and beam 430G-300-A (b) aggregate interlock and concrete crushing 93
Figure 4-21: Concrete and steel rebar strain response of beams strengthened with Sikawrap 430G-300 mm wide strips..... 94
Figure 4-22: Stirrup strain response of beams strengthened with Sikawrap 430G-300 mm wide strips 94
Figure 4-23: FRP strain response of beam 430G-300-NA 95
Figure 4-24: FRP strain response of beam 430G-300-A 96
Figure 4-25: Load vs. deflection of beams repaired with Sikawrap 430G-800mm wide strips 98
Figure 4-26: Aggregate interlock and FRP debonding failure of beam PC-430G-800-NA ... 98
Figure 4-27: Diagonal tension end anchorage failure of beam PC-430G-800-A 99
Figure 4-28: Diagonal tension end anchorage failure of beam PC-430G-800-FW 99
Figure 4-29: Concrete & steel rebar strain response of PC-430G-800mm wide GFRP beams 100
Figure 4-30: Stirrup strain response of PC-430G-800 mm wide GFRP beams..... 100
Figure 4-31: FRP strain response of beam PC-430G-800-NA 102
Figure 4-32: FRP strain response of beam PC-430G-800-A 103
Figure 4-33: FRP strain response of PC-430G-800-FW..... 104
Figure 4-34: Load vs. deflection of beams repaired with Sikawrap 100G-1100mm wide strips 105
Figure 4-35: Aggregate interlock & FRP debonding failure of beam PC-100G-1100-NA.. 106
Figure 4-36: Diagonal tension end anchorage failure of beam PC-100G-1100-A 106
Figure 4-37: Concrete & steel rebar strain response of PC-100G-1100mm wide beams..... 107
Figure 4-38: Stirrup strain response of PC-100G-1100mm wide GFRP beams..... 107

Figure 4-39: FRP strain response of PC-100G-1100-NA 109
Figure 4-40: FRP strain response of PC-100G-1100-A 110
Figure 4-41: Flexural failure of control slab (series II) 112
Figure 4-42: Load vs. deflection of control slab (series II) 112
Figure 4-43: Concrete and steel rebar strain response of control beam (series II) 113
Figure 4-44: FRP rupture of 230C-1L-NA 113
Figure 4-45: Load vs. deflection of slab 230C-1L-NA 114
Figure 4-46: Concrete and steel rebar strain response of 230C-1L-NA 115
Figure 4-47: FRP strain response of 230C CFRP strengthened slab 115
Figure 4-48: FRP debonding failure of slab 230C-2L-NA 116
Figure 4-49: Concrete cone anchor failure and anchor rupture of slab 230C-2L-8A 116
Figure 4-50: Load vs. deflection of slabs 230C-2L-NA and 230C-2L-8A 117
Figure 4-51: Concrete and steel rebar strain response of slabs 230C-2L-NA & 230C-2L-8A 118
Figure 4-52: FRP strain response of slab 230C-2L-NA 119
Figure 4-53: FRP strain response of slab 230C-2L-8A 119
Figure 4-54: FRP debonding of slab 600C-1L-NA 119
Figure 4-55: Load vs. deflection of a slab 600C-1L-NA 120
Figure 4-56: Concrete and steel rebar strain response of slab 600C-1L-NA 121
Figure 4-57: FRP strain response of slab 600C-1L-NA 121
Figure 4-58: Concrete cover failure (a-d) of slabs 600C-2L-NA and 600C-2L-8A and intermediate flexural shear crack induced interfacial debonding (e,f) of slab 600C-2L-12A 122
Figure 4-59: Load vs. deflection of slabs 600C-2L-NA, 600C-2L-8A & 600C-2L-12A 123
Figure 4-60: Concrete and steel rebar strain response of slabs 600C-2L-NA, 600C-2L-8A and 600C-2L-12A 123
Figure 4-61: FRP strain response of slab 600C-2L-NA 125
Figure 4-62: FRP strain response of slab 600C-2L-8A 125
Figure 4-63: FRP strain response of slab 600C-2L-12A 125
Figure 5-1: Failure of beam 430G-200-NA 127
Figure 5-2: Failure of beam 430G-200-A 128

Figure 5-3: Failure of beam 100G-200-NA 130
Figure 5-4: Failure of beam 100G-200-A 130
Figure 5-5: Failure of beam 430G-300-NA 131
Figure 5-6: Failure of beam 430G-300-A 132
Figure 5-7: Failure of beam 430G-800-NA 133
Figure 5-8: Failure of beam 430G-800-A 134
Figure 5-9: Full wrap (a) and Diagonal end anchorage failure (b) of beam 430G-800-FW 134
Figure 5-10: FRP debonding failure of beam 100G-1100-NA 135
Figure 5-11: Diagonal tension end anchorage failure of 100G-1100-A 135
Figure 5-12: Failure modes of shear critical beams 137
Figure 5-13: Strain gauge layout 138
Figure 5-14: Shear crack scheme of beams strengthened with u-wrap GFRP sheets: (a) without GFRP anchors and (b) with GFRP anchors 139
Figure 5-15: GFRP strain response – Sheet 2 140
Figure 5-16: GFRP strain response – Sheet 3 140
Figure 5-17: Load vs. deflection of 430G & 100G strengthened beams 142
Figure 5-18: Strength increase of 430G & 100G strengthened beams over control 143
Figure 5-19: Increase in maximum deflection of 430G & 100G beams over control 144
Figure 5-20: Stirrup strain at failure of Sikawrap 430G and 100G strengthened beams 145
Figure 5-21: GFRP strain at failure of Sikawrap 430G and 100G strengthened beams 145
Figure 5-22: FRP strain profile of beams strengthened with 200 mm wide GFRP sheets ... 146
Figure 5-23: Load vs. deflection of pre-cracked beams 147
Figure 5-24: Strength increase of pre-cracked FRP strengthened beams over the control ... 148
Figure 5-25: Pre-cracked FRP width maximum deflection comparison 149
Figure 5-26: Stirrup strain at failure of continuous 800 mm & 1100 mm GFRP sheets 150
Figure 5-27: GFRP strain at failure of continuous 800 mm & 1100 mm GFRP sheets 151
Figure 5-28: FRP strain profile of beams strengthened with continuous GFRP sheets 151
Figure 5-29: Shear crack with multi-linear slopes 152
Figure 5-30: Load vs. deflection of 200 mm & 300 mm wide GFRP strengthened beams .. 153
Figure 5-31: Strength increase of 200 mm & 300 mm wide GFRP sheets over the control 154

Figure 5-32: Increase in maximum deflection of 200 & 300 mm GFRP sheets over control 155
Figure 5-33: Stirrup strain at failure of 200 & 300 mm wide strengthened beams 156
Figure 5-34: GFRP strain at failure of 200 & 300 mm wide strengthened beams 156
Figure 5-35: FRP strain response of 430G – 300 mm wide GFRP strengthened beams..... 157
Figure 5-36: Diagonal tension shear crack propagation of beam 430G-300-NA..... 157
Figure 5-37: Load vs. deflection of GFRP strengthened beams without & with anchors 159
Figure 5-38: Strength increase of anchored beams over companion unanchored beams 160
Figure 5-39: Increase in max deflection of anchored beams over companion unanchored beams 161
Figure 5-40: Stirrup strain at failure of unanchored & anchored beams 162
Figure 5-41: GFRP strain at failure of unanchored & anchored beams 162
Figure 5-42: Load vs. deflection of pre-cracked beams without & with anchors..... 164
Figure 5-43: Strength increase of anchored beams over the control 165
Figure 5-44: Full wrapped beam with end anchorage failure 165
Figure 5-45: Increase in maximum deflection of anchored beams over control 166
Figure 5-46: Stirrup strain at failure for different anchorage configurations 167
Figure 5-47: GFRP strain at failure for different anchorage configurations 167
Figure 6-1: Flexural failure of slab 230C-2L-NA..... 171
Figure 6-2: Concrete cone anchor failure (b,c) & anchor rupture (d,e) of slab 230C-2L-8A 172
Figure 6-3: Failure of slab 600C-2L-NA 173
Figure 6-4: Concrete cover failure at steel rebar interface (no anchors) 174
Figure 6-5: Failure of slab 600C-2L-12A 175
Figure 6-6: Failure of slab 600C-2L-8A 175
Figure 6-7: Failure modes of flexure critical slabs 177
Figure 6-8: Concrete cover failure at concrete/steel rebar interface 179
Figure 6-9: Load vs. deflection of slabs strengthened with Sikawrap 230C & 600C sheets 180
Figure 6-10: Strength increase of 230C & 600C CFRP strengthened slabs over the control181
Figure 6-11: Decrease in maximum deflection of 230C & 600C CFRP slabs over the control 182

Figure 6-12: CFRP strain at failure - 1 layer of Sikawrap 230C or 600C 184
Figure 6-13: CFRP strain at failure - 2 layers of Sikawrap 230C or 600C..... 184
Figure 6-14: Steel rebar strain at failure of Sikawrap 230C & 600C strengthened slabs..... 184
Figure 6-15: Load vs. deflection of unanchored and anchored 230C strengthened slabs 186
Figure 6-16: Concrete cone anchor failure and anchor rupture 186
Figure 6-17: Strength increase of unanchored and anchored 230C slabs over the control... 187
Figure 6-18: Decrease in maximum deflection of 1 & 2 layers of 230C sheets over control 188
Figure 6-19: CFRP strain at failure of unanchored and anchored Sikawrap 230C strengthened slabs..... 189
Figure 6-20: Flexural steel rebar strain at failure of unanchored and anchored Sikawrap 230C strengthened slabs 189
Figure 6-21: Eight and twelve anchor configuration 190
Figure 6-22: Load vs. deflection of unanchored and anchored 230C strengthened slabs 191
Figure 6-23: Strength increase of unanchored and anchored 230C slabs over the control... 192
Figure 6-24: Decrease in maximum deflection of slabs without and with anchors..... 193
Figure 6-25: CFRP strain at failure of Sikawrap 600C strengthened slabs 194
Figure 6-26: Steel rebar strain at failure of Sikawrap 600C strengthened slabs..... 194
Figure 7-1: FRP anchor installation procedure..... 197
Figure 7-2: Shear design iterative procedure for unstrengthened beams using the general method..... 198
Figure 7-3: Free body diagram of internal forces 200
Figure 7-4: Comparison of experimentally estimated & measured efficiency of FRP anchors 205
Figure 7-5: Comparison of experimentally estimated FRP strain in unanchored & anchored beams 206
Figure 7-6: Comparison of measured FRP strain in unanchored & anchored beams..... 206
Figure 7-7: Relationship between strength increase and anchor efficiency of Sikawrap 430G strengthened beams..... 207
Figure 7-8: Stress strain profile of a flexure critical slab..... 208
Figure 7-9: Layer-by-layer strain compatibility of a flexure critical slab 210

Figure 7-10: Comparison of effective FRP strain in unanchored and anchored slabs..... 215
Figure 7-11: Comparison of experimentally estimated FRP strain in unanchored & anchored slabs..... 216
Figure 7-12: Comparison of measured FRP strain in unanchored & anchored slabs..... 216
Figure 7-13: Relationship between strength increase and anchor efficiency of CFRP strengthened slabs..... 217

List of Tables

Table 2-1: Mechanical properties of FRP materials 9
Table 2-2: Mechanical properties of Adhesives 9
Table 2-3: Design for shear in flexural regions (CSA A23.3-04 & ISIS-M04) 20
Table 2-4: Design of FRP sheets for shear strengthening (ISIS-M04-09)..... 21
Table 2-5: Simplified and general method for shear design (CSA A23.3-04) 21
Table 2-6: Design for flexure with FRP strengthening (ISIS-M04)..... 26
Table 3-1: Shear & Flexural Strengthening Test Matrix 43
Table 3-2: Flexural Strengthening Test Matrix 43
Table 3-3: Concrete cylinder test results 54
Table 3-4: Steel reinforcement nominal yield strength..... 55
Table 3-5: FRP sheet material properties..... 56
Table 3-6: FRP Anchor material properties..... 56
Table 4-1: Series 1 - Summary of test results for GFRP strengthened beams..... 79
Table 4-2: Series 3 - Summary of test results for CFRP strengthened slabs 111
Table 6-1: CFRP strengthening and failure data..... 179
Table 7-1: Experimental and predicted ultimate loads for control beams 199
Table 7-2: Shear resistance of FRP strengthened members (CSA A23.3-04 & ISIS-M04). 200
Table 7-3: Calculated Shear Forces of RC FRP Strengthened Beams 203
Table 7-4: Effective Strain Comparisons of RC Beams 203
Table 7-5: Strength increase and anchor efficiency of Sikawrap 430G strengthened beams207
Table 7-6: Experimental and predicted ultimate load for control slab 209
Table 7-7: Calculated Shear Forces of RC FRP Strengthened Beams 213
Table 7-8: Effective Strain Comparisons of RC Slabs 213
Table 7-9: Strength increase and anchor efficiency of CFRP strengthened slabs 217
Table 7-10: FRP Material Properties 219

Chapter 1 – Introduction

1.1 Research Significance

Throughout the world concrete bridges and structures are in need of repair or complete replacement as they are approaching the end of their service life. Bridges and structures require restoration and repair from increased volume, traffic loads, and deterioration caused by the corrosion of reinforcing steel (Noel & Soudki, 2011). In the United States, 23% of the 163,000 single span concrete bridges are considered structurally deficient or functionally obsolete (Mabsout, et al., 2004).

The advancement of fiber-reinforced polymer (FRP) composites as a repair and strengthening material for reinforced concrete (RC) beams, slabs and columns in structural engineering applications has increased over the past twenty years (Cao, et al., 2005; Triantfillou & Antonopoulos, 2000; Bank, 2006; American Concrete Institute, 2008). The high strength to weight ratio and non-corrosive characteristics of FRP's make them a very desirable repair material and can result in increases in service life of structures (Noel & Soudki, 2011).

When applying external FRP sheets for strengthening, the goal was to utilize the full capacity of the FRP sheet such that failure occurs by rupture of the FRP fibers. It is common knowledge that external FRP sheets bonded to the concrete surface are a bond-critical application. Therefore, the shear contribution provided by FRP sheets is limited by the anchorage capacity of the FRP system. Obtaining proper anchorage to allow for the full utilization of FRP sheets without external anchorage will rarely if at all occur.

The tendency for FRP sheets to debond at loads below their tensile strength has led researchers to investigate various approaches and designs to increase the efficiency of the installed FRP sheets for shear strengthening of RC members (Bousselham & Chaallal, 2008; Chaallal, et al., 2002; Chen, et al., 2012; Chen, et al., 2010; Khalifa & Nanni, 2000; Quinn, 2009; Chen & Teng, 2003). Various anchors, wrapping techniques and clamps have been explored to postpone and/or delay the debonding process in externally bonded FRP members (Smith & Kim, 2008; Orton, et al., 2008; Kim & Smith, 2009). FRP anchors are of particular interest because they have the same material properties as the FRP sheets and can be installed simultaneously with the sheets

using the same adhesives (Kim & Smith, 2009; Teng, et al., 2004). However, research on the effectiveness of FRP anchors to secure externally bonded FRP sheets is limited. There are no current models to predict the effectiveness of anchors in RC members strengthened with FRP sheets.

Research is required to study the efficiency of FRP anchors used to secure externally applied FRP sheets to strengthen beams in shear and slabs in flexure. This research study has been designed to investigate the effectiveness of using commercially manufactured FRP anchors to control and/or eliminate the debonding of externally bonded FRP sheets used to strengthen RC beams in shear and RC slabs in flexure.

1.2 Research Objectives

This research program was initiated to investigate the efficiency of FRP anchors to secure externally bonded FRP sheets in strengthening RC beams in shear and slabs in flexure. The main objective of this study is to examine the structural behaviour of shear-critical beams and flexure critical slabs strengthened with externally bonded FRP sheets and FRP anchors.

The Specific objectives were:

- Determine the behaviour of various FRP shear reinforcement configurations with and without anchors to strengthen full scale shear critical RC beams.
- Determine the behaviour of various FRP flexural reinforcement configurations with and without anchors to strengthen full scale flexure critical RC slabs.
- Determine the effect of different types of FRP sheets and FRP anchors (CFRP vs. GFRP) used to secure FRP sheets.
- Quantify the strain distribution along a FRP sheet with and without anchors.
- Predict the structural capacity of FRP strengthened beams in shear and slabs in flexure using current design codes and compare with measured data.
- Develop a step-by-step procedure for the installation of FRP anchors in the field.
- Develop a model to predict the quantity of FRP anchors required to secure a FRP sheet to prevent/delay FRP debonding.

1.3 Scope of the Work

The research program consists of experimental and analytical phases. The experimental program was comprised of twenty nine specimens tested in a pilot and main study. The pilot study comprised nine shear critical RC beams. The main study included twenty RC specimens which were divided into two series: Series I (comprised of twelve shear critical RC beams) and series II (comprised of eight flexure critical slabs). The test variables included: the type of FRP strengthening material (GFRP, CFRP), FRP configuration and presence of FRP anchors.

The analytical work included the analysis of the control beams (unstrengthened) using the Canadian design code, CSA A23.3-04 – Design of concrete structures and strengthened beams and slabs using a model based on the Canadian design code, CSA A23.3-04 – Design of concrete structures and the ISIS-M04 design manual - Reinforcing concrete structures with fiber reinforced polymers. The experimentally estimated results using the design models were compared with the measured experimental results.

Based on the study results, a step-by-step FRP anchor installation procedure was developed. A model to predict the number of FRP anchors required to secure a FRP sheet has also been developed to assist in the design of future strengthening configurations.

1.4 Organization of Thesis

This thesis is organized into eight chapters and two appendices as follows:

- Chapter 1: Introduction – This chapter describes the research significance, problem statement, objectives of the research program, scope of work and thesis organization.
- Chapter 2: Background and Literature Review – This chapter provides a presumptive literature review and background information on the use of fiber reinforced polymers to repair concrete structures. Previous work on the use of anchorage to eliminate premature debonding failures of beams and slabs strengthened in shear and flexure is provided.
- Chapter 3: Experimental Program – This chapter presents the test program, test specimens, material properties, fabrication of the test specimens, FRP strengthening procedure, FRP anchor installation procedure, instrumentation, test setup and test procedure.

- Chapter 4: Experimental Results – This chapter presents the experimental results of the beam and slab specimens including failure modes, load-deflections and FRP strain responses.
- Chapter 5: Discussion of Shear Critical Beam Results – A discussion of the experimental results of the shear critical beams is presented including the effect of FRP strengthening configurations and presence of FRP anchors.
- Chapter 6: Discussion of Flexure Critical Slab Results – A discussion of the experimental results of flexure critical slabs is presented including the effect of the amount of FRP strengthening and presence of FRP anchors.
- Chapter 7: Efficiency of FRP Anchors – This chapter presents a step-by-step FRP anchor installation procedure, observed behaviour of beams and slabs, comparison with existing strength prediction models, experimental estimation of the effective strains in FRP sheets and a comparison of the experimentally estimated vs. measured results.
- Chapter 8: Conclusions and Recommendations – This chapter presents main conclusions from the study. Recommendations for future research are provided.
- Appendix A: Pilot Study – This appendix contains the experimental results, discussion and analysis of the pilot study.
- Appendix B: Sample Calculations – This appendix contains the calculations for the unstrengthened and strengthened beam and slab designs of the pilot study and main study.

Chapter 2 – Background and Literature Review

2.1 General

Reinforced concrete members (beams and slabs) can become deficient in shear or flexure for many reasons. Problems to develop a shear or flexural deficient member may begin prior to the member even going into service. Construction errors, poor design, faulty construction and bad detailing cause a member to be deficient in strength. Deterioration caused by fatigue, corrosion of reinforcement and chemical attack can also cause a member to become deficient over time. A member may become deficient in shear or flexure because of updates in design codes or changes in service conditions.

For example, a bridge designed based on the 1994 design code may become deficient in shear based on the 2004 design code. Loads and volumes of traffic that bridges and structures were originally designed for may also change over time. For example, a bridge that was initially constructed to carry local traffic was converted to a highway and thus will carry increased volume.

2.1.1 Shear Failure Modes

Shear failure of a reinforced concrete beam is sudden, brittle and has the potential for catastrophic consequences. Because of the unpredictable nature of shear failures, general guidelines require shear strength to be greater than the flexural strength of a beam in all regions (MacGregor & Bartlett, 2000; DeWolf, et al., 2006).

Three types of shear failure are possible (Figure 2-1):

1. Diagonal tension shear failure
2. Bond splitting (end anchorage shear failure)
3. Crushing of compression strut

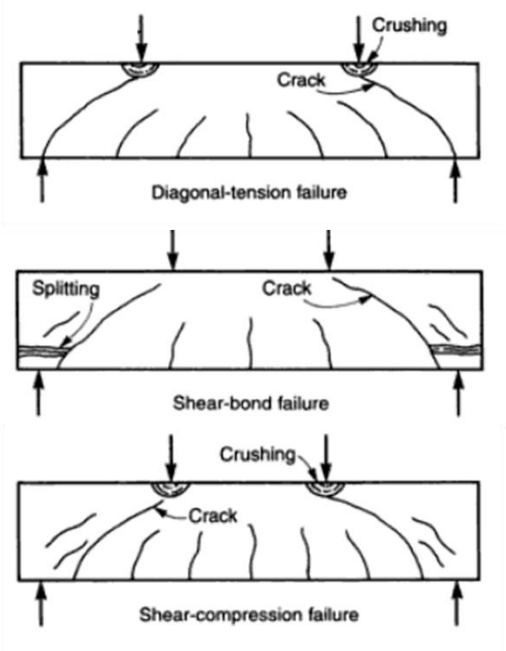

Figure 2-1: Shear failure modes (Williams, 2000)

2.1.2 Flexure Failure Modes

The flexural failure of a properly designed reinforced concrete beam or slab occurs by yielding of the steel reinforcing bars followed by crushing of the concrete (DeWolf, et al., 2006).

Two types of flexural failures are possible (Figure 2-2):

1. Steel yielding followed by concrete crushing (under-reinforced section)
2. Concrete crushing before steel yielding (over-reinforced section)

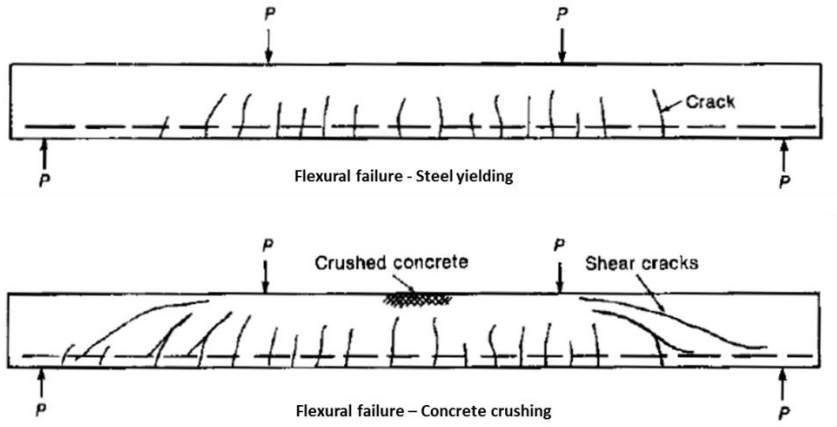

Figure 2-2: Flexural failure modes (MacGregor & Bartlett, 2000)

2.2 Techniques to Strengthen RC Members

Various factors can cause a RC structural member to become deficient in shear or flexure and thus would require repair and strengthening. The options and materials which are available to repair, rehabilitate or strengthen a member are limited (Stanley & Ng, 2005).

In this section the most common shear and flexural strengthening techniques that are in use today are highlighted. The repair/strengthening techniques for RC members include:

1. Section enlargement with steel reinforcement
2. Steel plate bonding
3. Epoxy or mortar injection
4. Concrete/polymer overlay
5. Near surface mounted reinforcement (NSM)
6. FRP reinforcement
7. External prestressing

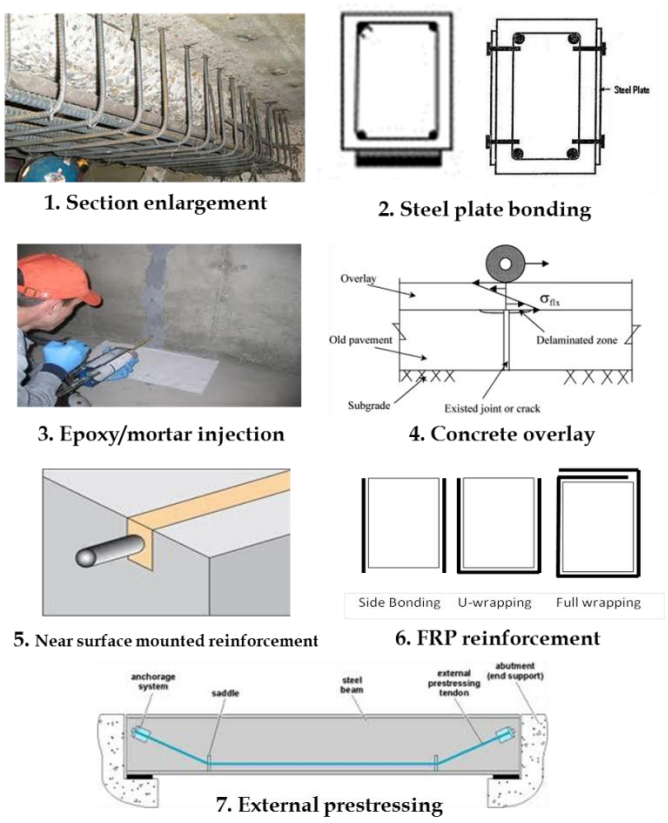

Figure 2-3: Shear & flexural strengthening techniques

2.3 Fiber Reinforced Polymers (FRP)

Over the past twenty years, the use of fiber reinforced polymers (FRP) for repair and strengthening of RC structures have gained rapid approval and have been implemented on many structures across the world.

FRPs have excellent physical characteristics and outstanding properties such as: high strength and stiffness (high strength to weight ratio), light weight, resistance to corrosion, easy handling and installation (ACI 440.2R-08). Corrosion will not occur because FRP have no iron and the epoxy resin will protect the FRP from becoming exposed to severe environmental conditions.

However, FRPs are expensive compared to other strengthening methods such as applying mortar or steel plates. Of the three main types of FRP's available, carbon (CFRP) has the highest cost and highest strength to weight ratio. FRPs are linear elastic until failure with low ultimate strain at failure ranging from 1.1% to 2.3%. In addition, FRPs are anisotropic materials with maximum strength aligned with the orientation of fibers (unidirectional), therefore FRPs do not have strength in the transverse direction. If strengthening is required in both directions, bi-directional sheets or two sheets must be installed perpendicular to each other.

FRPs are composite materials composed of two components: fibers which are the main load carrying component of the composite and the resin adhesive which is used to bond the fibers. FRP reinforcement is manufactured as sheets, pre-cured plates and rods. Fibers are made from glass, carbon or aramid fiber (GFRP, CFRP or AFRP). The resins are epoxy, polyester or vinylester with epoxy resin the most common choice. FRP sheets are susceptible to premature debonding at loads below 75% of their ultimate capacity (ACI 440.2R-08). To gain a better understanding of the FRP composite, its components will be reviewed individually.

FRP Sheets

FRP sheets that are commercially available vary in thickness from 0.381 to 1.30 mm. One of the main variables which affect the FRP strength is the density of fibers in a sheet. The density varies from 1.8 g/cm^3 for CFRP sheets to 2.5 g/cm^3 for GFRP sheets. Table 2-1 outlines typical mechanical properties of fibers, adhesives and composites.

On the micro level, fiber filaments (aramid, glass or carbon) of 7-10 micrometers form a single fiber strand. These strands are layered to a desired thickness and then woven together with a perpendicular thread to produce a monolithic fabric sheet (Kobayashi, et al., 2001). The sheets are flexible and can be rolled up into a coil.

Table 2-1: Mechanical properties of FRP materials

FIBRE TYPE		Tensile Strength [MPa]	Modulus of Elasticity [GPa]	Elongation [%]	Coefficient of Thermal Expansion [x10^{-6}]	Poisson's Ratio
CARBON						
PAN	High Strength	3500	200-240	1.3-1.8	(-1.2) to (-0.1) (α_{frpL}) 7 to 12 (α_{frpT})	-0.2
	High Modulus	2500-4000	350-650	0.4-0.8		
Pitch	Ordinary	780-1000	38-40	2.1-2.5	(-1.6) to (-0.9) (α_{frpL})	N/A
	High Modulus	3000-3500	400-800	0.4-1.5		
ARAMID						
Kevlar 29		3620	82.7	4.4	N/A	0.35
Kevlar 49		2800	130	2.3	-2.0 (α_{frpL}), 59 (α_{frpT})	
Kevlar 129		4210 (est.)	110 (est.)	--	N/A	
Kevlar 149		3450	172-179	1.9	N/A	
Twaron		2800	130	2.3	(-2.0) (α_{frpL}), 59 (α_{frpT})	
Technora		3500	74	4.6	N/A	
GLASS						
E-Glass		3500-3600	74-75	4.8	5.0	0.2
S-Glass		4900	87	5.6	2.9	0.22
Alkali Resistant Glass		1800-3500	70-76	2.0-3.0	N/A	N/A

Adhesives

Epoxy is the most common type of adhesive used to impregnate dry FRP sheets and bond them to the RC member. Kobayashi, et al., (2004) concluded that mixing the proper ratio of the two-part epoxy adhesives has a significant influence on the effectiveness of the installed FRP system. The distribution of epoxy on the surface of the concrete member is also very important. Areas which have insufficient or excess epoxy adhesive can create weak regions leading to delamination, debonding or premature failure (Kobayashi, et al., 2004). The mechanical properties of different adhesives are presented in Table 2-2.

Table 2-2: Mechanical properties of Adhesives

Resin	Specific Gravity	Tensile Strength [MPa]	Tensile Modulus [GPa]	Cure Shrinkage [%]
Epoxy	1.20-1.30	55.00-130.00	2.75-4.10	1.00-5.00
Polyester	1.10-1.40	34.50-103.50	2.10-3.45	5.00-12.00
Vinyl Ester	1.12-1.32	73.00-81.00	3.00-3.35	5.40-10.30

2.4 FRP Shear Strengthening/Repair of Reinforced Concrete Beams

2.4.1 Shear Strengthening Configuration

FRPs used for shear strengthening and repair can be applied in three configurations: full wrapping, u-wrapped or side bonded (Chen & Teng, 2003). The FRP sheets can be applied as intermittent strips (like stirrups) or a continuous sheet along the length of the member. These shear strengthening configurations are shown in Figure 2-4 and Figure 2-5.

Full Wrapping

In this repair technique the FRP sheet fully wraps the beam cross-section with the fibers fixed in the transverse direction along the beam (Figure 2-4). When the beam is fully wrapped, the probability of debonding is slim and the full capacity of the FRP sheet can be utilized. However, most FRP installations are done on existing structures and the top portion of the beam is usually supporting a concrete deck or slab and thus is not accessible. Therefore, full wrapping configuration is not feasible for applications in the field.

U-Wrapping

In this technique, the FRP sheet is applied to three sides of the beam's cross-section because the top face is not accessible (Figure 2-4). U-wrapping is more practical than the fully wrapped technique. A problem with the u-wrapping technique is that FRP sheets have the tendency to debond from the concrete surface. However, this technique is more effective than side bonded FRP (Chen & Teng, 2003).

Side Bonded

The FRP side bonded technique is used when the bottom face of the beam is not accessible. FRP sheets are applied on the two side faces of the beam (Figure 2-4) and debonding can occur at either end of the FRP sheet. The maximum stress experienced in a side bonded FRP sheet is lower or equal to the maximum stress in a u-wrapped sheet (Chen & Teng, 2003).

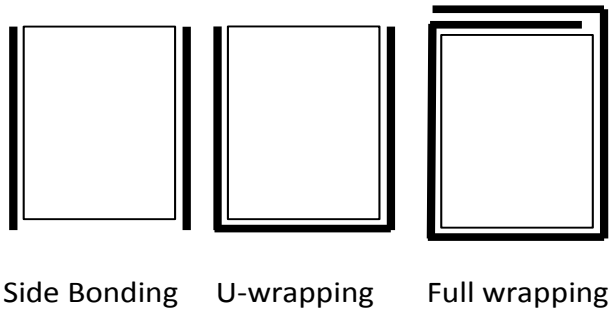

Figure 2-4: Shear strengthening schemes

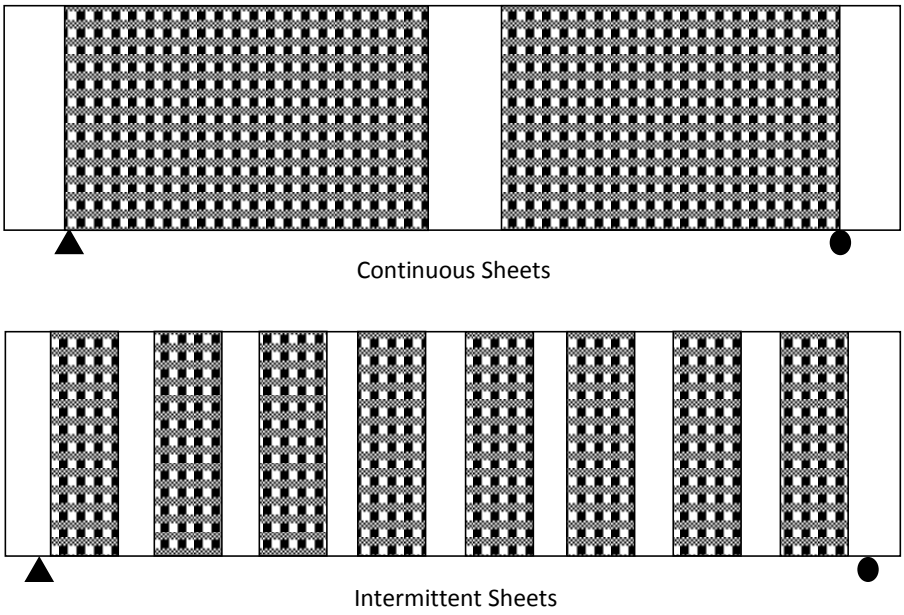

Figure 2-5: FRP wrapping configurations

2.4.2 FRP Failure Modes in Shear Strengthening

2.4.2.1 FRP Debonding

FRP debonding is the process where an FRP sheet peels off the concrete surface to which it is bonded to. In shear strengthening of RC beams, both u-wrapped and side bonded sheets have the tendency to debond from the concrete prior to the FRP sheet reaching its ultimate tensile capacity (Chen & Teng, 2003; Au & Buyukozturk, 2006; Lu, et al., 2007; Teng, et al., 2003; Yao, et al., 2002; Au & Buyukozturk, 2006). This can be attributed to two free ends which debonding can initiate from and less bonded area.

Many variables that affect the probability of FRP sheets to debond include: the thickness of the FRP sheet, concrete strength, surface preparation, development length of the FRP sheet, epoxy strength and presence of anchors. FRP debonding can occur on two surfaces: the FRP/epoxy interface or in the concrete substrate. When stresses at the FRP/epoxy interface or concrete substrate exceed the shear strength of concrete or epoxy, the bond will no longer hold and give way.

Failure at the FRP/Epoxy Interface

FRP debonding can occur at the FRP/epoxy adhesive interface and is initiated by the following factors: dust and debris on the FRP prior to bonding to concrete, substrate with high concrete strength and insufficient epoxy between the concrete and FRP.

This type of failure is less common and may occur in members with high concrete compressive strength. In this case, the bond between the FRP and epoxy is the weakest link and fails when the shear stresses exceed the strength of the epoxy.

Failure of the Concrete Substrate

Concrete substrate failure is the most common type of debonding failure. High stresses develop in the FRP strengthening system of RC members after cracking. Most reinforced concrete members have concrete strengths that vary from f'_c =15 MPa to 50 MPa with a tensile cracking strain between ε=0.0001 to 0.002 (Burgoyne, 1993; Swaddiwudhipong, et al., 2003). Epoxies used in FRP systems have strains ranging from ε=0.01 to 0.08. Thus the bond strength of the concrete interface layer is much weaker than the bond strength of the epoxy adhesive. Therefore, most debonding failures occur by peeling off of the FRP sheet with a thin layer of concrete substrate bonded to the epoxy and FRP. This can be seen in Figure 2-6a and b for strengthened beams that failed in flexure.

Figure 2-6: FRP debonding in the concrete substrate: (a) shear (b) flexure

In beams strengthened with u-wrapped FRP sheets, debonding will begin at the ends of the FRP sheet. However, debonding can occur at the top or bottom of the sheet for beams with side bonded FRP sheets. Once this begins, the sheet will slowly continue to debond as the area of FRP able to resist the tensile load decreases. Figure 2-7 shows the region in a FRP strengthened beam where debonding will most commonly occur with side bonded and u-wrapped FRP sheets.

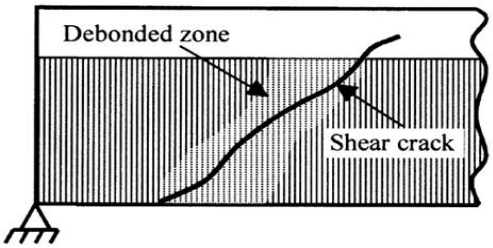

Figure 2-7: Debonding zones for side bonded & u-wrapped FRP strips (Chen & Teng, 2003)

A flexural or shear crack crossing the path of a FRP sheet will create localized stresses and start the debonding process (Figure 2-8a,b). When localized debonding occurs, the surrounding area of the FRP sheet will experience increased stress to compensate for the loss in bond. As loading continues, the stresses will increase causing successive FRP sections to debond. This process will continue until enough FRP has debonded causing the crack to propagate and member to fail (Figure 2-8c) or the ultimate strain in the FRP is obtained and the FRP sheet ruptures (Figure 2-8d).

Localized FRP debonding at a crack location is required to engage FRP sheets to resist the applied loads (Uji, 1992; Triantfillou & Antonopoulos, 2000). Large strains observed in the FRP sheet near cracks are due to the strain incompatibilities with the concrete substrate. This is similar to how internal stirrups resist loads. Internal stirrups require cracking in the concrete to engage them in resisting the shear forces (Quinn, 2009). Figure 2-9 shows how a crack in the concrete will produce localized debonding of the FRP at the crack location.

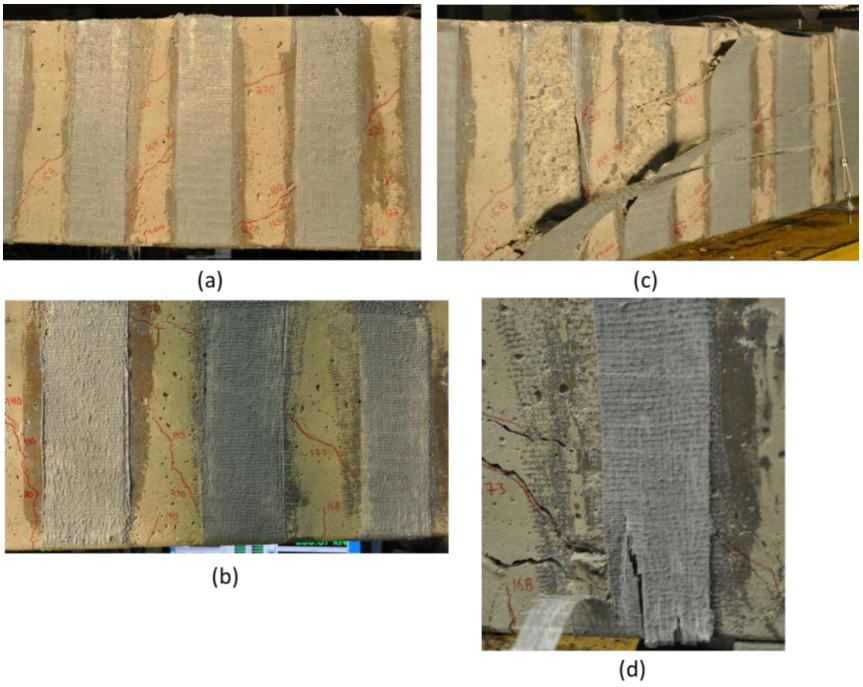

Figure 2-8: Shear crack crossing FRP sheets & debonding

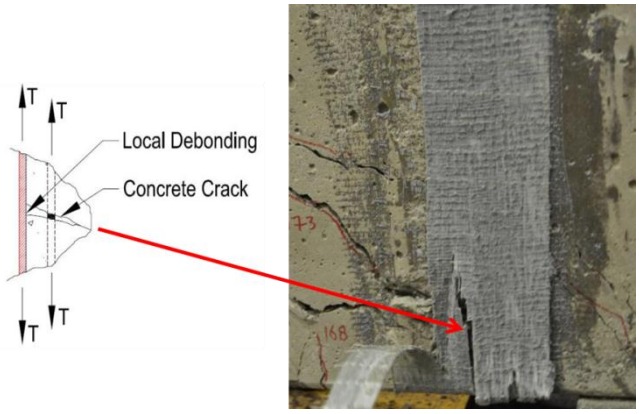

Figure 2-9: Debonding of FRP after cracking (Quinn, 2009)

Factors affecting FRP Debonding

Three main factors which affect FRP debonding are listed below. Each is individually discussed in the subsequent sections.

1. Concrete surface preparation
2. Bond and development length
3. Axial stiffness of FRP

1. Concrete Surface Preparation

Proper concrete surface preparation is one of the most important factors to safeguard against premature FRP debonding from occurring (Jayaprakash, et al., 2008). This will enable the best adhesion of the epoxy. Without proper bond, the tensile force transfer from the concrete surface to the FRP is not possible. Therefore, the FRP strengthening system (FRP sheet and epoxy) is dependent on the bond between the concrete surface, and the FRP epoxy interface.

ACI 440.2R-08 recommends detailed concrete surface preparation for any bond critical FRP application. The recommended preparation technique is summarized below:

1. Concrete must be free of loose or unsound material.
2. Surface preparation can be accomplished by using abrasive or water-blasting techniques.
3. All laitance, dust, dirt, oil, curing compound, existing coatings and any other matter that could interfere with the bond of the FRP to the concrete should be removed.
4. All surfaces should be dry as recommended by the FRP manufacturer.
5. The corners should be rounded to a minimum 13 mm radius to prevent stress concentrations and voids between the FRP system and the concrete.
6. The surface should be air-blasted to remove any dust and loose particles.

2. Bond and Development Length

The development bond length of a FRP sheet that is bonded to concrete has a direct effect on the ability of the sheet to resist shear forces and stresses which cause debonding. If sufficient bond length is provided, the full strength of the FRP sheet can be utilized. Any additional bond

length that is provided beyond the effective bond length will not decrease the stresses which cause debonding to occur (Chen & Teng, 2003).

Maeda, et al. (2007) observed that the larger the bonded length above the diagonal tension shear crack, the less likely the sheet will debond from the concrete surface. Therefore, the closer a shear crack is to the ends of a u-wrapped or side bonded FRP strip, the less tensile force the strip can carry before debonding occurs.

Madea, et al. (1997) revealed that the location a shear crack crossing a FRP sheet has a significant effect on the capacity to resist the tensile forces. He stated that "when a shear crack is created on a side bonded or u-wrapped beam, the bonded length of the FRP sheet above the shear crack is reduced significantly." The bonded area of a FRP sheet above a shear crack must provide anchorage for the entire tensile force. The stresses that were transferred from the concrete through the entire FRP sheet are now transferred through a much smaller area (the area of the bonded FRP sheet above the shear crack).

3. Axial Stiffness of FRP

Axial stiffness is the longitudinal stiffness of the FRP sheet in the direction of fibers. The product of multiple FRP layers is a very stiff FRP sheet. Triantifillou, (1998) reported that "The effective bond length required to obtain the ultimate tensile force of the FRP is proportionately dependent on the axial stiffness associated with FRP strips." The axial stiffness of a FRP system can be calculated using Equation 2-1 with FRP reinforcement ratio (ρ_{frp}) given in Equation 2-2.

$$\rho_{frp} E_{frp} \qquad \textbf{Equation 2-1}$$

$$\rho_{frp} = \frac{2 t_{frp} w_{frp}}{b \cdot s_{frp}} \qquad \textbf{Equation 2-2}$$

where

E_{frp}= the elastic modulus of the FRP
t_{frp} = the thickness of the FRP
w_{frp}= the width of the FRP
s_{frp}= the spacing of the FRP (center to center)

The axial stiffness of the FRP plays an important role in the mode of failure. A thin and slender FRP sheet has a higher possibility of rupturing compared to a thick and wide FRP sheet which is expected to debond (Quinn, 2009; Triantifillou, 1998; Teng, et al., 2004). Therefore, as the FRP stiffness increases, the development length must also be increased (Triantifillou, 1998).

2.4.2.2 FRP Rupture

FRP rupture occurs when the ultimate tensile strength of the material is reached causing the fibers to fracture. Prior to FRP rupture, local debonding of the sheet will occur at a shear crack. This localized debonding is essential to allow the FRP sheet to carry the tensile forces being transferred from the cracked concrete. A shear crack means the concrete is no longer providing any tensile resistance and the FRP sheet is now resisting all the tensile force. As loading is increased, the shear cracks become larger, wider and more strain is induced in the FRP sheet. The strain in the FRP will continually increase until it reaches the strain capacity of the FRP sheet and rupture occurs.

In u-wrapped beams rupture of the FRP sheet will occur close to mid-depth of the FRP sheet. This is consistent with the location the shear crack crosses the FRP sheet (Figure 2-10). At that location, strains are known to be highest (Chen & Teng, 2003).

Figure 2-10: Ruptured GFRP u-wrapped sheet

FRP sheets crossing the lower portion of a shear crack will rupture first. This location has the highest stress which is transferred to the FRP sheet. Once the FRP sheet ruptures the stresses in the member redistribute to the remaining sheets and the process of sheet rupture is repeated until the member completely fails (Figure 2-11).

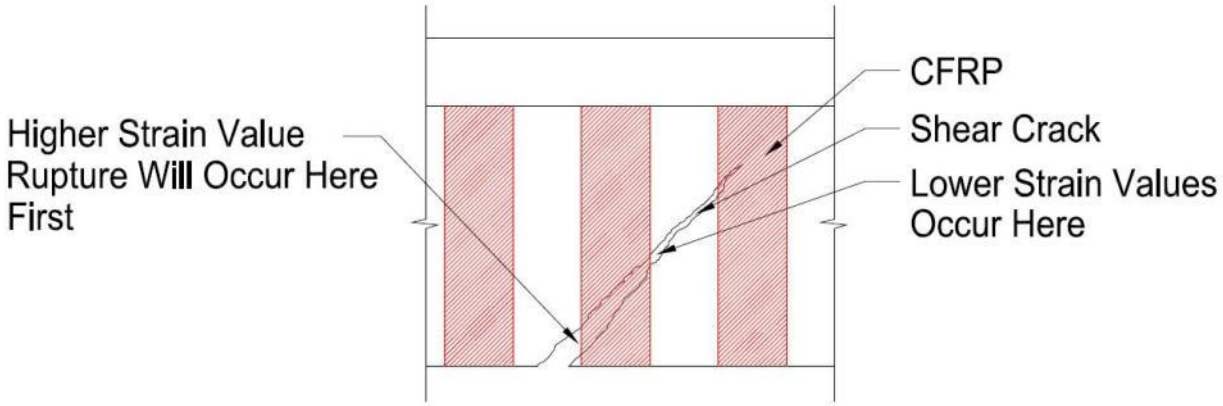

Figure 2-11: Shear crack crossing FRP strips (Quinn, 2009)

FRP fracture can be caused by localized stress concentrations due to surface imperfections and sharp edges at bends in the member's cross section. Therefore, when applying FRP as fully wrapped and u-wrapped configurations to strengthen RC beams, all corners in the cross-section must be rounded to a radius of 12.7 mm (ACI 440.2R-08). Rounding the corners will allow for a smoother transition of the tensile forces and eliminate the localized stress concentration on the FRP sheet.

Therefore, FRP rupture most commonly occurs when a diagonal tension shear crack is present and the beam is fully wrapped (Chen & Teng, 2003; Teng, et al., 2004). To date securing a FRP sheet to reach strains high enough to cause rupture with u-wrapped or side bonded strips has proven to be very difficult. Providing proper anchorage for the FRP sheet will delay if not eliminate the debonding process from occurring and allow the FRP sheet to reach its ultimate tensile capacity and rupture.

2.4.3 Shear Strength Prediction of FRP Strengthened Slender Beams

The shear capacity of a reinforced concrete beam with external FRP reinforcement is difficult to predict. Researchers are working to improve the prediction formulas for the shear capacity of a RC beam with external FRP (Chen, et al., 2012; Chen, 2010; Chen, et al., 2010; Ali, et al., 2006; Grande, et al., 2009; Pellegrino & Modena, 2002).

When calculating the shear strength of RC beams, several prediction models exist which fulfill either equilibrium and compatibility conditions, or just equilibrium conditions. The models which satisfy only equilibrium conditions include; the 45^0 truss model, variable angle truss

model, modified truss model and strut and tie model. The models which satisfy both equilibrium and compatibility conditions are the compression field theory, modified compression field theory, rotating angle softened truss model and fixed angle softened truss model (El-Sayed, 2006; Azam, 2010).

The most common shear prediction model used for deep beams is the strut and tie model (CSA A23.3-04 and ACI 318M-08). The most popular shear prediction models for slender beams are: the modified compression field theory (CSA A23.3-04) and the 45^o truss model (ACI 318M-08). The current Canadian design code (CSA A23.3-04) has adopted the modified compression field theory (MCFT) as the basis of both the General Method and Simplified Method for shear design of reinforced concrete beams.

When using the CSA A23.3-04 design procedure, two methods are available to determine the values of β and θ. The Simplified method is the more basic method which uses predetermined values from statistical regression models for typical slender beams. The General Method is a more detailed analysis where β and θ are calculated by iteration. Both of these methods are outlined in Table 2-5.The total shear capacity of a reinforced concrete beam designed using the CSA A23.3-04 code and ISIS-M04 is provided in Table 2-3and Table 2-4.

The shear resistance components are shown in Figure 2-12. The factored shear resistance 'V_r' is calculated by summing the individual contributions calculated for concrete 'V_c', steel stirrups 'V_s' and external fiber reinforced polymer (FRP) composites 'V_{frp}' as given in Equation 2-3.

$$V_r = V_c + V_s + V_{frp} \qquad \textbf{Equation 2-3}$$

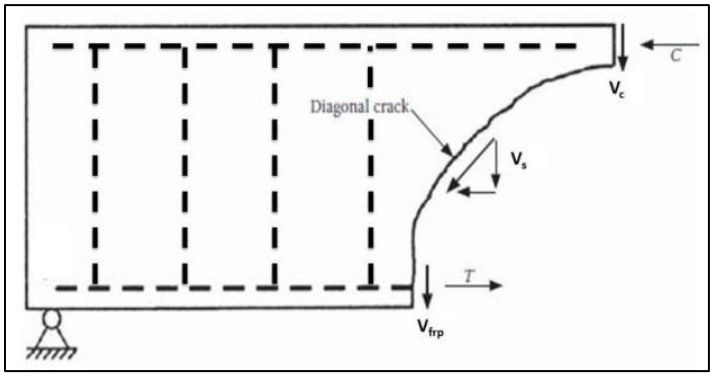

Figure 2-12: Mechanisms of shear transfer (Robert Park, 2006)

Table 2-3: Design for shear in flexural regions (CSA A23.3-04 & ISIS-M04)

Expression	Notation
$V_r = V_c + V_s + V_{frp}$	V_r= factored shear resistance V_c= shear resistance from concrete V_s= shear resistance from steel V_{frp}= shear resistance from FRP
$V_c = \phi_c \lambda \beta \sqrt{f_c'} b_w d_v$	Φ_c=resistance factor for concrete λ= factor to account for low density concrete β= factor accounting for shear resistance of cracked concrete f'_c=specified compressive strength of concrete b_{wt}= beam web width d_v= effective shear depth (greater of 0.9d or 0.72h)
$V_s = \frac{\phi_s A_v f_y d_v cot\theta}{s}$	Φ_c= resistance factor for concrete A_v= area of shear reinforcement with a distance s f_y= specified yield strength of non-prestressed reinforcement θ= angle of inclination of the diagonal compressive stresses s= spacing of shear reinforcement
$V_{frp}{}^* = \frac{\phi_{frp} E_{frp} \varepsilon_{frp} A_{frp} d_{frp} (cot\theta + cot\beta) sin\beta}{s_{frp}}$	Φ_{frp}= resistance factor of FRP material E_{frp}= modulus of elasticity of FRP material ε_{frp}= effective strain of FRP material A_{frp} = cross-section area of FRP material d_{frp}= effective depth θ= angle of inclination of diagonal cracks in the concrete β= angle of the FRP stirrups s_{frp}= spacing of the FRP stirrups

*FRP shear contribution (V_{frp}) is determined using ISIS-M04

Table 2-4: Design of FRP sheets for shear strengthening (ISIS-M04-09)

Expression	Notation
$\varepsilon_{frp} =$ smallest of $(\varepsilon_{frpe1}, \varepsilon_{frpe2}, \varepsilon_{frpe3})$ $\varepsilon_{frpe1} = 0.75\varepsilon_{frpu}$ $\varepsilon_{frpe2} = 0.004$ $\varepsilon_{frpe3} = K_v\varepsilon_{frpu}$ where	ε_{frpe1}= ultimate strain from FRP strength ε_{frpu}= ultimate strain of FRP material ε_{frpe2}= ultimate strain from aggregate interlock ε_{frpe3}= ultimate strain from bond capacity k_v= bond reduction coefficient for externally bonded FRP stirrups
$K_v = \frac{K_2 K_1 L_e}{11900\varepsilon_{FRPu}}$ where $K_1 = \left(\frac{f'_c}{27}\right)^{2/3}$ $K_2 = \frac{d_{frp} - L_e}{d_{FRP}}$ $K_v = \frac{23300}{(t_{FRP}E_{FRP})^{0.58}}$	k_1= concrete strength factor k_2= FRP bond configuration factor L_e= effective anchorage length t_{frp}= thickness of FRP d_{frp}= greater of 0.72h or 0.9d

Table 2-5: Simplified and general method for shear design (CSA A23.3-04)

Simplified Method	General Method	Notation
β= 0.18 or $\beta = \frac{230}{(1000 + d_v)}$	$\beta = \frac{0.4}{1 + 1500\varepsilon_x} \cdot \frac{1300}{1000 + s_{ze}}$ where $\varepsilon_x = \frac{\frac{M_f}{d_v} + V_f + 0.5N_f}{2(E_s A_s)}$ $s_{ze} = \frac{35s_z}{15 + a_g}$	ε_x= longitudinal strain at mid-depth of cross-section S_{ze}= equivalent crack spacing parameter M_f= moment due to factored loads d_v= effective shear depth V_f= factored shear force N_f= factored axial load normal to the cross-section E_s= modulus of elasticity of reinforcement A_s= area of longitudinal reinforcement S_z= crack spacing parameter a_g= nominal maximum size of coarse aggregate
$\theta = 35^0$	$\theta = 29 + 7000\varepsilon_x$	ε_x= longitudinal strain at mid-depth of cross-section

2.5 Flexure Strengthening/Repair of Reinforced Concrete Beams & Slabs

2.5.1 FRP Flexural Strengthening Configuration

The use of FRP for flexural strengthening and repair of reinforced concrete beams and slabs have been extensively researched in the past three decades. FRPs used for flexural strengthening and repair are applied by externally bonding FRP sheets or plates to the tension face of a beam or slab with the longitudinal fibers running along the length of the member (Figure 2-13). FRP strengthening has been proven to provide increased flexural capacity of RC slabs (Oehlers & Seracino, 2004). However, the FRP sheets are susceptible to premature debonding at the ends of the member or intermediate debonding within the member. FRP debonding occurs at strains well below the ultimate rupture strain of the FRP (Smith , et al., 2011).

Figure 2-13: Flexural strengthened slab with CFRP sheets

2.5.2 FRP Failure Modes in Flexural Strengthening

Six different types of flexural failure modes in beams strengthened with FRP exist. Each is summarised below:

1. FRP Rupture – Flexural failure occurs by yielding of the longitudinal steel followed by the rupture of the FRP plates (Figure 2-14a).
2. Crushing of the Concrete – Failure occurs by crushing of the concrete in the compressive zone. This can occur before or after yielding of the tensile steel and FRP is not ruptured (Figure 2-14b).
3. Shear Failure – FRP flexural strengthening may exceed the shear capacity of the beam and lead to cracking near the support. This crack can propagate as an inclined crack and cause shear failure (Figure 2-14c).

4. Concrete Cover Separation – Cracking along the tensile reinforcement causes failure in the concrete cover. High interfacial shear and normal stresses at the FRP plate end cause an initial crack to form and propagate to the tensile reinforcement. As the cracking extends along the bottom of the tensile steel, the concrete cover begins to separate (Figure 2-14d).
5. Plate-End Interfacial Debonding – Failure occurs in the concrete substrate with debonding of a thin layer of concrete attached to the FRP plate. High interfacial shear and normal stresses at the plate end exceed the tensile strength of the concrete substrate causing the weakest bond to fail (Figure 2-14e).
6. Intermediate Crack Induced Debonding – Cracking in the concrete is initiated in the high moment region (middle) by a vertical flexural or shear crack. This crack will propagate along the length of the beam at the FRP/concrete interface towards the plate end until failure occurs (Figure 2-14f, g). This type of debonding occurs when a major flexural crack begins to open and propagate towards the end of the sheet (Lu, et al., 2007; Teng, et al., 2003; Au & Buyukozturk, 2006).

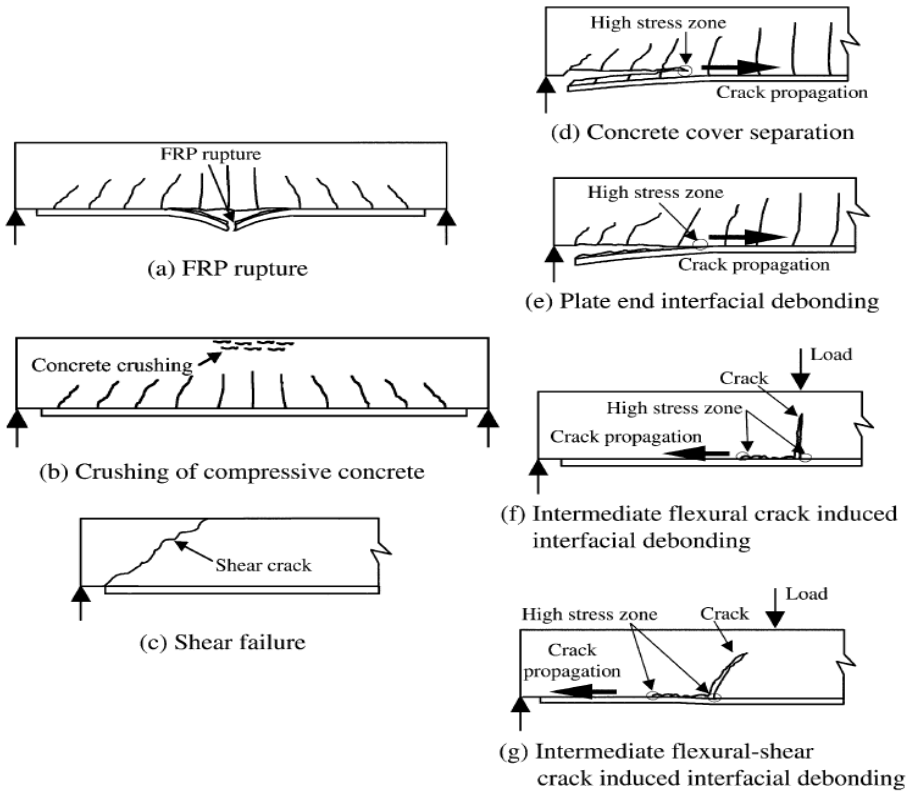

Figure 2-14: Failure modes of RC beams with FRP flexural strengthening (Teng, et al., 2003)

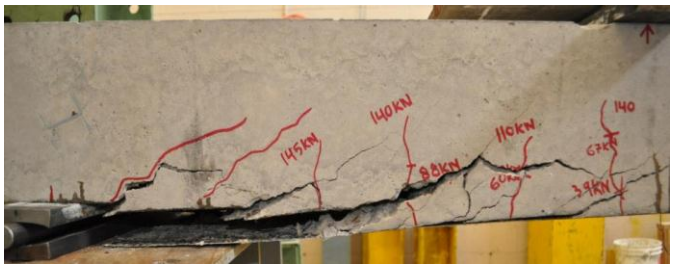

Figure 2-15: Intermediate crack induced debonding

Figure 2-16: Plate end debonding

Interfacial Stresses and Debonding

The mechanics behind FRP debonding are outlined in this section. A beam strengthened in flexure will most commonly debond from intermediate crack debonding or plate end debonding. Lu, et al. (2007) highlighted that FRP-strengthened beams have two types of the interfacial shear stresses acting on the FRP sheet. The first stress is the shear stress from the applied loads (τ_s) as shown in Figure 2-17a, the second stress is shear stress caused by the opening-up of flexural cracks (τ_c) displayed in Figure 2-17b.

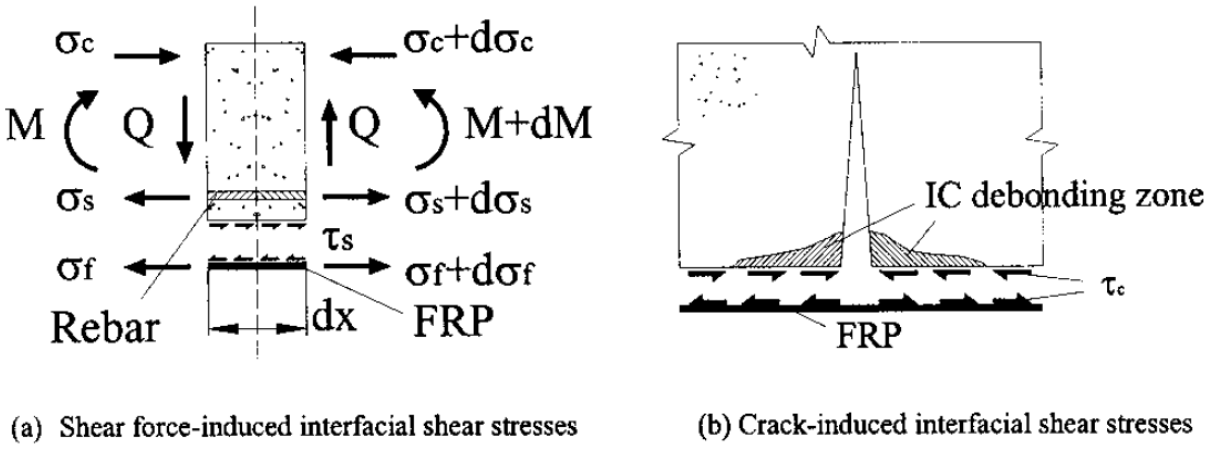

(a) Shear force-induced interfacial shear stresses (b) Crack-induced interfacial shear stresses

Figure 2-17: Interfacial shear stresses (Lu, et al., 2007)

During loading, once a large flexural or shear crack is formed tensile stresses are transferred to the bonded FRP. As the load is increased, the crack widens and the interfacial stresses between the FRP and concrete surface increase. Once the stress becomes larger than the tensile strength of the concrete, debonding occurs. Debonding of the FRP sheet will then propagate along the length of the member towards its end until failure. This process is displayed in Figure 2-18. The peak stress experienced in the FRP sheet which has debonded will be nearly equal regardless if it is induced from a flexural-shear crack or pure flexural crack (Teng, et al., 2003).

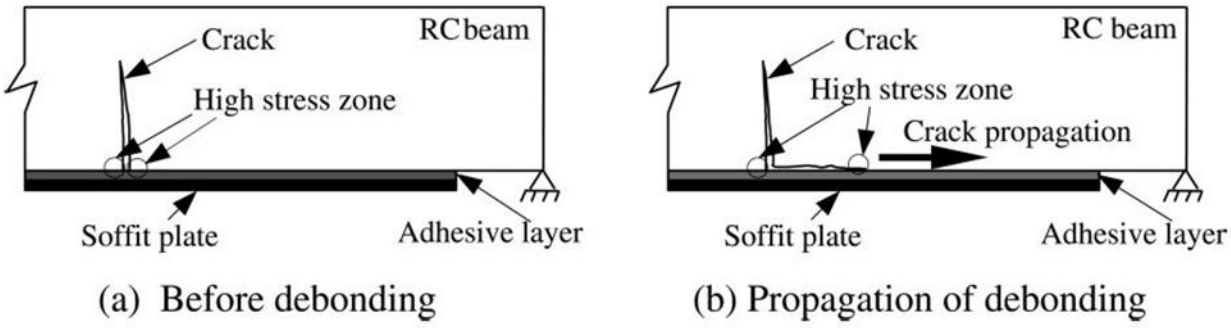

Figure 2-18: Intermediate crack induced debonding (Teng, et al., 2003)

In previous experimental studies, beams tested in four point bending experienced IC debonding under one of the loading points. Under these loading points, the maximum shear force and bending moment is reached. Both the interfacial shear stress (τ_s) and crack induced shear stress (τ_c) are at their highest values (Fang, 2002; Rahimi & Hutchinson, 2001).

2.5.3 Flexural Strength Prediction of FRP Strengthened Slabs

The flexural strength of a RC beam or slab is determined based on strain compatibility and force equilibrium (ACI 440.2R-08 and ISIS-M04). A diagram of a beam section, stress and strain profile of a singly-reinforced concrete beam strengthened in flexure with externally-bonded FRP materials is shown in Figure 2-19. The flexural moment resistance 'M_r' for a RC beam or slab with FRP strengthening is calculated by summing the moment contributions of the steel and FRP, as given in Equation 2-4 and Table 2-6. The variables are described in Table 2-6.

$$M_r = T_s\left(d_s - \frac{\beta c}{2}\right) + T_{frp}\left(h - \frac{\beta c}{2}\right) \qquad \textbf{Equation 2-4}$$

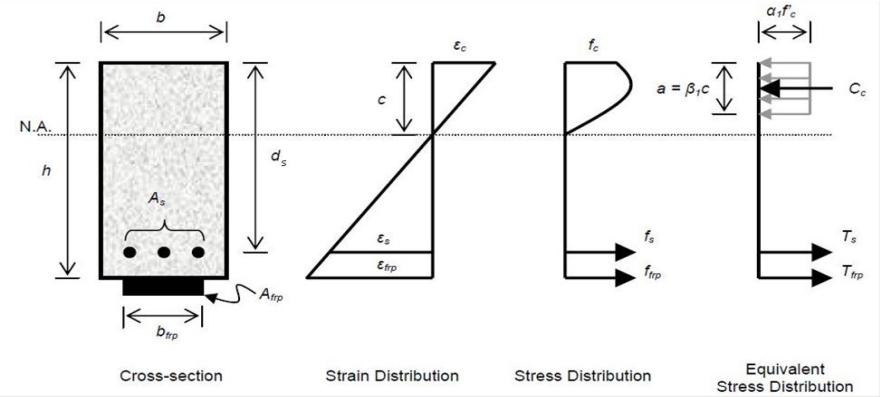

Figure 2-19: Stress & strain profile of beam strengthened in flexure with FRP (ISIS-M04)

Table 2-6: Design for flexure with FRP strengthening (ISIS-M04)

Expression	Notation
$M_r = T_s\left(d_s - \frac{\beta c}{2}\right) + T_{frp}\left(h - \frac{\beta c}{2}\right)$	M_r= factored flexural resistance T_s= tensile resistance of steel reinforcement T_{frp}= tensile resistance of FRP d_s= distance from extreme compression fiber to centroid of tension reinforcement β= depth ratio c= distance from extreme compression fiber to neutral axis h= overall height of member
$T_s = \phi_s f_y A_s$	Φ_s=resistance factor for steel reinforcement f_y=specified yield strength of steel reinforcement A_s= Area of tensile steel reinforcement
$T_{frp} = \phi_{frp}\varepsilon_{frp}E_{frp}A_{frp}$ where	Φ_{frp}= resistance factor of FRP material ε_{frp}= effective strain of FRP material E_{frp}= modulus of elasticity of FRP material A_{frp}= cross-sectional area of FRP material
$\varepsilon_{frp} =$ smallest of $(\varepsilon_{frpu}, \varepsilon_{frpd}, \varepsilon_{frpt})$ where $\varepsilon_{frpu} =$ material specific $\varepsilon_{frpt} = 0.006$ $\varepsilon_{frpd} = 0.41\sqrt{\frac{f'_c}{nE_t t_f}}$ $A_{frp} = t_{frp} w_{frp}$	ε_{frpu}= ultimate strain of externally bonded FRP material ε_{frpt}= maximum strain of externally bonded FRP material ε_{frpd}= strain at which debonding may occur w_{frp}= width of the FRP material t_{frp}= thickness of FRP material n_{frp}= modular ratio (E_{frp}/E_c)

2.6 Anchors for FRP Sheets

Researchers reported that some sort of anchorage (mechanical or otherwise) at the ends of FRP sheets is required to prevent debonding from occurring (Teng, et al., 2003; Lu, et al., 2007; Chen & Teng, 2003; Quinn, 2009; Khalifa & Nanni, 2000; Khalifa, et al., 1999; Orton, et al., 2008; Kim & Smith, 2009).

When any anchorage device is utilized to secure the FRP sheet, the debonding failure is almost always prevented and the mode of failure is changed to rupture of the FRP sheet (Khalifa, et al., 1999; Teng, et al., 2004). Without an anchorage system, the strength provided by an FRP system is entirely dependent on the bond between the FRP sheet and the concrete interface. All relevant information regarding anchors used for FRP strengthening is discussed in the subsequent sections.

2.6.1 Types of Anchors

Many types of anchors have been explored to deal with the problem of FRP debonding. Some of the anchors used to secure FRP sheets to concrete include: mechanically fastened metallic anchors, u-wrap with near surface mounted rod, modified anchor bolt system, embedded metal threads and FRP anchors (Smith , et al., 2011; Au & Buyukozturk, 2006; Sharif, et al., 1994; Khalifa, et al., 1998; Khalifa & Nanni, 2000; Kalfat, et al., 2011). A description of each of these anchors is given below.

U-jacket Anchorage

The u-jacket anchoring system is a u-wrap FRP strip that is transversely bonded at the ends of a longitudinal FRP sheet. The u-jacket provides confinement for the longitudinal FRP sheet to resist the tensile peeling stresses and longitudinal crack propagation at the FRP ends or intermediate crack location on the FRP sheet (Kalfat, et al., 2011). Figure 2-20 shows an inclined u-jacket (u-wrap) installed to anchor a FRP sheet used for flexural strengthening.

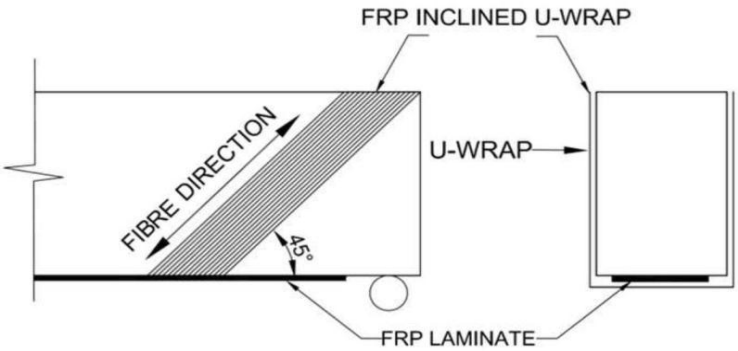

Figure 2-20: U-jacket anchor detail (Kalfat, et al., 2011)

U-jackets are placed at the ends of the FRP sheet but can also be placed along the length of the member. This is done to prevent intermediate crack induced debonding. In a study by Al-Amery, et al. (2006) u-jackets spaced throughout the length of a CFRP strengthened beam were used to anchor a CFRP flexural sheet from debonding from concrete substrate. The u-jackets reduced the interfacial stresses and allowed the flexural CFRP sheet to be completely utilized before failure. In comparison to the control beam, a 95% increase in strength was measured when the u-jacket anchors were installed to secure the longitudinal FRP sheet and only a 15% increase in strength was observed when the FRP sheet was applied without anchorage (Al-Amery & Al-Mahaidi, 2006).

U-Anchor with Near Surface Mounted Rod

The u-anchor with near surface mounted rod (NSMR) was invented by Khalifa, et al. (1999). It utilizes a FRP rod placed inside a pre-cut groove in the concrete member and used to anchor a FRP sheet. The anchor system can be used to secure the ends of FRP sheets in strengthening beams, slabs and columns (Figure 2-21).

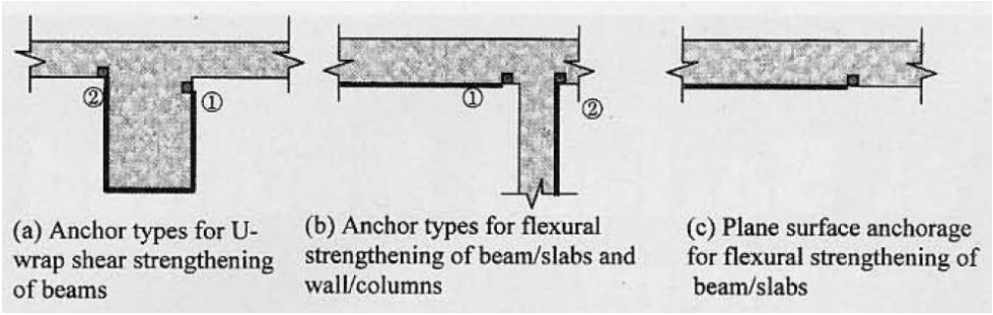

Figure 2-21: Application examples for u-wrap anchors (Khalifa, et al., 1999)

This anchor system works by embedding the end portion of the FRP sheet with a FRP rod (transverse to the sheet) into a pre-cut groove in the concrete member (Khalifa, et al., 1999). The groove is cut in the concrete cover by making two parallel saw cuts to a predetermined depth. After the two saw cuts are made, the concrete can be chipped away to create the groove. Prior to embedding the rod with the FRP sheet, the groove is half filled with epoxy and the rod is pressed lightly ensuring sufficient epoxy covers the FRP sheet and rod. The groove is then completely filled with epoxy until the surface is level. It should be noted that because the groove is made in the cover of the concrete member, shear forces are not transferred to the concrete and the surrounding internal steel reinforcement. Figure 2-22 shows a detail of this system.

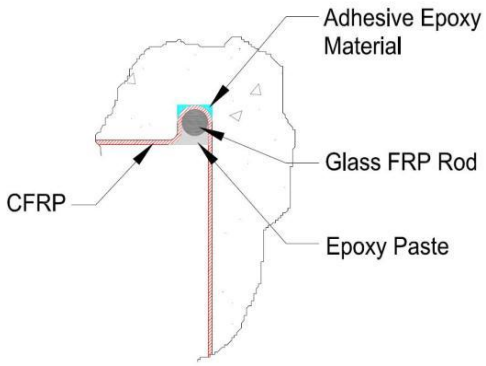

Figure 2-22: U-anchor with Near Surface Mounted Rod Detail (Khalifa, et al., 1999)

This anchor system eliminates any drilling and reduces the possibility of damaging the internal steel. Khalifa, et al. (1999) reported that in comparison to the control beam, this method of securing FRP sheets increased the shear capacity by 42% compared to beams strengthened with unanchored sheets and changed the failure mode from debonding to a flexural failure by crushing of the concrete.

Steel Clamps

Steel clamp anchor system is composed of three components; a threaded rod, steel plates and steel angles which act as clamps for the FRP material. In a rectangular beam with FRP u-wraps the clamp anchors uses steel plates and rods placed through the web of the section to secure the FRP sheet against debonding. For T-beams with u-wrap FRP sheets, the clamp anchor uses angle sections at the web/flange corner to secure the FRP sheet and eliminate debonding. Figure 2-23 shows details of three types of clamp anchors.

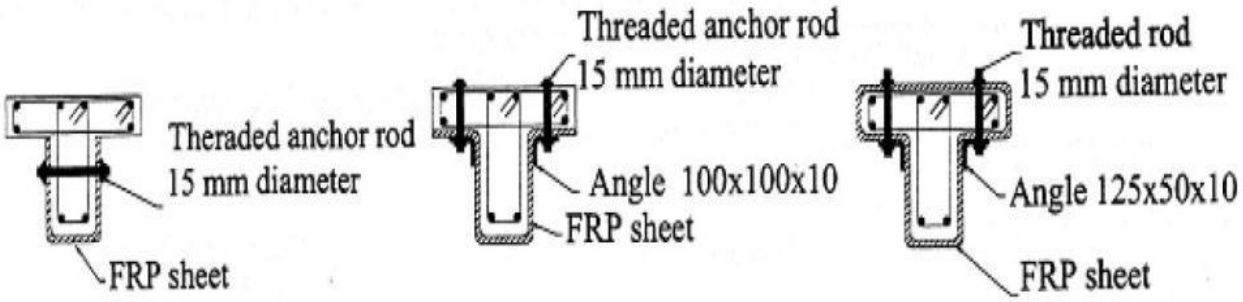

Figure 2-23: Embedded metal thread configurations (Deifalla & Ghobarah, 2006)

This method of anchoring FRP sheets has proven to work quite well. However, this system is labor intensive and costly. Steel angle sections are used and can corrode when exposed to the environment.

Mechanically Fastened Metallic Anchors

The mechanically fastened metallic anchor system also known as the hybrid bonded system, works by applying special mechanical fasteners which are nailed into the concrete substrate manually or with a powder actuated fastening gun. If done manually, holes are pre-drilled into the concrete substrate to allow for the fasteners to be hammered into place. Epoxy is placed on the FRP sheet to bond the mechanical fastener to the FRP sheet (Wu & Huang, 2008). Figure 2-24a shows a typical mechanical fastener used to anchor FRP sheets. For slabs strengthened in flexure, mechanical fasteners can be installed at discrete locations along the longitudinal FRP reinforcement as shown in Figure 2-24b.

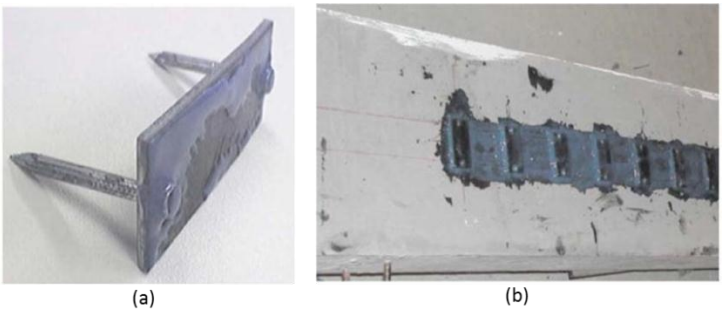

Figure 2-24: The mechanical fastener system (Wu & Huang, 2008)

This system is different from the traditional mechanical fasteners (steel clamps) because it doesn't depend on FRP. This makes the anchor applicable to any FRP strip, plate or sheet. Bond and interfacial shear resistance components differentiate this system from other mechanically anchored systems. The first is the presence of the additional epoxy between the FRP sheet and the fastener which provides additional adhesion and the second is the frictional resistance from the normal pressure exerted on the FRP strip by the mechanical fastener.

Wu, et al. (2008) reported that the increase in flexural strength of FRP strengthened slabs with mechanical fasteners varied from 79%-248%. The wide range is dependent on the number of FRP layers (2, 4, 6) that were used to strengthen the slab. Significant strength increases were observed with this anchorage system. The bond strength provided by the mechanically anchored system was greater than the tensile strength of the two and four ply FRP sheets but less than that of the stiffest six layered FRP strengthened slab. It was concluded that the more mechanical fasteners that are installed, the higher the bond strength is obtained.

Limitations of this anchoring system are due to the extensive labor involved to predrill and the use of steel as the fastener material. A metallic anchor is susceptible to corrosion and can deteriorate when exposed to the environment.

Modified Anchor Bolt System

The modified anchor bolt system also known as the wedge anchor system, works by looping a u-wrapped FRP sheet around a steel or FRP plate. A second plate is used to lock the sheet and a concrete wedge anchor and steel bolt secures the three layer connection. This system can be installed using continuous or discontinuous FRP plates bonded to the top and bottom of FRP sheets. Figure 2-25 shows the detail of this system.

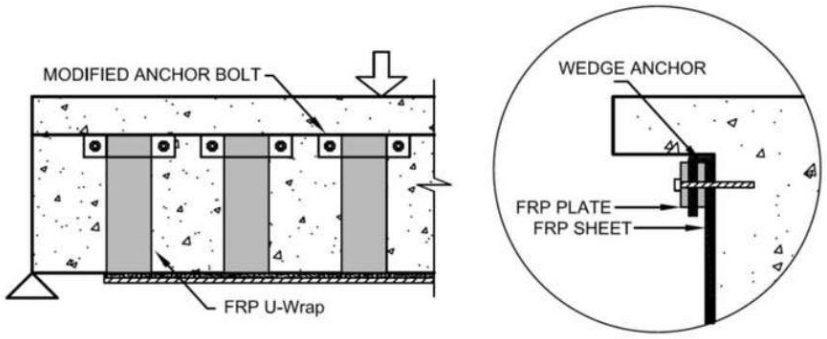

Figure 2-25: Modified anchor bolt system detail (Kalfat, et al., 2011)

The initial design of this anchor by Ortega, et al. (2009) used a three layer connection with one continuous steel plate mechanically anchored. This proved ineffective because the steel plate buckled due to the curvature of the beam at failure. Also, the u-wrapped CFRP sheet slipped inside the anchor preventing the sheet from reaching its ultimate tensile capacity (Ortega, et al., 2009). Mofidi, et al. (2012) proposed a modified anchor bolt system using a three layer connection and four layer connection. Strengthened beams with the three layer connection had a 30% increase in shear strength over the control (unstrengthened) and the mode of failure was maintained as a shear failure. The modified system with a four layer connection increased the shear capacity by 43% over the control (unstrengthened), changing the mode of failure from a shear to flexural failure. In comparison, the strengthened beam without anchors had a 25% increase over the control (Mofidi, et al., 2012).

FRP Anchors

Fiber reinforced polymer (FRP) anchors are relatively new method to anchor FRP sheets used in flexural or shear strengthening of RC beams and slabs. FRP anchors are composed of a tight bundle of fibers which are inserted into predrilled holes and adhered to the concrete and FRP sheet surface with high strength epoxy. Overall, FRP sheet debonding was prevented when a greater number of smaller anchors were used as opposed to a lesser quantity of larger anchors used to secure the FRP sheets.

The first FRP anchors were developed by the Shimizu Corporation in Japan (Jinno & Tsukagishi, 1998; Kobayashi, et al., 2001). FRP anchors were explored because they have the same material characteristics and benefits as the FRP sheets used for strengthening the member. The first type

of FRP anchors were constructed by hand using the same material as the FRP sheet. It was found that the presence of a one fan anchor in a shear coupon test can increase the strength and slip capacity of the FRP-to-concrete interface from 70% to 800% (Smith, 2010; Zhang, et al., 2011). Currently, FRP anchors are utilized to secure FRP sheets applied for shear and flexure strengthening of concrete members. They can be used to secure u-wraps and side bonded FRP sheets (Figure 2-26).

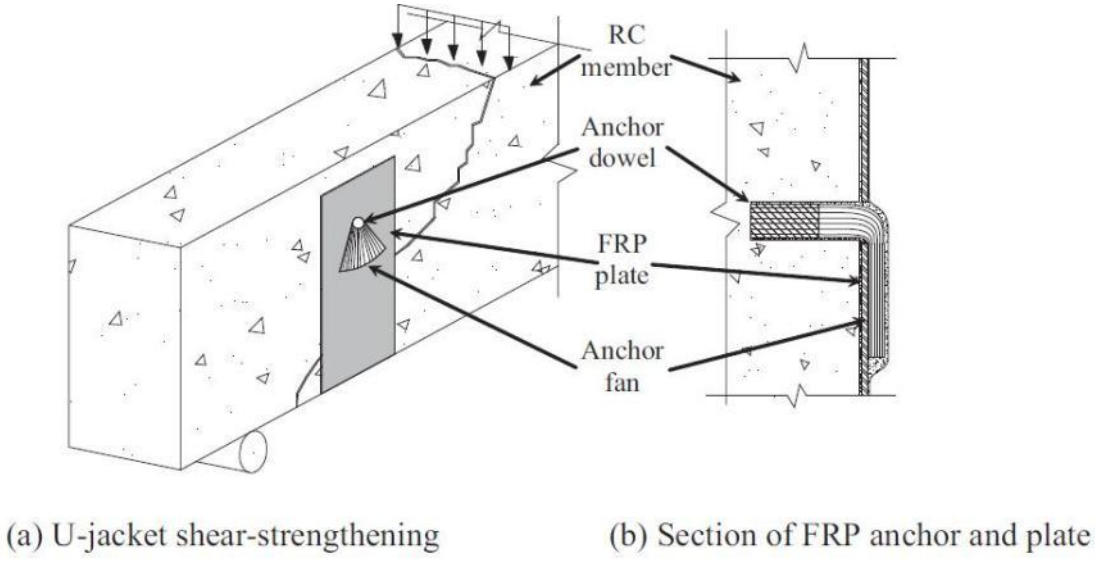

Figure 2-26: U-wrapped FRP sheet with FRP anchor (Zhang, et al., 2011)

FRP anchors can be fanned in two ways depending on the type of system. Anchors installed to secure u-wrapped or side bonded FRP sheets for shear strengthening will use a 30^o anchor fan. Anchors installed to secure flexural FRP sheets will use a 30^o or 360^o fan or a combination of both depending if the anchor is located in the center of the sheet or at the end of the sheet. Anchors located at either end of the FRP sheet will have a 30^o fan and anchors located in the shear span will have a 360^o fan. Figure 2-27 shows a diagram of a 360^o fan used on a slab with flexural strengthening.

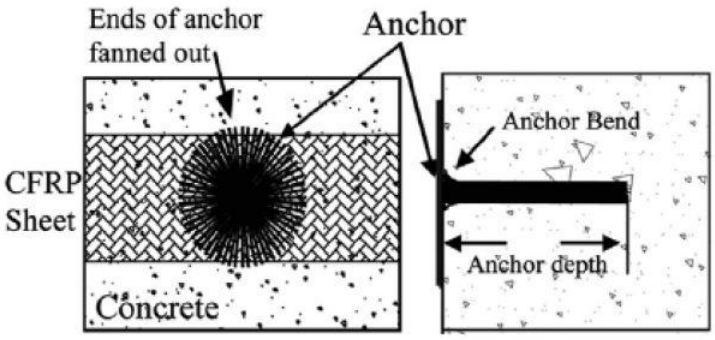

Figure 2-27: FRP anchor with 360 degree fan (Orton, 2007)

Orton and Kim, (2007) showed that strains in the FRP sheet are significantly higher with the presence of FRP anchors. The full tensile capacity of anchored FRP sheets was reached when no bond was present between the FRP reinforcement and the concrete surface. This proved that the anchors alone have the ability to develop the ultimate tensile capacity of the FRP sheets regardless of the quality of the surface preparation. Kim, et al. (2009) reported that FRP anchors can be installed to stop the propagation of debonding cracks in flexural strengthening of pre-cracked slabs.

2.6.2 Load Transfer Mechanism for Anchors

The load transfer mechanisms for anchors include: mechanical interlock, friction, chemical bond or a combination. FRP anchors installed in pre-drilled holes rely on chemical bond as the primary load transfer mechanism. The tensile stresses in the FRP sheet are transferred to the concrete substrate through the embedded portion of the FRP anchor and anchor fan. The tensile forces are transferred from the anchor into the concrete and the surrounding reinforcing steel (Ozdemir, 2005).

To understand the stress transfer mechanism when FRP anchors are used to secure an FRP sheet, a free body diagram of the forces acting on the FRP sheet and the anchor is shown in Figure 2-28. The debonding force from the CFRP sheet on the anchor is distributed into the concrete member through the anchor hole and is represented by component forces (dF and dF2). The forces (dF and dF2) are transferred through the anchor fan into component forces (dF1 and dF3). Force (dF2) acts on the inside wall of the predrilled hole at the anchor bend. This force changes the direction of the tensile force (dF) so it can be distributed throughout the anchor fan. Force (dF3) represents the epoxy or adhesive and acts orthogonally to the FRP sheet (Kobayashi, et al., 2001).

The stresses which act at the inserted portion of the anchor include both pull-out and shear stresses. Inside the hole, interfacial shear stresses exist between the anchor and epoxy. Close to the edge of the hole (where anchor bends from a vertical to horizontal direction) the anchor resists bearing stresses. Away from the hole location, the tensile forces in the FRP sheet are resisted by bonding stresses between the FRP sheet and the FRP anchors (Quinn, 2009).

Details of the forces acting on the embedded portion of a 30 degree fanned FRP anchor are displayed in Figure 2-29.

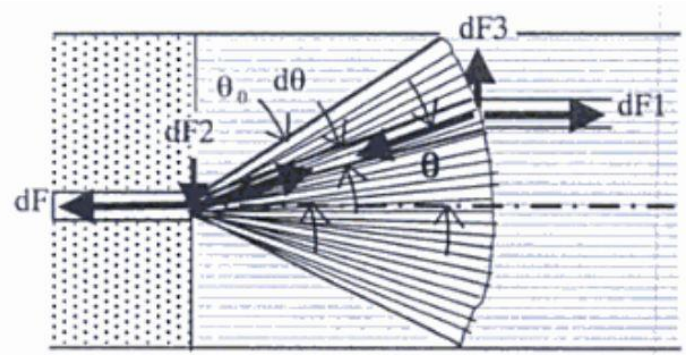

Figure 2-28: FRP anchor load transfer mechanism (Kobayashi, et al., 2001)

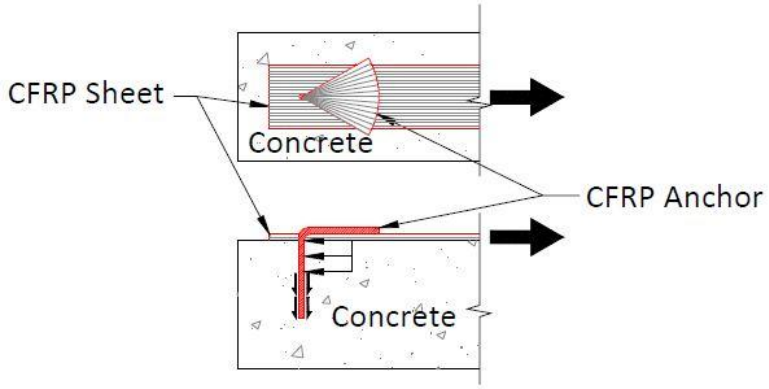

Figure 2-29: Force stress diagram of a 30 degree fan FRP anchor (Quinn, 2009)

2.6.3 Failure Modes of Anchors

The typical failure modes observed when using metallic and FRP anchors include: anchor pry-out with local concrete failure, concrete edge failure, anchor pull-out, anchor rupture or a combination of these failure modes. For example anchor pry-out with local concrete failure is

displayed in Figure 2-30. It is evident that the concrete around the anchor failed in a cone profile while the FRP anchor was completely intact and still bonded to the concrete.

Zhang, et al. (2011) reported that two failure modes exist for dry and impregnated anchors. For dry anchors, the primary mode of failure was pullout and for impregnated anchors the primary mode of failure was rupture of the fibers at the bend region. Figure 2-31 shows an FRP anchor pullout failure while Figure 2-32 shows a FRP anchor that failed by rupture.

In addition, Kim, et al. (2009) reported that the effectiveness of FRP anchors can be significantly improved if the anchor is positioned closer to the ends of the FRP sheet.

Figure 2-30: FRP anchor pry-out with local concrete failure

Figure 2-31: FRP anchor pull-out failure (Zhang, et al., 2011)

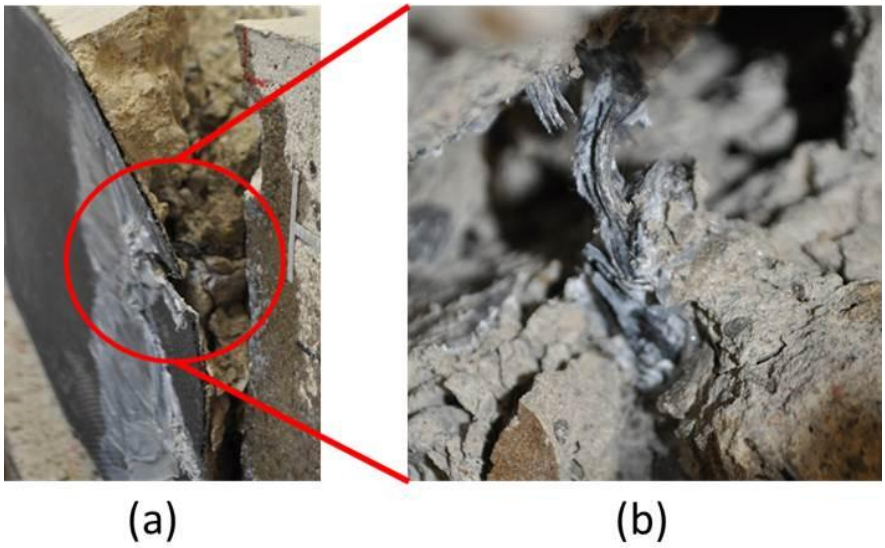

Figure 2-32: FRP anchor rupture

2.6.4 Design of FRP Anchors

The bond stress along the surface of the anchor hole decreases the deeper an anchor is embedded into the member. The bond stress distribution along the depth of the anchor hole is not uniform. In practice, an anchor must have a minimum embedment depth into the concrete member to enable the full capacity of the FRP anchor to be achieved (Ozdemir, 2005; Ozbakkaloglu & Saatcioglu, 2009; Orton, et al., 2008).

The embedment depth required for the full development of an FRP anchor was studied by Ozdemir, (2005). He reported that the anchor must be embedded into the core of a concrete specimen to effectively transfer the stresses from the anchor to the concrete and the surrounding reinforcing steel. There is an effective embedment depth beyond which the capacity of the anchor will not increase. This depth was found to be 100 mm for 14-20 mm diameter anchors in 10-20 MPa concrete.

Another concern in the design of FRP anchors is the interaction of the FRP anchor with the edge of the anchor hole, anchor size and bend radius. Previous research has shown that there is a direct relationship between a roughed concrete anchor hole edge and the stress concentration induced on an anchor. A rough concrete edge causes stress concentrations in the FRP anchor causing it to fail prematurely by rupture at the bend.

Orton, et al. (2008) recommended that the radius of the bend of the anchor hole be at least four times greater than the anchor diameter. Therefore, a 12.7 mm diameter CFRP anchor would require an anchor hole to be a radius of 50.8 mm. It is clear that this requirement is unrealistic with small anchor hole sizes. A different approach developed by the Japanese Society of Civil Engineers (JSCE) predicts the reduction in FRP strength due to the bend radius at the opening of the anchor hole (Equation 2-5).

$$\frac{f_a}{f_u} = 0.09\frac{\mathrm{r}}{\mathrm{d}} + 0.3 \qquad \textbf{Equation 2-5}$$

where f_a=the reduced capacity of the material, f_u=the ultimate capacity of the material, r=radius of the bend, d=anchor diameter

For a 12.7 mm diameter anchor with an elongation at beak of 0.74%, based on Equation 2-5 the reduction in strength in the FRP anchor will be 39% of the ultimate capacity of the FRP anchor (Orton, et al., 2008).

Knowing the size and strength of each anchor is essential in determining the number of anchors required to provide sufficient anchorage for the FRP sheet. In a study by Kobayaski, et al. (2001) it was reported that the capacity of a FRP anchor increases as the ratio of the amount of material in the anchor to the amount of material in the main FRP sheet increases. It was recommended that the amount of material contained within the anchor be at least more than the amount of material contained in the main FRP sheet (Kobayashi, et al., 2001). This is consistent with the recommendations of Kim, et al. (2009) and Orton, (2007) which suggest that the amount of material in an anchor should be 1.5 to 2 times the amount of material contained in the main FRP sheet that is being anchored.

When determining the length of an anchor, two things must be considered; the embedment depth of the anchor and the length of the bonded portion (anchor fan). As was discussed above the minimum embedment depth of an anchor is 100 mm. The length of the anchor fan is dependent on the bond strength developed between the fan and the main FRP sheet. It is recommended that the anchor fan should be long enough to completely cover the width of the main FRP sheet and the angle of the fan is less than 90 degrees (Kobayashi, et al., 2001; Orton, et al., 2008).

2.6.5 Construction of FRP Anchors

The first type of FRP anchors were made by hand. These anchors were relatively easy to construct. First a strip was cut from a roll of FRP sheet. Next the strip was saturated with epoxy and inserted into a predrilled hole in the concrete member. Saturating the anchor with epoxy ensures that the anchor and sheet form a monolithic composite. The last step required the ends of the anchor to be fanned out over the FRP sheet (Orton, et al., 2008).

Zhang, et al. (2005) outlined the steps to construct two types of handmade bow-tie FRP anchors (dry and impregnated). Construction of the dry bow-tie anchor begins with rolling the pre-cut FRP sheet by hand keeping the fibers reasonably compressed together (Figure 2-34a). Next a 25 mm portion of the dowel end is tied with wire (Figure 2-34b). Once this is complete the anchors can be inserted into the predrilled holes, and the ends of the anchors can be fanned out over the FRP sheet.

The process for making impregnated bow-tie anchors is the same as that for the dry anchor with the exception that the dowel end is not tied with wire, but covered with epoxy (Figure 2-35a) and placed into a mould (Figure 2-35b) to form an epoxy coated dowel end (Figure 2-35c).

Making FRP anchors by hand can be an extremely labor intensive task. Workmanship in the construction of FRP anchors is essential with poor workmanship reducing the capacity of a FRP anchor by 50% (Ozbakkaloglu & Saatcioglu, 2009).

Commercially manufactured carbon and glass FRP anchors are produced by Sika Canada Inc. and Fyfe Co. LLC. Different diameters are available with 10 mm diameter anchors the most common. These anchors are supplied as a 10 meter coiled rope with a protective gauze sock on the exterior shell to keep the fibers together. Figure 2-33 shows a photo of commercially manufactured CFRP and GFRP anchors.

Figure 2-33: Commercially manufactured CFRP and GFRP anchors

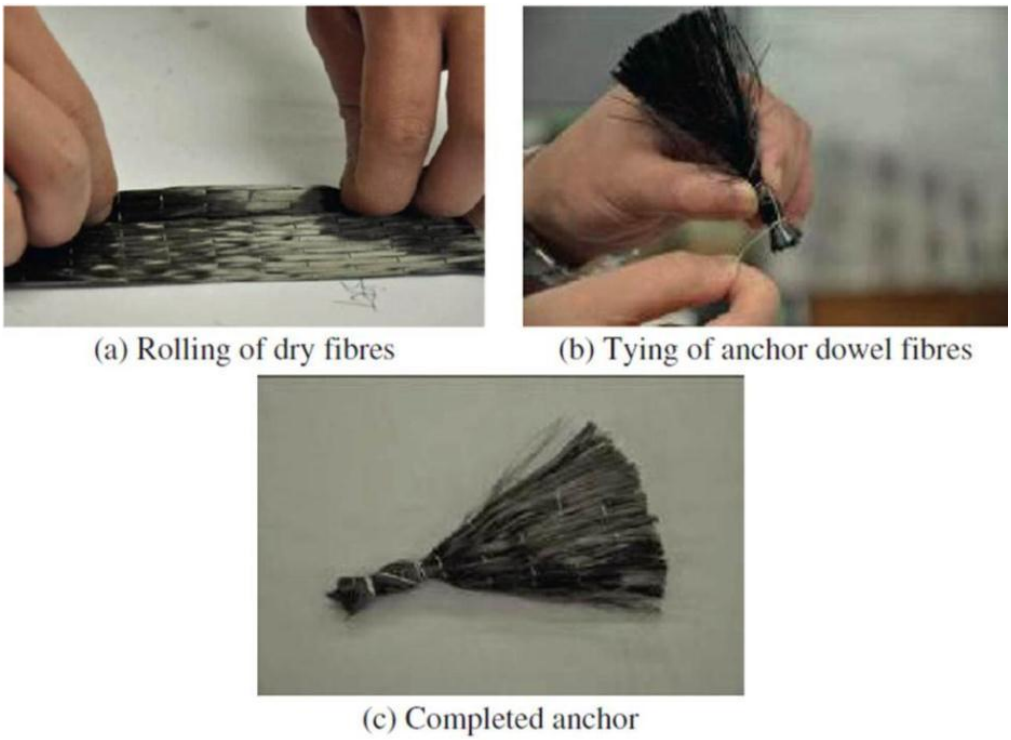

Figure 2-34: Dry anchor construction (Zhang, et al., 2011)

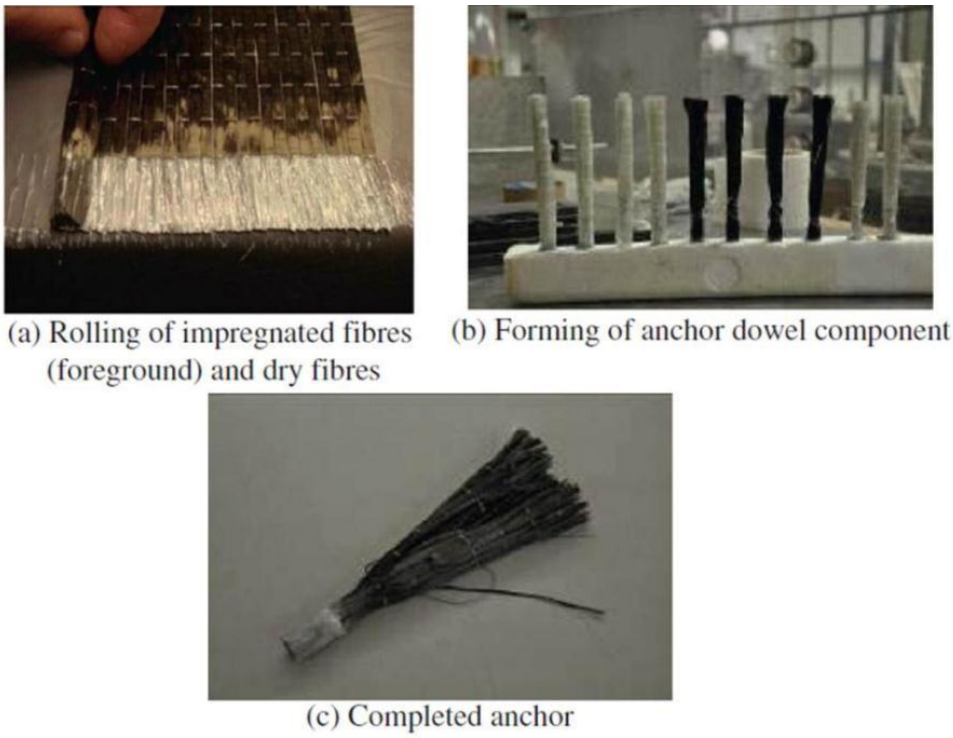

Figure 2-35: Wet anchor construction (Zhang, et al., 2011)

2.7 Gaps in Current Knowledge

Many studies in the literature have reported the results and benefits of FRP strengthening beams and slabs to increase their flexural and shear capacity. The problem of FRP debonding was addressed through the use of mechanical and other types of anchoring devices which were not very effective. The use of FRP anchors to secure FRP sheets was studied by several researchers (Zhang, et al., 2011; Teng, et al., 2003; Orton, et al., 2008; Orton, 2007; Quinn, 2009). Gaps in the current research include:

1. Limited design data are available for commercially manufactured FRP anchors and thus more testing is required to set codes and guidelines (Orton, et al., 2008).
2. Research on the strength and behaviour of FRP anchors is limited and currently there are no design procedures for FRP anchors (Quinn, 2009; Teng, et al., 2003).
3. Development of analytical and numerical models for use by engineers to design FRP anchors is still needed (Zhang, et al., 2011).

To the author's knowledge, there is no previous study on the behaviour of commercially manufactured FRP anchors to secure u-wrapped FRP shear strengthened rectangular RC beams or FRP flexural strengthened RC slabs. This study aims to fill this gap in the literature.

2.8 Literature Review Summary

The mechanics of RC shear and flexural failures were presented in this chapter. The methods to strengthen RC beams or slabs were discussed and the FRP materials used in repair & strengthening were introduced. A review of the previous work on FRP flexural and shear strengthening of RC structures was given. An overview of previous anchors and their failure modes, design and construction of FRP anchors was presented.

Chapter 3 – Experimental Program

3.1 Introduction

The experimental program was designed to investigate the feasibility of using commercially manufactured FRP anchors to secure FRP sheets installed to strengthen RC beams in shear or slabs in flexure. Details of the test specimen design, instrumentation, test setup and test procedure are presented in the following sections.

3.2 Test Program

A total of thirty one RC specimens were tested: twenty one shear deficient beams and eight flexural deficient slabs. The experimental program was divided into three series: an initial pilot study consisting of nine shear deficient RC beams, series I consisting of an additional twelve shear deficient RC beams and series II consisting of eight flexural deficient RC slabs. The complete test matrix for the beams is given in Table 3-1 and slabs in Table 3-2. The beam and slab designation used in the test matrix is as follows: XX-YY-ZZ with XX=Type of FRP material, YY=FRP strip width or number of layers of FRP and ZZ=Presence of anchors. For the pre-cracked or partial depth shear critical beams an additional term (PC or PD) is added in front of the specimen designation.

The test variables included the type of FRP sheets (CFRP, GFRP, FRCM), the presence and type of anchor (CFRP or GFRP), number of FRP layers, and u-wrapping schemes (full depth vs. partial depth). A more detailed description of the specimens in each series is discussed in the following subsections.

Table 3-1: Shear & Flexural Strengthening Test Matrix

Nomenclature	Specimen Description	No Anchors	With Anchors	Full wrap
Pilot Study				
Control	Control	1		
230C-200-NA 230C-200-A	230C-200 mm-No anchors 230C-200 mm-Anchors	1	 1	
350G-200-NA 350G-200-A	350G-200 mm- No anchors 350G-200mm-Anchors	1	 1	
430G-100-NA	430G-100 mm-No anchors	1		
PD-430G-100-NA PD-430G-100-CA PD-430G-100-GA	PD-430G-100mm-No anchors PD-430G-100mm-C Anchors PD-430G-100 mm-G Anchors	1	 1 1	
Series I				
Control	Control	1		
430G-200-NA 430G-200-A	430G-200 mm-No anchors 430G-200 mm-Anchors	1	 1	
100G-200-NA 100G-200-A	100G-200 mm-No anchors 100G-200 mm-Anchors	1	 1	
430G-300-NA 430G-300-A	430G-300 mm-No anchors 430G-300 mm-Anchors	1	 1	
PC-430G-800-NA PC-430G-800-A PC-430G-800-FW	PC-430G-800 mm-No anchors PC-430G-800 mm-Anchors PC-430G-800 mm-Full wrap	1	 1	 1
PC-100G-1100-NA PC-100G-1100-A	PC-100G-1100 mm-No anchors PC-100G-1100 mm-Anchors	1	 1	

Table 3-2: Flexural Strengthening Test Matrix

Series II				
Nomenclature	**Specimen Description**	**No Anchors**	**8 Anchors**	**12 Anchors**
Control	Control	1		
230C-1L-NA	230C-1 layer-No anchors	1		
230C-2L-NA 230C-2L-8A	230C-2 layers-No anchors 230C-2 layers-8 Anchors	1	 1	
600C-1L-NA	600C-1 layer-No anchors	1		
600C-2L-NA 600C-2L-8A 600C-2L-12A	600C-2 layers-No anchors 600C-2 layers-8 anchors 600C-2 layers-12 anchors	1	 1	 1

3.3 Conceptual Design

A preliminary study was conducted to determine the influence of different variables and their effects on flexural and shear strength of RC members. This information was critical in establishing the most optimal beam and slab designs. The results of this pilot study are detailed in Appendix A.

All beams and slabs were designed according to the Canadian design code - design of concrete structures (CSA A23.3-04) and FRP rehabilitation of RC structures design manual (ISIS-M04-09). In the pilot study and series I, the beams were designed so that the flexural capacity exceeded the shear capacity of the FRP strengthened beams. This enabled shear failure to govern which allowed for the determination of the capacity of a FRP sheet anchored with FRP anchors.

In series II, the slabs were designed so that the shear capacity exceeded the flexural capacity of the FRP strengthened slab. This would force a flexural mode of failure and further result in obtaining the capacity of a slab strengthened with FRP sheets secured with FRP anchors. The slabs (series II) had very closely spaced stirrups with minimal flexural reinforcement. Transverse reinforcement (stirrups) contributes significantly to the shear strength of an RC member. It is known that as the number of stirrups in a member increases; the shear capacity of the member will increase. These beams were designed using the maximum allowable stirrup spacing (0.7dv=180 mm o/c) based on CSA A23.3-04.

The beams were designed with a shear span-to-depth ratio over 2.5. A shear span-to-depth ratio over 2.5 gives a slender beam and will promote shear failures through the formation of a diagonal tension shear crack. These cracks generally form at a 45^{o} angle and extend from the support to the loading point. Beams with a shear span-to-depth ratio of less than 2.5 are deep beams and will encounter shear failure due to crushing of the concrete. This failure occurs in the concrete strut which forms between the support and the loading point.

For all test series, the specimens were designed with a low concrete strength of 30 and 40 MPa. A low concrete strength will result in a smaller concrete shear strength contribution because the tensile strength of the concrete is related to its compressive strength. The tensile strength of concrete is determined using Equation 3-1.

$$f_r = 0.6\lambda\sqrt{f'_c}$$ **Equation 3-1**

where

f_r= modulus of rupture of concrete
λ= density of concrete factor
f'_c= compressive strength of concrete

Externally bonded FRP sheets were used to provide shear strengthening of the RC beams and flexural strengthening for the RC slabs according to ISIS-M04-09. In the pilot study and series I, the beams were strengthened with FRP sheets applied in the transverse direction while in series II, the slabs were strengthened with FRP sheets applied in the longitudinal direction.

It should be noted that the ISIS-M04-09 design manual assumes that the FRP sheets are not anchored and thus have a high probability of debonding prior to reaching their rupture strain value. To account for potential premature debonding, strain limits are provided. In designing the beams and slab which contained anchors, the debonding limits set by ISIS-M04-09 were not considered and an assumption was made that the full tensile capacity of the FRP could be achieved i.e. the sheet would rupture at failure.

The theoretical shear capacity of each beam was determined based on the approach presented in section 2.4.3 by summing the individual contributions from the concrete, steel and FRP. The theoretical flexural capacity was determined by force equilibrium and strain compatibility accounting for the concrete, steel and FRP contributions (refer to section 2.5.3).

3.4 Test Specimens

3.4.1 Pilot Study

The beams measured 150 mm wide by 350 mm deep by 2440 mm long. The top compression reinforcement consisted of two 2-15M bars. The shear reinforcement consisted of stirrups made using 6 mm smooth bars spaced every 180 mm on center with standard 90^0 hooks. The bottom concrete cover was 40 mm while the top and side covers were 30 mm. The shear span to depth ratio of the beams in this series was 3.11 with tension and compression reinforcement ratios of 3.5% and 1%, respectively. A schematic of the specimen geometry and reinforcement detail are shown in Figure 3-1.

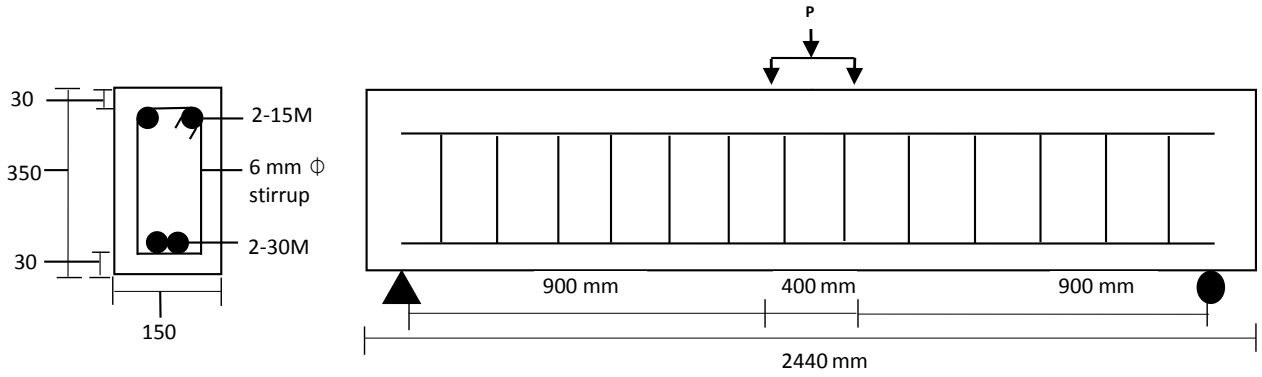

Figure 3-1: Pilot study beam geometry and steel reinforcement details (units in mm)

The concrete used to construct the beams was supplied with ready-mixed Portland cement with a maximum coarse aggregate size of 19 mm. The average compressive strength of the concrete after 28-days was 50.7 ± 1 MPa and the average strength at the day of testing was 50.1 ± 1 MPa.

The longitudinal reinforcements consisted of Grade 400 reinforcing steel bars with yield strength of 475 MPa and the stirrups having a yield strength of 384 MPa as reported by the manufacturer.

The FRP system consisted of FRP sheets or FRCM grid and FRP anchors. Three different FRP strengthening materials (CFRP, GFRP and FRCM) and two types of FRP anchors (CFRP and GFRP) provided by Sika® Canada were applied to strengthen the beams in shear.

The FRP system was installed as intermittent u-wraps around the cross-section along the beam length with orientation of fibers in the transverse direction. The wraps were 100 mm or 200 mm wide, spaced at 200 mm or 275 mm center to center and extended the full-depth or partial depth (50 mm below the top surface) of the cross-section. FRP anchors were used in half of the strengthened beams with one FRP anchor on each u-wrap for a total of eight anchors per beam. Figure 3-2 and Figure 3-3 illustrate the FRP and FRCM grid strengthening schemes.

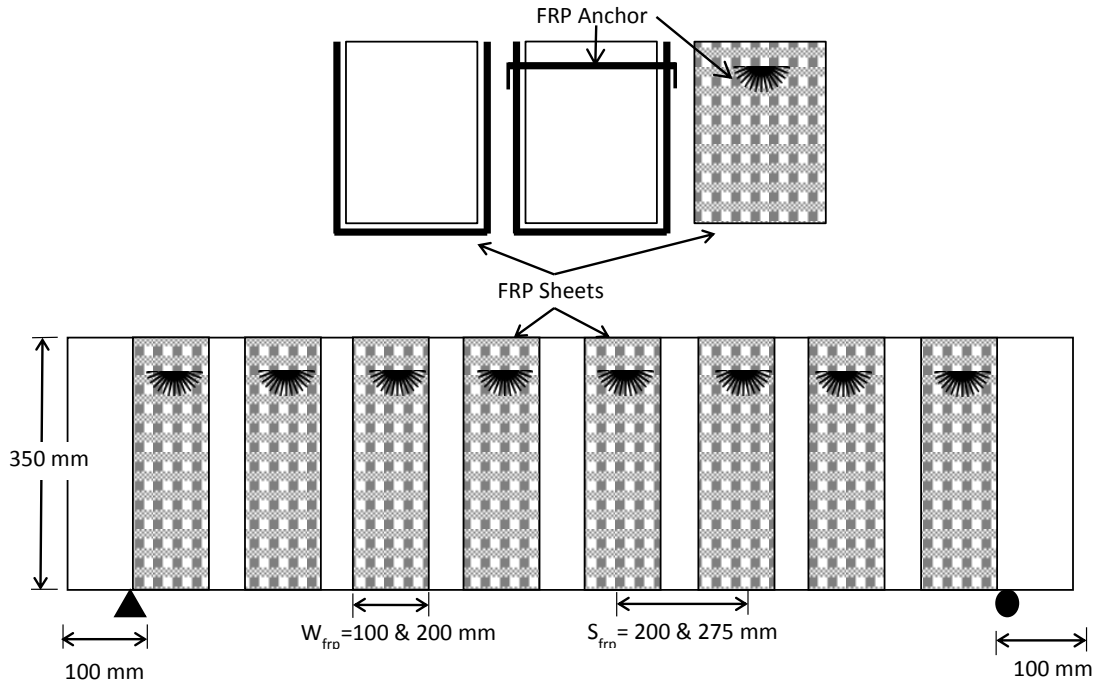

Figure 3-2: Beam with full-depth FRP u-wraps

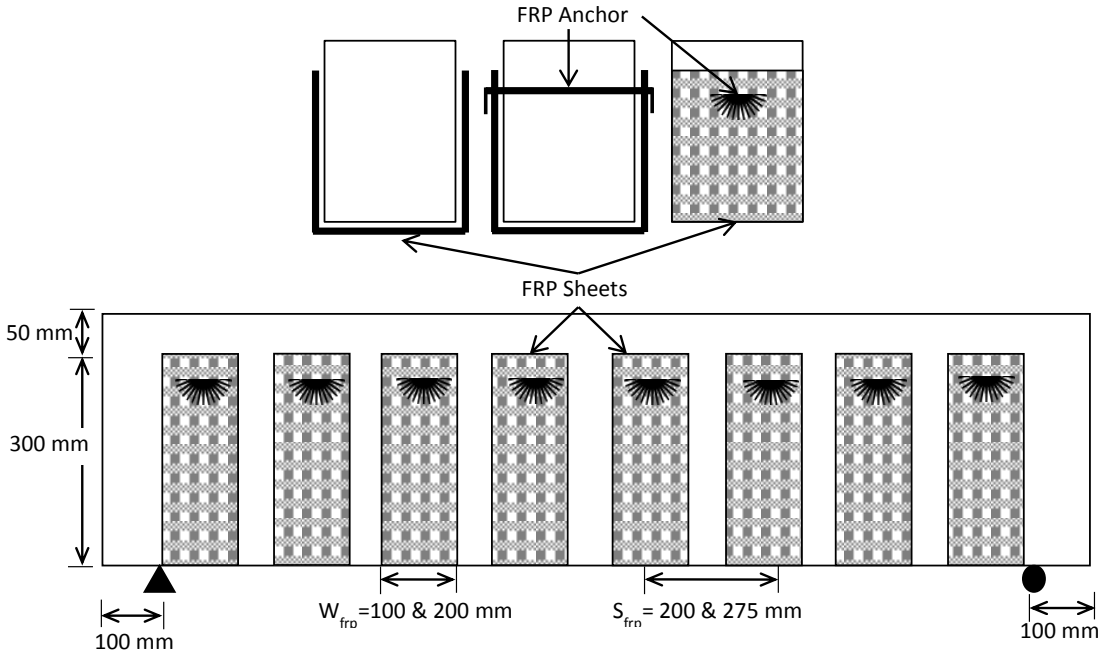

Figure 3-3: Beam with partial depth FRP u-wraps

3.4.2 Series I

The beams in series I were 150 mm wide x 350 mm deep by 2440 mm long. The flexural steel reinforcement was different in this series based on the results from the pilot study beams. The flexural capacity of these beams was increased to avoid flexural failure with certain FRP shear strengthening designs. The flexural reinforcement steel consisted of 4-25M bars with two 25M bars bundled on each side. The top compression reinforcement consisted of two 2-25M bars for symmetry. The shear reinforcement consisted of stirrups made using 6 mm smooth bars spaced every 180 mm on center with standard 90^o hooks. The bottom concrete cover was 40 mm while the top and side covers were 30 mm. The shear span to depth ratio of the beams in this series was 3.0 with a tension and compression reinforcement ratio of 5.1% and 2.5%, respectively. A schematic of the specimen geometry and reinforcement detail are shown in Figure 3-4.

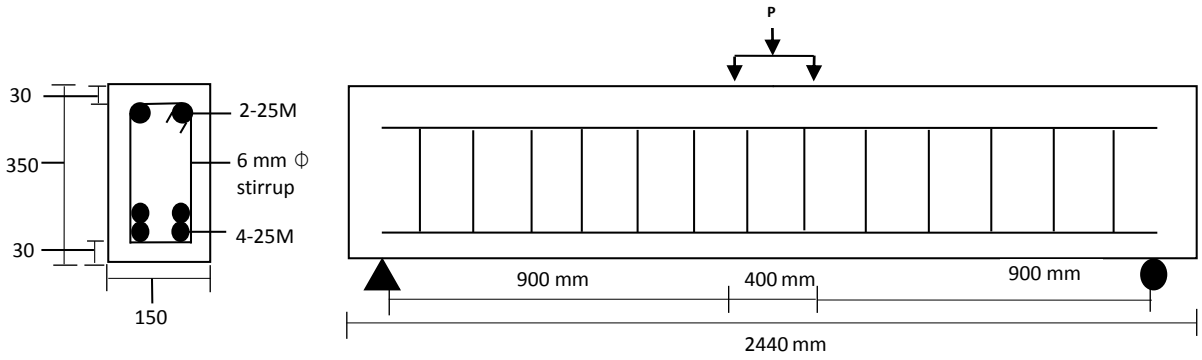

Figure 3-4: Series I beam geometry and steel reinforcement details (units in mm)

The concrete used to construct the beams was supplied with ready-mixed Portland cement with a maximum coarse aggregate size of 19 mm. The average compressive strength of the concrete obtained after 28-days was 27.5 ± 1 MPa and the average strength at the day of testing was 32.0 ± 1 MPa. The longitudinal reinforcements consisted of Grade 400 reinforcing steel bars with yield strength of 427 MPa and the stirrups had a yield strength of 384 MPa as reported by the manufacturer.

The FRP system consisted of GFRP sheets and anchors. Two different GFRP strengthening materials and one type of GFRP anchors provided by Sika® Canada were applied to strengthen the beams in shear.

The FRP system was installed as intermittent u-wraps or continuous u-wraps around the cross-section. FRP anchors were used in half of the strengthened beams with one or multiple FRP anchors on each u-wrap. The intermittent and continuous FRP sheets were applied along the beam with the orientation of fibers in the transverse direction. The intermittent u-wraps were 200 mm wide at 275 mm o/c as shown in Figure 3-5 or 300 mm wide at 375 mm o/c in the shear span and one 200 mm wide u-wrap at mid-span as shown in Figure 3-6. The continuous u-wraps were 800 mm or 1100 mm wide within the shear span as shown in Figure 3-7 and Figure 3-8, respectively. The full wrap sheets were 1100 mm wide within the shear span as shown in Figure 3-9. The u-wraps extended the full depth of the cross-section and the full wraps completely wrapped the section with an overlap on the top of the beam. The number of anchors per FRP sheet was determined using the Baggio FRP anchor design procedure presented in chapter 7.

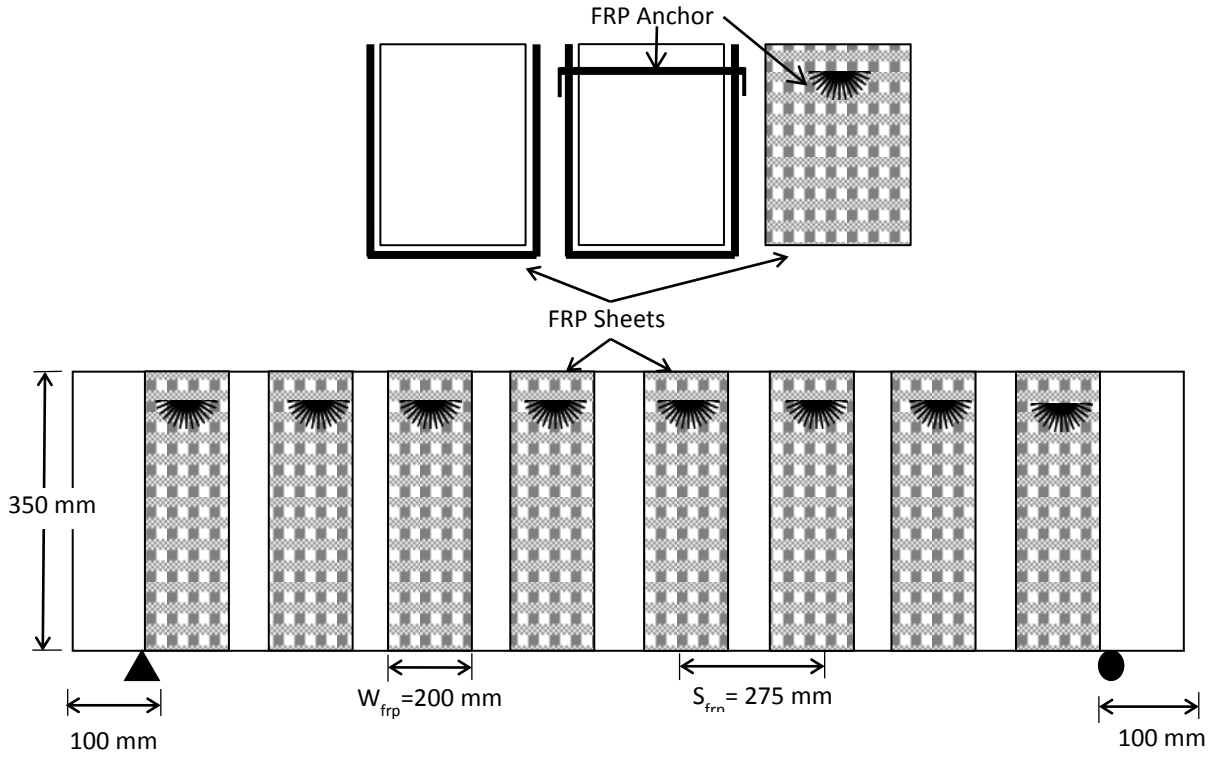

Figure 3-5: Beams with 200 mm full depth FRP u-wraps

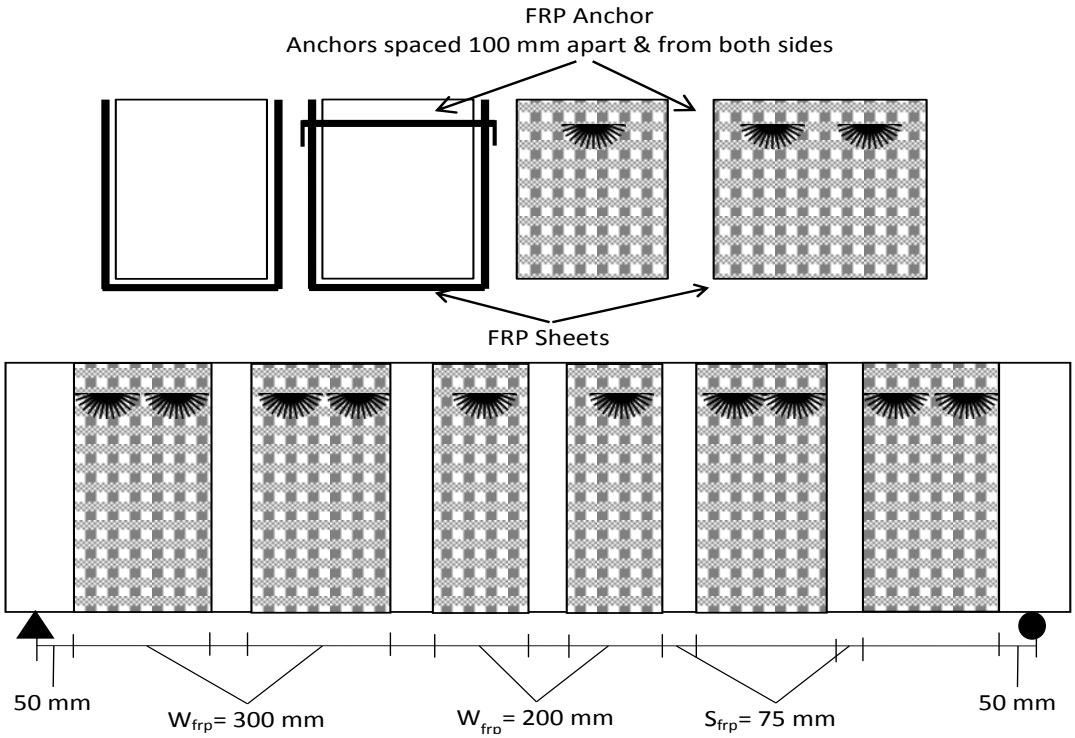

Figure 3-6: Beams with 300 mm full depth FRP u-wraps

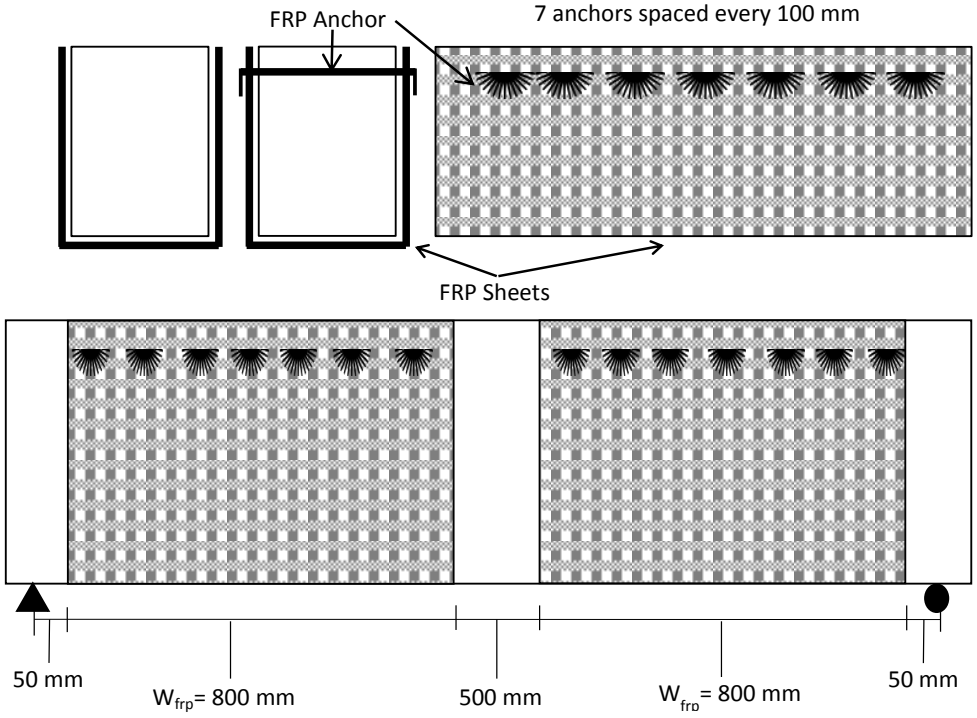

Figure 3-7: Beams with 800 mm full depth FRP u-wraps

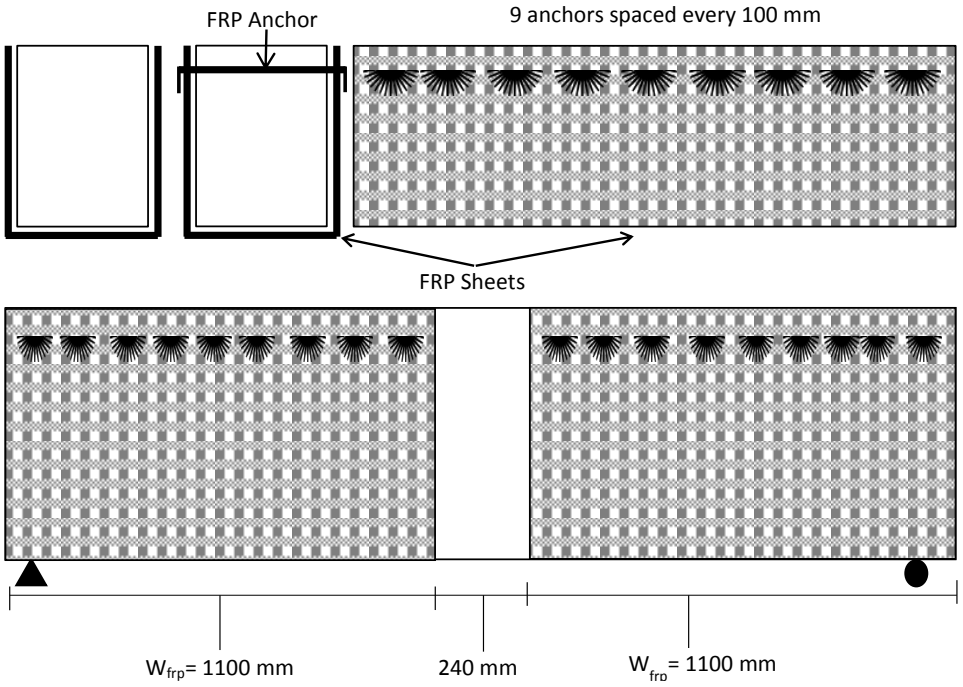

Figure 3-8: Beam with 1100 mm full depth FRP u-wraps

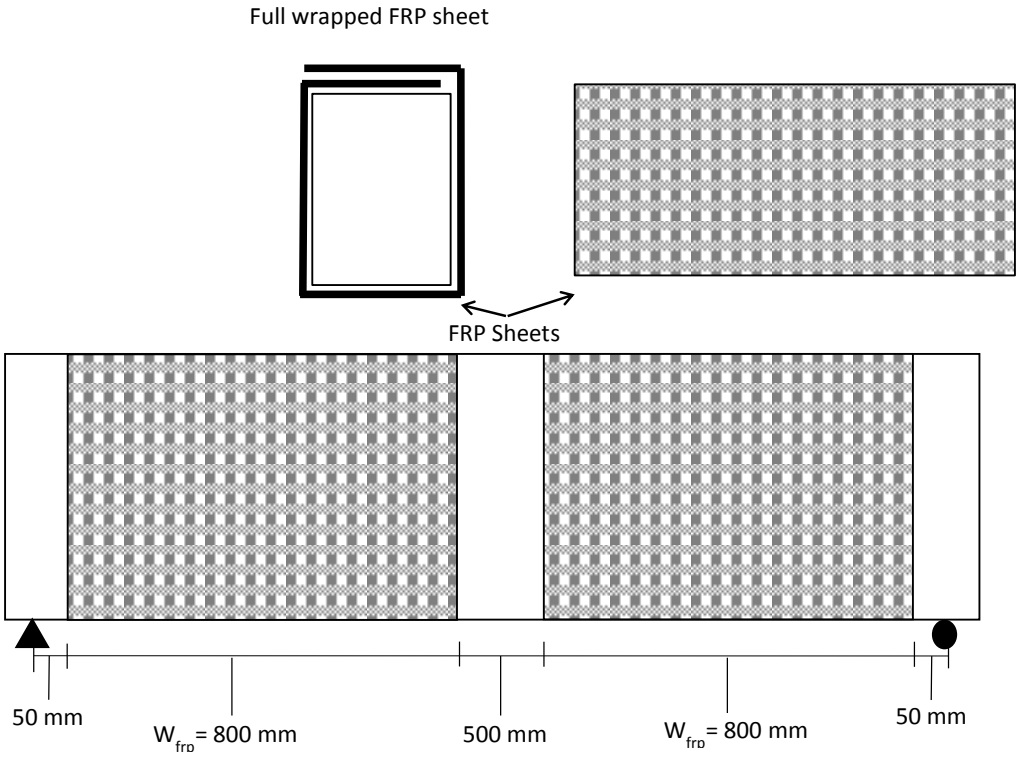

Figure 3-9: Beam with fully wrapped FRP sheets

3.4.3 Series II

The slabs measured 350 mm wide by 200 mm deep by 2200 mm long. The flexural steel reinforcement consisted of 3-15M bars. The top compression reinforcement consisted of two 2-10M bars. The shear reinforcement consisted of stirrups made using 10M bars spaced every 100 mm on center with standard 90^{o} hooks. The concrete cover was 20 mm around the entire slab. The shear span to depth ratio of the slabs in this series was 4.61 with a tension and compression reinforcement ratio of 1% and 0.35%, respectively. A schematic of the specimen geometry and reinforcement detail are shown in Figure 3-10.

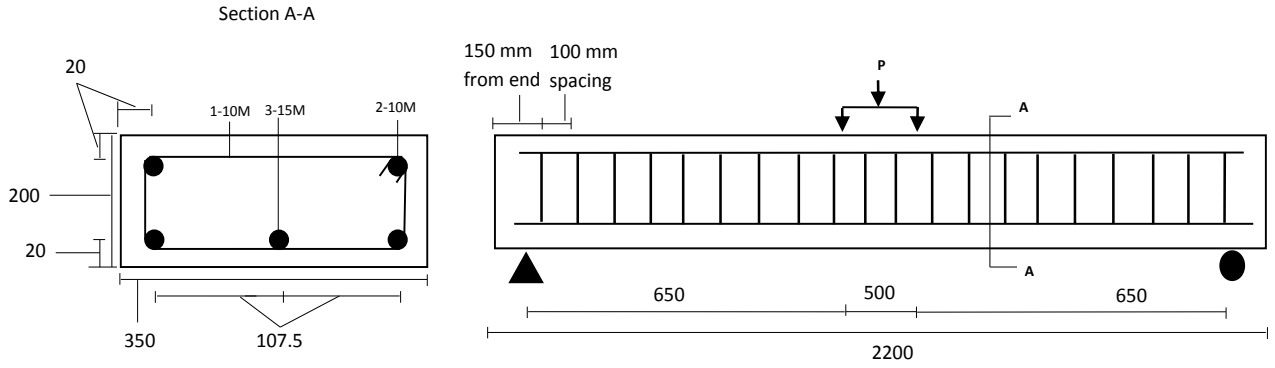

Figure 3-10: Series II slab geometry and steel reinforcement details (units in mm)

The concrete used to construct the slabs was supplied with ready-mixed Portland cement with a maximum coarse aggregate size of 19 mm. The average compressive strength of the concrete after 28-days was 34.1 ± 1 MPa and the average strength at the day of testing was 34.0 ± 1 MPa. The longitudinal reinforcements consisted of Grade 400 reinforcing steel bars. As reported by the manufacturer, the 15M flexural reinforcement had a yield strength of 487 MPa, the 10M compression reinforcement had a yield strength of 431 MPa, and the 10M stirrups had a yield strength of 462MPa.

The FRP system consisted of FRP sheets and FRP anchors used for flexural strengthening of the slabs. Two different CFRP strengthening materials (Sikawrap 230C and 600C) and CFRP anchors provided by Sika® Canada were used.

The FRP sheets were installed onto the slab tension soffit with the orientation of fibers in the longitudinal direction of the slab. All sheets were 300 mm wide and extended for 1700 mm along the length of the beam. FRP anchors were used in three out of seven strengthened slabs with two FRP anchors located under the loading points and at the ends of the bonded sheet. The anchors were placed at the ends of the boned sheet to eliminate debonding initiating from the FRP sheet ends and the anchors located under the loading point were placed to ensure the applied force does not cause the FRP sheet to debond directly under the loading point. Figure 3-11 illustrates the FRP strengthening scheme.

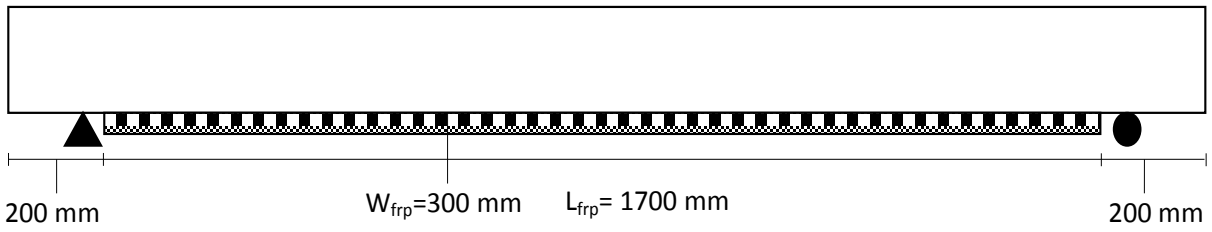

Figure 3-11: Slab with FRP flexural strengthening

3.4.4 Material Properties

3.4.4.1 Concrete

The concrete used to construct the beams and slabs was supplied by Hogg ready-mix concrete. One concrete truck was ordered for the pilot study and each series (Figure 3-12). It is common practice when ordering ready mix concrete to receive the concrete with a 28-day compressive strength higher than what is specified. However, for this research project, any additional compressive strength could possibly prohibit shear failure from occurring. To address this issue, a lower 28-day compressive strength was ordered. In the pilot study the 28-day compressive strength delivered was 50MPa which was much higher than the code specified strength of 40 MPa. In series I and II the specified strength was 30 MPa. The 28-day compressive strength delivered was 32 MPa for series I and 34 MPa for series II respectively.

During casting, concrete was placed into the form work (Figure 3-12a,b), vibrated to ensure all voids were filled within the reinforcing cage (Figure 3-12c) and finished and leveled with trowels (Figure 3-12d).

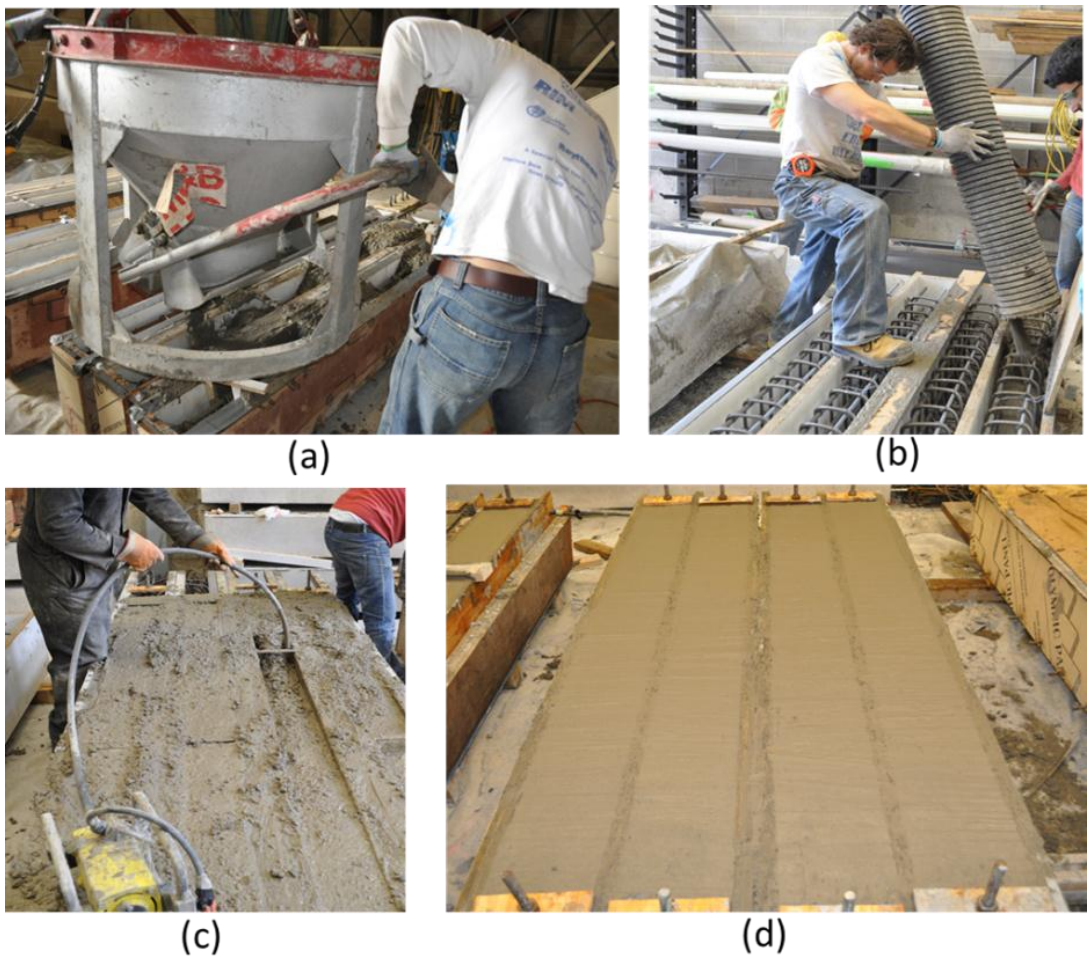

Figure 3-12: Pilot study casting

Multiple cylinders were batched from each cast to determine the 28-day compressive strength and the day of testing compressive strength. A total of ten cylinders were cast for the pilot study, fifteen cylinders for series I and twelve cylinders for series II. Figure 3-13 shows the molds during cylinder casting and the axial load test. Table 3-3 gives the average cylinder test results from each series.

Table 3-3: Concrete cylinder test results

Series	Design Strength (MPa)	28-day Strength (MPa)	Day of Testing Strength (MPa)
Pilot Study	40	50.7	50.1
I	30	27.5	32.0
II	30	34.1	34.0

Figure 3-13: Concrete cylinder testing

3.4.4.2 Reinforcing Steel

In all three series, grade 400 reinforcing steel bars were used as longitudinal reinforcement. Stirrups for the pilot study and series I were 6 mm smooth bars made from grade 350 steel and stirrups for series II were 10M reinforcing bars made from grade 400 steel. Table 3-4 presents the nominal yield strength of the reinforcing steel in the pilot study, series I and II.

Table 3-4: Steel reinforcement nominal yield strength

Series	Compression Longitudinal Steel (MPa)	Tension Longitudinal Steel (MPa)	Stirrups (MPa)
Pilot Study	475	475	384
I	427	427	384
II	487	431	462

3.4.4.3 Fiber Reinforced Polymers (FRP)

Various types of FRP sheets were used to strengthen the beams in shear and the slabs in flexure. CFRP, GFRP and GFRCM grid were externally applied on beams in the pilot study. Series I beams were strengthened with externally applied GFRP sheets and slabs in series II were strengthened with two types of CFRP sheets (different thicknesses). Table 3-5 gives the physical and mechanical properties of the different FRP systems used in the test program as reported by the manufacturer (Sika Canada Inc®).

Table 3-5: FRP sheet material properties

Series	Material	Thickness (mm)	Elastic Modulus (GPa)	Elongation at Rupture (%)
Pilot Study	CFRP – 230C	0.381	65	1.33
	GFRP – 430G	0.508	26	2.21
	GFRCM – 350G	1.170	75	2.80
I	GFRP – 430G	0.508	26	2.21
	GFRP – 100G	1.016	25	2.31
II	CFRP – 230C	0.381	65	1.33
	CFRP – 600C	1.333	24	1.55

Two types of FRP anchors were used and installed to secure the FRP sheets. The pilot study used CFRP and GFRP anchors, series I used only GFRP anchors and series II used only CFRP anchors. Table 3-6 gives the diameter, elastic modulus and elongation at rupture of the CFRP and GFRP anchors used in all three series.

Table 3-6: FRP Anchor material properties

Material	Diameter (mm)	Elastic Modulus (GPa)	Elongation at Rupture (%)
GFRP – Anchor G	10	70	3.99
CFRP – Anchor C	10	215	0.74

3.5 Fabrication of Specimens

The beams in the pilot study and series I were cast in formwork which consisted of wooden sides and a steel bases as shown in Figure 3-14a. Prior to casting, the formwork was lubricated with form oil for ease of stripping. The reinforcement cages were hung from the top of the formwork using metal wire (Figure 3-14b). This ensured proper cover was provided on the main longitudinal reinforcement and side stirrups. For each series, all specimens were cast from the same batch of concrete. Immediately after casting, the specimens were covered with wet burlap and plastic sheets to prevent any loss of moisture (Figure 3-15c). The plastic and burlap remained for seven days at which time the beams were stripped from the formwork and stored in the laboratory until they reached 28 day strength. For ease of transportation, two eye hooks were installed inside each beam so that it could be lifted by a crane. Figure 3-14c shows a photo of an eye hook that was installed and Figure 3-16 shows the beam being transported by the crane.

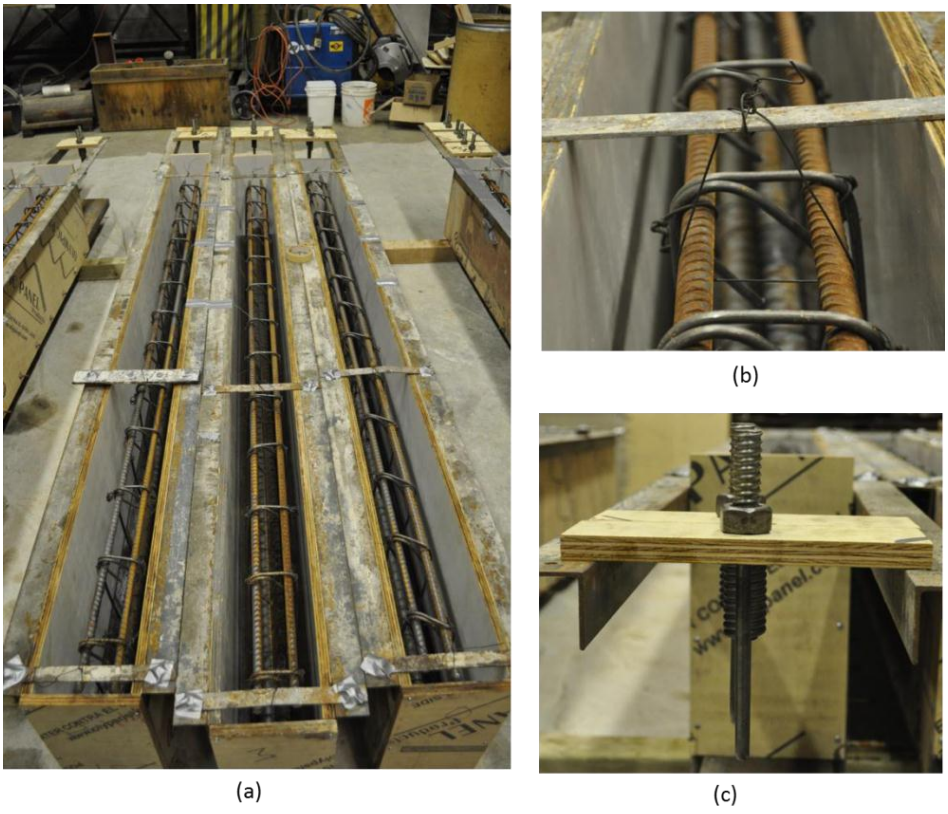

Figure 3-14: Caging and fabrication of the beam specimens

The slabs in series II were cast in wooden formwork as shown in Figure 3-15a. Again prior to casting, the formwork was lubricated with form oil for ease of stripping the slabs. The reinforcement cages were placed on top of plastic chairs which provided the proper cover (Figure 3-15b). All specimens were cast from the same batch of concrete and again immediately after casting, the specimens were covered with wet burlap and plastic sheets to prevent any loss of moisture. The plastic and burlap remained for seven days at which time the slabs were stripped from the formwork and stored in the laboratory until they reached their 28 day strength.

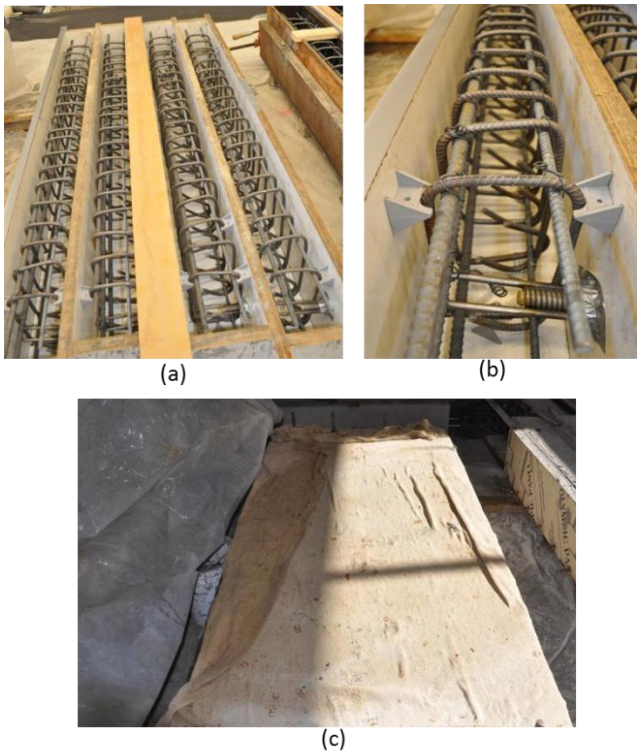

Figure 3-15: Caging and fabrication of slab specimens

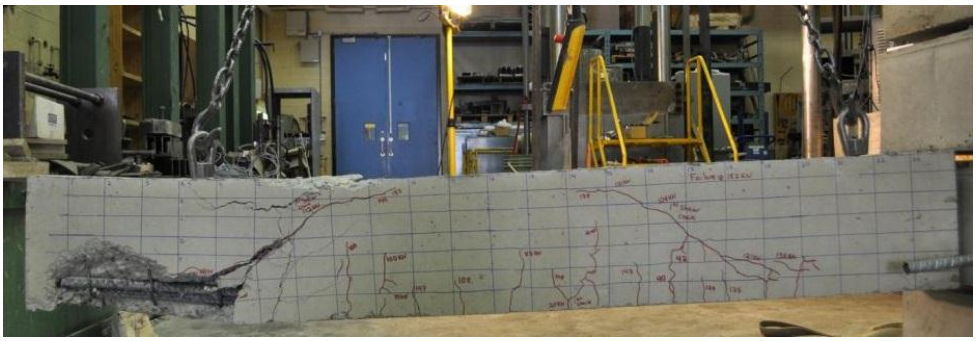

Figure 3-16: Lifting and transportation of a beam by overhead crane

For specimens with FRP anchors, the process of installing the anchors required holes to be drilled either partially or entirely through the width of the beam or depth of the slab. Prior to drilling, the location of the internal steel stirrups is required to avoid drilling a hole and striking the steel stirrup.

For this research study the location of the stirrups was determined prior to casting. The location of the stirrups was marked on the side of the form work after the cages were installed and hung (Figure 3-17a-d). The beams were cast and left to cure in the formwork. Prior to stripping the formwork and removing the beam, the locations of the stirrups were marked on the beam (Figure 3-17e,f). This method worked very well with all beams that required FRP anchor holes to be drilled to ensure that no anchor holes intercepted stirrups during the drilling process.

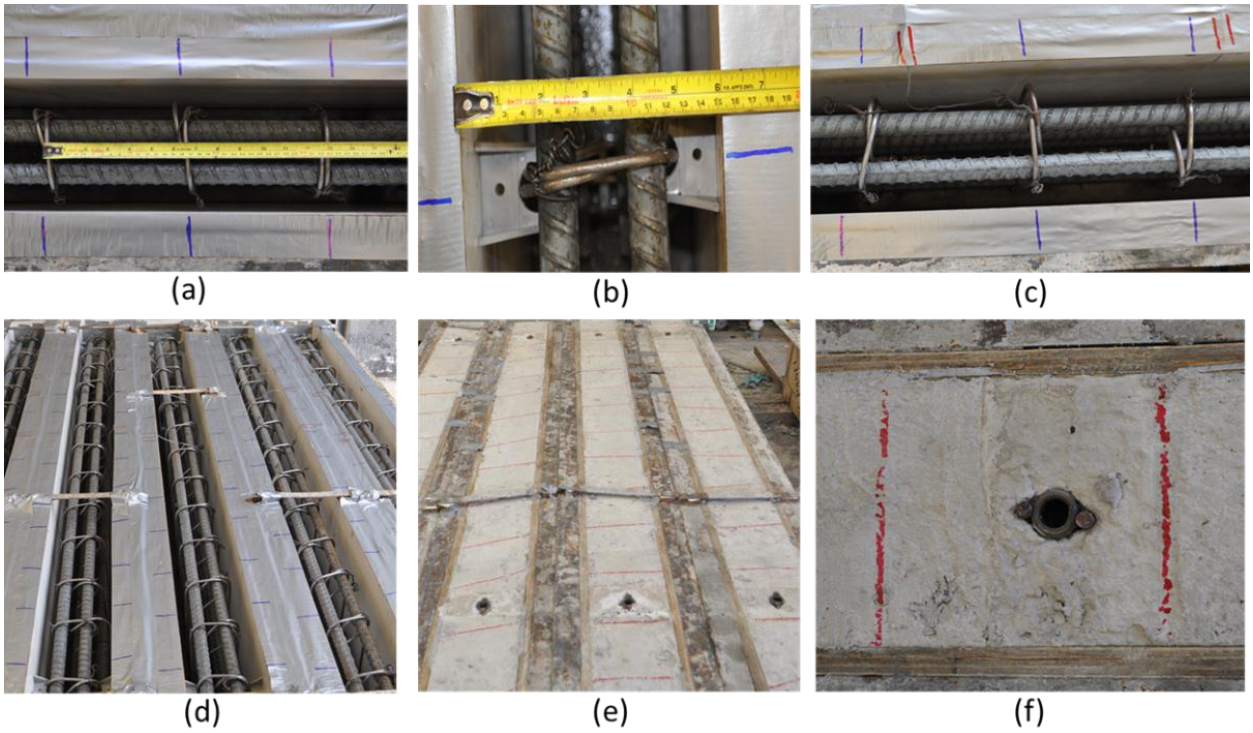

Figure 3-17: Internal stirrup locations

3.6 Strengthening of Specimens

3.6.1 FRP Sheet Installation

The FRP system was installed on the concrete specimens using a dry lay-up procedure as recommended by Sika® Canada. The beam and slab surface preparation and FRP installation procedure was as follows:

1) The bottom edges of the beam's cross-section were rounded to a radius of 12.7 mm (½"). This was essential to mitigate any stress concentrations on the FRP sheet (Figure 3-18a-c)
2) The concrete surface was sandblasted to roughen the surface and remove the smooth concrete paste for a better bonding surface (Figure 3-18d,e).
3) Hydrating the concrete, the beam surface was sprayed with water until damp (Figure 3-19d). This was required to ensure the concrete surface did not extract the moisture from the epoxy resin or cement mortar which would decrease the workability time.
4) Sikadur® 330 epoxy was prepared as per the manufacturers specifications. The two component epoxy was weighed and mixed by pouring component B into component A. The epoxy was mixed for three minutes with a low speed mixing drill until one monolithic color was observed (Figure 3-19a to c).
5) The specimens were flipped upside down with the top surface facing the ground. This allowed for easy installation of the u-wrap FRP sheets (Figure 3-20a,b).
6) The location and spacing of each FRP sheet was marked on the specimen to outline where to place the epoxy and FRP sheet (Figure 3-20a).
7) Sikadur® 330 epoxy was first applied to the concrete surface to a thickness of 0.7-1.2 kg/m^2 and for the FRCM grid, the mortar was applied to the concrete substrate as a 3 mm thick scrub coat (Figure 3-20b).
8) The FRP sheets were applied by hand onto the beam surface and pressed until the fabric was saturated and for the FRCM grid, after the grid was applied a second lift (layer) of the mortar was placed and finished covering the FRCM grid (Figure 3-20c).
9) The FRP sheets were rolled with a fluted roller (3/16" deep notch) to remove any air pockets, excess epoxy and irregularities as well as to squeeze the epoxy out of the rovings of the fabric (Figure 3-20d,e). Figure 3-18, Figure 3-19 and Figure 3-20 show step-by-step photos of the process of FRP strengthening for beams and slabs as outlined above.

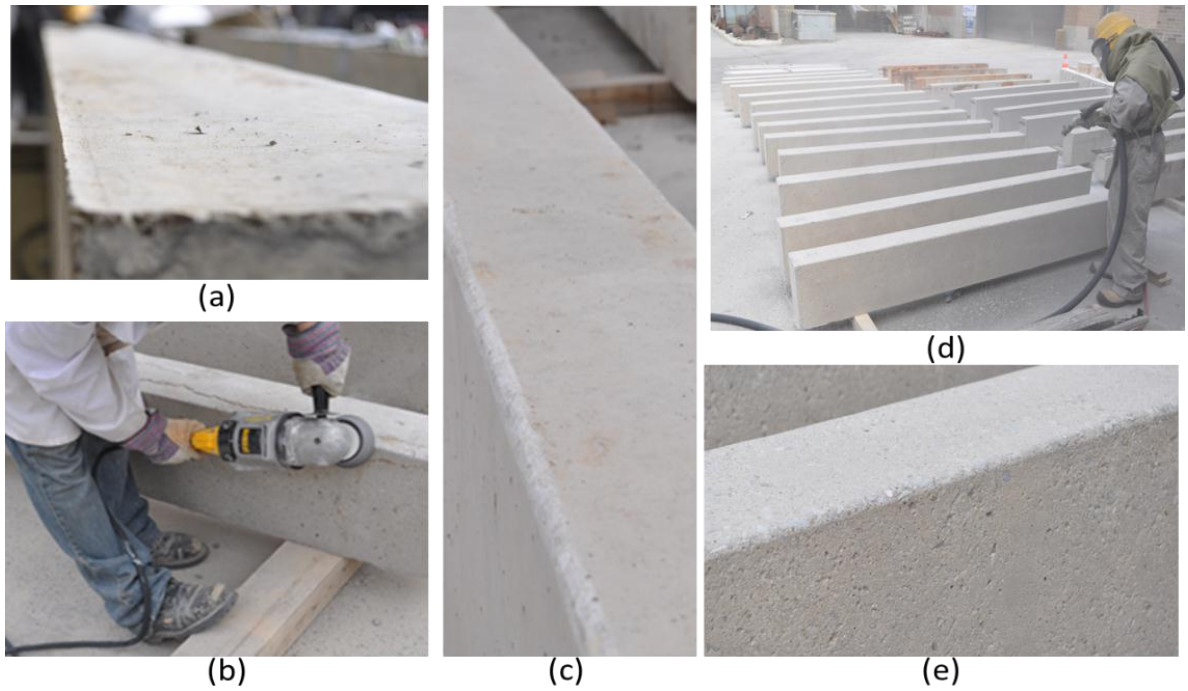

Figure 3-18: Specimen grinding and sandblasting preparation

Figure 3-19: Specimen preparation and mixing of epoxy

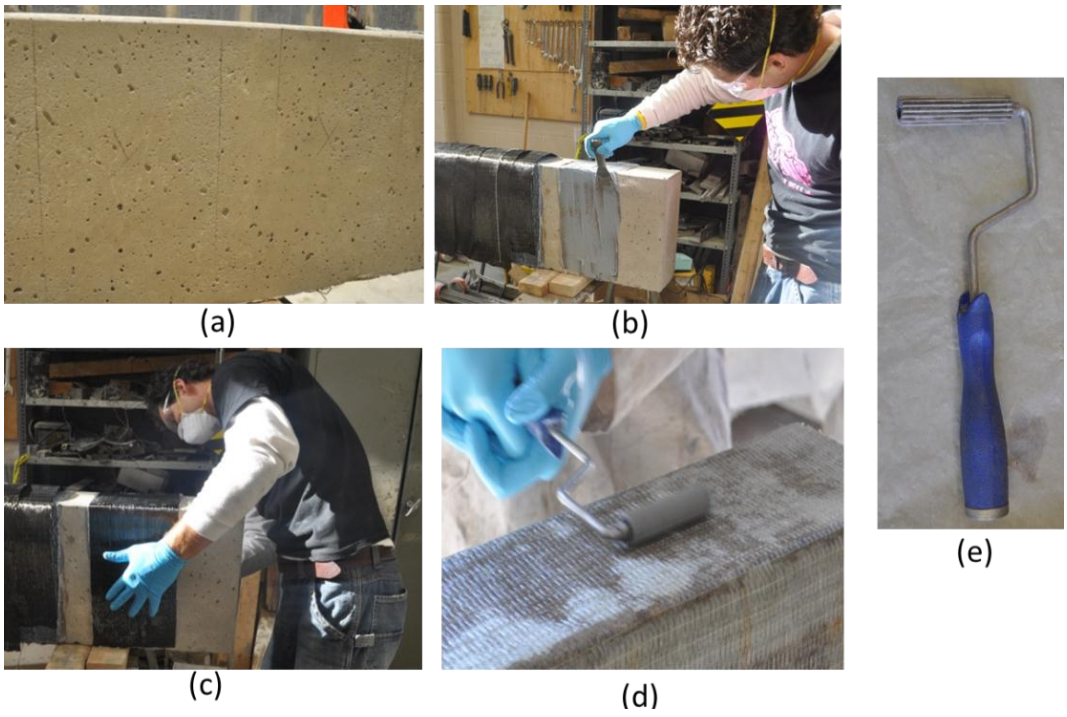

Figure 3-20: Epoxy and FRP application

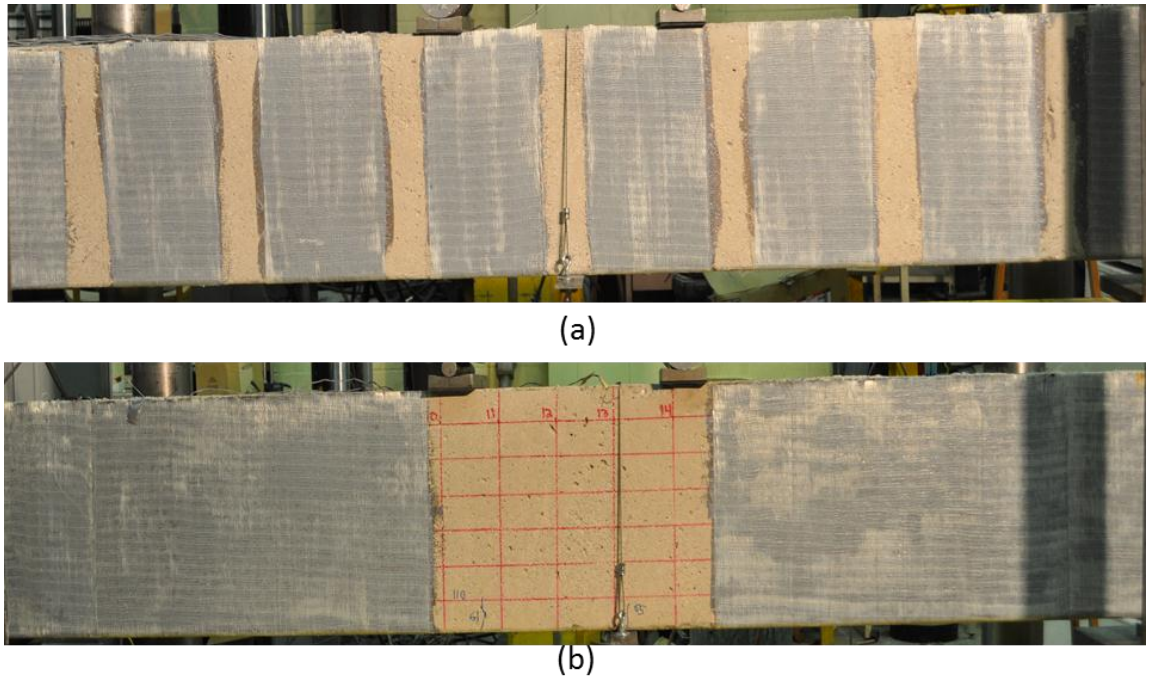

Figure 3-21: Intermittent vs. continuous FRP u-wrapped shear strengthened beam

3.6.2 FRP Anchor Installation

Specimens with FRP anchors required additional steps compared to those with only FRP sheet installation (section 3.6.1). Currently, there is no recommended procedure to install FRP anchors which extend through the entire width of a beam or partial depth of a slab. The FRP sheet and anchor system was installed using a combination of trial and error, expert advice and procedures recommended by Sika® Canada. The installation of anchors in the pilot study and series I were different from those in series II as outlined below.

Pilot Study and Series I – Anchor Installation

The FRP anchor installation procedure for beams with FRP shear strengthening was conducted as follows:

1) The anchor holes were located at mid-width in the FRP sheet. The vertical location of the holes varied: 55 mm from the top of the beam for the sheets that extended the full depth of the beam and 90 mm from the top of the beam for the beams with sheets that extended to partial depths.
2) The location of the anchor holes were predetermined to ensure no internal reinforcing steel was crossing the proposed hole locations.
3) The holes were drilled with a Hilti hammer drill with a 9/16” reinforced concrete drill bit (size of anchor holes were 40% larger than the FRP anchor diameter). The anchor holes were drilled from each side of the beam and connected in the middle of the section. This technique was employed to avoid pop-out and concrete surface breakoff around each hole. To increase the productivity of the drilling process, a special wood template was fashioned with the exact hole locations pre-drilled on each side of the beam (Figure 3-22).
4) Once the holes were drilled, the FRP sheets were installed as described in the previous section. Finishing nails were inserted through the weave of the FRP to mark the location of each pre-drilled hole.
5) After 24 hours, when the epoxy was tack dry, the finishing nails were removed and the holes were re-opened by drilling through the hardened FRP sheet.
6) When the hole was re-opened, dust and debris was removed by blowing out the hole from each end with compressed air.

7) The FRP anchors were cut to 300 mm lengths which included provision for 75 mm fans on each side of the beam. One end of the anchor was tied with a twist tie. This was done to cap the end and hold the mesh sock on the anchors to keep the fibers together (Figure 3-23a).
8) The fibers of the FRP anchor were impregnated with Sikadur® 330 epoxy (Figure 3-23b-d). The gauze sock was pulled down after impregnation to keep the anchor intact and the fibers in a linear direction.
9) Once all anchors were impregnated, the pre-drilled holes in the beam were filled with Sikadur® 330 epoxy (Figure 3-24a,b).
10) The anchors were then pushed through the hole with a metal rod inside the beam's cross-section (Figure 3-23d and Figure 3-24c,d).
11) Finally, FRP anchor ends were fanned out to a 30^{o} angle on both sides of the beam (Figure 3-24e,f).

Figure 3-22: Anchor hole drilling

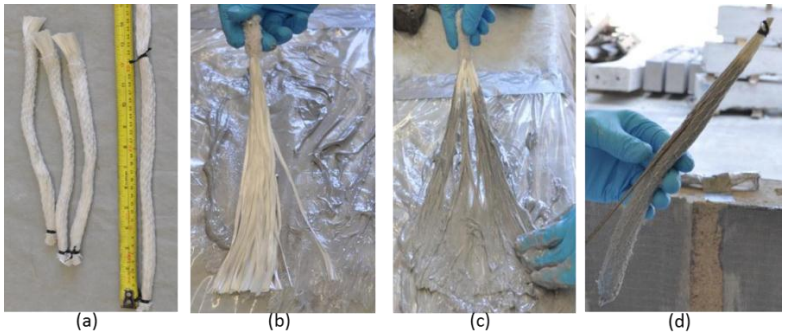

Figure 3-23: FRP anchor preparation

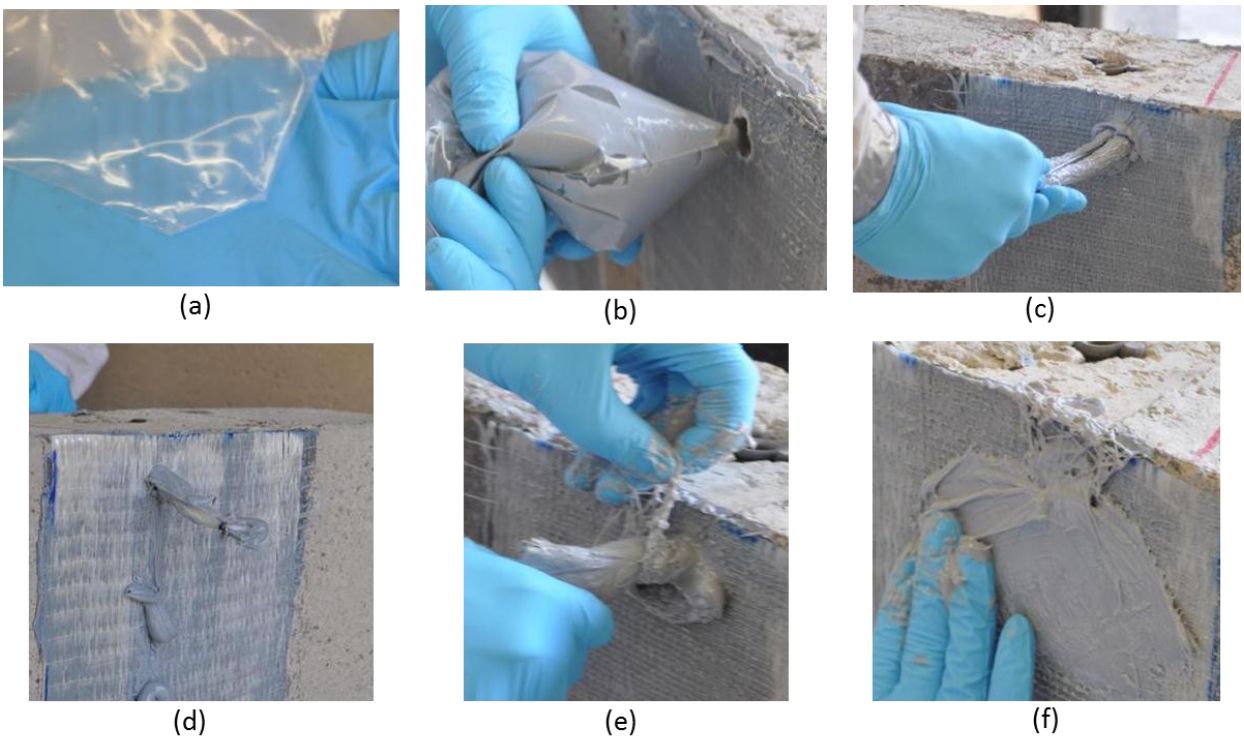

Figure 3-24: FRP anchor installation

Series II – Anchor Installation

The FRP anchor installation procedure for slabs with FRP flexural strengthening varied from that of the shear strengthened beams as described above. In this case, anchors were not drilled through the entire depth of the slab. The FRP anchor installation procedure for slabs is as follows:

1) The anchor holes were located under the loading points and at the ends of the FRP sheet. The x and y location of these holes were: x= 125 mm from each side of the beam, y= 280 mm and y= 850 mm from each end of the beam. These coordinates corresponded to anchors placed at 80 mm from the end of the FRP sheet and spaced every 100 mm along the sheet width.
2) The holes were drilled using a Hilti hammer drill with a 9/16” reinforced concrete drill bit to a depth of 100 mm and 150 mm into the slab (Figure 3-28a,b).
3) Once the holes were drilled the FRP sheets were installed as described in section 3.6.1. Finishing nails were inserted through the weave of the FRP to mark the location of each pre-drilled hole.

4) After 24 hours, when the epoxy was tack dry, the finishing nails were removed and the holes were re-opened by drilling through the hardened FRP sheet.
5) When the holes were re-opened, the dust and debris were removed by blowing out the hole with compressed air.
6) The FRP anchors were cut to a length of 175 mm for the 100 mm deep holes or 225 mm for the 150 mm deep holes. Regardless of the depth of the hole a provision for a 75 mm anchor fan was included. One end of the anchor was tied with a twist tie. This was done to cap the end and hold the mesh sock on the anchor to keep the fibers together (Figure 3-23a).
7) The fibers of the FRP anchor were impregnated with Sikadur® 330 epoxy (Figure 3-23b-d). The gauze sock was pulled down after impregnation to keep the anchor intact and the fibers in a linear direction.
8) Once all anchors were impregnated, the pre-drilled holes in the slab were filled with Sikadur® 330 epoxy (Figure 3-24a,b).
9) The anchors were then pushed into the hole with a metal rod (Figure 3-23d and Figure 3-24c).
10) Finally the FRP anchor ends were fanned out to a 30^{o} angle at the ends of the slab and a to a 360^{o} angle at mid-span and under the loading points (Figure 3-25e,f).

The layout of the FRP anchors in the beam of the pilot study, series I and series II are shown in Figure 3-26, Figure 3-27 and Figure 3-28 respectively.

An important component in the FRP anchor installation process is the 75 mm long 30^{o} fan portion of the anchor. A 30^{o} fan was suggested by Sika® Canada to distribute the forces across the FRP strip. The decision to use 75 mm as the length of the fan was determined from an ancillary study of three different anchor fan lengths. The test assessed the performance and ease of installation of the three lengths (50 mm, 75 mm, 100 mm). The result, found the 75 mm anchor fan performed best in both categories. Figure 3-29 details the FRP anchors installed in all series.

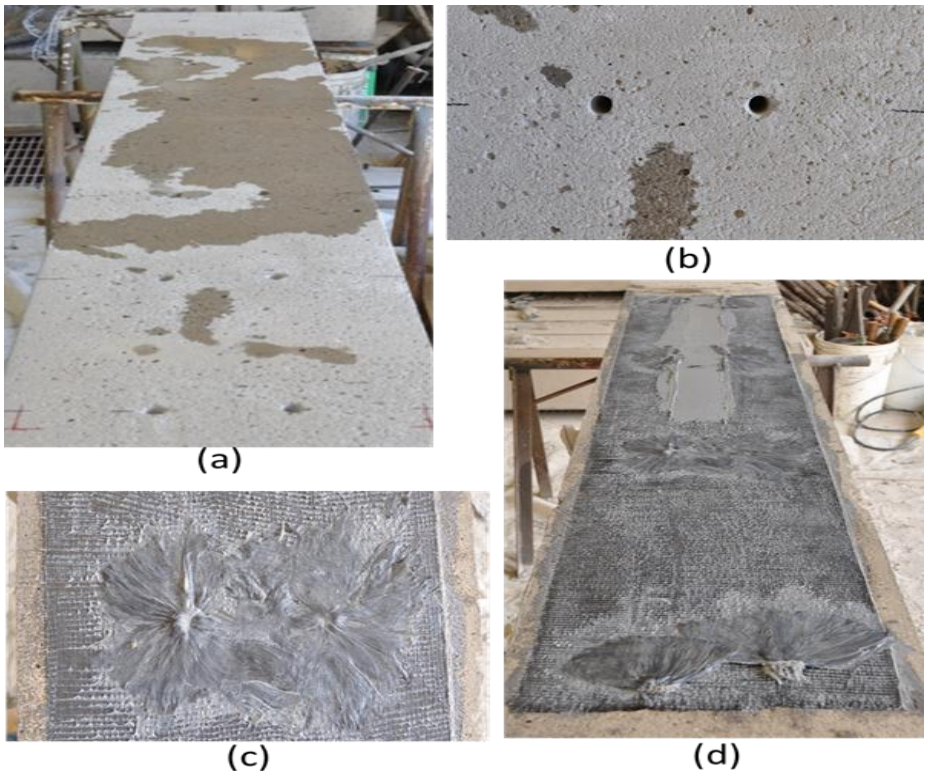

Figure 3-25: FRP anchor slab installation

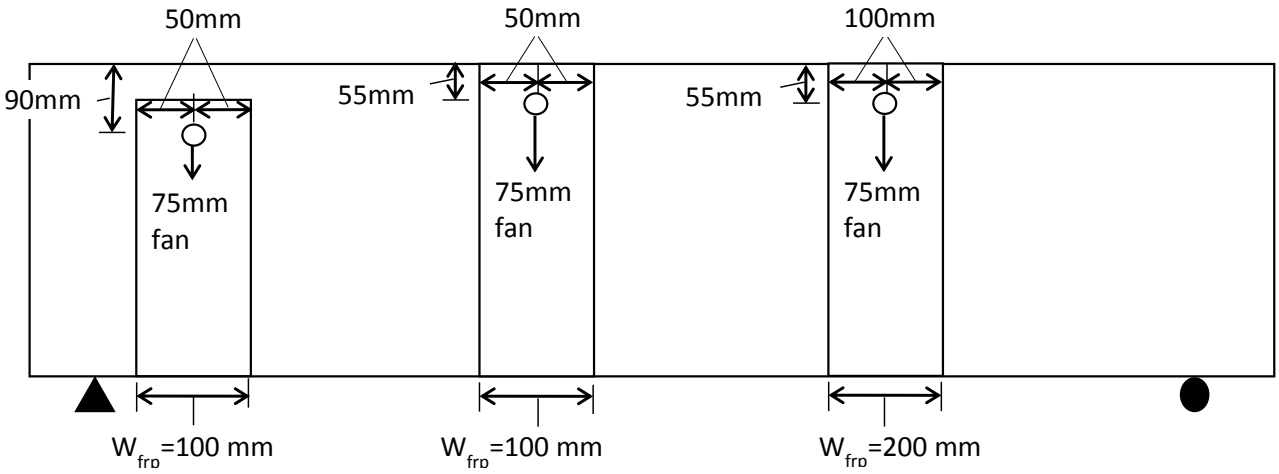

Figure 3-26: Pilot study anchor locations

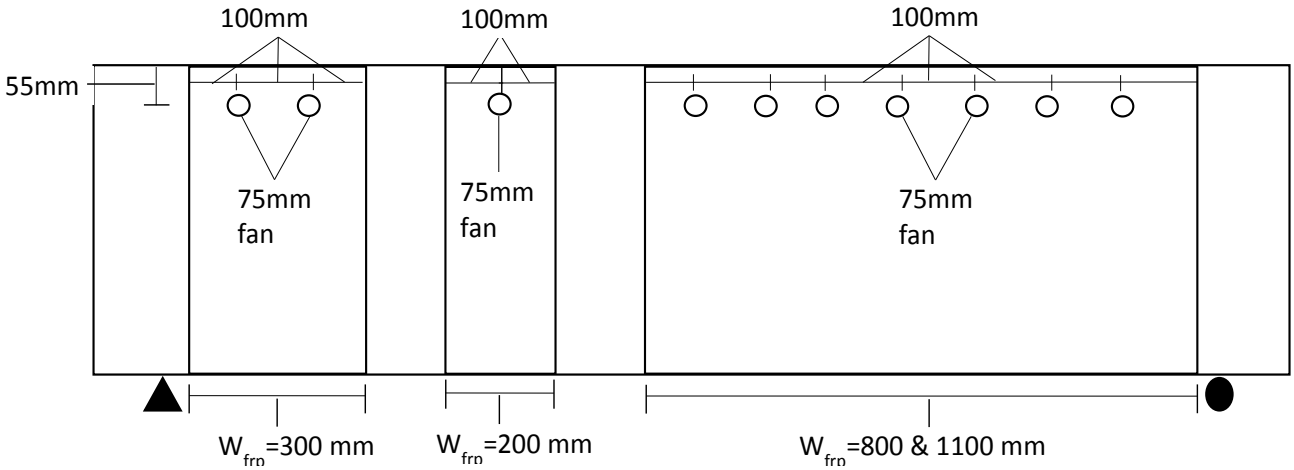

Figure 3-27: Series I anchor locations

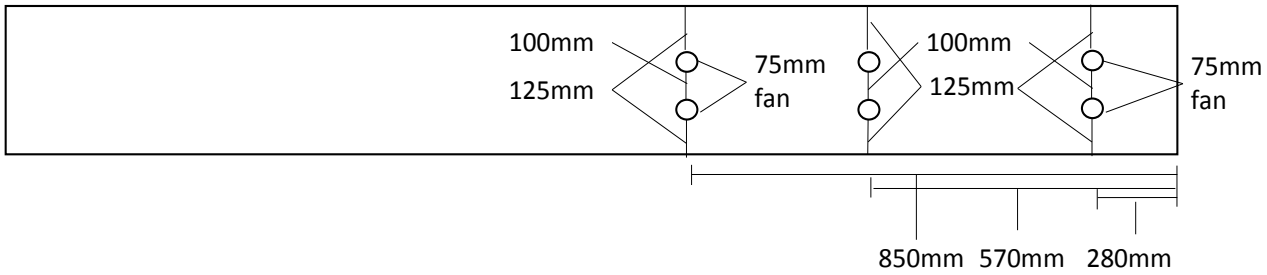

Figure 3-28: Series II anchor locations

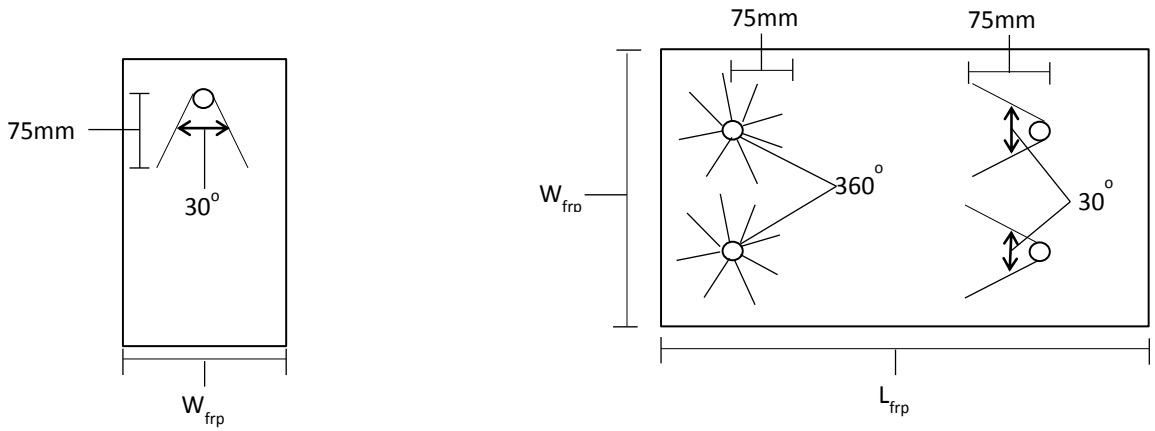

Figure 3-29: Anchor detail

3.7 Instrumentation

Electrical resistance strain gauges were used to measure the strain in the steel (5 mm, 120Ω), FRP sheet (5 mm and 30 mm, 120Ω), and concrete (60 mm, 120Ω). The concrete strain gauge was installed on the top surface between the two loading points. The number and location of the strain gauges per specimen varied in each series as described below.

Pilot Study

A total of three 5 mm strain gauges were installed in each beam: one gauge was attached onto the longitudinal rebar at mid-span (Figure 3-33a,b) and two gauges were installed onto two stirrups (2nd stirrup and 4th stirrup) located in the shear region (Figure 3-33c,d). To measure the strain in the FRP sheets, five 5 mm strain gauges were applied to the FRP or GFRCM. Figure 3-30 illustrates a schematic of the location of each of the strain gauges applied on the concrete, steel and FRP.

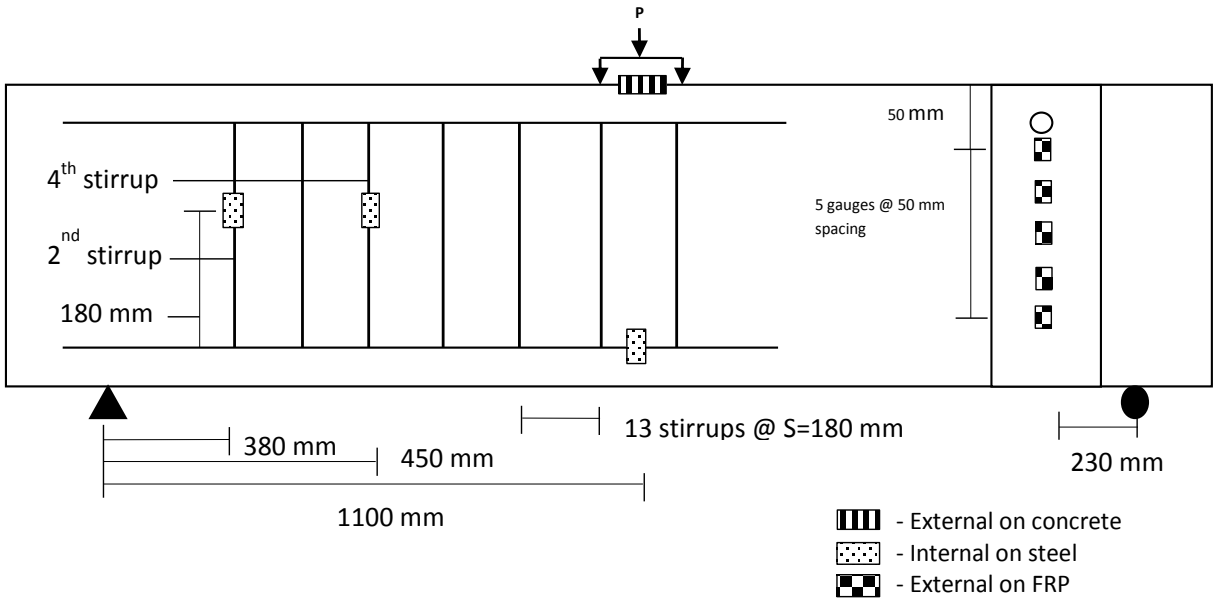

Figure 3-30: Pilot study strain gauge detail

Series I

A total of four 5 mm strain gauges were installed on each beam, one gauge was attached to the longitudinal rebar at mid-span (Figure 3-33a,b) and three gauges were installed on three stirrups located in the shear region (Figure 3-33c,d). The three gauges were placed at different locations on the stirrup. This procedure was undertaken to ensure that the strain gauges would be in the area of the stirrup that is experiencing the highest strain as the shear crack progresses. The strain gauges were placed at 95 mm from the bottom of the "2nd stirrup" or the equivalent of 1/3 the distance from the bottom, 145 mm from the bottom of the "3rd stirrup" or the equivalent of ½ the distance from the bottom and 190 mm from the bottom of the "4th stirrup" or the equivalent of 1/3 the distance from the top of the stirrup.

To measure the strain in the FRP sheet, six 30 mm strain gauges were mounted to the FRP surface. Figure 3-31 shows a schematic of the location of these strain gauges.

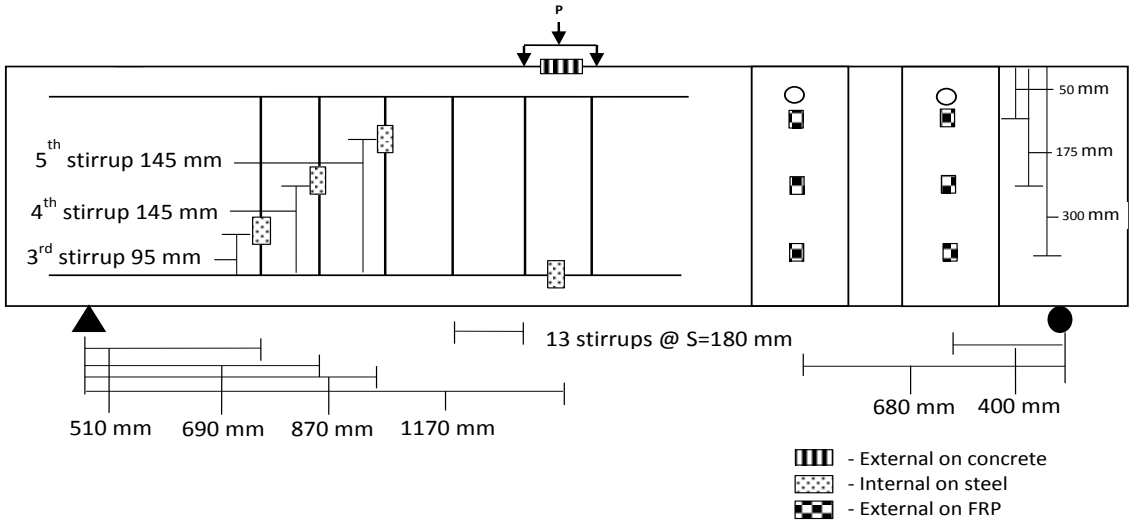

Figure 3-31: Series I strain gauge detail

Series II

Two 5 mm strain gauges were installed on the two outside longitudinal rebar at mid-span. One 60 mm gauge was mounted on the concrete surface at mid-span. Three 30 mm strain gauges were mounted on the FRP sheet at 350 mm, 850 mm from the end of the slab and at mid-span. Figure 3-32 depicts the location of each of these strain gauges.

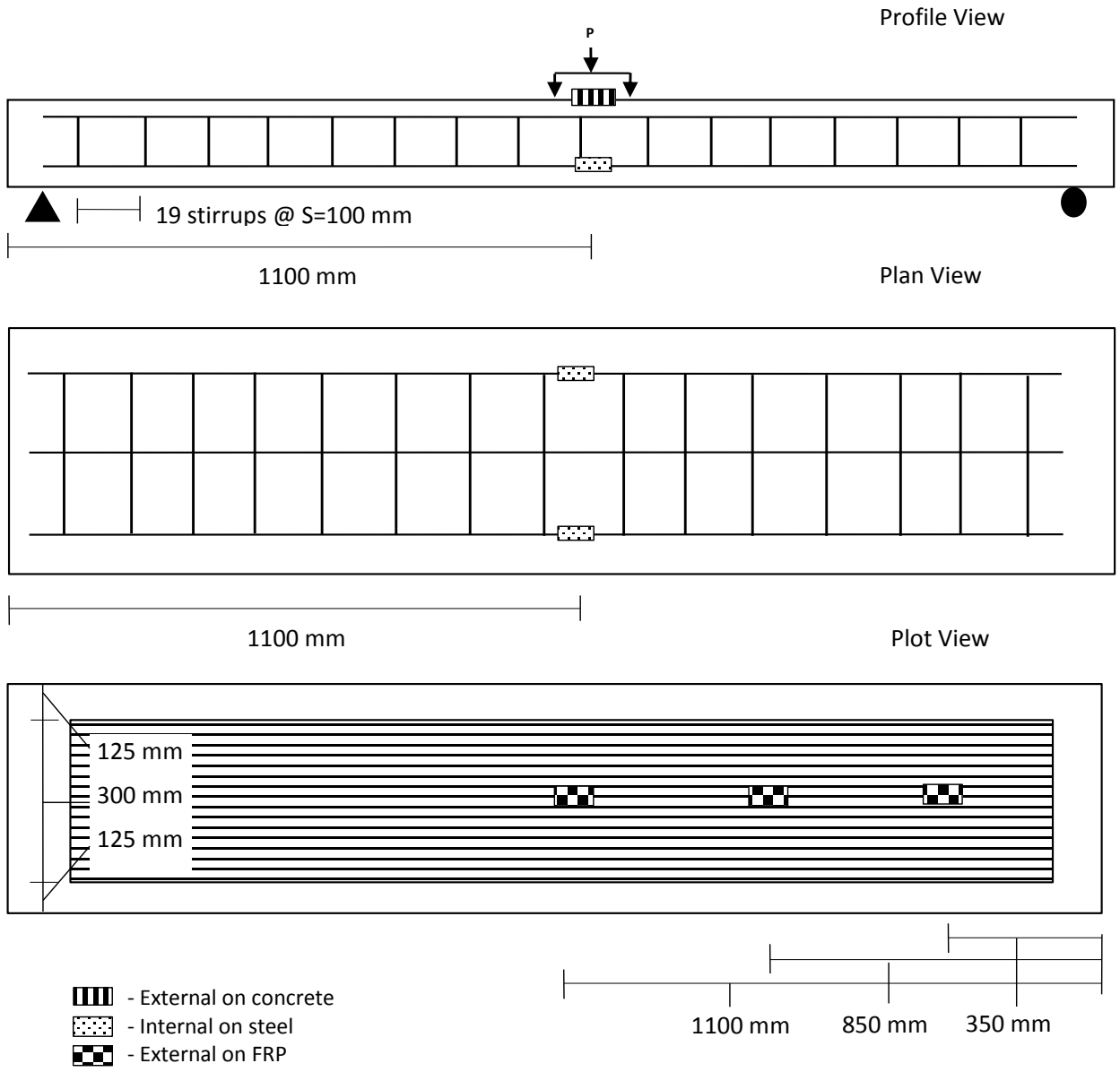

Figure 3-32: Series II strain gauge detail

Figure 3-33 shows photos of strain gauges installed on the steel rebar. The installation of the gauges onto the FRP system required a different procedure compared to that for steel and concrete installation. Prior to application of the strain gauges on the FRP, a layer of Sikadur® 330 epoxy was poured over a local section of the FRP and left to dry. This provided a smooth surface to mount the gauges. In total each beam contained 5-6 strain gauges and each slab had 3 strain gauges mounted on the FRP. Photos of the epoxy layer and the strain gauges attached to the FRP are shown in Figure 3-34.

One linear variable differential transformer (LVDT) with a 25 mm range was used to measure the mid-span deflection of the beams and slabs (Figure 3-35).

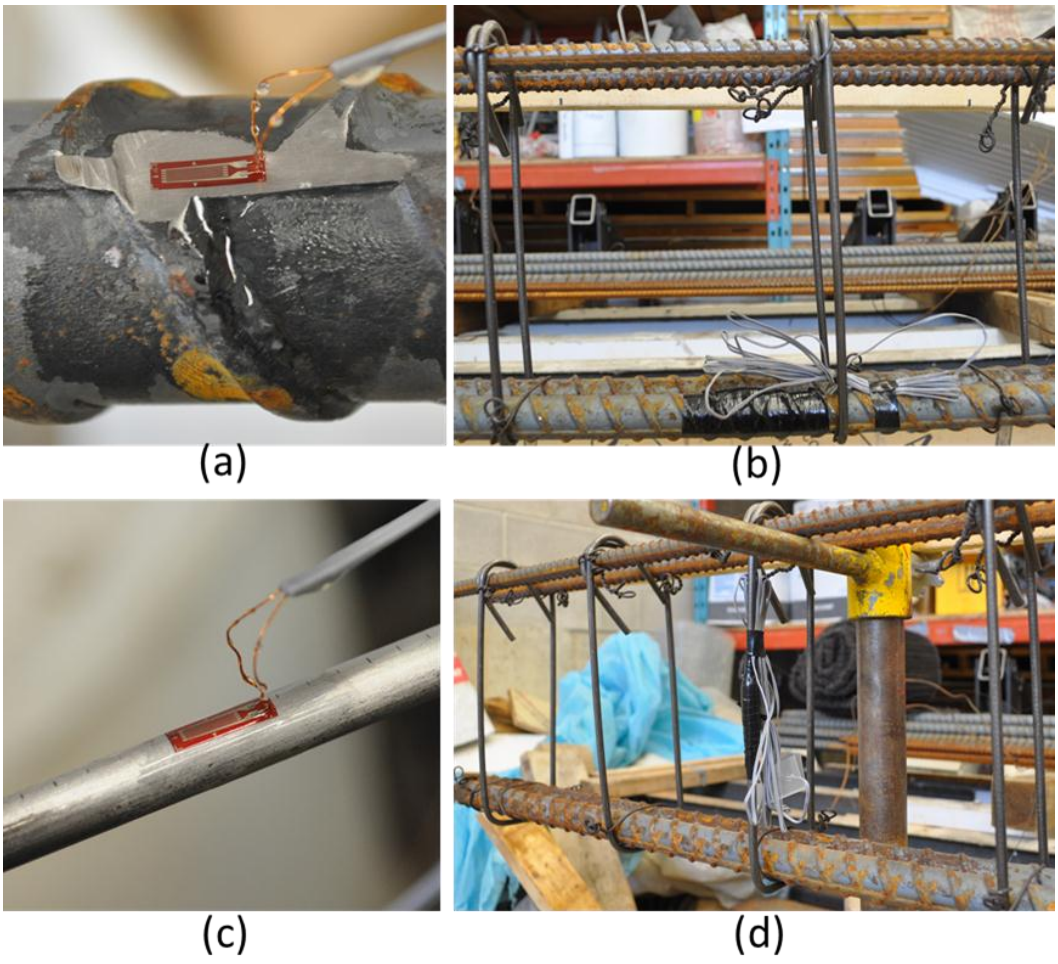

Figure 3-33: Strain gauge installation on the steel rebar & stirrups

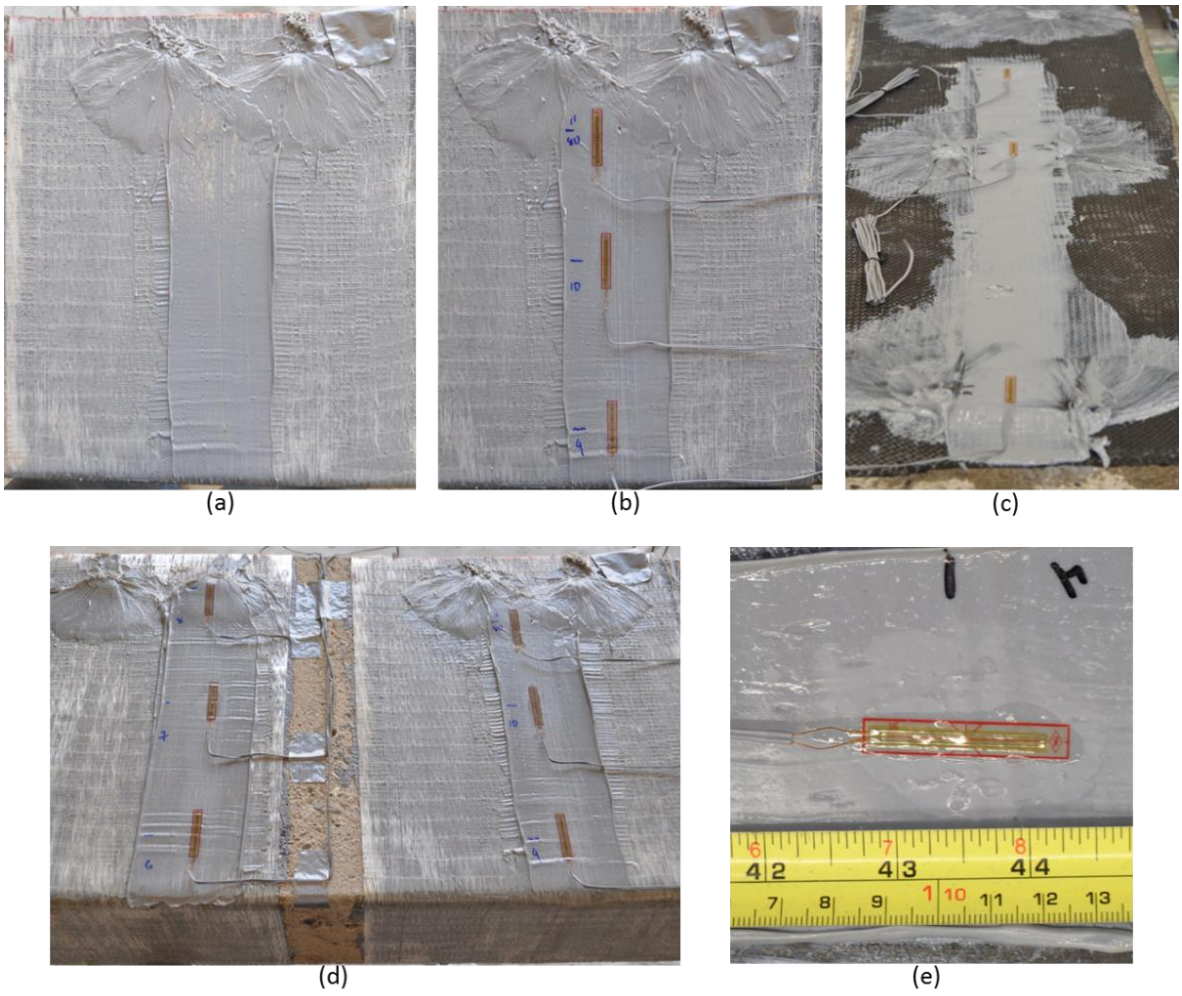

Figure 3-34: FRP strain gauge application

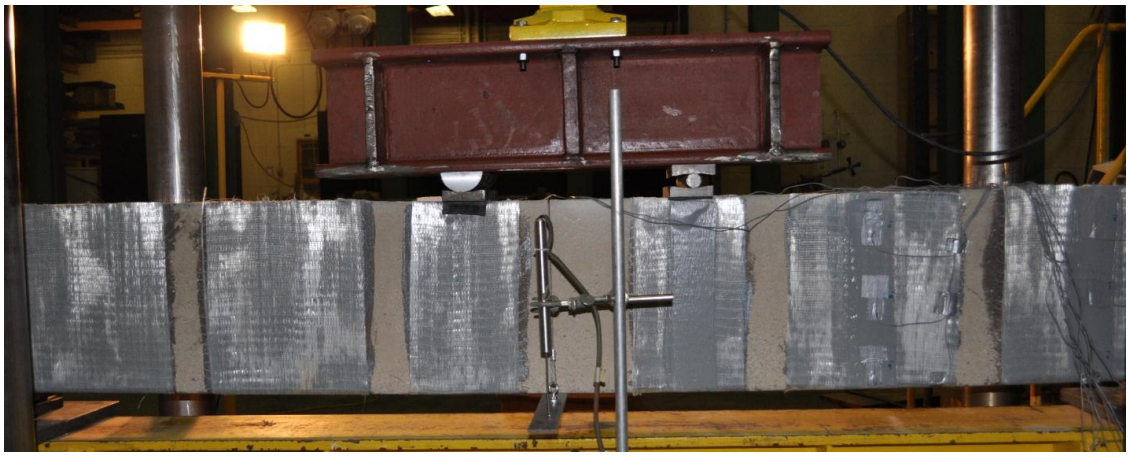

Figure 3-35: LVDT setup during beam testing

3.8 Test Setup and Procedure

All beams and slabs were tested using four point bending employing a closed-loop hydraulic MTS actuator with a 500 kN capacity in a MTS 322 test frame. Two different test setups were used for beams and slabs as discussed below.

Pilot Study and Series I

The beams in the pilot study and series I were simply supported with a clear span of 2200 mm and 400 mm spacing between the two loading points resulting in a shear span of 900 mm. The supports and loading points consisted of a pin and roller connection. Load was applied through a spreader beam mounted on the actuator. The test setup is shown Figure 3-36.

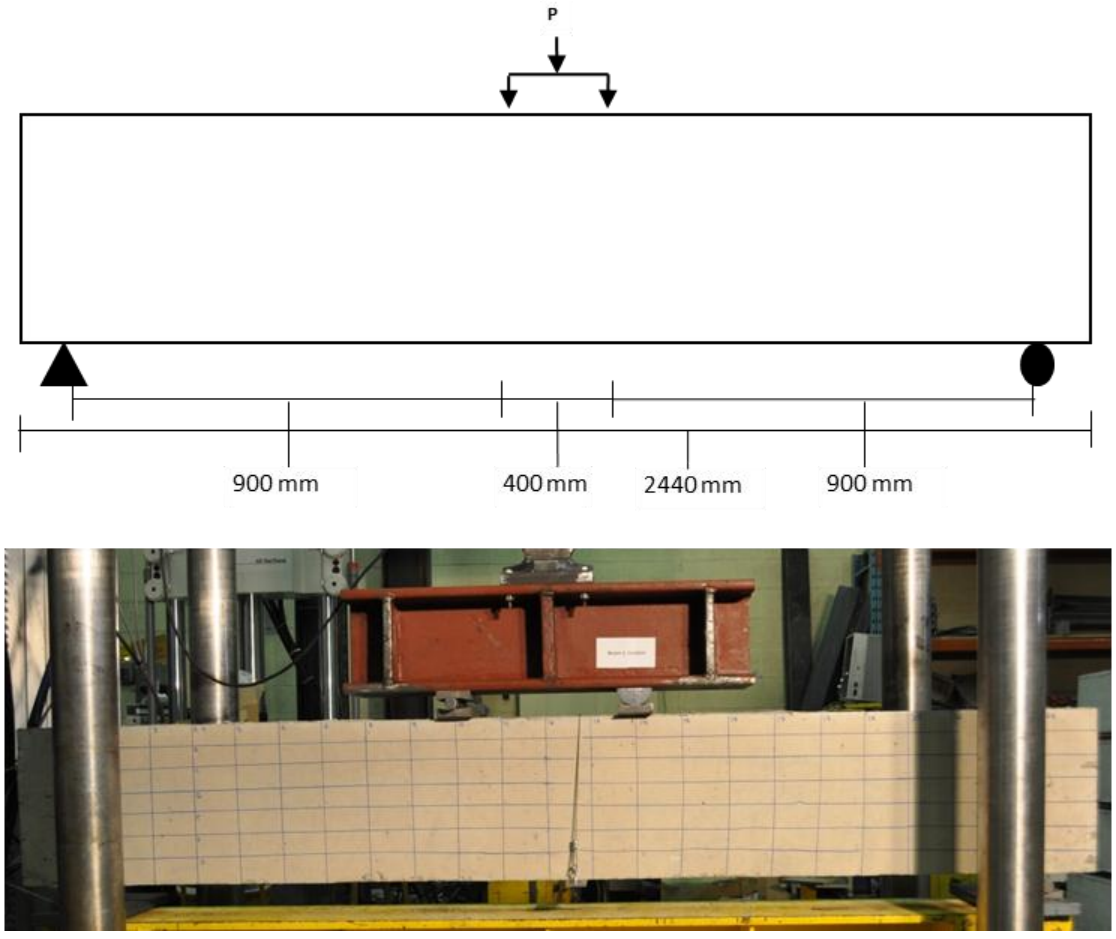

Figure 3-36: Pilot study and Series I beam test setup

Series II

The slabs in series II were simply supported with a clear span of 1800 mm, 500 mm spacing between the two loading points and a shear span of 650 mm. The supports and loading points consisted of a pin and roller connection. The test setup is shown Figure 3-37.

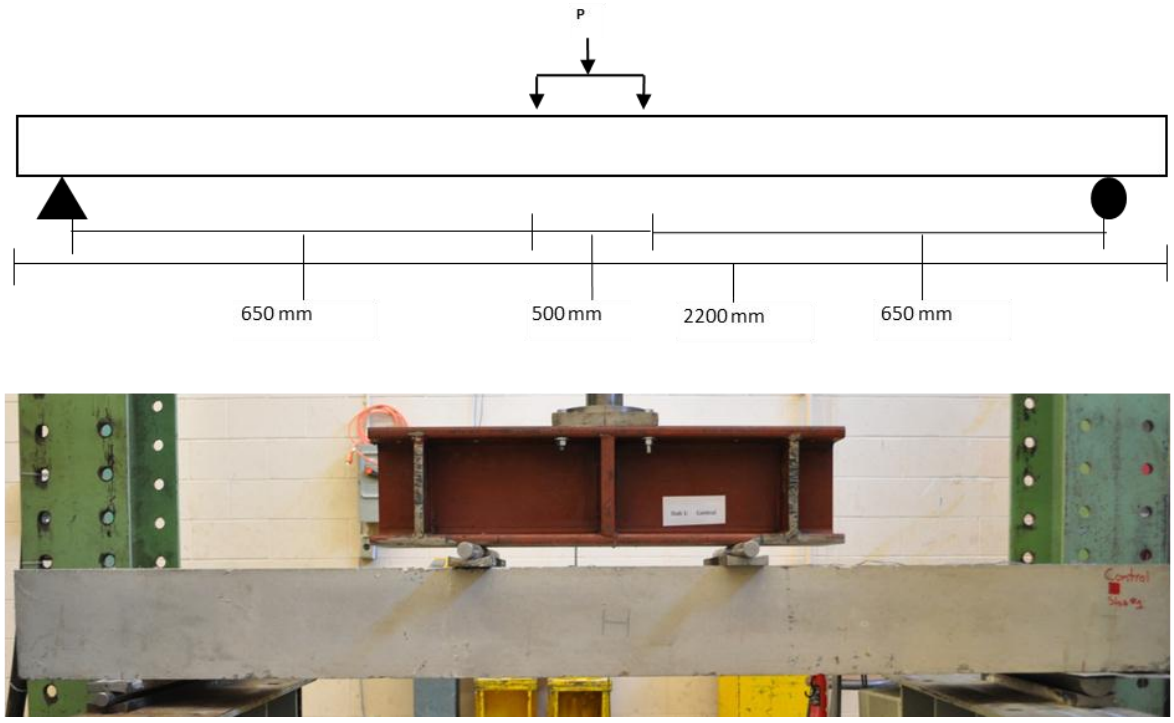

Figure 3-37: Series II slab test setup

The test procedure for the three series was as follows:

1) Each specimen was placed on the pin and roller supports, leveled and centered under the two point load system.
2) After each beam was centered and leveled, the LVDT was mounted at mid-span.
3) The instrumentation (strain gauges and LVDT) were connected to the data acquisition system and calibrated.
4) The data acquisition system was started prior to loading to ensure data was being recorded before loading began.
5) Each specimen was preloaded to a load of 20-30 kN

6) The load was increased by displacement control at a rate of 0.3 mm/min for beams and 1 mm/min for slabs.
7) The initiation and progression of cracks was monitored to gain a better understanding of the behaviour and failure mode.
8) The test was stopped when the load dropped after reaching the peak value.

In series I, six beams were pre-cracked, repaired and tested. The beams were preloaded to 85% (155kN) of the failure load of the control beam (182 kN) to induce large shear cracks and replicate a beam requiring repair. These tests were conducted analogous to the method described above and stopped when the load reached 155 kN. The beams were repaired with FRP and then tested until failure as outlined previously.

A national instrument data acquisition system recorded all readings from the instrumentation (strain gauges and LVDT's). Cracks and their development were recorded and monitored visually for every test. The complete setup with instrumentation is displayed in Figure 3-38.

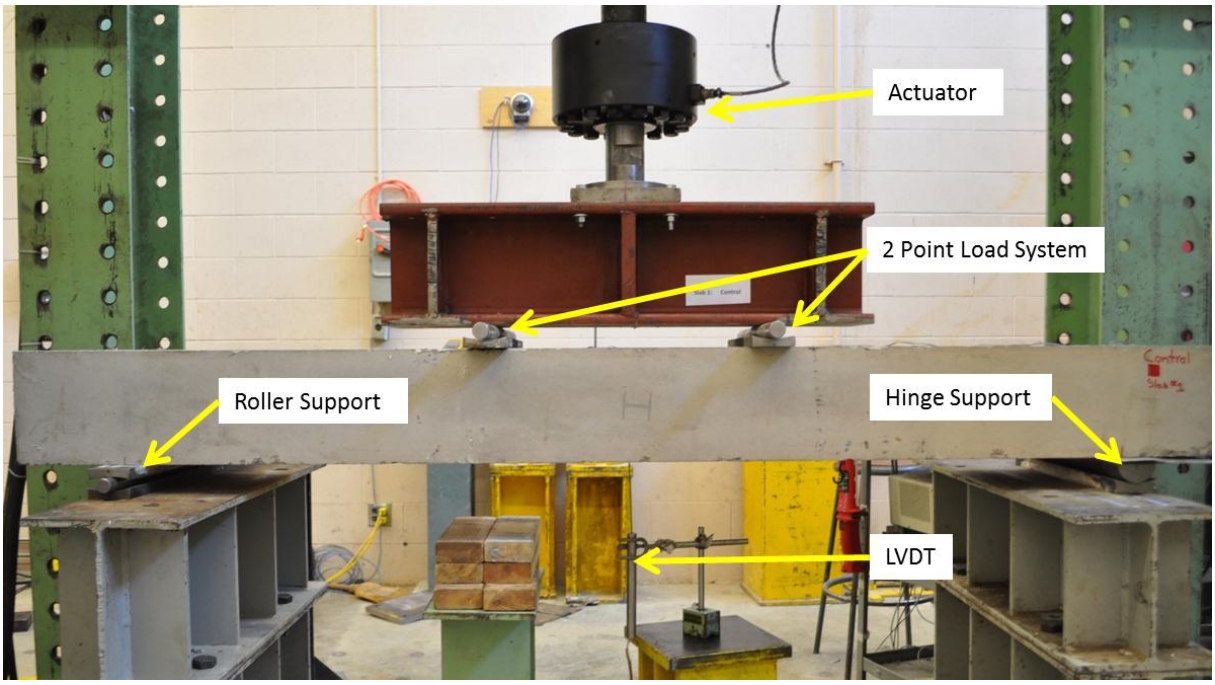

Figure 3-38: Test setup

Chapter 4 – Experimental Results

4.1 Introduction

In this chapter the experimental results of the main study specimens are presented. The results of the pilot study are presented in Appendix A. The test program is comprised of two series: series I – shear strengthened slender beams (a/d ratio = 2.99) and series II – flexural strengthened slabs (a/d ratio = 4.61). The test results include the following information:

- Observed behaviour and failure modes
- Load-displacement behaviour
- Steel and concrete strain response
- FRP strain response

4.1.1 Nomenclature

The nomenclature for the test specimen consists of three parts (Figure 4-1). The first part indicates the type of FRP reinforcement, the second part indicates the FRP strip width or number of layers and the third part indicates if anchors were present or not. For the pre-cracked shear critical beams an additional term (PC) is added in front of the specimen designation.

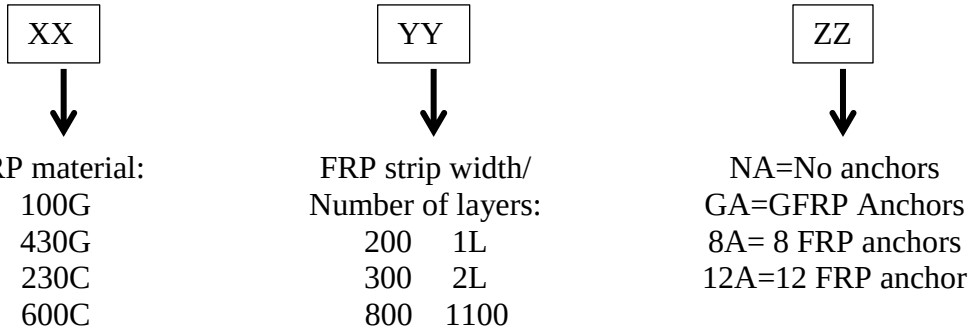

Figure 4-1: Experimental nomenclature used in this study

4.2 Shear Critical Beams – Series I

Twelve shear critical beams were strengthened with two types of GFRP sheets. One beam was tested as control (unstrengthened), six beams were strengthened with intermittent u-wrap GFRP sheets and five beams were pre-cracked then repaired with continuous u-wrap GFRP sheets. The test variables were:

1. Type of GFRP sheet: Sikawrap 430G and Sikawrap 100G
2. GFRP configuration in shear span: Intermittent strips (200 mm vs. 300 mm wide) and Continuous sheet (800 mm vs. 1100mm wide)
3. Use of FRP anchors: No anchors vs. GFRP anchors

The GFRP sheets were applied as u-wraps around the cross-section running the full depth of the beam. A summary of the test results including, the ultimate load, deflection at ultimate load, percent increase over the control and mode of failure for all beams is provided in Table 4-1. The failure mode notation highlights the principal failure mode which caused failure in each beam. Descriptions of each acronym are provided at the bottom of the table. Determining if FRP debonding and FRP rupture occurred was verified visually and recorded. However, loss of aggregate interlock was determined by using a differential diagnosis procedure. This procedure consists of determining all possible causes of failure of a shear critical beam, followed by a process of elimination until only one failure mode remains. The differential diagnosis procedure used on each beam to determine if aggregate interlock governed as the primary failure mode is outlined below:

1. Did FRP debonding occur prior to failure – No
2. Did FRP rupture occur prior to failure – No
3. Did flexural failure occur? - No
4. Did shear failure occur? – Yes
5. Is a diagonal tension shear crack present? – Yes
6. Did the diagonal tension shear crack widen as the applied load increased? – Yes

Therefore, by a process of elimination all failure modes were eliminated until loss of aggregate interlock was the only remaining mode of failure.

Table 4-1: Series 1 - Summary of test results for GFRP strengthened beams

Nomenclature	Specimen Description	Ultimate Load (kN)	Deflection at ultimate load (mm)	Percent increase over the control (%)	Failure mode
Control	Control	182	6.52	-	• DT-SF
430G-200-NA 430G-200-A	430G-200 mm-No anchors 430G-200 mm-Anchors	332 332	15.7 14.0	81.4 81.4	• AI & FRP D • AI & FRP R
100G-200-NA 100G-200-A	100G-200 mm-No anchors 100G-200 mm-Anchors	363 369	15.1 13.6	98.4 101.4	• AI & FRP D • AI
430G-300-NA 430G-300-A	430G-300 mm-No anchors 430G-300 mm-Anchors	313 346	11.9 13.9	71.0 89.1	• AI & FRP D • AI & CC
PC-430G-800-NA PC-430G-800-A PC-430G-800-FW	PC-430G-800 mm-No anchors PC-430G-800 mm-Anchors PC-430G-800 mm-Full wrap	304 358 357	10.7 12.6 15.3	66.1 95.6 95.1	• AI & FRP D • FRP R DT-EAF • FRP R DT-EAF
PC-100G-1100-NA PC-100G-1100-A	PC-100G-1100 mm-No anchors PC-100G-1100 mm-Anchors	352 395	16.7 21.5	92.3 115.8	• AI & FRP D • DT-EAF

where: SF=Shear failure, AI=Loss of aggregate interlock, FRP D=FRP Debonding, FRP R= FRP Rupture, CC=Concrete crushing, DT=Diagonal tension and EAF=End anchorage failure

4.2.1 Control Beam

The failure mode of the control beam was by shear diagonal tension failure. The load deflection response of the control beam is shown in Figure 4-2 and the diagonal tension shear crack of the failed beam is shown in Figure 4-3. The strain response for the concrete top fiber and the longitudinal steel reinforcement at mid-span are shown in Figure 4-4 and the stirrup strain response is presented in Figure 4-5.

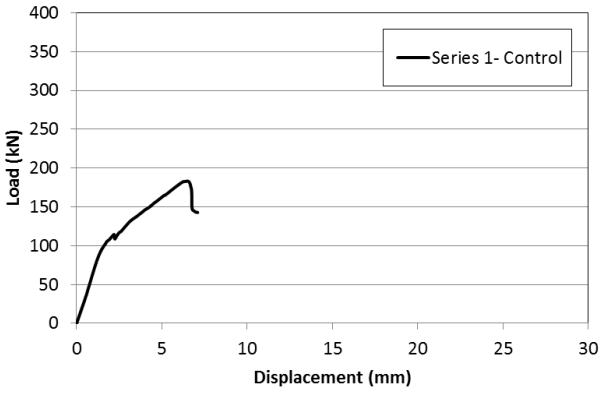

Figure 4-2: Load vs. deflection of control beam (series I)

The load deflection curve in Figure 4-2 showed a bi-linear response. Cracking initiated as flexural cracks between the two loading points with the first crack appearing at a load of 20 kN. As the load was increased, inclined cracks began to develop in the shear span and propagated between the support and loading points. A slight drop in the load was caused by crack development in the shear spans at a load of 112 kN. The load deflection curve further increased when the internal stirrups began to resist shear forces. This is evident in the stirrup strain response curves in Figure 4-5. The beam failed suddenly in shear (diagonal tension) immediately after the peak load (182 kN) was reached indicating the brittle nature of shear failure. The deflection at maximum load was 6.5 mm. After failure, a sudden drop in load with deflection was exhibited.

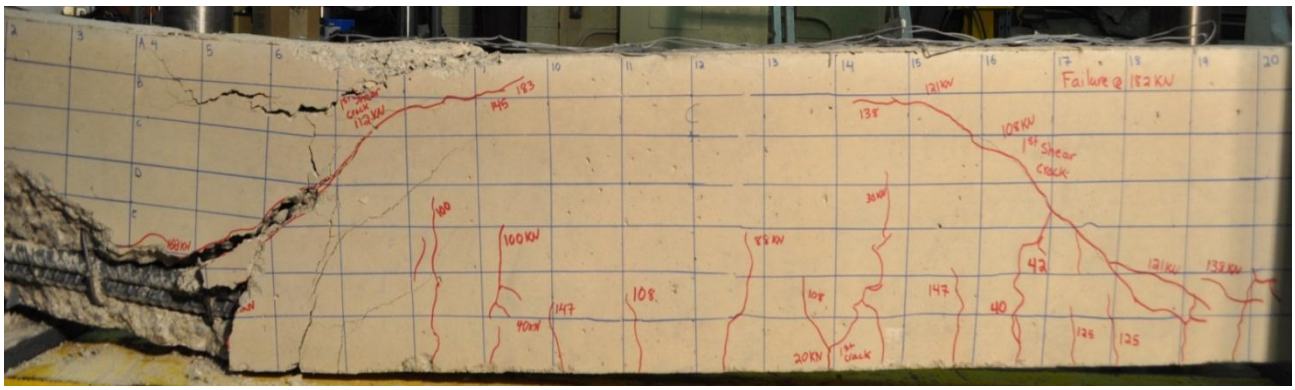

Figure 4-3: Diagonal tension failure of control beam (series I)

The strain in the concrete at beam failure was below the strain to cause concrete crushing and the strain in the longitudinal steel rebar was below the yield strain of steel (Figure 4-4). The strain response in the stirrups (Figure 4-5) indicated that the 4th stirrup yielded reaching a maximum strain of 2400 με. The 3rd and 4th stirrups did not yield reaching maximum strains of 1780 με.

In both cases the strain in the stirrups had a bi-linear response. Almost no strain was recorded in the stirrups for the first 100 kN beyond which the tensile capacity of concrete was reached and cracking occurred. After cracking the shear cracks widened and the stirrups became engaged in resisting the diagonal tension. Once the stirrups were engaged in resisting the tensile force, a gradual increase in strain was recorded as the load was increased.

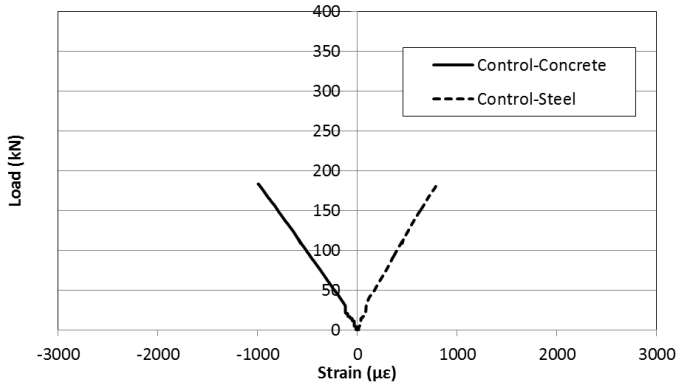

Figure 4-4: Concrete and steel rebar strain response of control beam (series I)

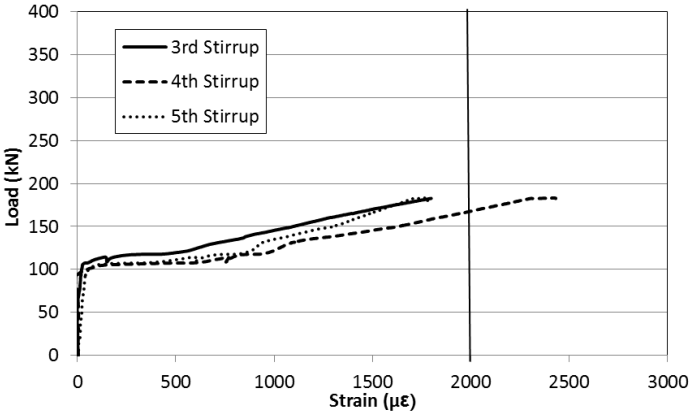

Figure 4-5: Stirrup strain response of control beam (series I)

4.2.2 Beams Strengthened with Sikawrap 430G – 200 mm wide U-wraps

Two beams were strengthened with Sikawrap 430G-GFRP sheets as u-wraps (200 mm wide at a spacing of 275 mm o/c). The Sikawrap 430G sheets were 0.508 mm thick and were applied with Sikadur 330 epoxy. The failure mode of beam 430G-200-NA was loss of aggregate interlock with FRP debonding (Figure 4-6a) and the failure mode of beam 430G-200-A was loss of aggregate interlock with FRP rupture (Figure 4-6b).

The load deflection curves of the two GFRP-430G strengthened beams are shown in Figure 4-7. The strain response for the concrete top fiber and longitudinal steel reinforcement at mid-span are shown in Figure 4-8. The strain response in the stirrups is presented in Figure 4-9. Figure 4-11 and Figure 4-12 show the GFRP strain response across the depth of the beam.

The load deflection curve showed a tri-linear response with three distinct stages (Figure 4-7). The first flexural cracks appeared at a load of 20 kN for beam 430G-200-NA. As the load increased, inclined cracks began to develop in the shear span at a load of 163 kN and 160 kN for beams 430G-200-NA and 430G-200-A, respectively.

The crack development occurred in both shear spans with the GFRP sheets in beam 430G-200-NA debonding at the top end of the sheet at 297 kN. This caused the load to drop to 291 kN then increase again. Beam 430G-200-A exhibited minor debonding at 327 kN because of the presence of GFRP anchors. Both beams failed suddenly in shear (diagonal tension) immediately after the peak load of 332 kN. The maximum deflection at failure for beams 430G-200-NA and 430G-200-A was 15.7 mm and 14.0 mm, respectively. The post peak behaviour of the load vs. deflection curve shows the brittle nature of this type of failure in both beams.

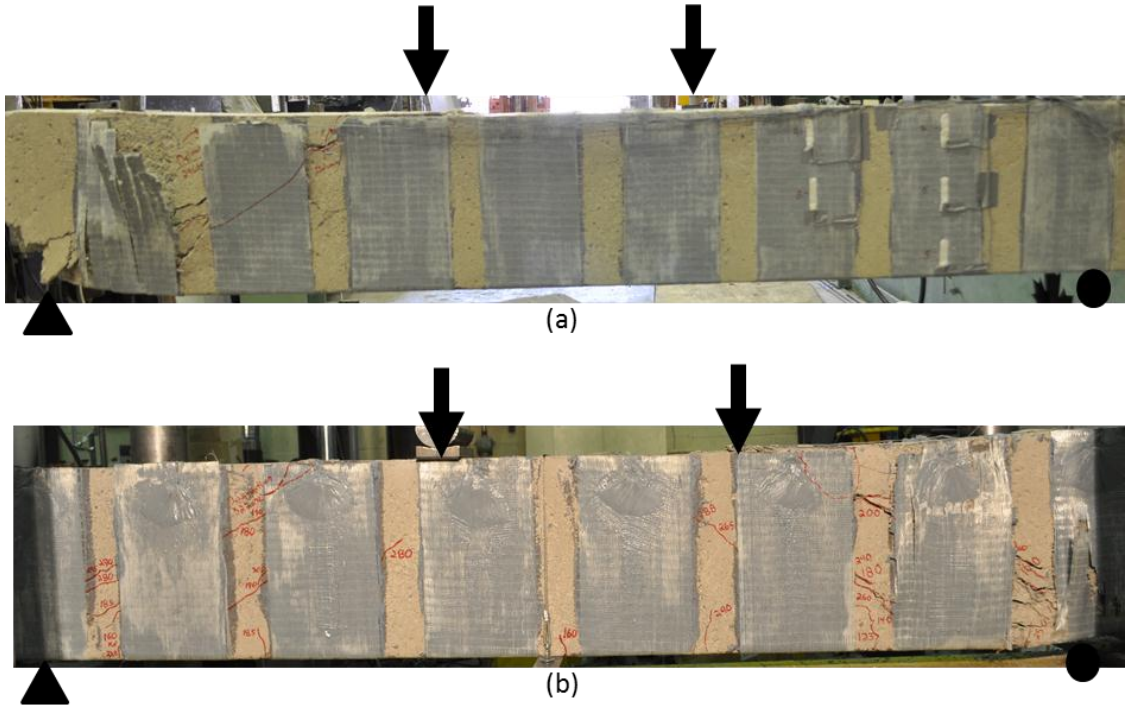

Figure 4-6: Failure mode of beam 430G-200-NA (a) aggregate interlock and FRP debonding and beam 430G-200-A (b) aggregate interlock and FRP rupture

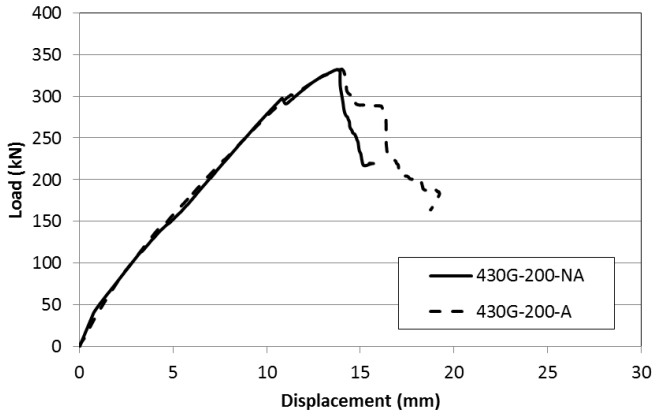

Figure 4-7: Load vs. deflection of beams strengthened with Sikawrap 430G-200mm strips

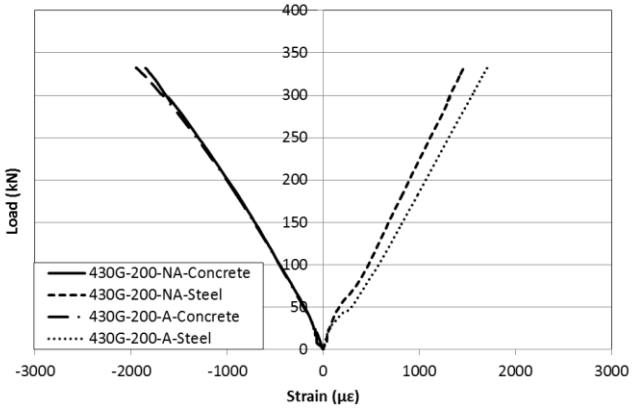

Figure 4-8: Concrete and steel rebar strain response of 430G-200 mm wide GFRP beams

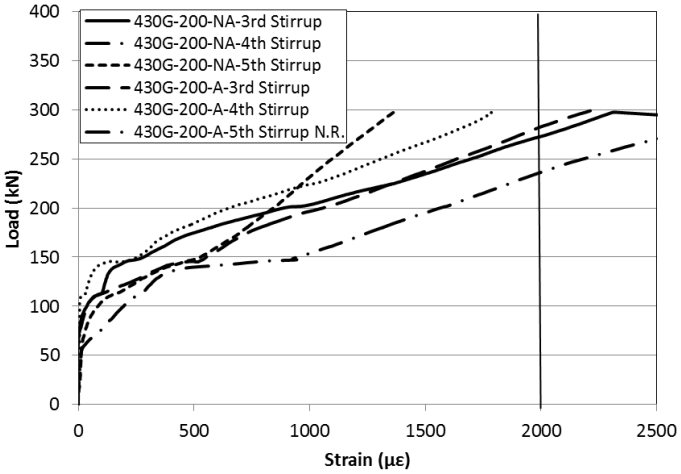

Figure 4-9: Stirrup strain response of 430G-200 mm wide GFRP beams

The concrete top fiber strain at failure was below the crushing strain of concrete and the steel strain was below the yield strain of steel (Figure 4-8). The strain response in the stirrups (Figure 4-9) showed that three stirrups had strains above the yield strain, reaching maximum strains of 5000 με (430G-200-NA-3rd stirrup), 3000 με (430G-200-NA-4th stirrup) and 2200 με (430G-200-A-3rd stirrup).

Each beam had of two FRP sheets which contained strain gauges. Sheet 2 was located at 400 mm from the support and sheet 3 was located at 680 mm from the support. Sheet 2 and 3 had three strain gauges, one gauge was placed 50 mm from the top of the beam, one gauge was located at mid-depth and one gauge was placed 300 mm from the top of the beam.

The GFRP strain response across the depth of beam 430G-200-NA showed very high strains at 50 mm from the bottom of the beam and at mid-depth in sheet 2 and 3 (Figure 4-11). The highest strain recorded in beam 430G-200-NA was 5000 με at mid-depth. This corresponds with post mortem cracking under the GFRP sheet in Figure 4-10 which shows that the diagonal tension shear crack was propagating at a 45^{o} angle towards the loading point.

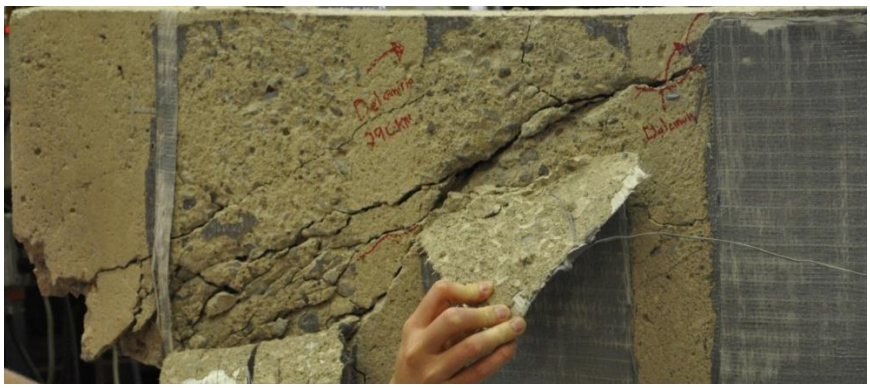

Figure 4-10: Diagonal tension shear crack in 430G-200-NA

The GFRP strain response across the depth of beam 430G-200-A behaved similarly to the strain response recorded in beam 430G-200-NA. High strains were recorded at 50 mm from the bottom of the beam in sheet 2 and at mid-depth in sheet 3 (Figure 4-12). The highest strain recorded in beam 430G-200-A was 8000 με at mid-depth. The location along the depth of the GFRP sheet coincided with the shear crack progressing from the bottom support to the top fiber through sheet 3 at mid-span.

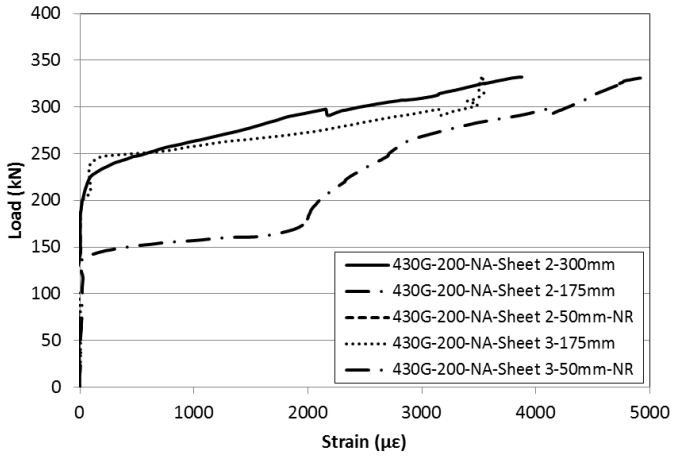

a) Load-strain curves

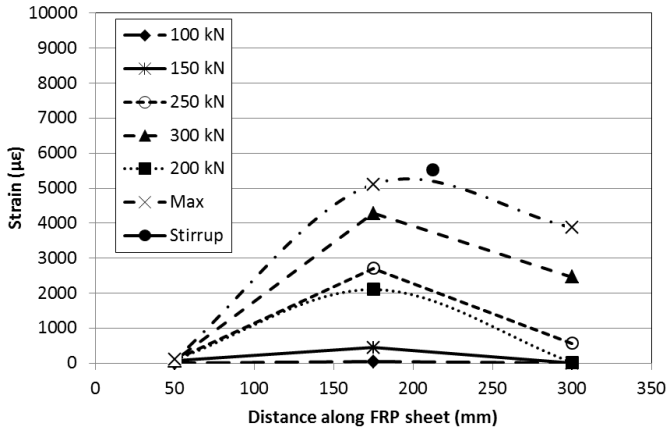

b) Strain profile - sheet 2

Figure 4-11: FRP strain response of beam 430G-200-NA

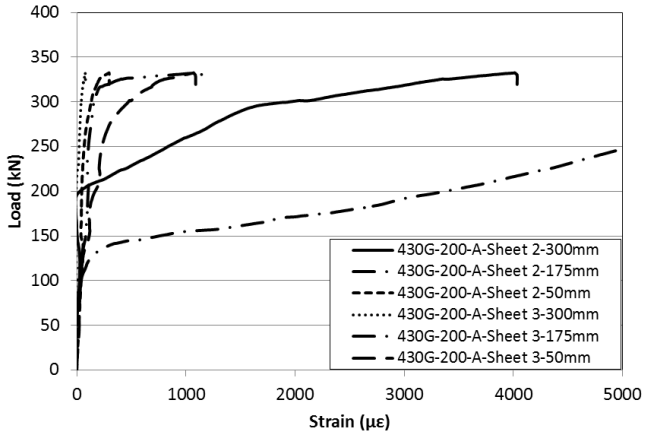

a) Load-strain curves

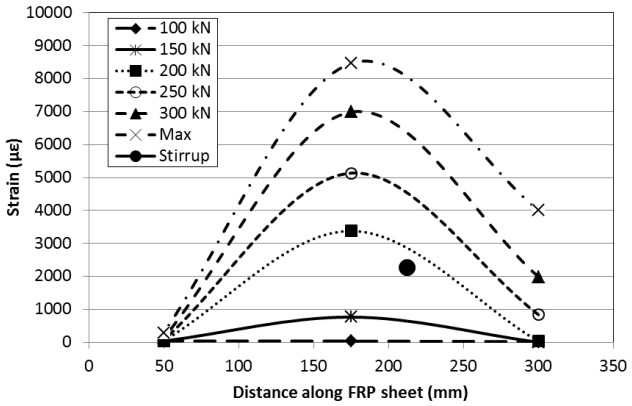

b) Strain profile - sheet 2

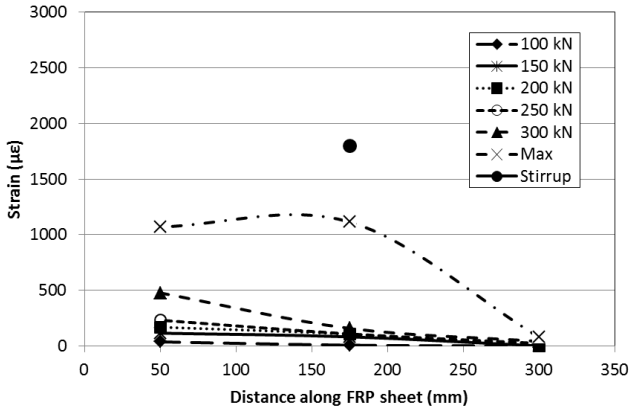

c) Strain profile - sheet 3

Figure 4-12: FRP strain response of beam 430G-200-A

4.2.3 Beams Strengthened with Sikawrap 100G-200 mm wide U-wraps

Two beams were strengthened with Sikawrap 100G-GFRP sheets as u-wraps (200 mm wide at a spacing of 275 mm o/c). The Sikawrap 100G sheets were 1.016 mm thick and were applied with Sikadur 330 epoxy. The failure mode of beam 100G-200-NA was loss of aggregate interlock with FRP debonding (Figure 4-13a) and the failure mode of beam 100G-200-A was loss of aggregate interlock (Figure 4-13b). The load deflection response of GFRP strengthened beams with Sikawrap 100G sheets is shown in Figure 4-14. The strain response for the concrete top fiber and longitudinal steel reinforcement at mid-span is shown in Figure 4-15. The strain response of the stirrups is presented in Figure 4-16. Figure 4-17 and Figure 4-18 show the GFRP strain response for each beam.

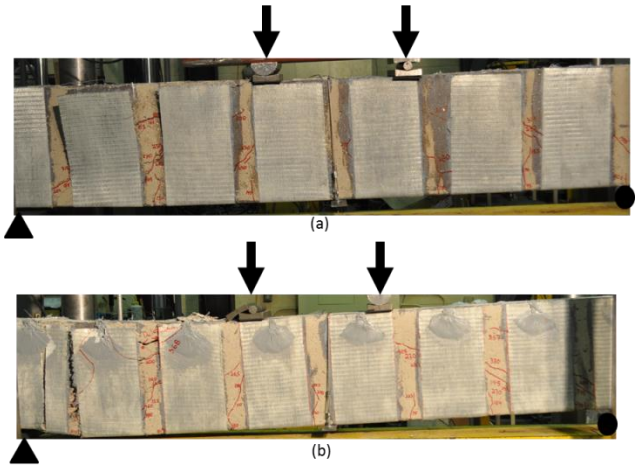

Figure 4-13: Failure mode of beam 430G-100-NA (a) aggregate interlock and FRP debonding and beam 430G-100-A (b) aggregate interlock

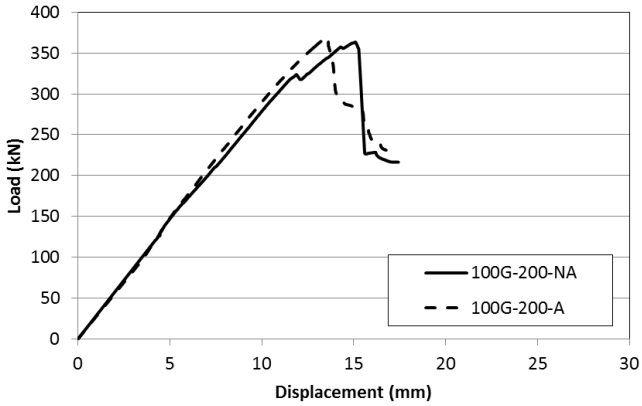

Figure 4-14: Load vs. deflection of beams strengthened with Sikawrap 100G-200 mm strips

The load deflection curve showed a linear response with two distinct stages. The first flexural cracks appeared at a load of 43 kN and 75 kN for beams 100G-200-NA and 100G-200-A, respectively. As the load increased, inclined cracks began to develop in the shear span at a load of 130 kN and 145 kN for beams 100G-200-NA and 100G-200-A, respectively.

The crack development occurred in both shear spans with the GFRP sheets in beam 100G-200-NA debonding at the top end of the sheet. This occurred at a load of 323 kN causing the load to drop to 319 kN before increasing again to 363 kN. Beam 100G-200-A had no premature debonding and failure occurred at a load of 368 kN. The presence of GFRP anchors eliminated the premature FRP debonding. Both beams had sudden (diagonal tension) shear failure with loss of aggregate interlock immediately after their peak loads were reached (363 kN and 369 kN).

The maximum deflection recorded for each beam at failure was 15.1 mm and 13.6 mm, respectively. The post peak behaviour of the load vs. deflection curve shows the brittle nature of shear failure.

The concrete strain at failure was below the crushing strain of concrete (Figure 4-15). The steel strain response was below the yield strain of steel recording 1957 με (Figure 4-15). The strain response in the stirrups (Figure 4-16) showed that four stirrups exceeded the yield strain, reaching maximum strains of 2400 με (100G-200-NA-3rd stirrup), 3000 με (100G-200-NA-4th stirrup) and 2188 με (100G-200-A-3rd stirrup).

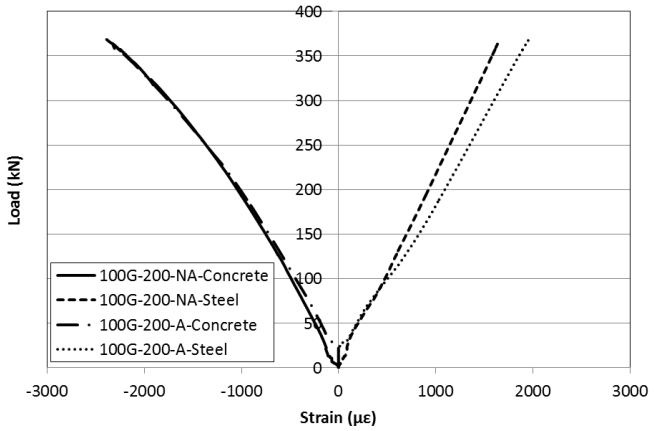

Figure 4-15: Concrete and steel rebar strain response of beams strengthened with Sikawrap 100G-200 mm wide strips

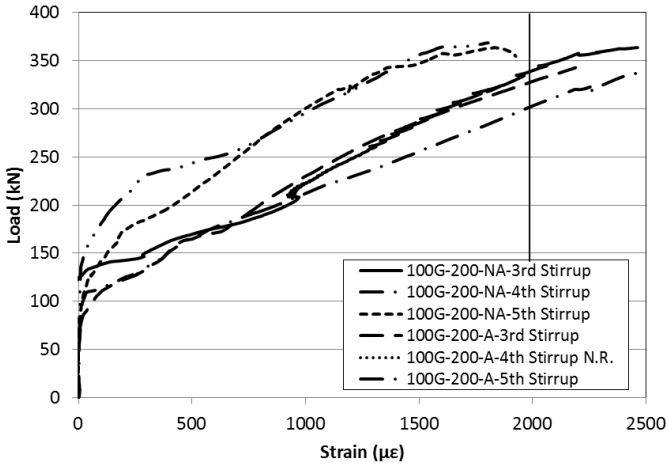

Figure 4-16: Stirrup strain response of beams strengthened with Sikawrap 100G-200 mm wide strips

The GFRP strain response across the depth of beam 100G-200-NA (Figure 4-17) showed high strains at 50 mm from the top of the beam in sheet 2 (400 mm from the support) and mid-depth of sheet 3 (680 mm from the support). The highest strain recorded in beam 100G-200-NA was 4600 με at 50 mm from the top in sheet 2 and 2600 με at mid-depth in sheet 3.

The GFRP strain response across the depth of beam 100G-200-A (Figure 4-18) recorded high strains at 50 mm from the top of the beam in both sheet 2 (400 mm from the support) and sheet 3 (680 mm from the support). The maximum strain recorded was 5566 με which occurred at 50 mm from the top in sheet 2. The remaining strain gauges recorded moderate strain values between 1000 με - 2000 με. Beam 100G-200-A with GFRP anchors was able to withstand substantially higher strains than beam 100G-200-NA which was not anchored. This can be attributed to the anchorage provided by the FRP anchors which allowed the FRP sheet to develop higher strains as opposed to debonding.

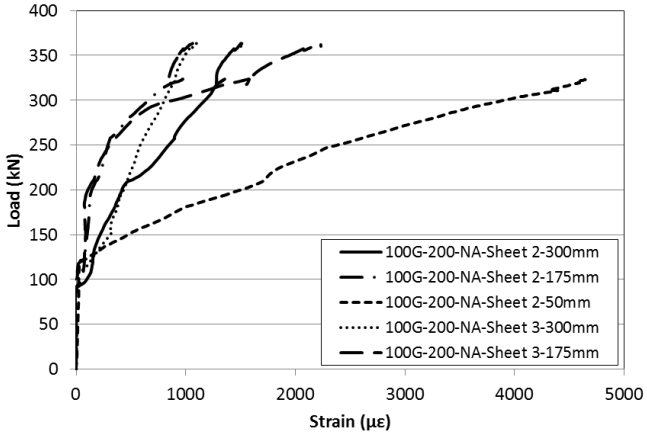

a) Load-strain curves

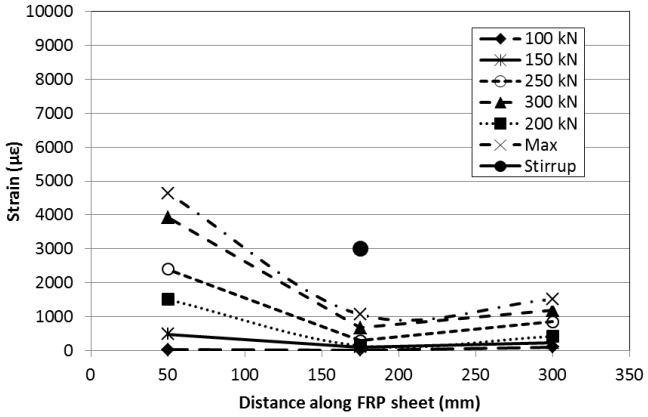

b) Strain profile – sheet 2

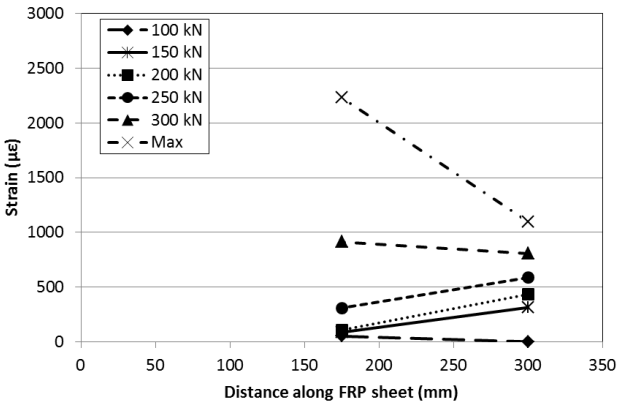

c) Strain profile – sheet 3

Figure 4-17: FRP strain response of beam 100G-200-NA

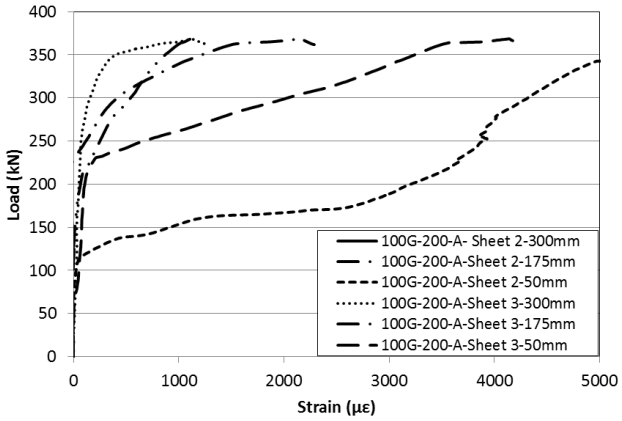

a) Load-strain curves

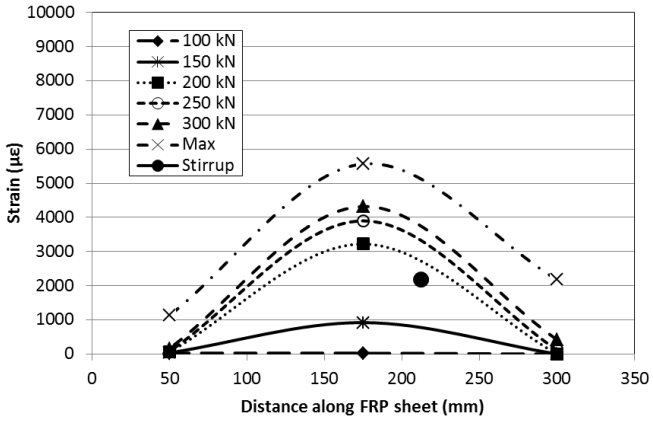

b) Strain profile – sheet 2

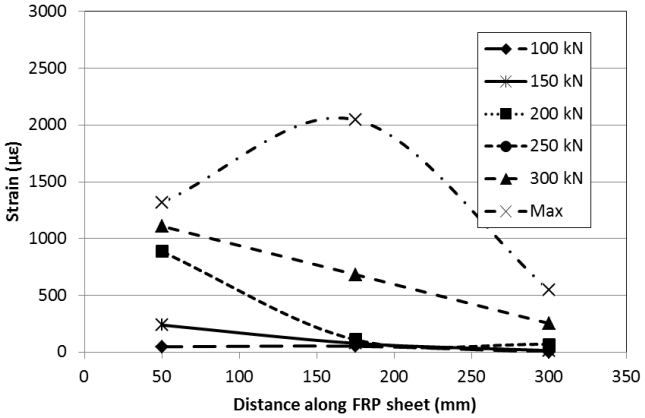

c) Strain profile – sheet 3

Figure 4-18: FRP strain response of beam 100G-200-A

4.2.4 Beams Strengthened with Sikawrap 430G-300 mm wide U-wraps

Two beams were strengthened with Sikawrap 430G-GFRP sheets (300 mm wide strips at a spacing of 375 mm o/c) placed as u-wraps. The failure mode of beam 430G-300-NA was in shear by loss of aggregate interlock with FRP debonding. The failure mode of beam 430G-300-A was in shear by loss of aggregate interlock with FRP rupture. The load deflection response of the GFRP strengthened beams with Sikawrap 430G sheets is shown in Figure 4-19. The strain response for the concrete at the top fiber and longitudinal steel reinforcement at mid-span is shown in Figure 4-21 and the strain response in the stirrups is presented in Figure 4-22. Figure 4-23 and Figure 4-24 show the GFRP strain response of the two beams.

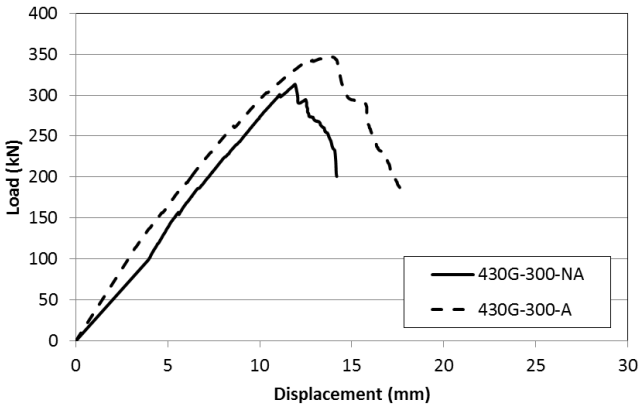

Figure 4-19: Load vs. deflection of beams strengthened with Sikawrap 430G-300 mm strips

The load deflection curves had a linear response with two stages. The first stage, flexural cracks appeared at a load of 65 kN and 55 kN for beams 430G-300-NA and 430G-300-A, respectively. As the load increased, inclined cracks began to develop in the shear span at a load of 160 kN and 188 kN for beams 430G-300-NA and 430G-300-A, respectively. It was observed that the diagonal tension shear cracks had a very steep slope between FRP sheets and a much shallower slope behind the FRP sheets (Figure 4-20a). Crack development occurred in both shear spans with the GFRP sheets in beam 430G-300-NA debonding from the top of the sheets at a load of 300 kN causing the load to drop 3 kN before increasing again to a load of 313 kN at which point the beam failed in shear.

Beam 430G-300-NA failed in shear by loss of aggregate interlock followed by FRP debonding at a load of 313 kN with maximum deflection of 11.9 mm. Beam 430G-300-A had no premature FRP debonding due to the presence of GFRP anchors. Failure initiated with a diagonal tension shear crack extending to the top of the beam. As the load was increased the crack progressed across the top surface of the beam until it reached the loading point (Figure 4-20b,c). Beam 430G-300-A failed in shear by loss of aggregate interlock with FRP sheet rupture at a load of 346 kN with a maximum deflection of 13.9 mm.

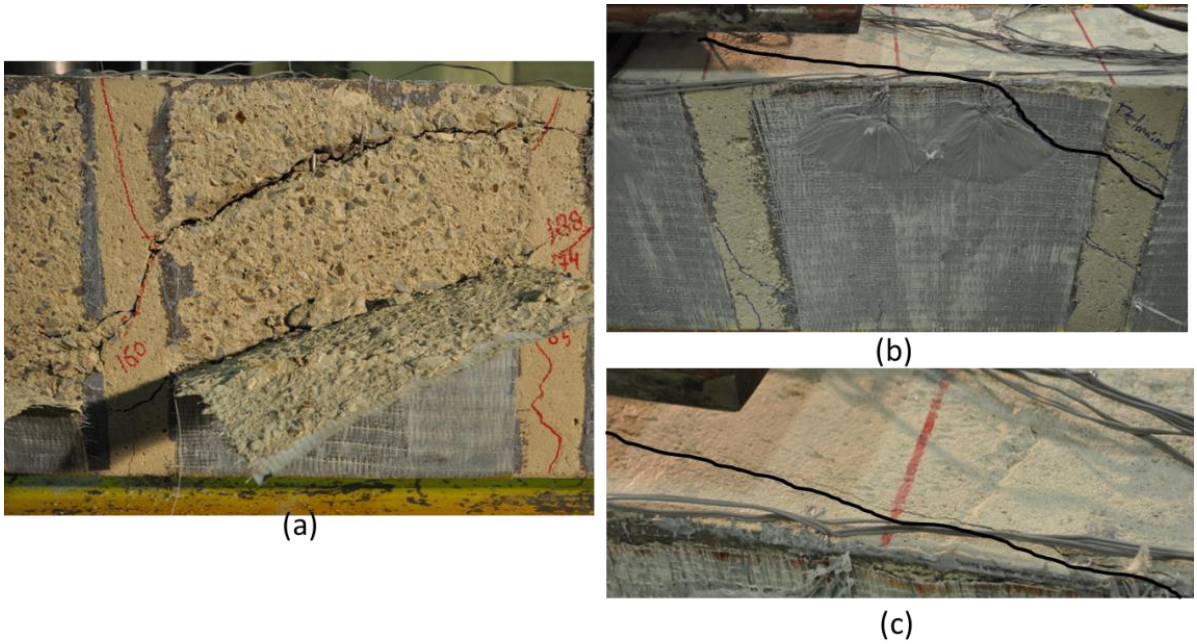

Figure 4-20: Failure mode of beam 430G-300-NA (a) aggregate interlock and FRP debonding and beam 430G-300-A (b) aggregate interlock and concrete crushing

The concrete strains at failure were below the crushing strain of concrete for both beams (Figure 4-21). The steel rebar strains were well below the yielding strain of steel recording 1416 με for beam 430G-300-NA. The strain gauges on the steel rebar in beam 430G-300-NA were not functioning (Figure 4-21). The strain response in the stirrups (Figure 4-20) showed that three stirrups exceeded the yield strain, reaching maximum strains of 2447 με (430G-300-NA-4th stirrup), 4450 με (430G-300-A-3rdstirrup) and 2109 με (430G-300-A-4th stirrup).

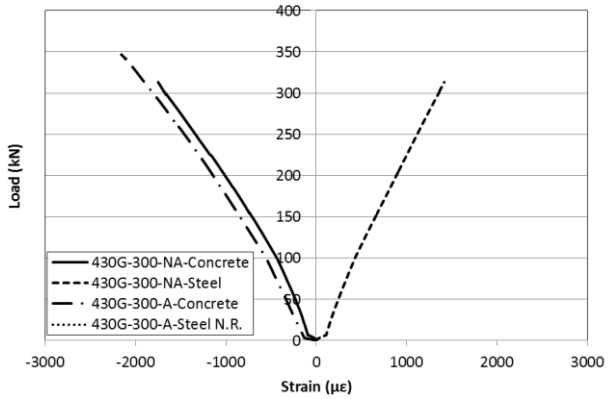

Figure 4-21: Concrete and steel rebar strain response of beams strengthened with Sikawrap 430G-300 mm wide strips

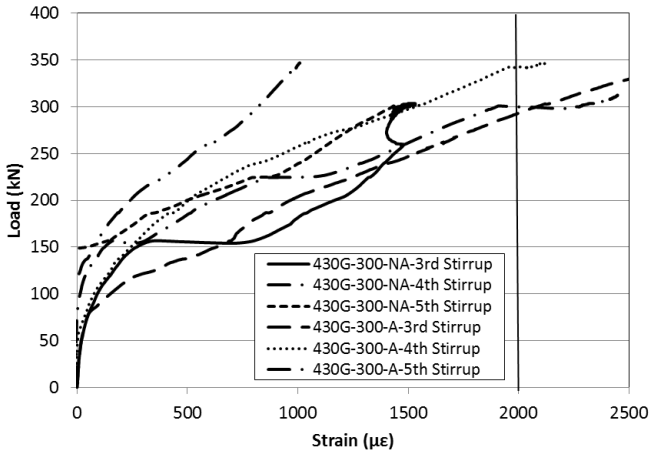

Figure 4-22: Stirrup strain response of beams strengthened with Sikawrap 430G-300 mm wide strips

The GFRP strain response across the depth of beam 430G-300-NA showed that three strain gauges recorded strains greater than 5000 με (Figure 4-23). The high strains were recorded on sheet 2 at 300 mm from the top of the beam and sheet 3 at mid-depth and 50 mm from the top of the beam. This showed that the shear crack propagated towards the top loading point as it travelled from sheet 2 (400 mm from the support) to sheet 3(680 mm from the support). The highest strain recorded in beam 430G-300-NA was 4694 με at 300 mm from the top in sheet 2 and 6331 με at 50 mm from the top in sheet 3.

The GFRP strain response across the depth of beam 430G-300-A exhibited higher FRP strains due to the presence of GFRP anchors (Figure 4-24). Four strain gauges recorded strains greater than 5000 με. The highest strain recorded on sheet 2 was at 50 mm from the top of the beam

(7592 με) and at mid-depth (6897 με). The highest strain recorded on sheet 3 was at mid-depth (5006 με) and 50 mm from the top of the beam (5087 με). Beam 430G-300-A with GFRP anchors was able to withstand higher strains in both sheets 2 and 3 over the unanchored beam 430G-300-NA. This shows that the presence of GFRP anchors increased the efficiency of the GFRP sheet.

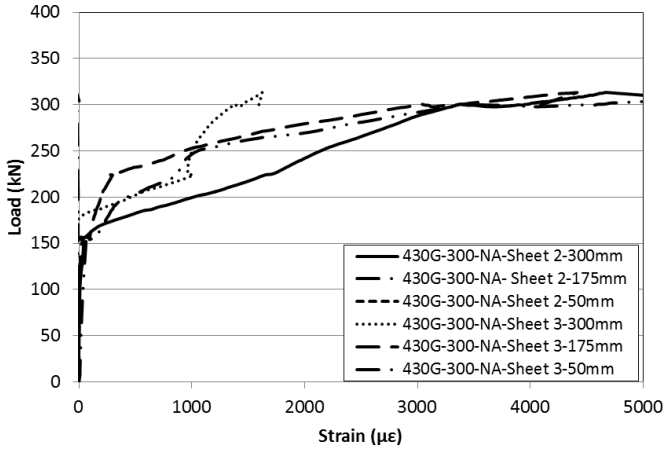

a) Load-strain curves

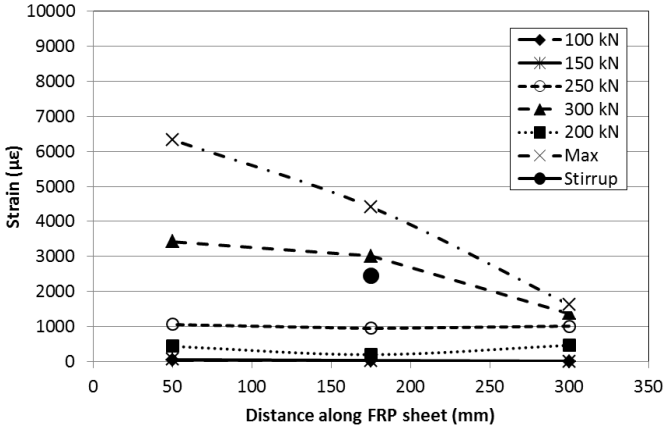

b) Strain profile – sheet 3

Figure 4-23: FRP strain response of beam 430G-300-NA

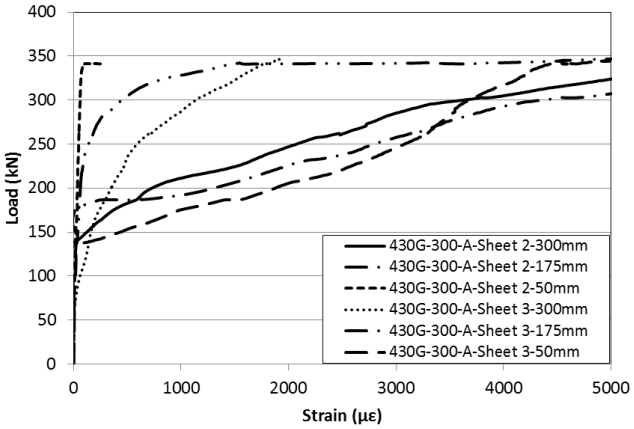

a) Load-strain curves

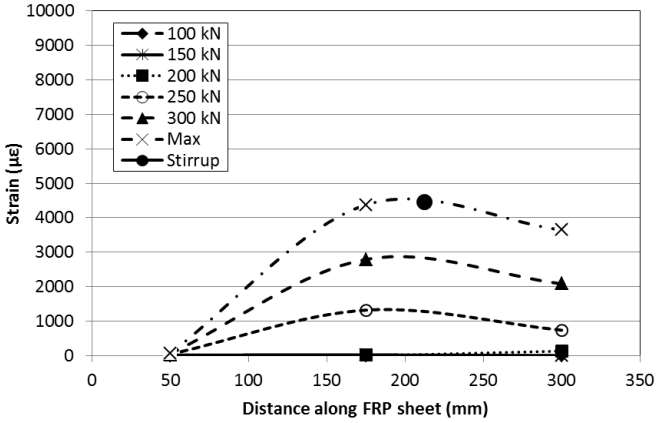

b) Strain profile – sheet 2

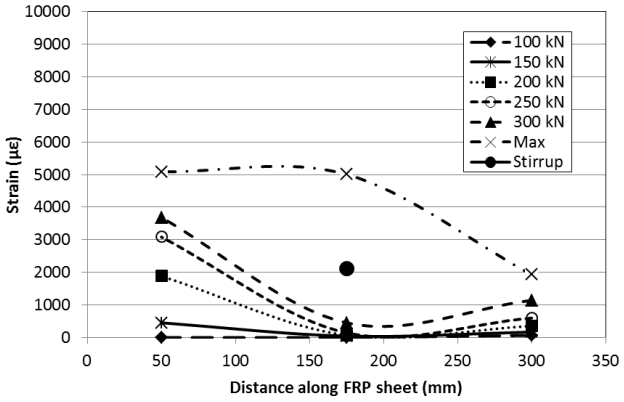

c) Strain profile – sheet 3

Figure 4-24: FRP strain response of beam 430G-300-A

4.2.5 Pre-cracked Beams Repaired with Sikawrap 430G-800 mm wide U-wraps

Three beams were pre-cracked to simulate a repair scenario. The beams were loaded to 85% of the ultimate capacity of the control beam (182 kN) to induce shear cracks and then unloaded. In the pre-cracking phase, the largest shear cracks that appeared in each of the beams were:

- PC-430G-800-NA - 615 mm long, 1.25 mm thick at an angle of 34.0^{o}
- PC-430G-800-A - 800 mm long, 1.25 mm thick at an angle of 21.8^{o}
- PC-430G-800-FW - 487 mm long, 0.50 mm thick at an angle of 28.1^{o}

After pre-cracking the beams, each beam was repaired with Sikawrap 430G sheets applied as continuous u-wraps (800 mm wide) in both shear spans. After GFRP repair, the beams were loaded until failure.

The failure mode of beam PC-430G-800-NA was in shear by loss of aggregate interlock followed by FRP debonding. Both anchored beams PC-430G-800-A and PC-430G-800-FW fully wrapped failed in shear by diagonal tension end anchorage failure followed by FRP rupture.

The load deflection curves of the three repaired beams with Sikawrap 430G sheets are shown in Figure 4-25. Monitoring the progression of cracks in the shear spans was difficult because they were covered with GFRP sheets. Flexural cracks at mid-span appeared at a load of 61 kN, 54 kN and 71kN for beams PC-430G-800-NA, PC-430G-800-A and PC-430G-800-FW, respectively.

The failure mode of beam PC-430G-800-NA occurred by GFRP sheet debonding and concrete splitting in the shear span. As the load was increased, debonding of the GFRP sheet occurred at 280 kN beginning from the top of the sheet. Because the entire shear span was wrapped, the crack did not reach the loading point. Instead the shear crack extended to the top surface of the beam and propagated longitudinally towards the loading point (Figure 4-26 a,b). When the crack reached the loading point failure occurred at 304 kN with a maximum deflection of 10.7 mm.

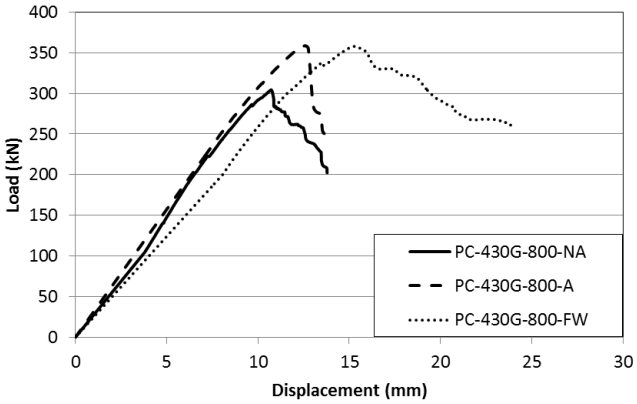

Figure 4-25: Load vs. deflection of beams repaired with Sikawrap 430G-800mm wide strips

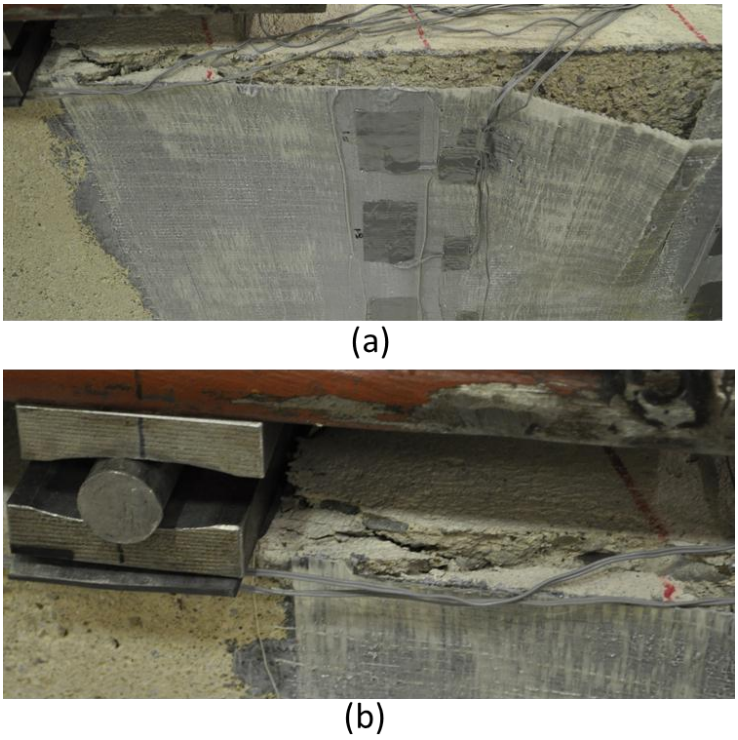

Figure 4-26: Aggregate interlock and FRP debonding failure of beam PC-430G-800-NA

The cracking in beam PC-430G-800-A advanced through the propagation of the existing shear cracks which were created during the pre-cracking stages. As the load was increased, no GFRP debonding occurred due to the presence of FRP anchors that were spaced every 100 mm. Because the entire shear region was wrapped, the cracks were not able to progress towards the loading point. Instead the shear crack extended to the un-wrapped area around the support end zone as shown in Figure 4-27. Failure occurred at 358 kN at a maximum deflection of 12.6 mm.

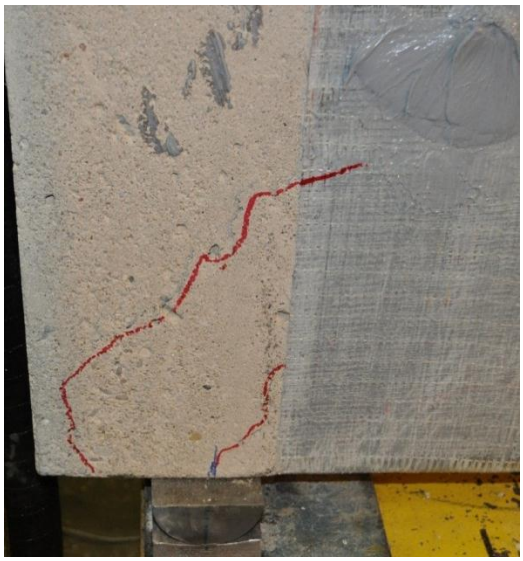

Figure 4-27: Diagonal tension end anchorage failure of beam PC-430G-800-A

Beam PC-430G-800-FW was completely wrapped, i.e. the GFRP sheet was wrapped around the entire cross-section of the beam with a 150 mm lap splice. The cracking in beam PC-430G-800-FW advanced through the propagation of existing shear cracks which were created in the pre-cracking stage. As the load was increased, no debonding of the GFRP sheet occurred. Because the entire shear region was fully wrapped, the shear crack did not progress towards the loading point. Instead the shear crack extended to the un-wrapped zone close to the support and end anchorage failure occurred (Figure 4-28). The load at failure was 358 kN with a maximum deflection of 15.3 mm.

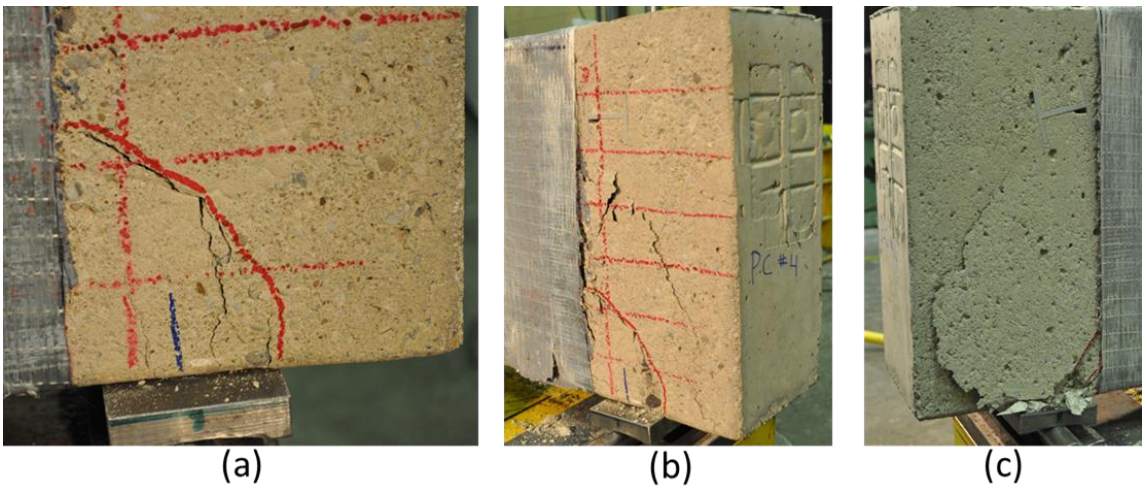

Figure 4-28: Diagonal tension end anchorage failure of beam PC-430G-800-FW

The post peak load vs. deflection behaviour showed the brittle nature of shear failure in both u-wrapped beams (PC-430G-800-NA, PC-430G-800-A). The fully wrapped beam exhibited shear failure with a gradual drop in load. The strain response for the concrete top fibers and longitudinal steel reinforcement at mid-span is shown in Figure 4-29. The strain response in the stirrups is presented in Figure 4-30. Figure 4-31, Figure 4-32 and Figure 4-33 show the GFRP strain response for these beams.

The maximum steel and concrete strains at failure were below the crushing strain of concrete and yield strain for steel in all beams (Figure 4-29). The strain response in the stirrups (Figure 4-30) showed three stirrups exceeded the yield strain, reaching maximum strains of 2704 με (PC-430G-800-NA-3rd stirrup), 2000 με (PC-430G-800-A-4th stirrup) and 2309 με (PC-430G-800-FW-4th stirrup).

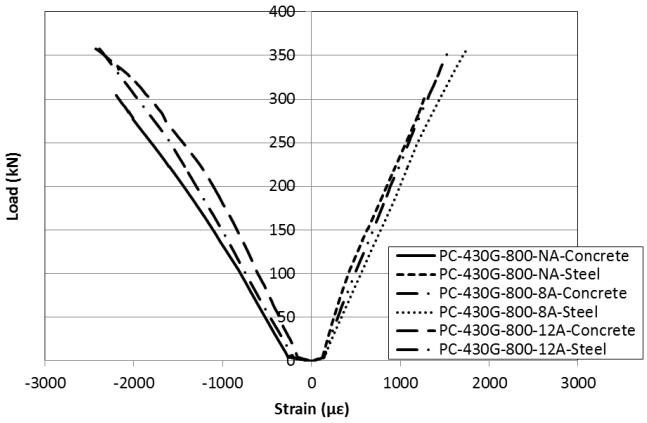

Figure 4-29: Concrete & steel rebar strain response of PC-430G-800mm wide GFRP beams

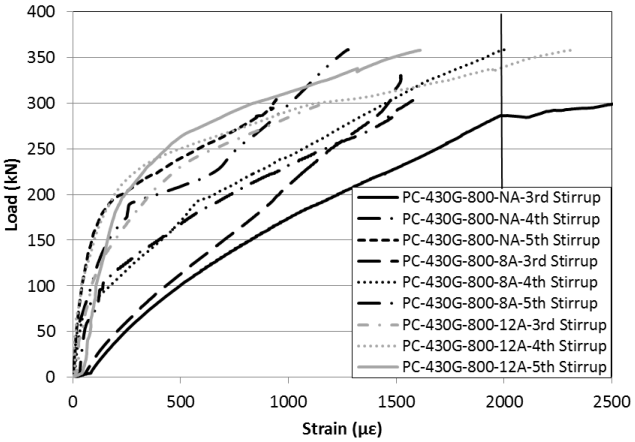

Figure 4-30: Stirrup strain response of PC-430G-800 mm wide GFRP beams

Each beam had two sets of FRP strain gauges per sheet; located at 300 mm and 600 mm from the support. Each set contained three strain gauges: one gauge was placed 50 mm from the top of the beam, one gauge was located at mid-depth and one gauge was placed 300 mm from the top of the beam.

The GFRP strain response of beam PC-430G-800-NA showed that two strain gauges recorded strains greater than 3000 με (Figure 4-31). The high strains were 3343 με (300 mm from the support and 300 mm from the top of the beam) and 3490 με (600 mm from the support and 50 mm from the top of the beam). This shows that the induced shear crack behind the GFRP sheet in the shear span was causing stresses in the continuous GFRP sheet to propagate from the bottom support towards the top loading point.

The GFRP strain response of beam PC-430G-800-A showed higher FRP strains (Figure 4-32), this can be attributed to the presence of GFRP anchors. Two strain gauges recorded strains greater than 4000 με. The highest strains were recorded at mid-span in both set 1(4680 με, 300 mm from the support) and set 2 (4043 με, 600 mm from the support). These results indicate that the presence of GFRP anchors spaced every 100 mm along the length of the sheet caused the strain in the FRP sheet to be distributed equally preventing any localized strains in the FRP sheet due to the diagonal tension shear crack.

The GFRP strain response of beam PC-430G-800-FW (Figure 4-33) showed higher FRP strains than the anchored sheet in beam PC-430G-800-A. This can be attributed to the use of full wrapping. Two strain gauges recorded strains greater than 6000 με. The highest strains were recorded at mid-span in both set 1 (6391 με, 300 mm from the support) and set 2 (6966 με, 600 mm from the support). All strain gauges located at 600 mm from the support recorded strains above 3000 με.

Beam PC-430G-800-A with GFRP anchors was able to withstand higher strains in over the unanchored beam PC-430G-800-NA but did not reach the same strains experienced in the fully wrapped beam PC-430G-800-FW. These results show that the presence of GFRP anchors increased the efficiency of the GFRP sheets.

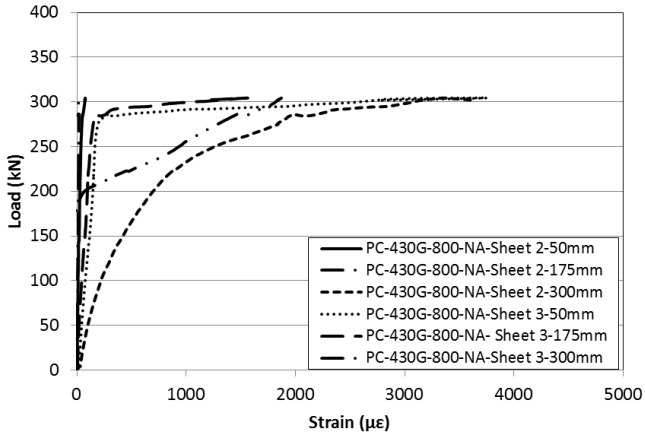

a) Load-strain curves

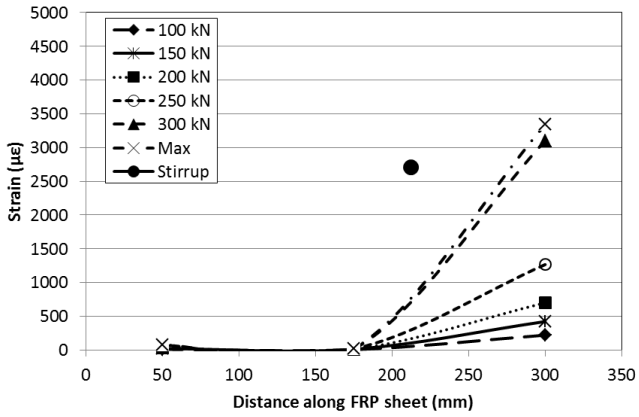

b) Strain profile for set 1 – 300 mm

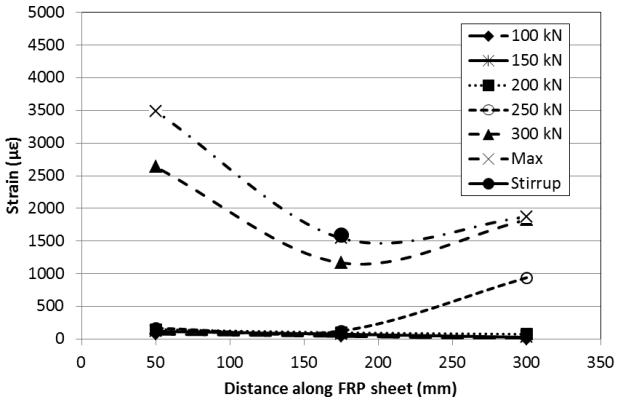

c) Strain profile for set 2 – 600 mm

Figure 4-31: FRP strain response of beam PC-430G-800-NA

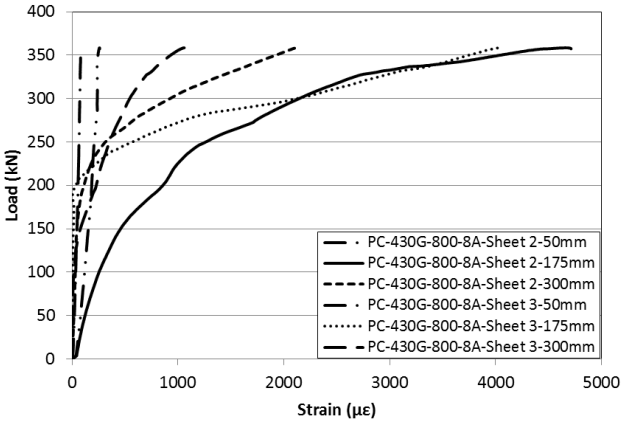

a) Load-strain curves

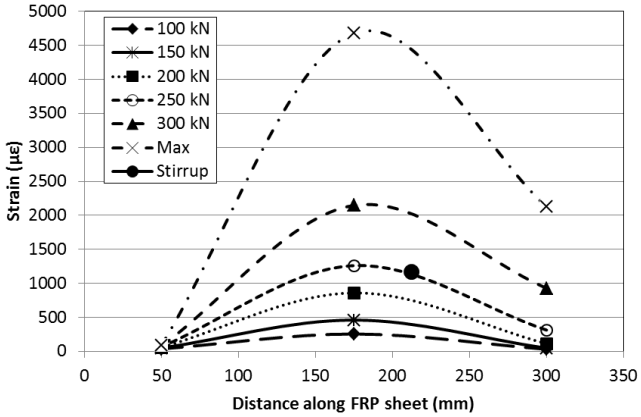

b) Strain profile for set 1 – 300 mm

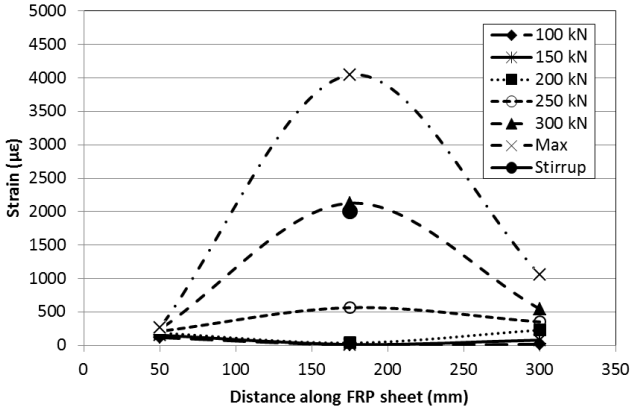

c) Strain profile for set 2 – 600 mm

Figure 4-32: FRP strain response of beam PC-430G-800-A

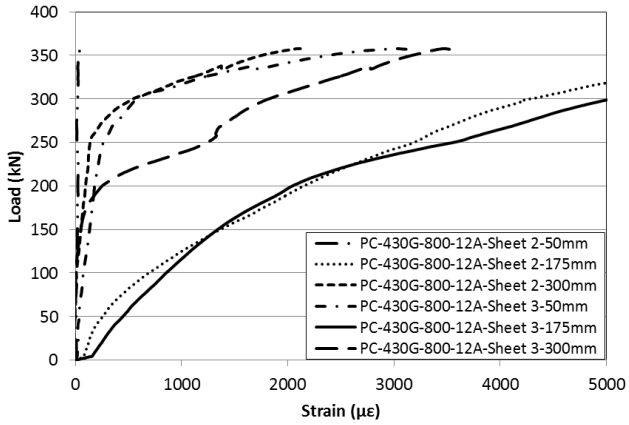

a) Load-strain curves

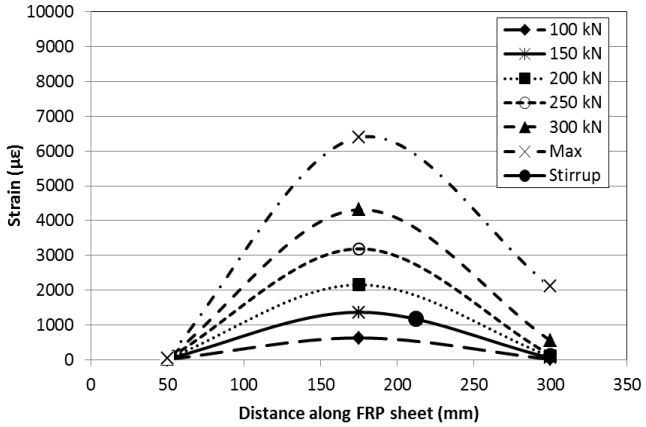

b) Strain profile for set 1 – 300 mm

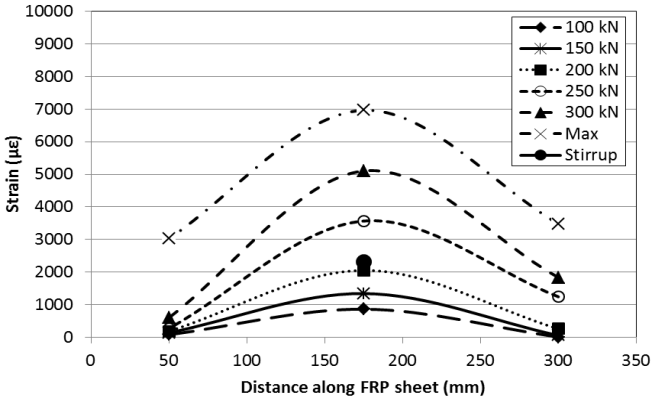

c) Strain profile for set 2 – 600 mm

Figure 4-33: FRP strain response of PC-430G-800-FW

4.2.6 Pre-cracked Beams Repaired with Sikawrap 100G-1100 mm wide U-wraps

Two beams were pre-cracked then repaired with GFRP wraps similar to those described in Section 4.2.5. These two beams were repaired with Sikawrap 100G sheets (1100 mm wide) applied as a continuous u-wrap in both shear spans. GFRP sheets extended 120 mm from the beam support and 100 mm past the loading point. The Sikawrap 100G sheets were 1.016 mm thick and were applied with Sikadur 300 epoxy.

In the pre-cracking phase, the largest shear cracks in the shear span of these beams were:

- PC-100G-1100-NA - 466 mm long, 0.40 mm thick at an angle of 31^{o}
- PC-100G-1100-A - 538 mm long, 0.80 mm thick at an angle of 34^{o}

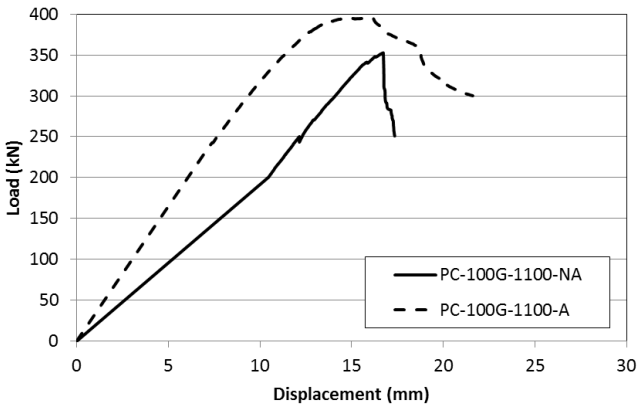

Figure 4-34: Load vs. deflection of beams repaired with Sikawrap 100G-1100mm wide strips

The load deflection curves of the two beams repaired with Sikawrap 100G sheets are shown in Figure 4-34. The load deflection curves showed a linear response up to failure. It was difficult to monitor the progression of the pre-existing shear cracks because the entire beam was covered with GFRP sheet. The failure mode of beam PC-100G-1100-NA was in shear by loss of aggregate interlock followed by FRP debonding. Beam PC-100G-1100-A with anchors failed in shear by diagonal tension end anchorage failure.

In beam PC-100G-1100-NA, as the load was increased debonding of the FRP sheet occurred at a load of 340 kN at the top of the sheet (Figure 4-35a). It was evident that the shear crack extended to the top face of the beam and progressed transversely towards the loading point (Figure 4-35b).

When the crack reached the loading point failure occurred at a load of 352 kN with a maximum deflection of 16.7 mm. The post peak behaviour showed the brittle nature of shear failure.

In beam PC-100G-1100-A, as the load was increased no FRP debonding occurred due to the presence of FRP anchors spaced every 100 mm. Because the entire shear region was wrapped, the crack did not progress towards the loading point. Instead the shear crack extended past the support where end anchorage failure occurred at 395 kN with a maximum deflection of 21.5 mm.

The strain response for the concrete top fibers and longitudinal steel reinforcement at mid-span is shown in Figure 4-37. The stirrup strain response is presented in Figure 4-38. Figure 4-39 and Figure 4-40 show the GFRP strain response for both beams.

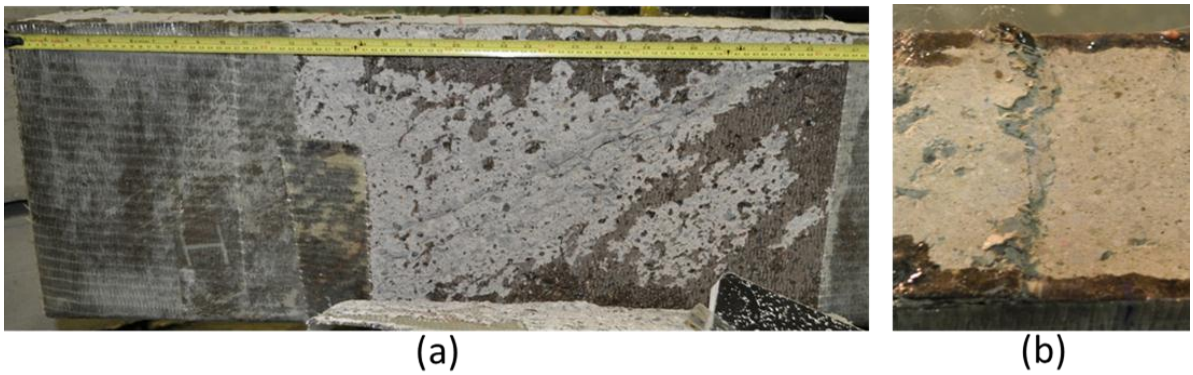

Figure 4-35: Aggregate interlock & FRP debonding failure of beam PC-100G-1100-NA

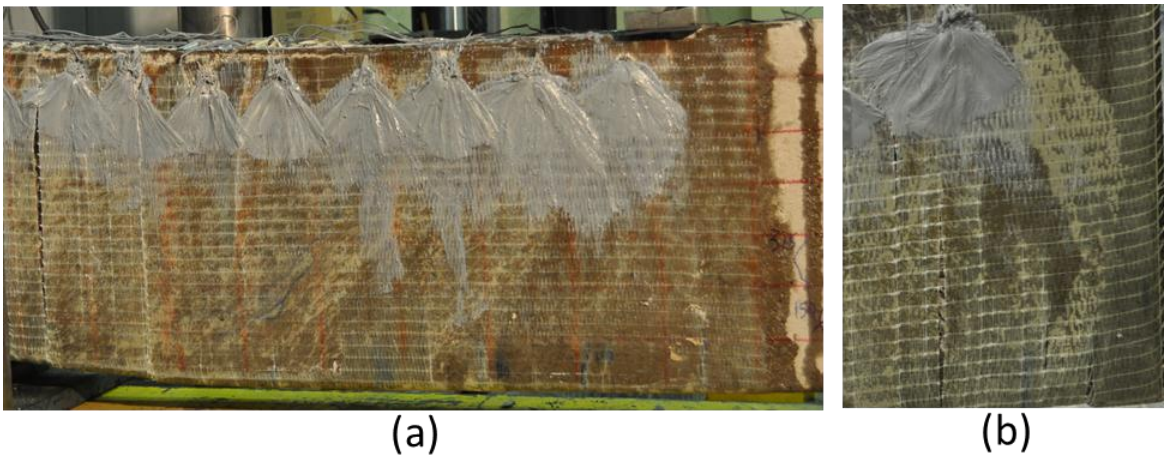

Figure 4-36: Diagonal tension end anchorage failure of beam PC-100G-1100-A

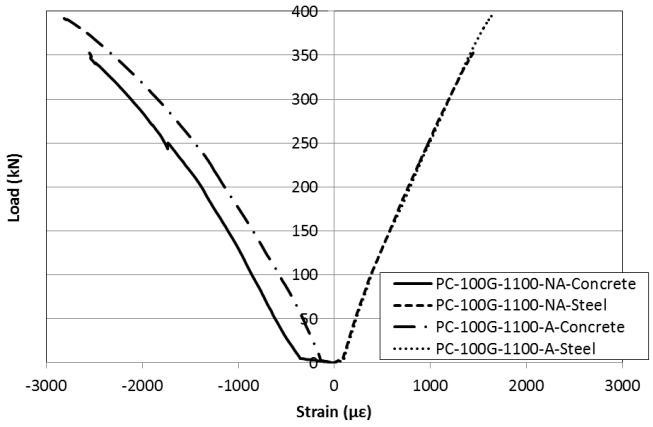

Figure 4-37: Concrete & steel rebar strain response of PC-100G-1100mm wide beams

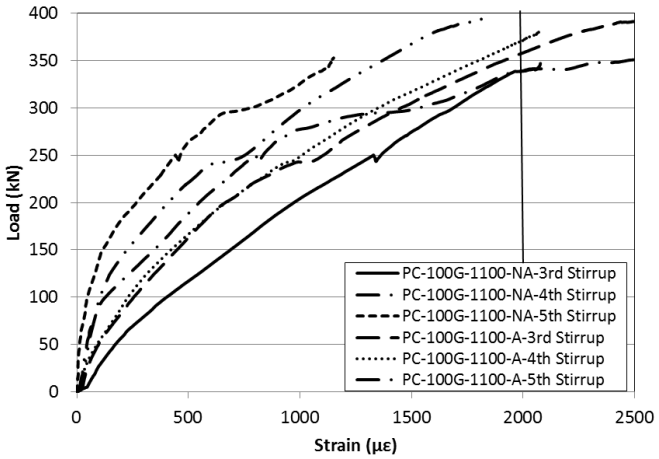

Figure 4-38: Stirrup strain response of PC-100G-1100mm wide GFRP beams

The steel and concrete strains at failure were below the crushing strain of concrete and yield strain for steel for all beams (Figure 4-37). The strain response in the stirrups (Figure 4-38) showed that four stirrups exceeded the yield strain (Beam 20 – 3rd and 4th and Beam 21 – 3rd and 4th), reaching maximum strains of 2077 με (PC-100G-1100-NA-3rd stirrup), 2532 με (PC-100G-1100-A-4th stirrup), 2700 με (PC-100G-1100-A-3rd stirrup) and 2080 με (PC-100G-1100-A-4th stirrup).

Each beam had of two sets of FRP strain gauges per sheet; located at 400 mm and 600 mm from the support. Each set contained three strain gauges: one gauge was placed 50 mm from the top of the beam, one gauge was located at mid-depth and one gauge was placed 300 mm from the top of the beam.

The GFRP strain response of beam PC-100G-1100-NA showed that four strain gauges recorded strains greater than 2000 με (Figure 4-39). The highest strains recorded on sheet 2 (400 mm from the support) were 3302 με and 2368 με at mid-depth and 100 mm from the top of the beam, respectively. The highest strains recorded on sheet 3 (600 mm from the support) were 2825 με and 2119 με at mid-depth and 100 mm from the top of the beam, respectively. This shows that a consistent strain was experienced throughout the continuous GFRP sheet in the shear span.

The GFRP strain response across the depth of beam PC-100G-1100-A showed even higher FRP strains were recorded over beam PC-100G-1100-NA. Three gauges recording strains greater than 4000 με and two gauges recorded strains greater than 2000 με (Figure 4-40).

The highest strains recorded on sheet 2 (400 mm from the support) were 6598 με at mid-depth and 5038 με, 100 mm from the top of the beam. The highest strains recorded on sheet 3 (600 mm from the support) were 2304 με at mid-depth and 4129 με, 100 mm from the top of the beam. These results indicate that the presence of GFRP anchors spaced every 100 mm along the length of the sheet caused the strain in the FRP sheet to be distributed equally preventing localized strains in the FRP sheet from the diagonal tension shear crack.

Therefore, beam PC-100G-1100-A with GFRP anchors was able to withstand higher strains over the unanchored beam PC-100G-1100-NA showing the benefits of providing FRP anchors.

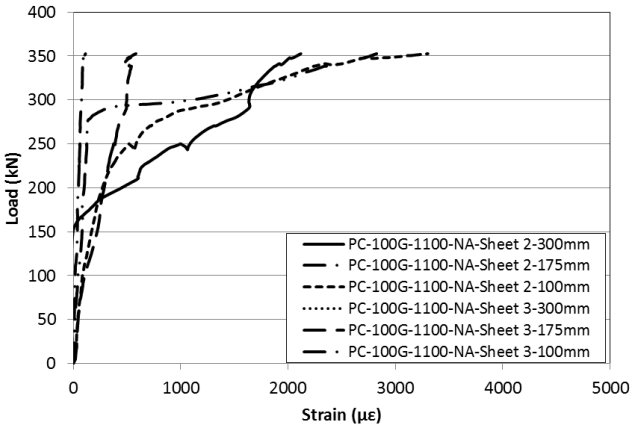

a) Load-strain curves

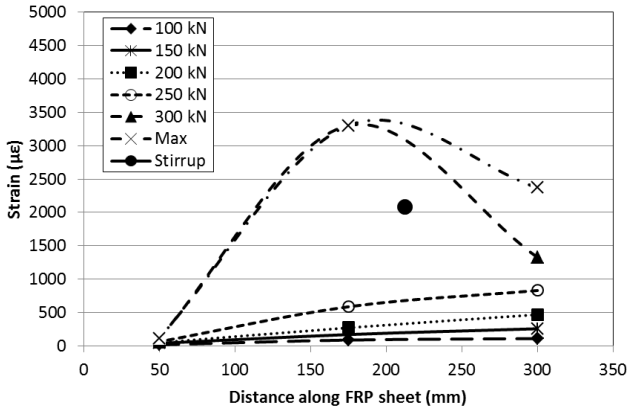

b) Strain profile for set 1 – 400 mm

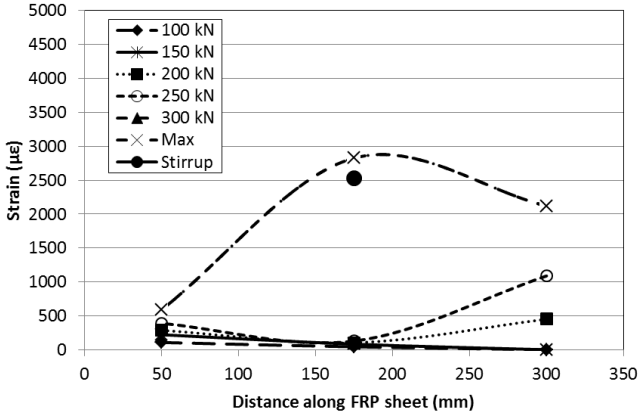

c) Strain profile for set 2 – 600 mm

Figure 4-39: FRP strain response of PC-100G-1100-NA

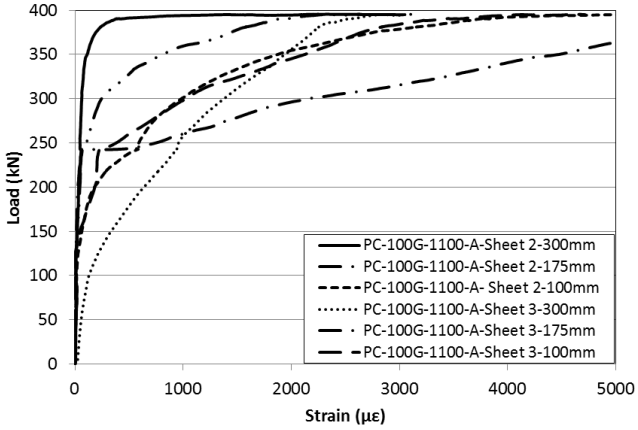

a) Load-strain curves

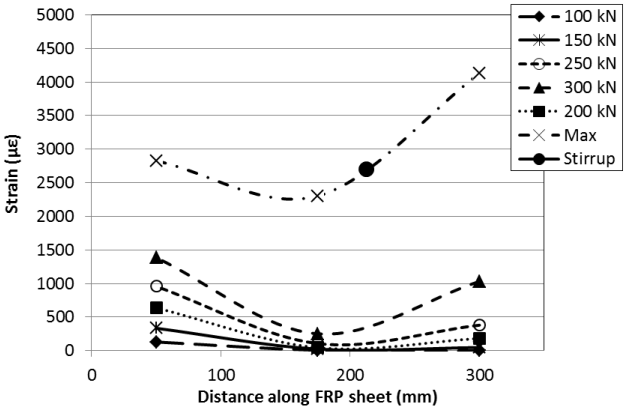

b) Strain profile for set 1 – 400 mm

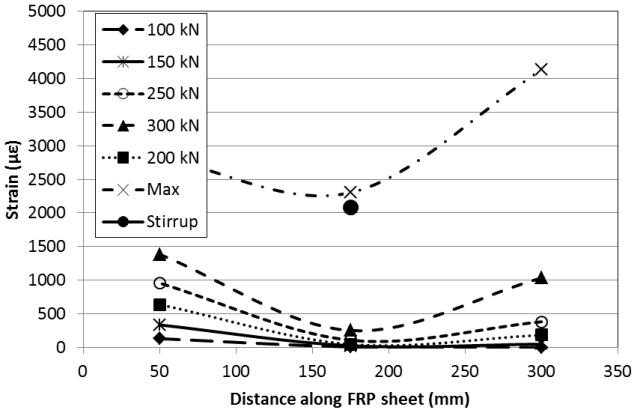

c) Strain profile for set 2 – 600 mm

Figure 4-40: FRP strain response of PC-100G-1100-A

4.3 Flexure Critical Slabs – Series II

Eight flexure critical slabs were strengthened with two types of CFRP sheets. One slab was tested as control (unstrengthened), three slabs were strengthened with Sikawrap 230C sheets and four slabs were strengthened with Sikawrap 600C sheets. The test variables were:

1. Type of CFRP sheet: Sikawrap 230C and Sikawrap 600C
2. Number of CFRP layers: 1 layer of 230C (t=0.381 mm)
2 layers of 230C (t=0.762 mm)
1 layer of 600C (t=1.30 mm)
2 layers of 600C (t=2.60 mm)
3. Use of FRP anchors: No anchors vs. CFRP anchors
4. Number of FRP anchors 8 anchors vs. 12 anchors

The CFRP sheets were applied as continuous sheets with fibers in the longitudinal direction on the bottom soffit of the slab. Table 4-2summarizes the test results including: ultimate load, deflection at ultimate load, percent increase over the control and mode of failure for all slabs. The failure mode notation highlights the principal failure mode which caused failure in each beam. Descriptions of each acronym are provided at the bottom of Table 4-2. Determining if FRP debonding FRP rupture or concrete cover failure occurred was verified visually and recorded.

Table 4-2: Series 3 - Summary of test results for CFRP strengthened slabs

Nomenclature	Specimen Description	Ultimate Load (kN)	Deflection at ultimate load (mm)	Percent increase over the control (%)	Failure mode
Control	Control	132	36.1	-	• FF
230C-1L-NA	230C-1 layer-No anchors	174	24.6	31.8	• FRP R
230C-2L-NA	230C-2 layers-No anchors	190	20.6	43.9	• FRP-D
230C-2L-8A	230C-2 layers-8 Anchors	201	20.1	52.3	• CAF & AR
600C-1L-NA	600C-1 layer-No anchors	186	15.1	40.9	• FRP-D
600C-2L-NA	600C-2 layers-No anchors	192	10.6	45.5	• FRP-D, CCF
600C-2L-8A	600C-2 layers-8 anchors	228	13.2	72.7	• CCF
600C-2L-12A	600C-2 layers-12 anchors	219	12.1	65.9	• IFSD

where: FF=Flexural failure with concrete crushing, FRP R=FRP rupture, FRP D=FRP debonding, CAF=Concrete cone anchor failure, AR=Anchor rupture, CCF=Concrete cover failure, IFSD=Intermediate flexural shear crack induced interfacial debonding

4.3.1 Control Slab

The failure mode of the control slab was a flexural failure by yielding of the longitudinal steel reinforcement followed by crushing of the concrete (Figure 4-41).

The load deflection response of the control slab is shown in Figure 4-42. The load deflection curve showed a tri-linear response with three distinct stages: the first stage before cracking, the second stage after cracking and third stage after yielding. Cracking initiated as flexural cracks at mid-span between the two loading points with the first crack appearing at a load of 21 kN. As the load increased, more flexural cracks began to develop.

The load vs. deflection curve began to flatten out when the longitudinal steel rebar yielded. This is confirmed by the steel strain response in Figure 4-43. The beam exhibited a very ductile response beyond the yield load up to the ultimate stage. The peak load of 132 kN was reached with a maximum deflection of 32.1 mm. After failure, a gradual drop in load with deflection was exhibited.

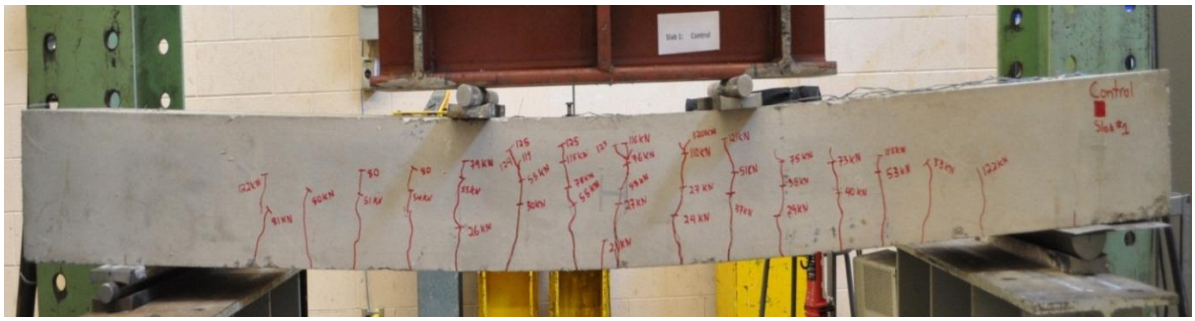

Figure 4-41: Flexural failure of control slab (series II)

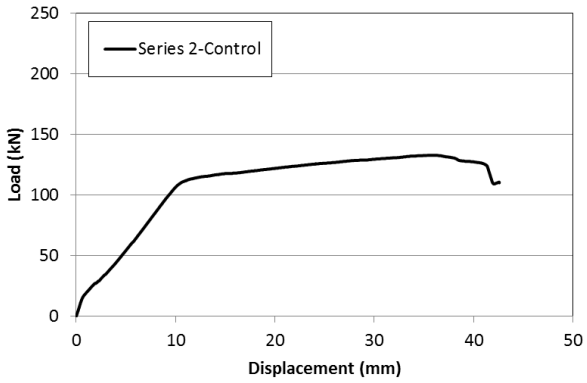

Figure 4-42: Load vs. deflection of control slab (series II)

The strain gauge readings for the concrete top fiber and the longitudinal steel reinforcement at mid-span are presented in Figure 4-43. The concrete strain exceeded the strain to cause concrete crushing (ε_{cu}= -3500 με) reaching a maximum strain of -4768 με (Figure 4-43). The strain in the longitudinal steel bars surpassed the yield strain (ε_s=2400 με) as shown in Figure 4-43. The strain response of the longitudinal steel indicates that both steel rebar yielded. The maximum strain in the longitudinal steel bars was 16,048 με. The strain data correlates with the load deflection curve indicating that the mode of failure was a ductile flexural failure.

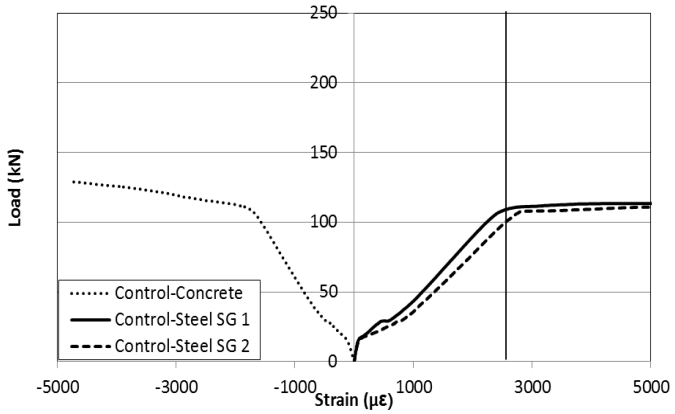

Figure 4-43: Concrete and steel rebar strain response of control beam (series II)

4.3.2 Slabs Strengthened with Sikawrap 230C – Single Layer

One slab was strengthened with one layer of Sikawrap 230C CFRP sheet (300 mm wide, 1700 mm long). The sheet extended the full length of the slab and was stopped at 250 mm from each slab end. The Sikawrap 230C sheet was 0.381 mm thick and was applied with Sikadur 330 epoxy. The failure mode of slab 230C-1L-NA was CFRP rupture (Figure 4-44). The load deflection response of the CFRP strengthened slab is shown in Figure 4-45.

Figure 4-44: FRP rupture of 230C-1L-NA

The load deflection curve showed a tri-linear response with three distinct stages. The first flexural crack appeared at a load of 34 kN. As the load increased, additional flexural cracks began to develop in the span. The strengthened specimen exhibited a less ductile response between the yielding and ultimate stages in comparison to the control (unstrengthened). Failure occurred when the CFRP sheet ruptured at a load of 174 kN and a maximum deflection of 24.6 mm. The post peak behaviour of the load vs. deflection curve shows a sudden brittle failure with rupture of the CFRP sheet.

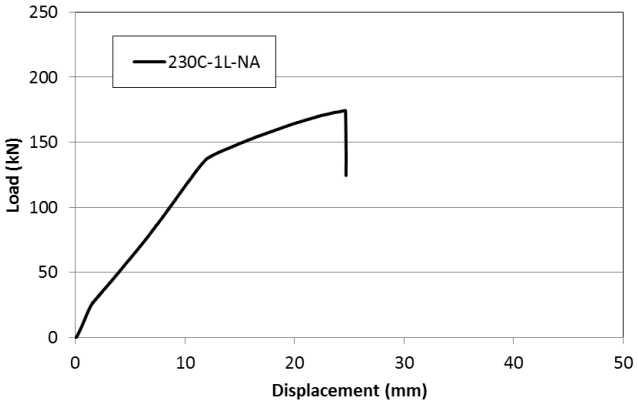

Figure 4-45: Load vs. deflection of slab 230C-1L-NA

The strain gauge response for the concrete top fiber and longitudinal steel reinforcement at mid-span are presented in Figure 4-46. Figure 4-47 shows the CFRP strain response. At failure, the concrete strain was -3516 με which exceeds the concrete crushing strain (ε_{cu}= -3500 με). The strain in the longitudinal steel bars were well above the yield strain (ε_s=2400 με). The maximum strain measured in the longitudinal steel bars was 17585 με.

The CFRP strain response had a tri-linear behaviour. Initially, little or no strain was resisted by the CFRP sheet at mid-span (stage 1). When the slab reached a load of 50 kN the sheet began to pick up strain and had a reduced slope (stage 2). This continued until the load reached 140 kN at which point the internal steel rebar began to yield. As yielding in the flexural steel reinforcement occurred, the CFRP sheet continued to resist the applied load causing the strain in the CFRP sheet to increase until failure (174 kN). The highest strain in the CFRP sheet was experienced at the mid-span and under the loading point as 10,000 με.

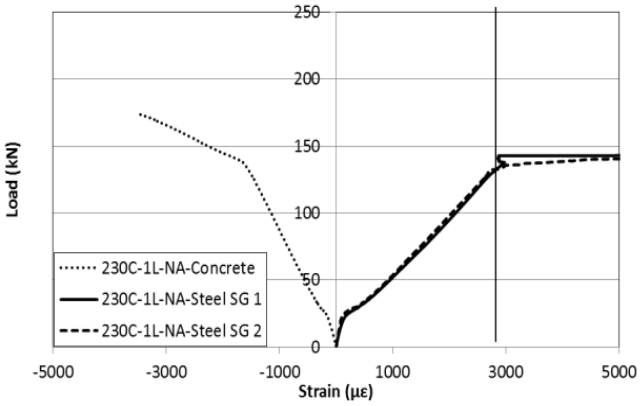

Figure 4-46: Concrete and steel rebar strain response of 230C-1L-NA

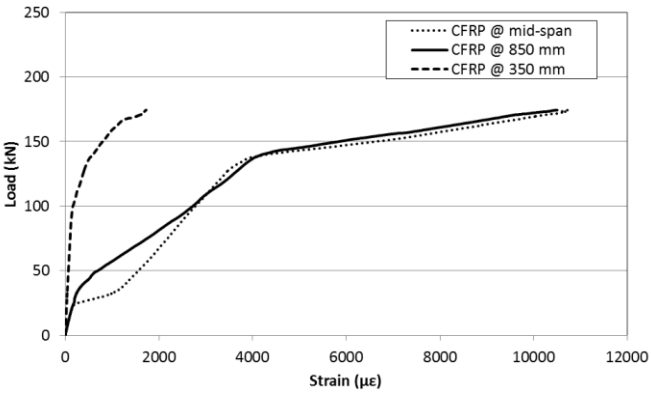

Figure 4-47: FRP strain response of 230C CFRP strengthened slab

4.3.3 Slabs Strengthened with Sikawrap 230C – Multi-layers

Two slabs were strengthened with two layers of Sikawrap 230C sheets (300 mm wide, 1700 mm long). The CFRP sheets extended the full length of the slab beginning at 250 mm from each end of the slab. The two layers of Sikawrap 230C sheets were 0.762 mm thick and were applied with Sikadur 330 epoxy one sheet on top of another. One slab had no anchors and the other slab had eight 175mm long CFRP anchors installed at 100 mm depth into the slab. Four anchors were placed on each side of the slab. The first set of two anchors was installed at 280 mm from each end of the slab (80 mm from the end of the CFRP sheet) spaced 100 mm apart. The second set of anchors was located directly under the loading point of the slab (570 mm from each end of the slab) spaced 100 mm apart.

The failure mode of slab 230C-2L-NA (with no anchors) was CFRP debonding which initiated from the end of the sheets and progressed inwards (Figure 4-48 a,b). The failure mode of slab

230C-2L-8A (with eight CFRP anchors) was concrete cone anchor failure at the end of the sheet (Figure 4-49 a-c) followed by FRP debonding and CFRP anchor rupture (Figure 4-49 d,e). The CFRP concrete cone anchor failure was consistent with failures observed in the literature (Chaallal, et al., 1998).

Figure 4-48: FRP debonding failure of slab 230C-2L-NA

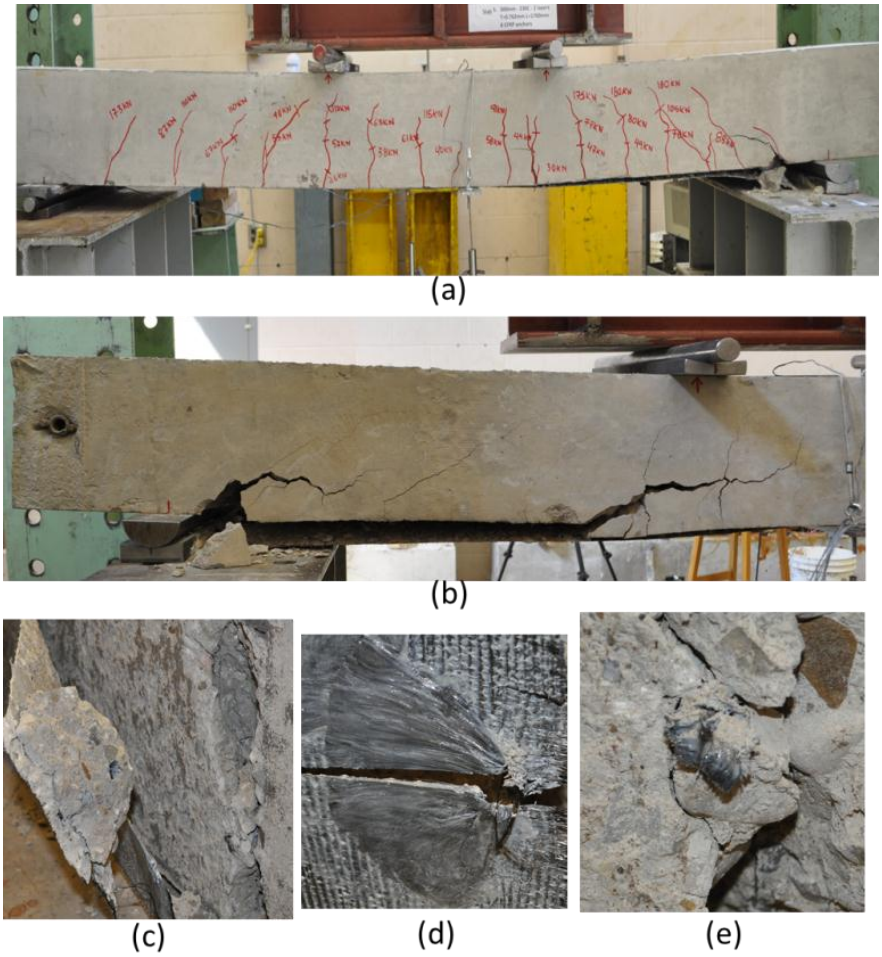

Figure 4-49: Concrete cone anchor failure and anchor rupture of slab 230C-2L-8A

The load deflection response of the multi-layered CFRP strengthened slabs is shown in Figure 4-50. The strain gauge response for the concrete top fiber and longitudinal steel reinforcement at mid-span is presented in Figure 4-51. Figure 4-52 and Figure 4-53 show the CFRP strain response.

The load deflection curves for both slabs showed a tri-linear response with three stages (Figure 4-50). Flexural cracks appeared at a load of 34 kN and 36 kN for slabs 230C-2L-NA and 230C-2L-8A, respectively. As the load increased, flexural cracks began to develop in the span.

Failure in slab 230C-2L-NA occurred when the CFRP sheet debonded at a load of 190 kN at a maximum deflection recorded of 20.6 mm. The post peak behaviour of slab 230C-2L-NA exhibited a gradual CFRP sheet debonding. Failure in slab 230C-2L-8A occurred when the concrete around the anchor failed prematurely as a cone and the CFRP anchor fibers ruptured. The maximum load recorded was 201 kN at a maximum deflection of 20.1 mm. The post peak behaviour of slab 230C-2L-8A showed a sudden brittle failure with a steep drop in load.

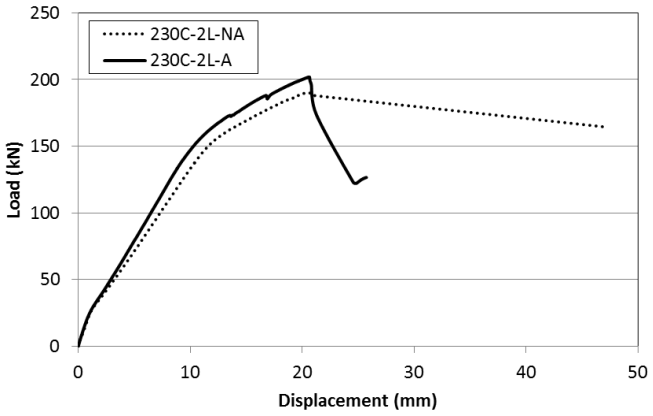

Figure 4-50: Load vs. deflection of slabs 230C-2L-NA and 230C-2L-8A

In slab 230C-2L-NA the concrete did not reach the crushing strain recording a maximum strain of -2689 με. However, in slab 230C-2L-A the concrete reached concrete crushing strain recording a maximum strain of -3500 με (Figure 4-51). The strain in the longitudinal steel rebar (Figure 4-51) exceeded the yield strain (ε_s=2400 με) in both slabs reaching maximum strains of 12,998 με and 21,785 με in slabs 230C-2L-NA and 230C-2L-8A, respectively.

The CFRP strain response for slab 230C-2L-NA showed a tri-linear behaviour (Figure 4-52). Initially little or no strain was resisted by the CFRP sheets at mid-span (stage 1). The CFRP sheet began to pick up strain when the slab reached a load of 50 kN with a reduced slope until the load reached 150 kN and the steel rebar began to yield (stage 2). As yielding in the flexural steel reinforcement occurred, the CFRP sheet continued to resist the applied load causing the strain in the CFRP sheet to increase until failure (190 kN). The highest strains in the CFRP sheet were experienced at mid-span (7798 με) and under the loading point (8018 με). These strain values were less than those experienced by the single layer of CFRP strengthening provided in slab 230C-1L-NA.

The CFRP strain response of the anchored slab 230C-2L-8A showed a tri-linear behaviour (Figure 4-53) with softer transitions. The CFRP sheet began to pick up strain at a much lower load (25 kN) with a reduced slope until the load reached 150 kN and the steel rebar began to yield. Again, as yielding in the flexural steel reinforcement occurred, the CFRP sheet continued to resist the applied load causing the strain in the CFRP sheet to increase until failure (201 kN). The CFRP strain response showed that the highest strains were experienced at mid-span (8978 με) and under the loading point (5195 με). Comparing these results to the unanchored slab, the presence of CFRP anchors allowed for an increase in strain of 1000 με in the CFRP sheet at mid-span before failure occurred.

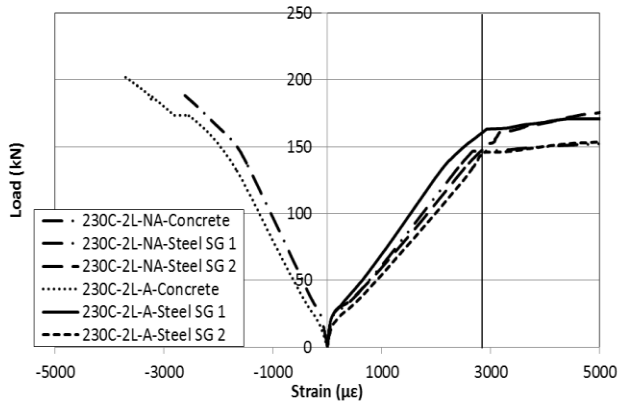

Figure 4-51: Concrete and steel rebar strain response of slabs 230C-2L-NA & 230C-2L-8A

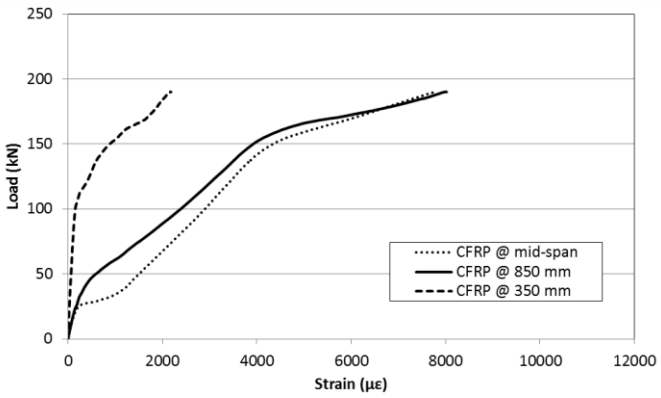

Figure 4-52: FRP strain response of slab 230C-2L-NA

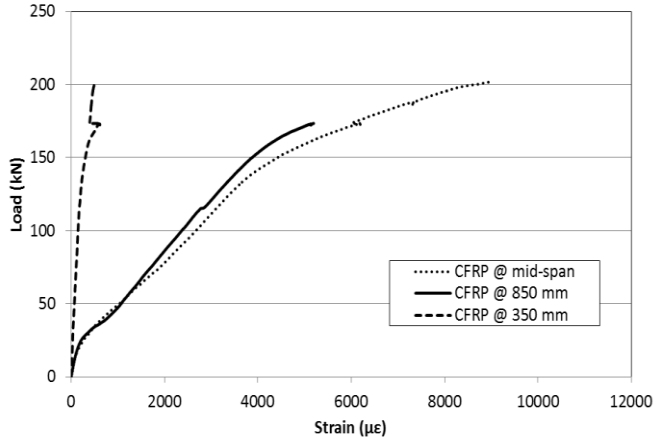

Figure 4-53: FRP strain response of slab 230C-2L-8A

4.3.4 Slabs Strengthened with Sikawrap 600C – Single Layer

Slab 600C-1L-NA was strengthened with one layer of Sikawrap 600C sheet (300 mm wide, 1700 mm long). The CFRP sheet extended the full length of the slab beginning at 250 mm from each end. The Sikawrap 600C sheet was 1.30 mm thick and was applied with Sikadur 300 epoxy. The failure mode of slab 600C-1L-NA was CFRP debonding that initiated at the end of the sheet and progressed inwards (Figure 4-54).

Figure 4-54: FRP debonding of slab 600C-1L-NA

The load deflection response of slab 600C-1L-NA is shown in Figure 4-55. The load deflection curve showed a tri-linear response with three stages. Flexural cracks appeared at a load of 26 kN. As the load increased, flexural cracks began to develop in the span of the slab. Failure occurred when the CFRP sheet debonded at a load of 186 kN at a maximum deflection of 15.1 mm. The post peak behaviour was a sudden, brittle failure by debonding of the CFRP sheet.

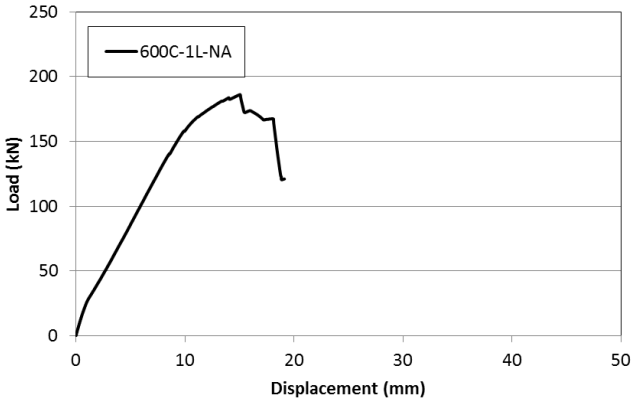

Figure 4-55: Load vs. deflection of a slab 600C-1L-NA

The strain response for the concrete at the top fiber and the longitudinal steel reinforcement are presented in Figure 4-56. The concrete strain at failure was below the crushing strain in the concrete and the strain in the steel rebar exceeded the yield strain (ε_s=2400 με). The maximum strain in the steel rebar was 15,950 με and 5461 με.

Figure 4-55 shows the CFRP strain response of slab 600C-1L-NA. The CFRP strain response showed a tri-linear behaviour. Initially no strain was recorded by the CFRP sheet (stage 1). The CFRP sheet began to pick up strain at a load of 25 kN with a lower slope until the load reached 160 kN and the steel began to yield (stage 2). The CFRP sheet continued to resist load causing the strain in the CFRP sheet to increase until failure (186 kN). The highest CFRP strains were experienced at mid-span (7006 με) and under the loading point (6666 με). The thicker Sikawrap 600C sheet experienced much lower strains at failure compared to the thinner Sikawrap 230C sheet in slab 230C-1L-NA.

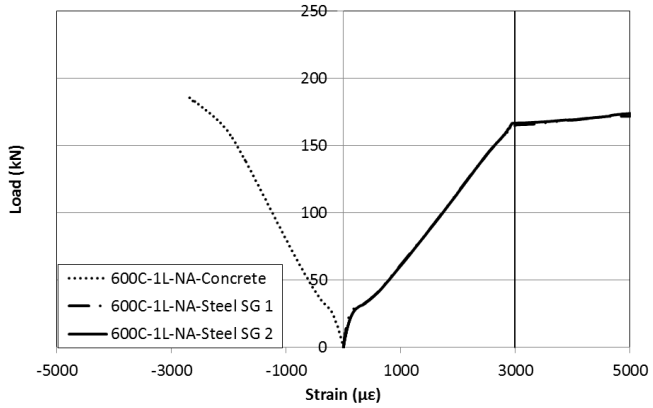

Figure 4-56: Concrete and steel rebar strain response of slab 600C-1L-NA

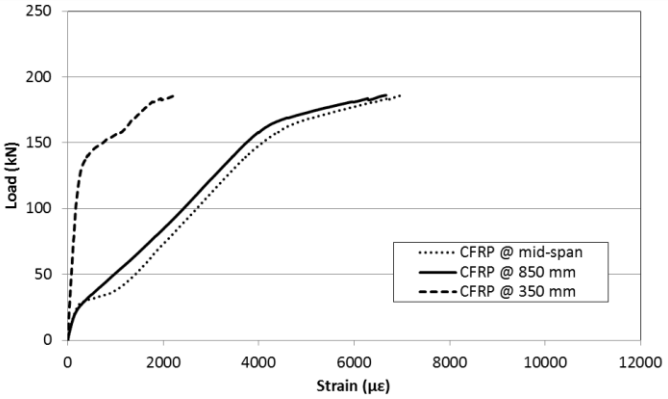

Figure 4-57: FRP strain response of slab 600C-1L-NA

4.3.5 Slabs Strengthened with Sikawrap 600C – Multi-layers

Three slabs were strengthened with two layers of Sikawrap 600C sheets (300 mm wide, 1700 mm long). The CFRP sheets extended the full length of the slab beginning at 250 mm from each end. The 600C sheets were 1.30 mm thick and were applied with Sikadur 300 epoxy with one sheet on top of another.

Slab 600C-2L-NA did not have any CFRP anchors installed and slab 600C-2L-8A had eight CFRP anchors installed to secure the CFRP sheets. Two anchors were installed at 30 mm and 600 mm from both ends of the CFRP sheet. Each anchor was 225 mm long, installed at 150 mm depth into the slab. Slab 600C-2L-12A contained twelve CFRP anchors used to secure the CFRP sheets. Six anchors were spaced 280 mm apart beginning at 30 mm from the end of the CFRP sheet. Each anchor was 350 mm long and was installed through the entire depth of the slab. The failure mode of slabs 600C-2L-NA and 600C-2L-8A was concrete cover failure (Figure 4-58 a

though d) and the failure mode of slab 600C-2L-12A was intermediate flexural shear crack induced interfacial debonding (Figure 4-58 e, f). The concrete cover delamination failure was consistent with failures observed in the literature (ACI 440.2R-08).

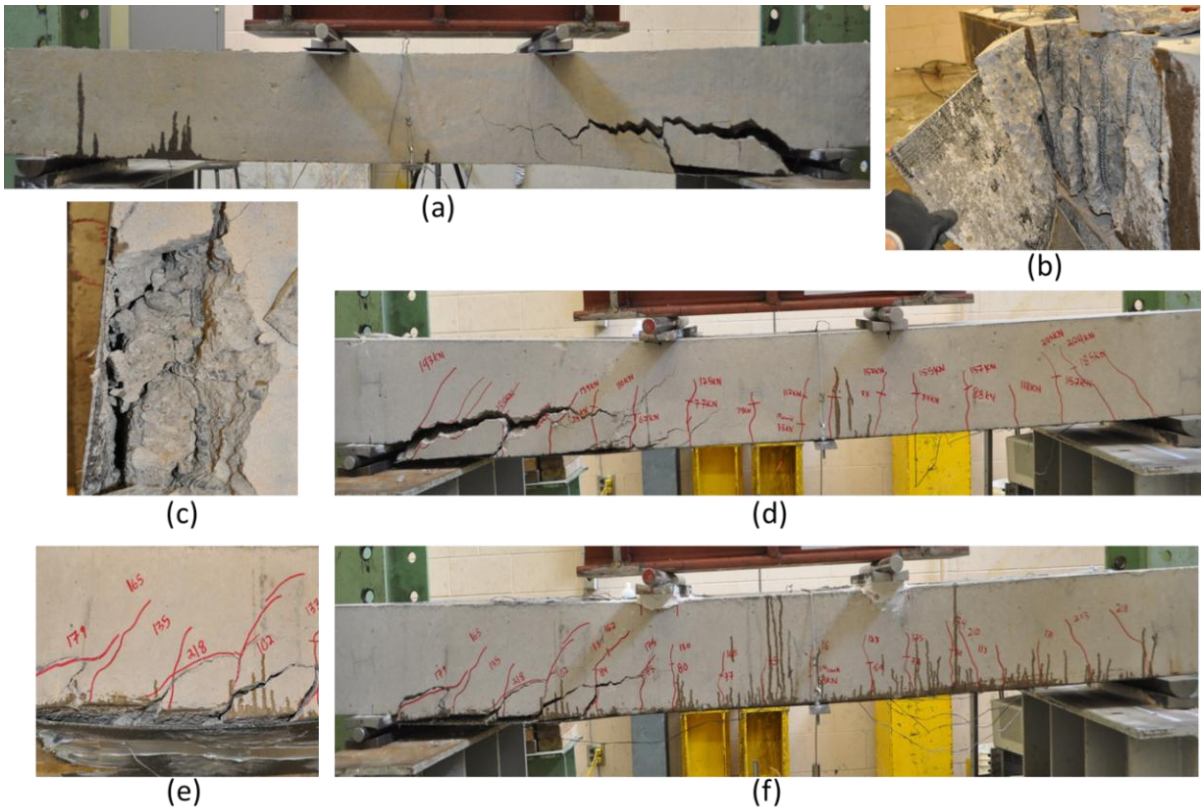

Figure 4-58: Concrete cover failure (a-d) of slabs 600C-2L-NA and 600C-2L-8A and intermediate flexural shear crack induced interfacial debonding (e,f) of slab 600C-2L-12A

The load deflection curves for the three multi-layered CFRP strengthened slabs had a linear response with two stages: pre-cracking and post-cracking (Figure 4-59). The initial stiffness of each slab was changed after the first flexural cracks appeared at a load of 24 kN, 35 kN and 63 kN for slabs 600C-2L-NA, 600C-2L-8A and 600C-2L-12A, respectively. As the load increased, flexural cracks began to develop in the span and the slabs experienced sudden brittle drop in load at failure.

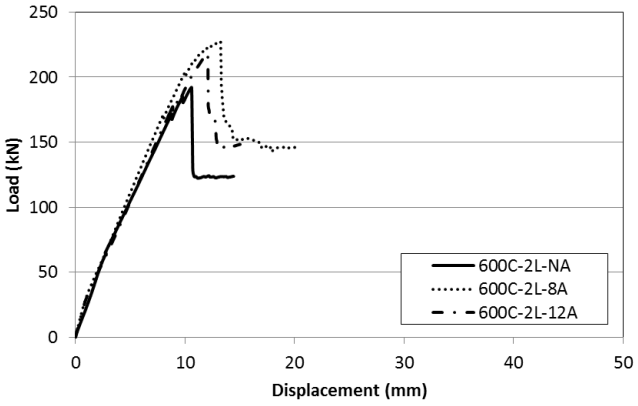

Figure 4-59: Load vs. deflection of slabs 600C-2L-NA, 600C-2L-8A & 600C-2L-12A

Failure in slabs 600C-2L-NA and 600C-2L-8A occurred with the concrete cover delaminating at the location of the longitudinal rebar. This occurred at a load of 192 kN and 227 kN with maximum deflection of 10.6 mm and 13.2 mm for slabs 600C-2L-NA and 600C-2L-8A, respectively. Failure in slab 600C-2L-12A occurred by intermediate flexural shear crack induced interfacial debonding. The maximum load recorded was 219 kN with a maximum deflection of 12.1 mm.

The strain response for the concrete at the top fiber and longitudinal steel reinforcement are presented in Figure 4-60. At failure, all slabs had concrete strains below the crushing strain of concrete. The strain response of the longitudinal steel bars indicated that all rebar yielded reaching maximum strains of 2,495 με and 4,044 με and 3575 με in slabs 600C-2L-NA, 600C-2L-8A and 600C-2L-12A, respectively.

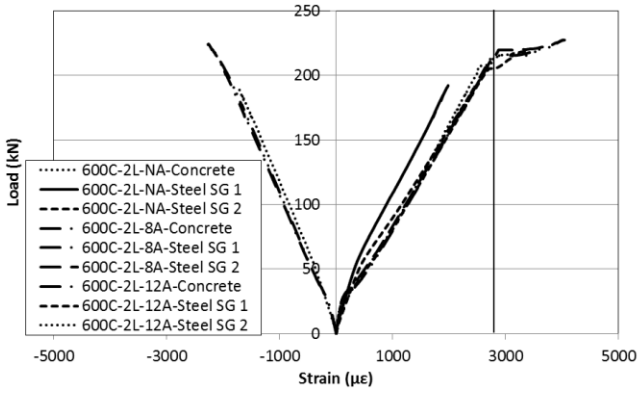

Figure 4-60: Concrete and steel rebar strain response of slabs 600C-2L-NA, 600C-2L-8A and 600C-2L-12A

Figure 4-61 through Figure 4-63 show the strain response in the CFRP sheets. The CFRP strain response for slab 600C-2L-NA shows a bi-linear behaviour. The CFRP sheet began to pick up strain when the slab reached a load of 12 kN and had the same steep slope until failure occurred at 192 kN. The highest strains in the CFRP sheet were experienced at mid-span (3627 με) and under the loading point (3535 με). The strains in the Sikawrap 600C sheets at failure were 4000 με lower in comparison to the strains in the thinner Sikawrap 230C sheet. This can be attributed to the additional area (A_{frp}) provided by the thicker Sikawrap 600C. The thinner Sikawrap 230C has less material to distribute and resist strain thus making the sheet more responsive.

The CFRP strain response of slab 600C-2L-8A showed a bi-linear behaviour similar to that of slab 600C-2L-NA. The CFRP sheet began to pick up strain at a load of 25 kN and maintained a steep slope until failure at 228 kN. The highest strains were experienced in the CFRP sheets at mid-span (4666 με) and under the loading point (3984 με). Comparing these results to the unanchored slab, the presence of CFRP anchors allowed for an increase in strain of 1000 με in the CFRP sheet at mid-span before failure occurred.

The CFRP strain response of the slab 600C-2L-12A showed a bi-linear behaviour in the CFRP sheet with soft transitions. The CFRP sheet began to pick up strain at a load of 25 kN and maintained a steep slope until failure at 228 kN similar to slab 600C-2L-8A. The highest strains in the CFRP sheets were experienced at mid-span (4579 με) and under the loading point (4069 με). Comparing these results to the slab with 8 anchors, there was no increase in the CFRP strain or load at failure. Thus no additional benefit was achieved by using 12 CFRP anchors vs. 8 CFRP anchors.

In summary, the CFRP strain response was affected by the thickness of the CFRP strengthening layers. The slabs strengthened with two layers of Sikawrap 600C (thicker) had a bi-linear behaviour and the slabs strengthened with two layers of Sikawrap 230C (thinner) had a tri-linear behaviour. The strain values experienced in the two layer Sikawrap 600C strengthened slabs were much lower than the strains experienced in the two layer Sikawrap 230C strengthened slabs. This can be attributed to the lower stiffness and increased area (A_{frp}) of Sikawrap 600C which has more material to distribute the strain resisted by the sheet.

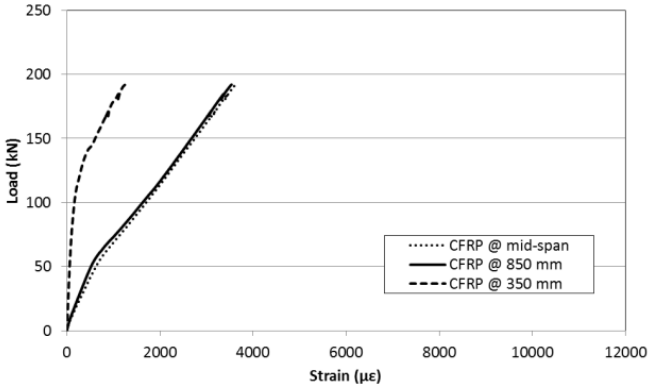

Figure 4-61: FRP strain response of slab 600C-2L-NA

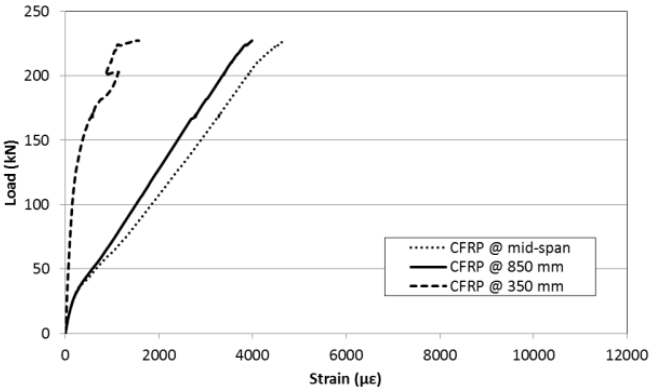

Figure 4-62: FRP strain response of slab 600C-2L-8A

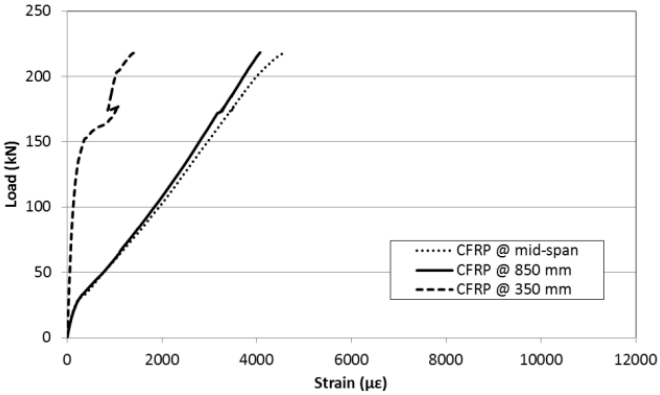

Figure 4-63: FRP strain response of slab 600C-2L-12A

Chapter 5 – Discussion of Shear Critical Beam Results

5.1 Introduction

Twelve shear critical beams were constructed and tested. One beam was tested as control (unstrengthened), six beams were strengthened with GFRP sheets and anchors (three beams were strengthened with GFRP sheets only) and five beams were pre-cracked then repaired with GFRP sheets and anchors (three beams were repaired with GFRP sheets only).

The strength and stiffness of the beams increased with FRP strengthening and repair. Yielding of internal steel rebar was delayed or did not occur with the application of FRP sheets. Shear failure occurred for all beams, the quality of the FRP sheet application was directly related to the strength contribution and quality of the FRP sheet bonded to the beam.

This chapter discusses the experimental results of the shear critical beams strengthened with GFRP sheets. The analysis is divided into the following sections:

- Section 5.2 - Observed Behaviour of Shear Critical Beams
- Section 5.3 - Failure Modes
- Section 5.4 – FRP Strain Profiles
- Section 5.5 - Effect of FRP Type
- Section 5.6 - Effect of FRP Configuration
- Section 5.7 - Effect of FRP Anchors
- Section 5.8 - Shear Critical Beam Section Highlights

5.2 Observed Behaviour of Shear Critical Beams

In this section, the observed behaviour and failure modes of the shear critical beams strengthened with external FRP sheets and FRP anchors is analyzed and discussed. Seven out of the twelve strengthened beams experienced increases in shear capacity when FRP anchors were installed.

5.2.1 Beams with No Increases in Shear Capacity when FRP Anchors were Used

Beams Strengthened with Sikawrap 430G Sheets

Four beams were strengthened with Sikawrap 430G or 100G FRP sheets with and without FRP anchors. These beams did not experience increases in their shear capacity with the addition of FRP anchors to secure the u-wrapped FRP sheets.

The failure load of both beams 430G-200-NA and 430G-200-A was 332 kN. During testing, the diagonal shear crack was observed to widen significantly in between the FRP sheets within the shear span (Figure 5-1). In beam 430G-200-NA as the major shear crack approached the top compression zone, it caused debonding of the top portion of the FRP sheet and progressed to the loading point. The ultimate load of this beam was attained when the crack reached the loading point.

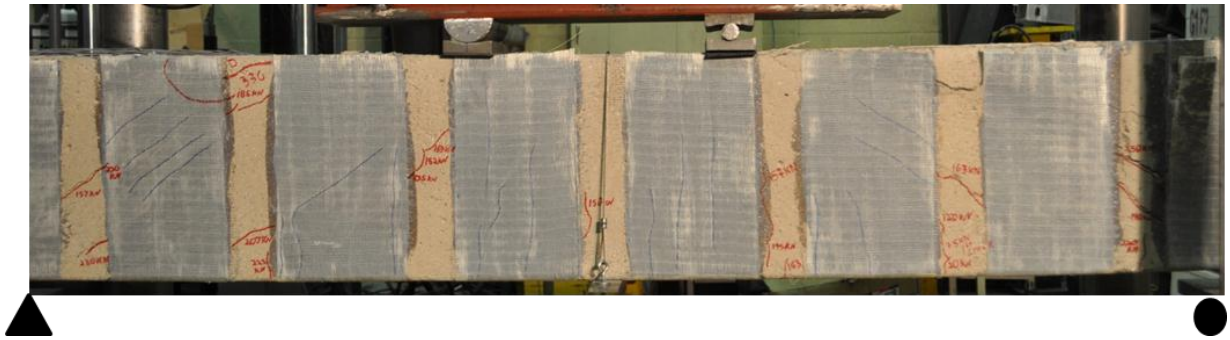

Figure 5-1: Failure of beam 430G-200-NA

Beam 430G-200-A had a similar failure mode. The diagonal shear crack widened in between the FRP sheets within the shear span. As the crack approached the top compression zone, it traveled above the location of the FRP anchors close to the loading point causing debonding of the sheet (Figure 5-2a) and local tension splitting of the concrete (Figure 5-2b). The presence of FRP anchors did not seem to affect the failure mode or the shear capacity of the beam. This can be attributed to both beams failing by loss of aggregate interlock. Because of the 200 mm wide intermittent u-wrap GFRP configuration, a 75 mm unstrengthened zone exists between each GFRP sheet. This can be attributed to the large areas within each beam which were unstrengthened and allowed for easy propagation of the diagonal tension shear crack. Because the shear crack was able to propagate and widen, failure occurred by loss of aggregate interlock regardless of the presence of anchors. Therefore, the effectiveness of providing GFRP anchors is diminished as the width of the GFRP strips decreases.

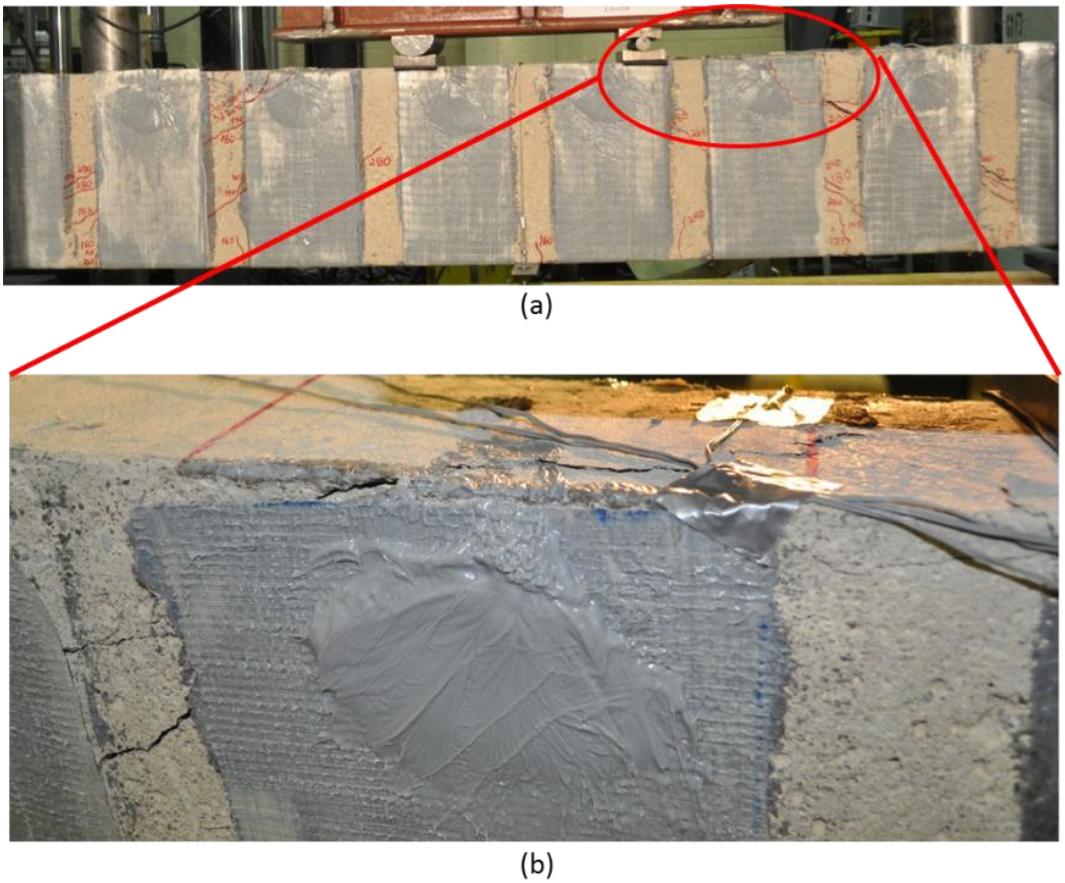

Figure 5-2: Failure of beam 430G-200-A

The initial observation from beam 430G-200-NA was that failure occurred due to FRP debonding because the top of the FRP sheets debonded from the concrete. However, a closer examination of the beam with FRP sheets removed revealed that failure occurred first by loss of aggregate interlock in the concrete. In beam 430G-200-A, the FRP anchors used to secure FRP sheets were not utilized because the shear crack propagated around the top of the FRP anchors causing tension splitting of the concrete. Failure was governed by aggregate interlock due to the use of narrow intermittent FRP sheets for shear strengthening of this beam. This explains the lack of performance of the FRP anchors and the similarity in the failure loads between the beams with and without anchors.

Beams Strengthened with Sikawrap 100G Sheets

The Sikawrap 100G sheets used on these beams 100G-200-NA and 100G-200-A are twice as thick as the Sikawrap 430G sheets used for the previous beams. Knowledge of mechanics indicates that thicker FRP sheets have a higher probability to debond over thinner FRP sheets. This was validated by beams 100G-200-NA and 100G-200-A which experienced debonding at a lower effective strain level compared to beams 430G-200-NA and 430G-200-A.

The failure loads of beams 100G-200-NA and 100G-200-A were 363 kN and 369 kN, respectively. The crack propagation and failure modes were similar to that of beams 430G-200-NA and 430G-200-A as discussed above. The diagonal shear crack widened significantly in between the FRP sheets within the shear span (Figure 5-3). In beam 100G-200-NA, the crack approached the top compression zone and caused the FRP sheet to debond in the top portion with horizontal cracking close to the loading point. The beam failed by aggregate interlock when the crack reached the loading point.

In beam 100G-200-NA, as the crack approached the top compression zone it traveled above the FRP anchors, debonding the unanchored top portion of the FRP sheet and causing concrete tension splitting close to the loading point (Figure 5-4). The presence of FRP anchors did not provide any increase in shear capacity.

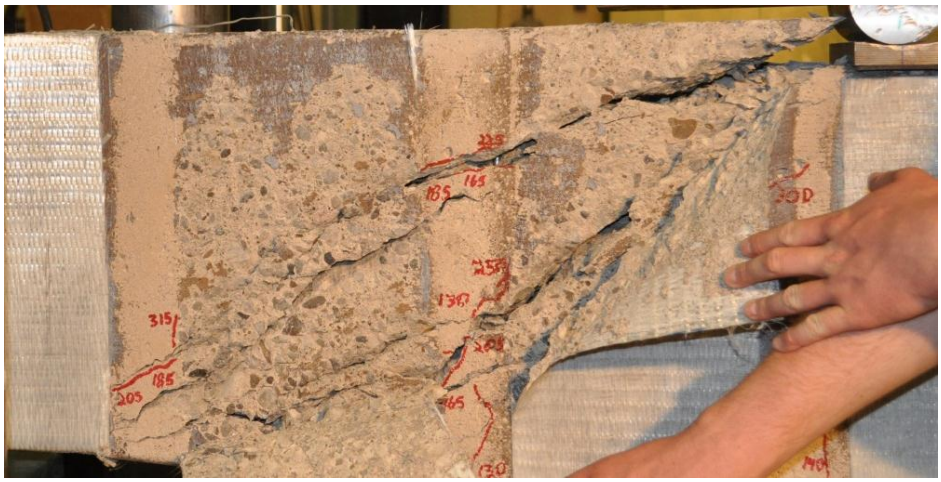

Figure 5-3: Failure of beam 100G-200-NA

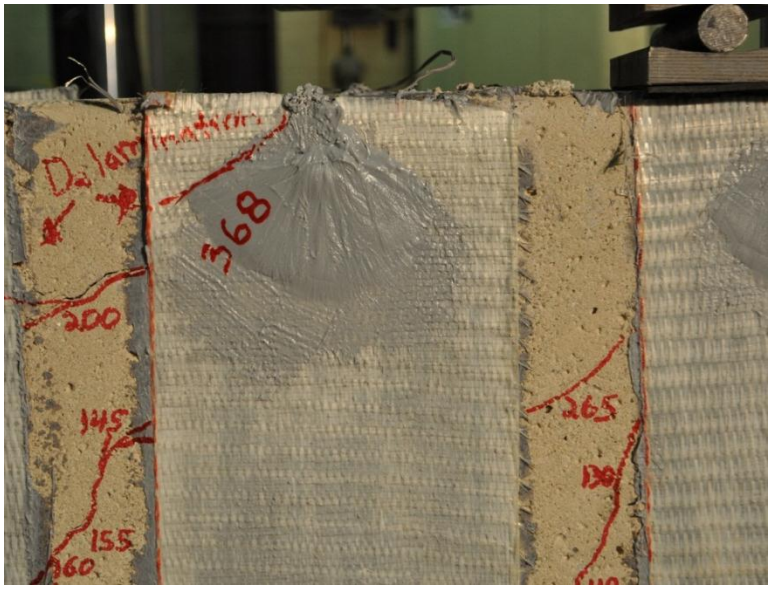

Figure 5-4: Failure of beam 100G-200-A

In summary, beams strengthened with 200 mm wide FRP sheets failed in shear by aggregate interlock. The narrow FRP strips did not sufficiently confine the member and delay crack propagation. The diagonal tension shear crack was allowed to propagate and widen as the load increased causing loss of aggregate interlock and failure. The presence of GFRP anchors had no effect because loss of aggregate interlock occurred before strains in the FRP sheet could reach levels to activate the GFRP anchors. Wider FRP strips are expected to reduce the effective stress from shear crack propagation and FRP anchors are expected to increase the effective failure stress in FRP strengthened beams.

5.2.2 Beams with Increases in Shear Capacity when FRP Anchors were used

Five beams were strengthened with Sikawrap 430G FRP sheets and two beams were strengthened with Sikawrap 100G FRP sheets. Intermittent 300 mm wide strips or continuous sheets were used. These beams experienced increases in shear capacity when FRP anchors were used to secure the u-wrapped FRP sheets.

Beams Strengthened with Sikawrap 430G Sheets

Beams 430G-300-NA and 430G-300-A are shear critical beams with internal stirrups spaced every 180 mm. Each beam was strengthened with external 300 mm wide Sikawrap 430G sheets, spaced every 375 mm o/c. The failure load of beam 430G-300-NA was 313 kN and the failure load of beam 430G-300-A was 346 kN. During testing, the diagonal shear crack propagated significantly in between the FRP sheets within the shear span (Figure 5-1). For beam 430G-300-NA (without anchors), the crack caused debonding in the top section of the 300 mm FRP sheet in the middle of the shear span and progressed to the loading point. The beam failed with premature FRP debonding and loss of concrete aggregate interlock.

Figure 5-5: Failure of beam 430G-300-NA

Beam 430G-300-A had a 10% increase in shear capacity over the companion beam without anchors. The increase in capacity can be attributed to the confinement provided by the wider FRP sheets that were anchored resulting in less unconfined concrete regions between sheets in the shear span. During testing, the diagonal tension shear cracks appeared and propagated in the shear span similar to the beams previously discussed. As the load increased, the crack progressed around the FRP anchors across the top of the beam to the loading point (Figure 5-6a). The wider FRP sheets with FRP anchors stopped the primary shear crack from crossing to the loading point along the side of the beam forcing the crack to travel across the top face of the beam. Failure

occurred when the crack reached the loading point and aggregate interlock in the concrete was lost (Figure 5-6b).

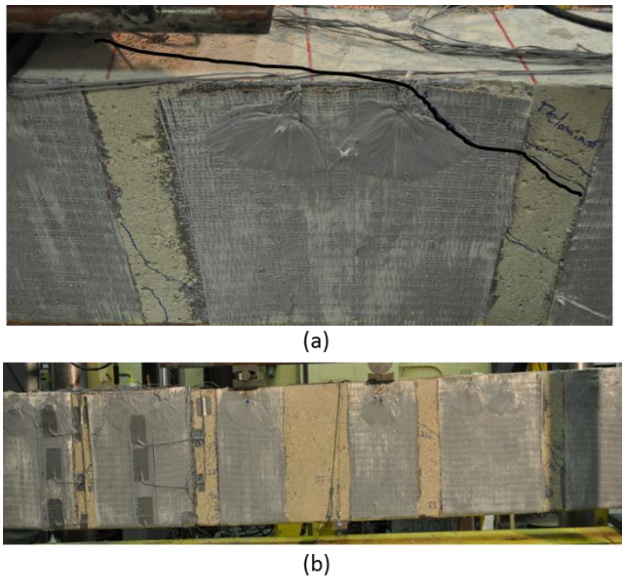

Figure 5-6: Failure of beam 430G-300-A

The presence of FRP anchors in combination with the increased width of the FRP sheets delayed the loss of aggregate interlock by confining the concrete in the shear span. The use of FRP anchors increased the beam capacity by 10% over the strengthened beam without anchors. However, failure occurred by loss of aggregate interlock in both beams.

Pre-cracked Beams Strengthened with 800 mm wide Sikawrap 430G Sheets

Beams 430G-800-NA, 430G-800-A and 430G-800-FW were pre-cracked and repaired with external 800 mm wide Sikawrap 430G sheets. The 800 mm sheets covered the entire shear span between the load points and supports on either side of the beam. The failure load of beam 430G-800-NA was 304 kN and the failure load of beams 430G-800-A and 430G-800-FW was 358kN. The observed behaviour of beam 430G-800-NA was FRP debonding at the top of the sheet followed by a diagonal shear crack propagating across the top of the beam (Figure 5-7a). The shear crack did not reach the loading point because of the continuous FRP configuration. Instead, the crack moved into the compression zone at the top face and propagated horizontally to the loading point (Figure 5-7b). Failure mode was premature FRP debonding followed by loss of aggregate interlock.

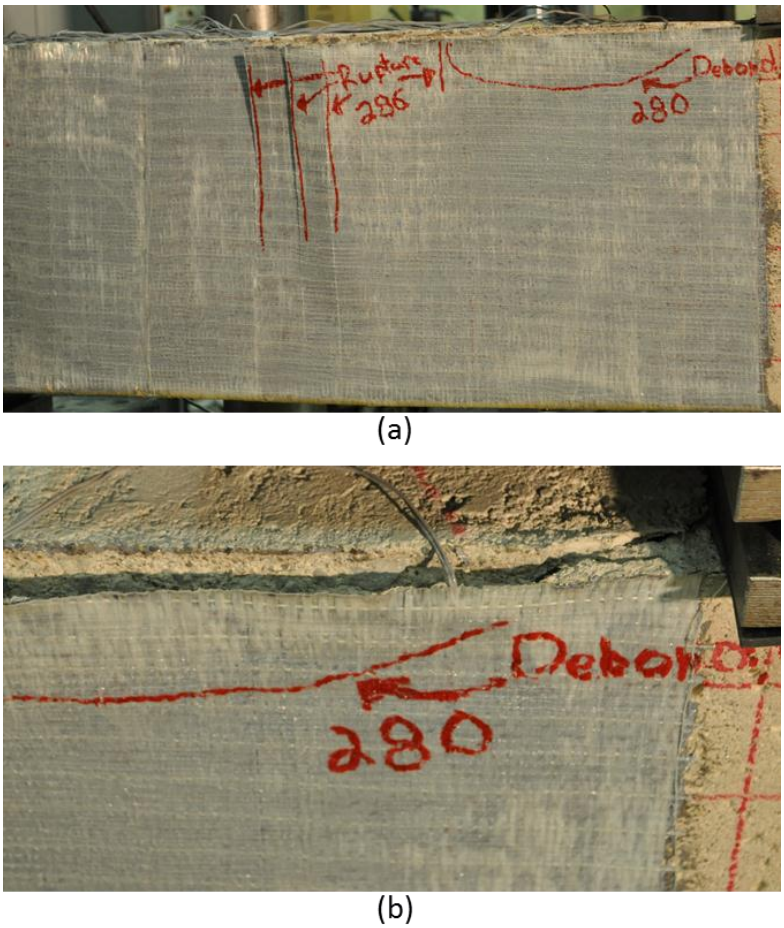

(a)

(b)

Figure 5-7: Failure of beam 430G-800-NA

Beams 430G-200-A (Figure 5-8) and 430G-200-FW (Figure 5-9a) had a 19% increase in the shear capacity over the strengthened beam without anchors. The increase in shear capacity can be attributed to the confinement of the shear span by the continuous FRP sheet configuration. No diagonal tension cracks were visible in both beams as the entire shear span was covered with a GFRP sheet.

The failure mode changed from loss of aggregate interlock observed for the beam without anchors to end anchorage failure in the zone outside the support (Figure 5-8 and Figure 5-9b). This type of failure occurred because the additional shear strengthening provided by the 800 mm wide FRP sheet with FRP anchors did not allow the diagonal tension forces to propagate towards the compression zone and loading point. Instead, the tension forces propagated outside the support zone causing failure in the weaker unstrengthened end zone.

Figure 5-8: Failure of beam 430G-800-A

Figure 5-9: Full wrap (a) and Diagonal end anchorage failure (b) of beam 430G-800-FW

Pre-cracked Beams Strengthened with 1100 mm wide Sikawrap 100G Sheets

Beams 100G-1100-NA and 100G-1100-A are shear critical beams with internal stirrups spaced every 180 mm. These beams were pre-cracked and repaired with external 1100 mm wide Sikawrap 100G GFRP sheets. The 1100 mm sheets covered the entire span leaving a 200 mm gap in the center of the beam in between the load points. The failure load of beam 100G-1100-NA was 352 kN and the failure load of beam 100G-1100-A was 395 kN. During testing, it was difficult to follow the propagation of shear cracks because the entire span was covered with a GFRP sheet. The failure mode of beam 100G-1100-NA was FRP debonding at the top of the sheet with loss of aggregate interlock (Figure 5-10).

Beam 100G-1100-A had a 12% increase in the shear capacity over the companion strengthened beam without anchors. The increase in capacity can be attributed to the confinement provided by the FRP anchors that prevented the FRP sheets from debonding. Providing proper anchorage to the u-wrapped FRP sheet changed the failure mode from FRP debonding and loss of aggregate interlock to diagonal tension end anchorage failure in the zone outside the support. Figure 5-11a shows the beam at failure. Cracking in the end anchorage area is not visible because the beam was completely covered with a GFRP sheet.

Based on observations during testing it was evident that beams strengthened with anchored FRP sheets do not fail by FRP debonding or loss of aggregate interlock. The presence of FRP anchors or full wrapping with continuous FRP configurations delays the loss of aggregate interlock by confining the shear span (Figure 5-11b).

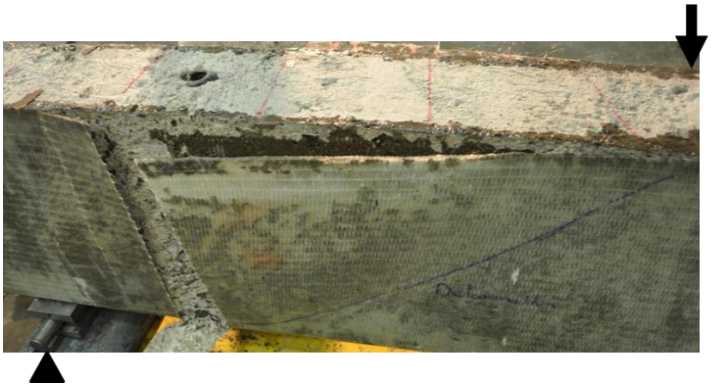

Figure 5-10: FRP debonding failure of beam 100G-1100-NA

Figure 5-11: Diagonal tension end anchorage failure of 100G-1100-A

5.3 Failure Modes

Shear failure occurred in all beams. Shear failure was characterized by the formation of diagonal tension shear cracks in the shear spans of the beam. Diagonal tension formed in between the compression and tension zones in the beam causing a 30^o to 45^o diagonal crack to form in the shear span. As loading was increased, the shear cracks propagated towards the loading point and support. Failure was sudden and occurred when the crack reached the loading point, support or when the concrete failed by crushing. Six different failure modes occurred:

- Diagonal tension shear failure - Figure 5-12a
- Loss of aggregate interlock - Figure 5-12b
- FRP debonding - Figure 5-12c
- FRP rupture - Figure 5-12d
- Shear failure with crushing of concrete - Figure 5-12e
- Diagonal tension end anchorage failure - Figure 5-12f

Observations of the six failure modes identified various trends based on the FRP strengthening and repair configuration. Five beams failed by FRP debonding (Figure 5-12c) as these beams did not have any FRP anchors. Three beams failed by FRP rupture (Figure 5-12d): two beams had FRP anchors installed to secure the FRP sheets and the third beam was fully wrapped. This observation implies that FRP anchors used to secure FRP sheets not only eliminated FRP debonding but also allowed the FRP sheets to reach their ultimate strength.

Applying FRP anchors to secure the ends of FRP u-wraps achieved the same capacity as a fully wrapped beam. This is a significant finding as fully wrapping a beam is not always possible or practical in field applications. Three beams experienced end anchorage failure (Figure 5-12f). These beams had FRP u-wraps across the entire shear spans that did not extend past the support overhang. As the load was increased, the diagonal tension forces did not propagate through the FRP repaired shear spans leading to premature end anchorage failure.

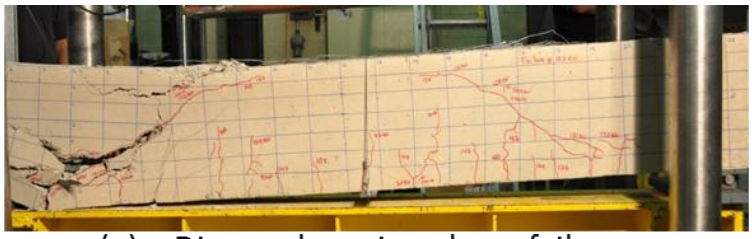

(a) – Diagonal tension shear failure

(b) – Loss of aggregate interlock

(c) – FRP debonding

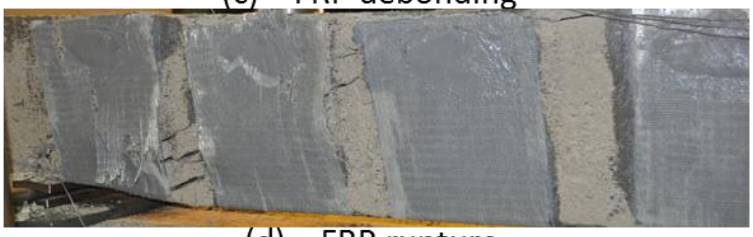

(d) – FRP rupture

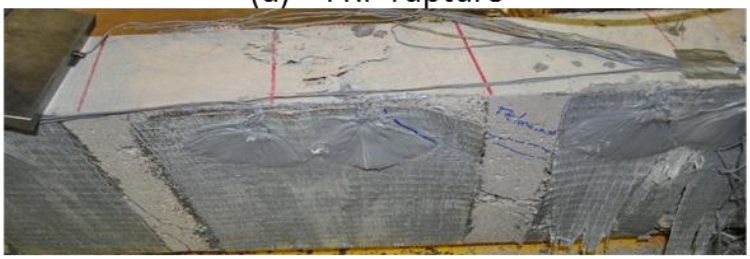

(e) – Shear failure with concrete crushing

(f) – Diagonal tension end anchorage failure

Figure 5-12: Failure modes of shear critical beams

5.4 FRP Strain Profiles

In this section, the FRP strain distribution with respect to the shear crack is discussed. Each FRP strengthened beam had six FRP strain gauges: three strain gauges across the depth of the beam (50 mm, 175 mm and 300 mm from the top of the beam) were installed on two GFRP sheets in the shear span (sheet 2: 400 mm from the support and sheet 3: 680 mm from the support). The strain gauge layout is shown in Figure 5-13.

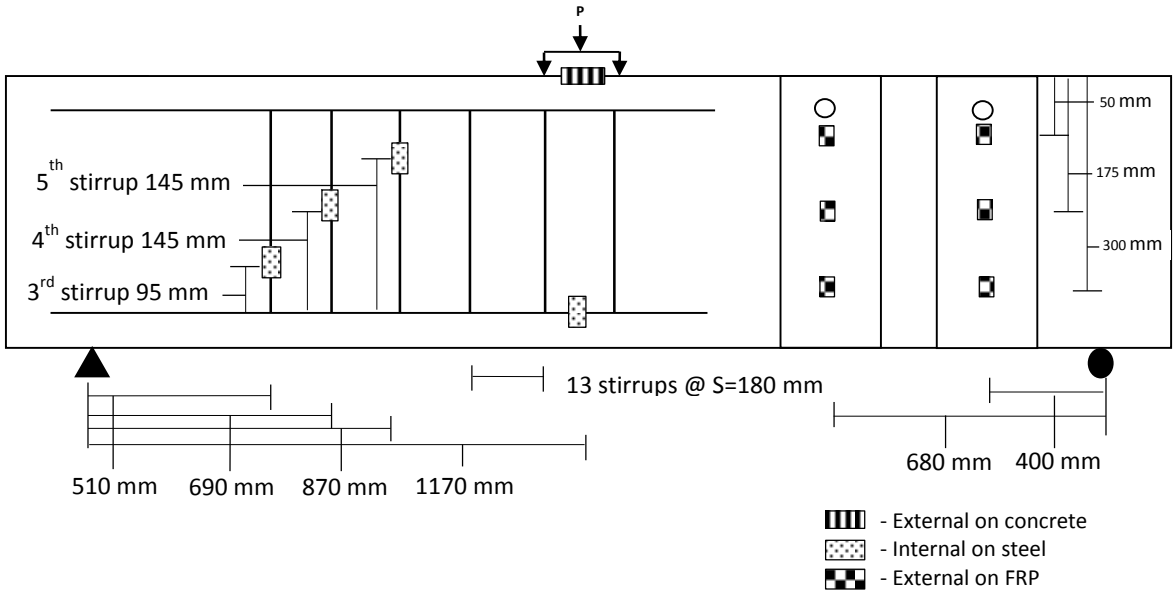

Figure 5-13: Strain gauge layout

Figure 5-14 show a schematic of the diagonal tension shear crack crossing the GFRP sheets for beams strengthened with GFRP sheets with and without anchors. When FRP anchors were used the shear crack went above the anchor location as shown in Figure 5-14b.

Two trends were observed in the GFRP strain response of all shear critical beams. A bell-shaped strain profile was experienced in GFRP sheets that intercepted the diagonal tension shear crack at mid-depth (175 mm) and an L-shaped strain profile was experienced in the GFRP sheets that intercepted the diagonal tension shear crack at the top of the sheet (50 mm).

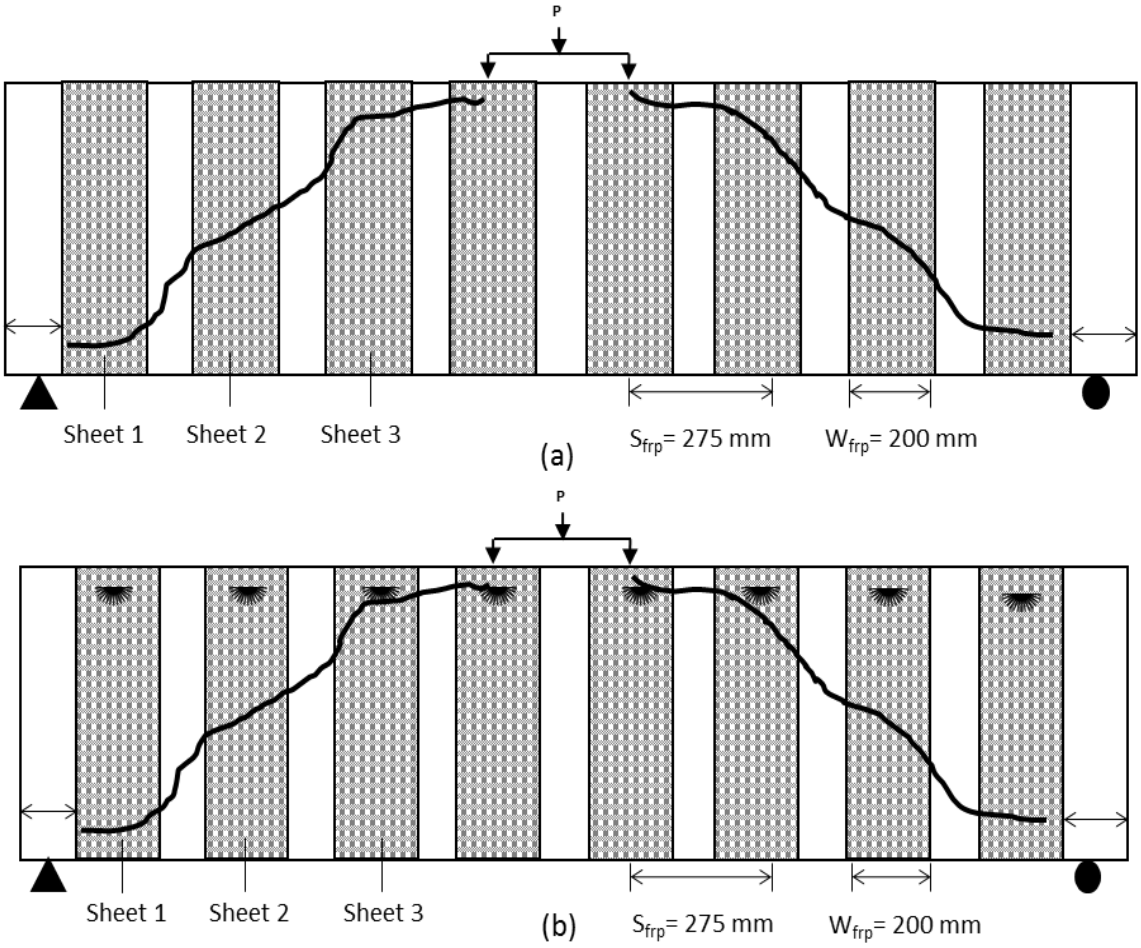

Figure 5-14: Shear crack scheme of beams strengthened with u-wrap GFRP sheets: (a) without GFRP anchors and (b) with GFRP anchors

Bell Curve Strain Response

When FRP sheets intercept a shear crack at mid-depth (sheet 2) a bell-shaped strain profile was recorded. An example of how the strain profile in FRP sheet 2 increased at different load levels is shown Figure 5-15. The highest strain in the GFRP sheet was experienced at mid-depth where the crack was intercepted and lower strains were experienced at each end of the sheet. The black circle shows the maximum strain experienced in the stirrup. Initially, the FRP strain was very low until the stirrup yielded (2000 με) at which point a large jump in the FRP strain response was experienced as can be seen at subsequent load levels until failure occurred.

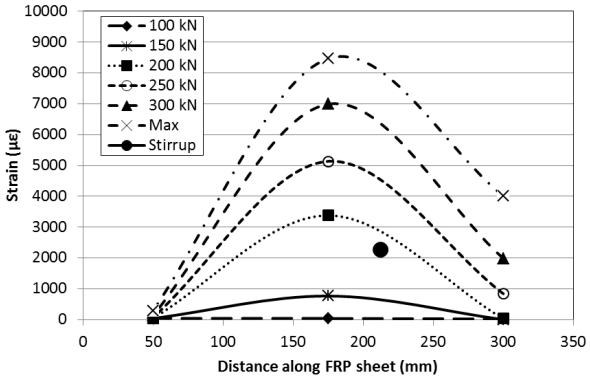

Figure 5-15: GFRP strain response – Sheet 2

L-shape Strain Response

When FRP sheets intercept a shear crack at the top of a u-wrap sheet (sheet 3) a L-shaped strain profile is recorded. An example of how the strain profile in FRP sheet 3 increased at different load levels is shown in Figure 5-16. The highest strain in the GFRP sheet was experienced at the top of the sheet where the crack was intercepted. Low strains were experienced at mid-depth and at the bottom of the sheet because no tension strain from the shear crack was being resisted by the GFRP sheet at that location.

The black circle shows the maximum strain experienced in the stirrup. The FRP strain was very low until the stirrup yielded (2000 με) at which point a large jump in the FRP strain was experienced at the top of the GFRP sheet (at 50 mm from beam top) at each load level until failure occurred. Low strains were recorded at the mid-depth and bottom locations of the GFRP sheet.

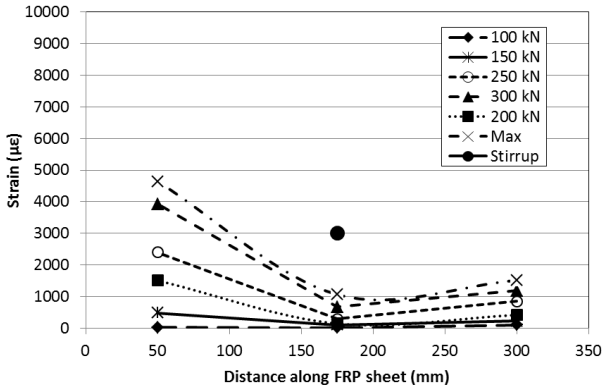

Figure 5-16: GFRP strain response – Sheet 3

5.5 Effect of FRP Type

In this section, the effect of the type of FRP used to strengthen or repair a shear critical beam on the load, stiffness, deflection and the strain response is discussed. The comparisons include beams with and without anchors:

5.5.1 Intermittent Glass FRP - 430G vs. 100G

Four shear critical beams were strengthened with two types of GFRP sheets. All four strengthened beams failed in shear as designed. The performance of beams strengthened with the thicker sheets (Sikawrap 100G) was slightly better obtaining higher shear strength over the beams strengthened with thinner sheets (Sikawrap 430G). Both beams without anchors failed by FRP debonding and the Sikawrap 430G anchored beam failed by FRP rupture. The Sikawrap 100G anchored beam did not rupture, instead diagonal tension shear failure occurred with the dominant shear crack developing between the FRP sheets close to the loading point.

The load vs. deflection curves of the two beams strengthened with Sikawrap 430G sheets and the two beams strengthened with Sikawrap 100G sheets are shown in Figure 5-17. All strengthened beams exhibited similar load-deflection responses. It is worth noting that the bi-linear load deflection response exhibited by the control beam was not evident when the beams were strengthened with GFRP sheets.

Beams strengthened with the thicker Sikawrap 100G sheets obtained the highest ultimate load. The post peak behaviour showed that the two unanchored beams failed with a sudden drop in load. The two anchored beams had a gradual drop in load which can be attributed to the presence of FRP anchors.

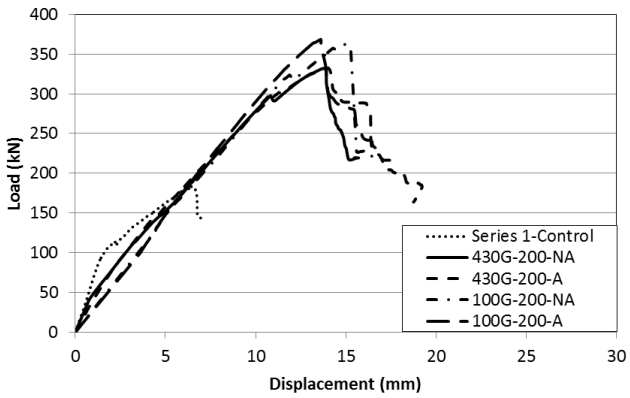

Figure 5-17: Load vs. deflection of 430G & 100G strengthened beams

Effect on Strength

A comparison of the strength increase over the control of beams strengthened with Sikawrap 430G and Sikawrap 100G sheets is shown in Figure 5-18. The increase in strength for beams 430G-200-NA and 100G-200-NA was 81.4% and 98.4% over the control and for beams 430G-200-A and 100G-200-A, it was 81.4% and 101.4%.

Beams strengthened with Sikawrap 100G sheets without anchors had a 17% increase in strength over beams strengthened with Sikawrap 430G sheets. This can be attributed to the thickness of the 100G sheet. In theory, the Sikawrap 100G sheet should provide double the strengthening capacity because it is twice as thick as the Sikawrap 430G sheet (t=1.016 mm vs. t=0.508 mm). However, beams strengthened with the thicker Sikawrap 100G sheet provided a 20% increase over the 430G sheet. The ultimate capacity of the Sikawrap100G sheets was not reached because the beam failed prematurely by loss of aggregate interlock. Therefore, the increase in strength provided by the anchored sheets could potentially be much greater if the FRP sheets are able to develop higher strains before failure occurs (loss of aggregate interlock).

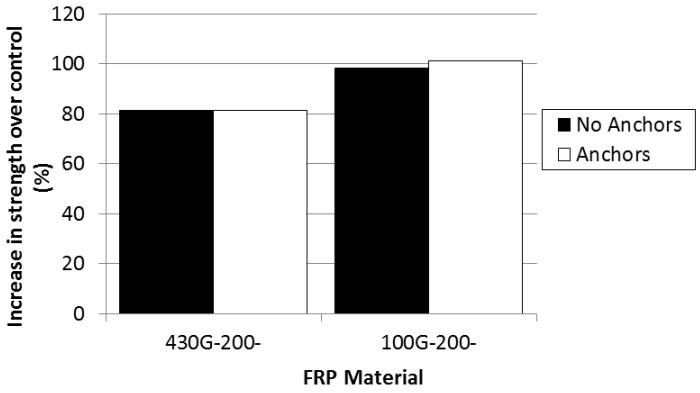

Figure 5-18: Strength increase of 430G & 100G strengthened beams over control

Effect on Stiffness

The beam stiffness was increased by 40% for the beams strengthened with Sikawrap 430G and Sikawrap 100G sheets over the post cracking stiffness of the control. Beams with thicker GFRP sheets (Sikawrap 100G) had the same stiffness (25 kN/mm) as beams with thinner GFRP sheets (Sikawrap 430G).

Effect on Deflection

Figure 5-19 compares the maximum deflection at failure of beams strengthened with Sikawrap 430G and Sikawrap 100G sheets. The strengthened beams experienced an average increase in deflection of 123% over the control. Thinner Sikawrap 430G sheets had a 7.5% higher deflection compared to the thicker Sikawrap 100G sheets. The presence of GFRP strengthening significantly increases the deflection at failure.

Unanchored beam 100G-200-NA experienced a decrease in deflection of 9% over unanchored beam 430G-200-NA. A further decrease in deflection of 6% was experienced in the anchored 100G-200-A beam over beam 430G-200-A. The presence of GFRP anchors decreased the deflection over the corresponding unanchored beams by 26% in 430G-200-A and 23% in 100G-200-A. The maximum deflection in a strengthened beam was affected by the type of FRP material used and the presence of FRP anchors.

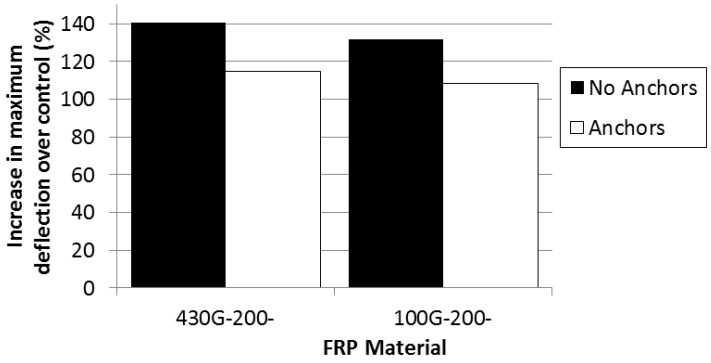

Figure 5-19: Increase in maximum deflection of 430G & 100G beams over control

Strain Response

The maximum strains at failure showed a large difference in strain recorded in the GFRP sheets and the internal steel stirrups between the beams strengthened with Sikawrap 430G and Sikawrap 100G sheets. The presence of GFRP anchors decreased the maximum strain in the stirrups at failure by 112% in beam 430G-200-A vs. beam 100G-200-A.

The highest strains in the FRP sheet were observed in the beams with anchors. Cross referencing the strain in the GFRP sheet with the failure mode observed, it can be concluded that the strain to cause FRP rupture in Sikawrap 430G sheets is 8000 με. This is lower than the rupture strain of 22,100 με reported by the manufacturer.

Figure 5-20 shows the strains in the stirrups of the GFRP strengthened beams. Comparing the strain in the stirrups of the beams strengthened with Sikawrap 430G and Sikawrap 100G sheets reveals that the thicker Sikawrap 100G sheets provided a larger shear strength contribution than the thinner Sikawrap 430G sheets. This is validated by the maximum strain recorded in the stirrups. Lower strains were experienced in the internal stirrups of the beams strengthened with Sikawrap 100G sheets due to the increased shear resistance by the thicker Sikawrap 100G sheet. This was more evident in the beams without anchors with a 45% decrease in stirrup strains while the beams with anchors had a slight decrease of 7% in the stirrup strains (Figure 5-20).

Figure 5-21 shows the GFRP strain for beams strengthened with Sikawrap 430G and 100G sheets. In general, the Sikawrap 100G sheet exhibited lower strains than the Sikawrap 430G sheet. The effect of sheet thickness on the FRP strain was less pronounced when the sheets were not anchored.

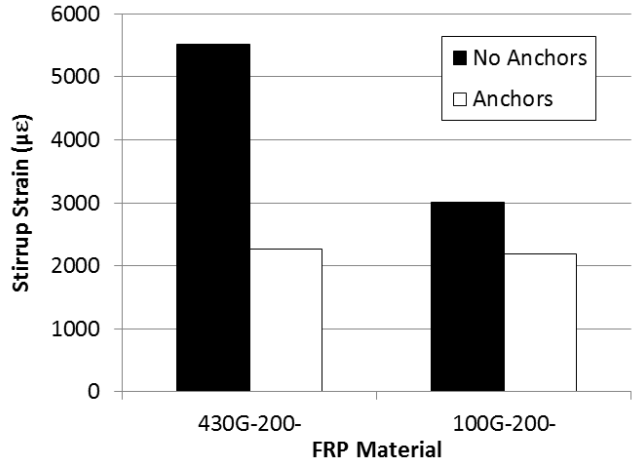

Figure 5-20: Stirrup strain at failure of Sikawrap 430G and 100G strengthened beams

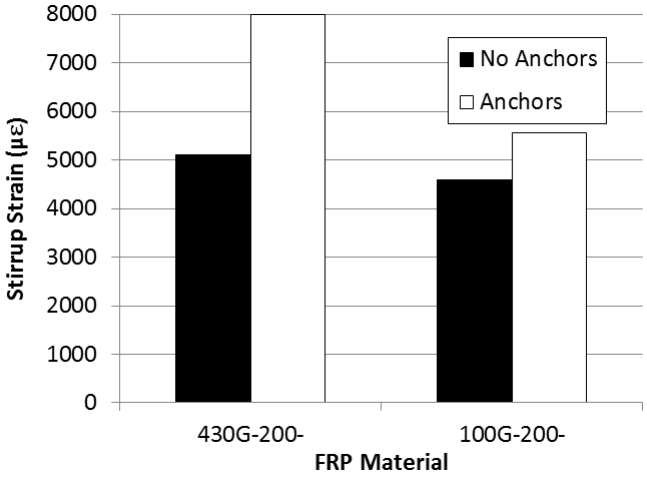

Figure 5-21: GFRP strain at failure of Sikawrap 430G and 100G strengthened beams

Both unanchored beams 430G-200-NA and 100G-200-NA experienced FRP debonding at failure. The strain to cause debonding in the Sikawrap 430G sheet was 5000 με and 4600 με for the Sikawrap 100G sheet. The theoretical debonding strain for Sikawrap 430G and 100G sheets is 5900 με and 4600 με, respectively (ISIS-M04). However, the data does not support this hypothesis with minimal difference in strains between measured Sikawrap 430G and Sikawrap

100G sheets. The small difference in FRP strain measured between each beam can be attributed to the concrete substrate failing when the strain in the FRP sheet was 4600 με.

The strain profiles across the depth of the beam for the GFRP strengthened beams are shown in Figure 5-22. It is evident that sheet 2 (400 mm form support) showed very high strains on both anchored beams. All beams recorded the highest strains at mid-depth of the GFRP sheets. There was no effect on the strain profile between beams strengthened with Sikawrap 430G or 100G sheets as both materials resembled a bell-shaped profile.

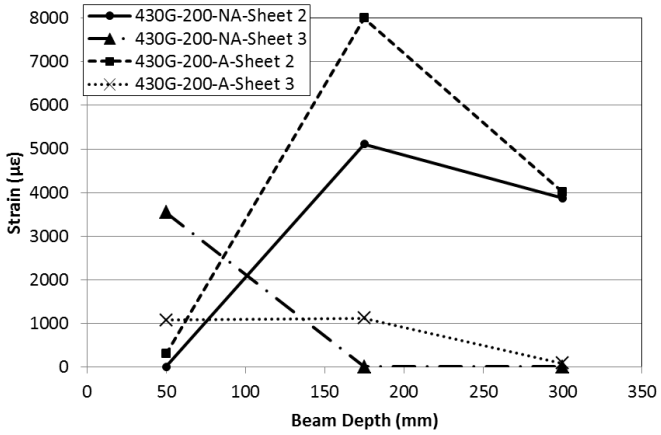

a) Sikawrap 430G Strengthening

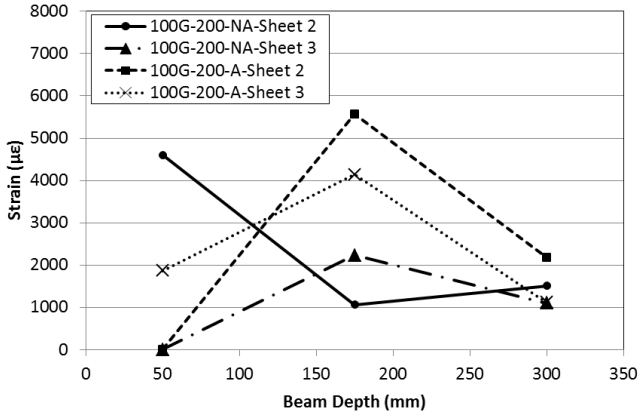

b) Sikawrap 100G Strengthening

Figure 5-22: FRP strain profile of beams strengthened with 200 mm wide GFRP sheets

5.5.2 Continuous Glass FRP - 430G vs. 100G

Four pre-cracked shear critical beams were repaired with two types of GFRP sheets. The beams with 800 mm wide continuous GFRP strengthening were u-wrapped with Sikawrap 430G GFRP on three sides of the shear span. The anchored beam (PC-430G-800-A) was secured with seven GFRP anchors spaced every 100 mm. The beams with 1100 mm wide continuous GFRP strengthening were u-wrapped with Sikawrap 100G on three sides of the shear span. The anchored beam (PC-100G-1100-A) was secured with nine GFRP anchors spaced every 100 mm.

The load vs. deflection curves of the four strengthened beams and the control are shown in Figure 5-23. The bi-linear load deflection response exhibited by the control beam was not evident when the beams were strengthened with GFRP sheets.

The two unanchored beams experienced FRP debonding at loads of 280 kN (PC-430G-800-NA) and 340 kN (PC-100G-1100-NA). The anchored beams with continuous FRP sheets failed by diagonal tension end anchorage failure at a maximum load of 358 kN (PC-430G-800-A) and 395 kN (PC-100G-1100-A). The post peak behaviour of beam PC-100G-1100-A had a less sudden failure mode compared to the other three breams.

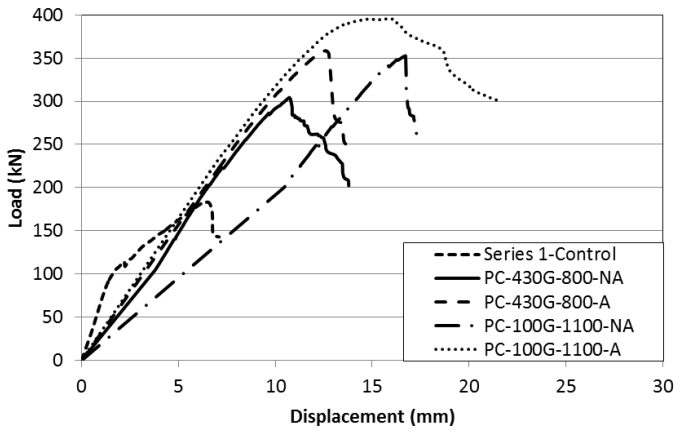

Figure 5-23: Load vs. deflection of pre-cracked beams

Effect on Strength

A comparison of the strength increase of each beam over the control beam is displayed in Figure 5-24. The additional strength provided by the beams with continuous Sikawrap 100G sheets was 26% (PC-100G-1100-NA) and 20% (PC-100G-1100-A) over the corresponding beams strengthened with Sikawrap 430G. The thicker Sikawrap 100G vs. Sikawrap 430G exhibited additional increase in shear capacity.

End anchor failure was observed in both the anchored Sikawrap 430G and 100G strengthened beams. The increased thickness of Sikawrap 100G did not prevent diagonal tension end anchorage failure from occurring, even though the beam ends were wrapped in this case.

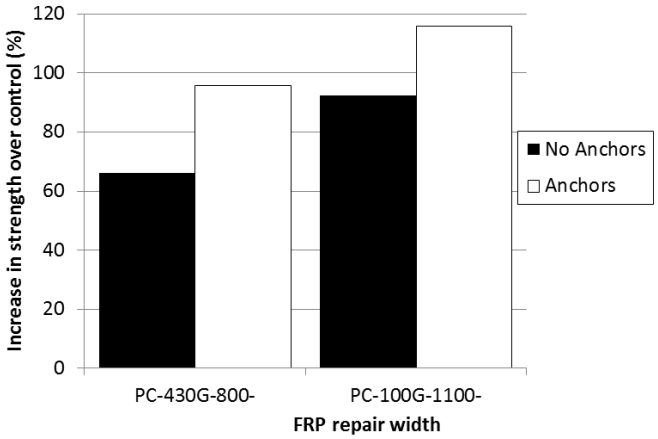

Figure 5-24: Strength increase of pre-cracked FRP strengthened beams over the control

Effect on Stiffness

Stiffness was increased by 50% for the beams strengthened with Sikawrap 430G and Sikawrap 100G sheets over the post cracking stiffness of the control (20 kN/mm). Beams with thicker GFRP sheets (Sikawrap 100G) had the same stiffness (30 kN/mm) as beams with thinner GFRP sheets (Sikawrap 430G). The 1100 mm wide unanchored beam (PC-100G-1100-NA) had an unusually low stiffness.

Effect on Deflection

Figure 5-25 compares the maximum deflection at failure for the 800 mm and 1100 mm continuous u-wrapped beams. All four beams experienced increases in the maximum deflection over the control at failure. Both the unanchored and anchored Sikawrap 100G strengthened beams experienced larger deflections than the equivalent Sikawrap 430G strengthened beams. Beams strengthened with Sikawrap 100G sheets had 92% and 136% greater maximum deflection at failure over the companion Sikawrap 430G strengthened beams.

Comparison of intermittently vs. continuously applied Sikawrap 430G and 100G sheets revealed that Sikawrap 430G sheets applied intermittently and continuously had an average increase in maximum deflection of 127% and 79%, respectively. Sikawrap 100G sheets applied intermittently and continuously had an average increase in maximum deflection of 120% and 193%, respectively. The results were contradictory and thus no trend was found for the effect of intermittent or continuous u-wrapped FRP sheets.

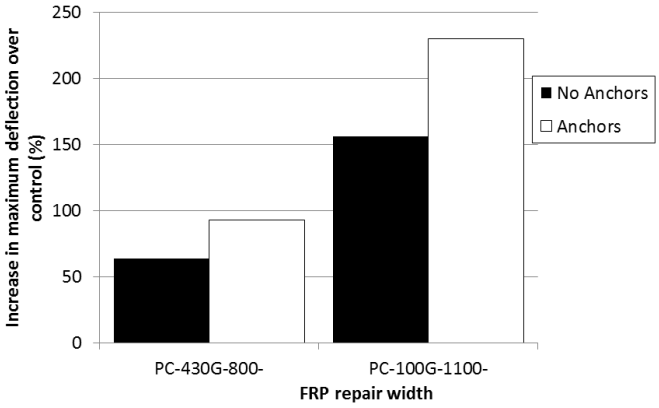

Figure 5-25: Pre-cracked FRP width maximum deflection comparison

Strain Response

The maximum strains at failure recorded in the GFRP sheets and the internal steel stirrups were quite different for beams strengthened with Sikawrap 430G and Sikawrap 100G sheets. Figure 5-26 shows the strains in the stirrups of the GFRP strengthened beams. In all four beams, all stirrups yielded recording strains greater than 2000 με. The maximum strain in the stirrups at failure was equal for both Sikawrap 430G and 100G strengthened beams with no

anchors. The maximum stirrup strain at failure for the anchored beams showed the Sikawrap 100G strengthened beams experienced a 35% increase in strain compared to the Sikawrap 430G strengthened beam.

Figure 5-27 shows the GFRP strain for beams strengthened with Sikawrap 430G and 100G sheets. In general, Sikawrap 100G sheets exhibited higher strains than Sikawrap 430G sheets. Correlating the strain in the GFRP sheet with the failure mode observed, it can be concluded that the strain to cause FRP debonding in Sikawrap 430G and Sikawrap 100G sheets was 3000 με. This is lower than the theoretical debonding strain of 5900 με for Sikawrap 430G and 4600 με for Sikawrap 100G. This is probable because debonding actually occurred in the concrete substrate when the strain in the FRP sheet was 3000 με.

The strain profiles across the depth of the beam for the GFRP strengthened beams are shown in Figure 5-28. All beams except PC-430G-800-NA recorded the highest strains at mid-depth of the GFRP sheets. Beam PC-430G-800-NA had an L-shape strain profile with the highest strains at the ends of the FRP sheet. The beam strengthened with anchored Sikawrap 430G sheets had a bell-shaped strain profile with the highest strain at mid-depth. Both the unanchored and anchored beams strengthened with Sikawrap 100G also had bell-shaped strain profiles with the highest strain occurring at mid-depth. Regardless whether continuous or intermittent configuration, the bell-shape strain profile was observed in Sikawrap 430G and 100G sheets.

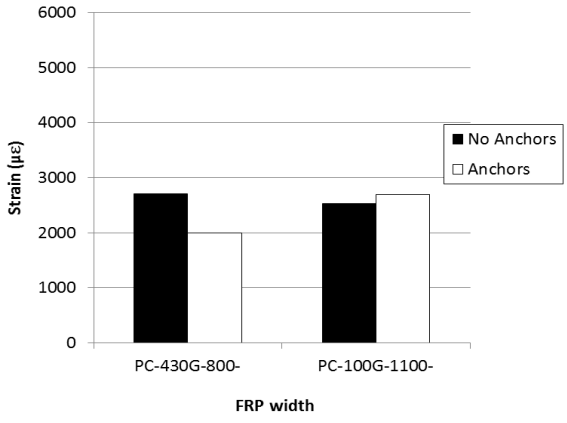

Figure 5-26: Stirrup strain at failure of continuous 800 mm & 1100 mm GFRP sheets

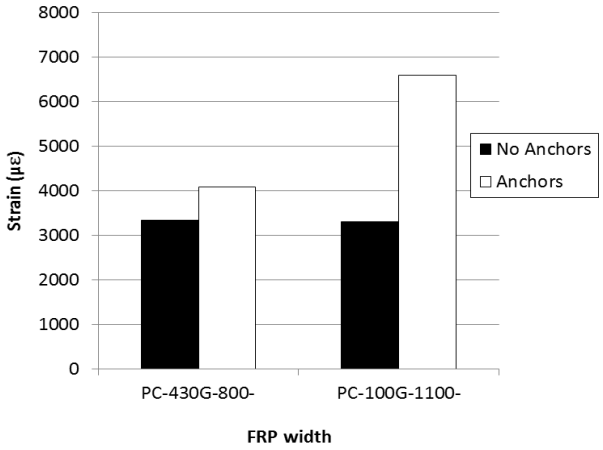

Figure 5-27: GFRP strain at failure of continuous 800 mm & 1100 mm GFRP sheets

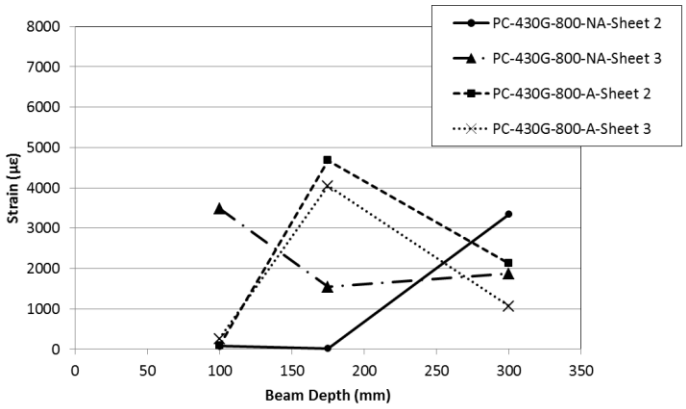

a) Sikawrap 430G Strengthening

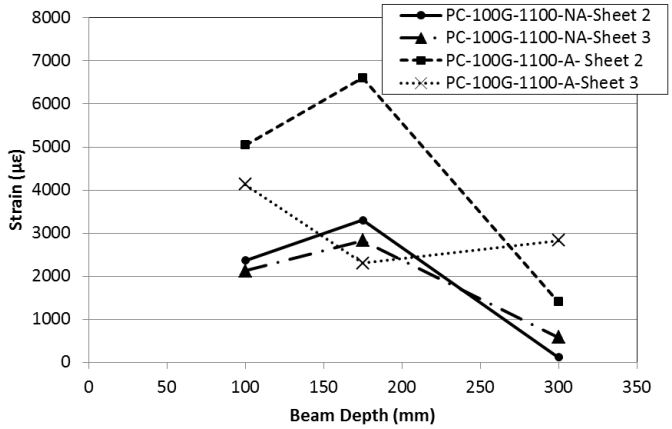

b) Sikawrap 100G Strengthening

Figure 5-28: FRP strain profile of beams strengthened with continuous GFRP sheets

5.6 Effect of FRP Configuration

In this section the effect of the FRP configuration used to strengthen or repair a shear critical beam on the load, stiffness, deflection and the strain response is analyzed and compared. Each comparison includes beams with and without anchors.

5.6.1 Intermittent 200 mm wide vs. 300 mm wide GFRP

Four shear critical RC beams were strengthened with 200 mm and 300 mm wide Sikawrap 430G sheets. Both unanchored beams (430G-200-NA, 430G-300-NA) failed by FRP debonding. Beam 430G-200-A with anchors failed by loss of aggregate interlock and beam 430G-300-A failed by crushing of concrete in the compression zone. The load deflection curves of the four strengthened beams vs. the control are shown in Figure 5-30. The bi-linear load-deflection response exhibited by the control beam was not evident when the beams were strengthened with GFRP sheets.

The presence of intermittent GFRP sheets changed the inclination of the diagonal tension shear crack. The angle of the shear crack varied as it propagated towards the loading point depending if the crack was behind a FRP u-wrap or if it was in between the FRP sheets. Figure 5-29 shows the difference in crack orientation between the exposed concrete sections of the beam and the u-wrapped sections. The slope of the shear crack was steeper in between the FRP sheets vs. under the u-wrap FRP sheet.

Figure 5-29: Shear crack with multi-linear slopes

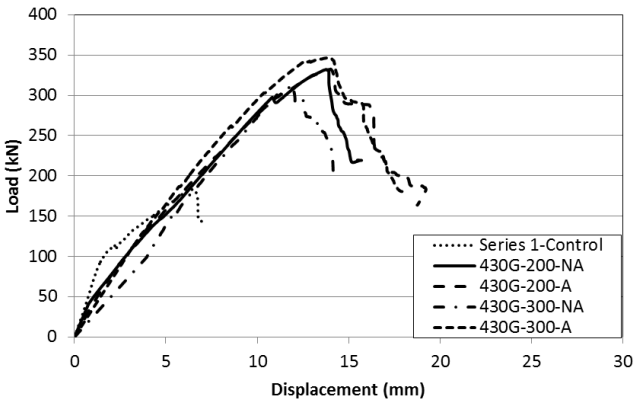

Figure 5-30: Load vs. deflection of 200 mm & 300 mm wide GFRP strengthened beams

Effect on Strength

A comparison of the strength increase over the control provided by 200 mm and 300 mm wide GFRP sheets is shown in Figure 5-31. The increase in strength over the control for the beams strengthened with 200 mm and 300 mm wide sheets was 81% for beam 430G-200-NA and 81% for beam 430G-200-A vs. 71% for beam 430G-300-NA and 89% for beam 430G-300-A.

The effect of using 200 mm vs. 300 mm wide GFRP sheets depended whether the sheets were anchored or not. In the anchored beams (430G-200-A, 430G-300-A), the 300 mm wide sheets provided an 8% increase in strength over the 200 mm wide sheets. In the unanchored beams (430G-200-NA and 430G-300-NA) the 200 mm wide sheets provide a 10% increase in strength over the wider 300 mm sheets. This can be attributed to the path the crack took once the FRP sheet debonded. The 300 mm wide sheet was wider and once it debonded the crack had an unrestricted path to the load point. In comparison, multiple 200 mm wide sheets would intercept the shear crack and both sheets would have to debond separately before the beam fails.

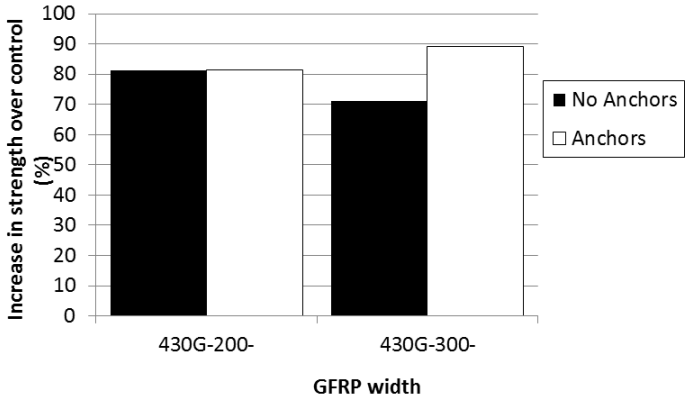

Figure 5-31: Strength increase of 200 mm & 300 mm wide GFRP sheets over the control

Effect on Stiffness

The beam stiffness was increased in all 200 mm and 300 mm wide strengthened beams. Beams with 200 mm wide GFRP sheets had the same stiffness (27 kN/mm) as beams with wider 300 mm wide GFRP sheets. In general, increasing the width of the GFRP sheet (from 200 mm to 300 mm) did not have an effect on beam stiffness. However, the beam strengthened with 300 mm wide sheets with anchors had a slightly higher stiffness compared to the other three strengthened beams.

Effect on Deflection

A bar chart comparing the maximum deflection at failure is shown in Figure 5-32. The strengthened beams showed an average increase in maximum deflection at failure of 113% over the control.

Beams strengthened with 300 mm wide sheets with and without anchors experienced smaller deflections than the companion beams strengthened with 200 mm wide GFRP sheets. The unanchored beam with 300 mm wide sheets (430G-300-NA) had a 58% decrease in deflection compared to the beam with 200 mm wide sheets (430G-200-NA). The anchored beam with 300 mm wide sheets (430G-300-A) experienced a 1.5% decrease in deflection vs. the beam with 200 mm wide sheets (430G-200-A). Therefore, on average the 300 mm wide sheet configuration (430G-300-A) experienced a decrease in maximum deflection of 30%.

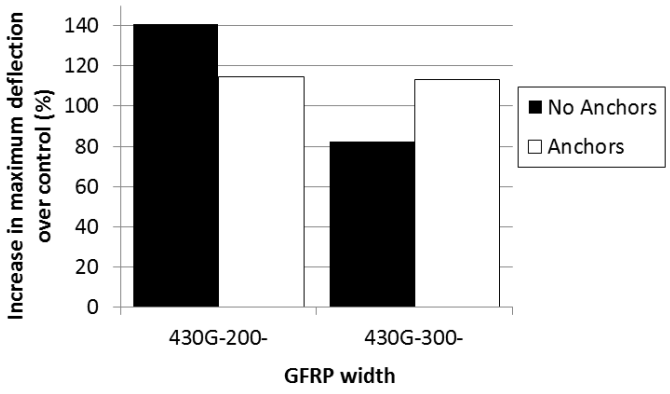

Figure 5-32: Increase in maximum deflection of 200 & 300 mm GFRP sheets over control

Strain Response

A bar chart comparison of the stirrup and GFRP strains at failure for the 200 mm and 300 mm wide GFRP sheet configuration is shown in Figure 5-33 and Figure 5-34, respectively.

Higher overall stirrup strain was recorded with the 200 mm wide configuration because more sections in the shear span were not covered with GFRP sheets which lead to localized areas with higher stirrup strain. The strain in the stirrup decreased in the unanchored beam when the wider (300 mm) sheets were provided (430G-300-NA).

The maximum stirrup strain at failure in the anchored beams decreased by 59% (430G-200-A) and increased by 81% (430G-300-A). The presence of FRP anchors with 200 mm wide configuration decreased the stirrup strain and the presence of anchors with 300 mm wide configuration increased the stirrup strain.

The largest strain in the GFRP sheets was measured in the anchored beams as 8000 με. This corresponds to the observed FRP rupture of the sheet which is lower than the rupture strain reported by the manufacturer (22,100 με).

Both unanchored beams 430G-200-NA and 430G-300-NA experienced FRP debonding at failure (Figure 5-36). The strain to cause debonding in the 200 mm and 300 mm wide sheets was 5000 με and 6000 με, respectively. The theoretical debonding strain for a Sikawrap 430G sheet is 5900 με. The slight difference in the measured strain to cause debonding between the 200 mm and 300 mm wide sheets can be attributed to the bonded area of the GFRP sheet.

The strain profiles across the depth of the beam for the 200 mm and 300 mm wide configurations are shown in Figure 5-35. It is evident that sheet 2 (400 mm form support) showed very high strains on both anchored beams. Both beams with 200 mm wide strips had a bell-shaped profile compared to beam 430G-300-A with 300 mm wide strips which had an L-shaped strain profile. These results indicate that the wider 300 mm sheet distributed the strain evenly throughout the depth compared to the 200 mm wide sheet which had a peak in the strain at mid-depth.

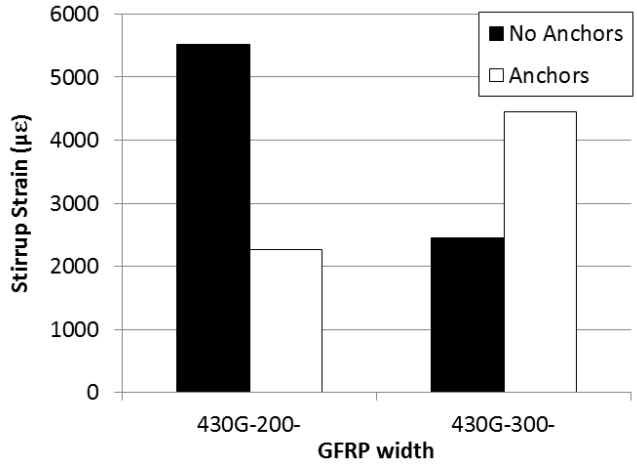

Figure 5-33: Stirrup strain at failure of 200 & 300 mm wide strengthened beams

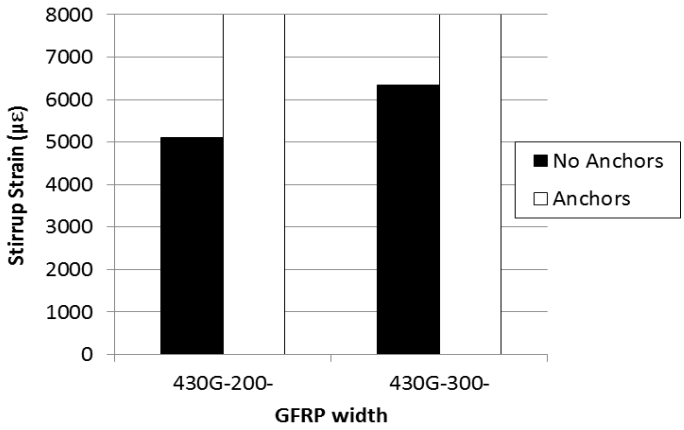

Figure 5-34: GFRP strain at failure of 200 & 300 mm wide strengthened beams

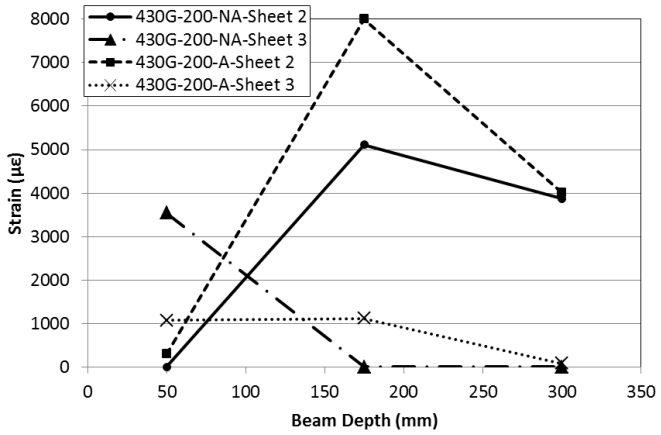

a) 200 mm wide sheets

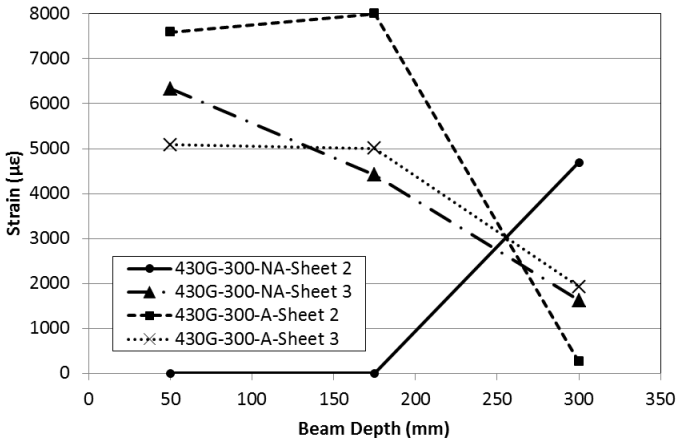

b) 300 mm wide sheets

Figure 5-35: FRP strain response of 430G – 300 mm wide GFRP strengthened beams

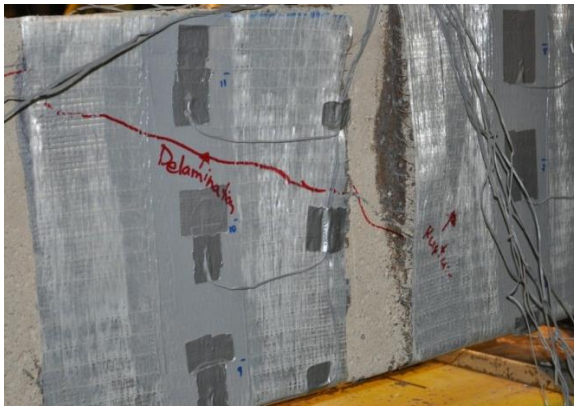

Figure 5-36: Diagonal tension shear crack propagation of beam 430G-300-NA

5.7 Effect of FRP Anchors

In this section the effect of FRP anchors on FRP strengthened and repaired shear critical beams is discussed.

Key findings include: (1) Anchored beams do not have a large drop in load in the post peak behaviour compared to unanchored beams. (2) The presence of FRP anchors increased the shear capacity in u-wrapped GFRP strengthened beams with GFRP sheets ≥ 300 mm. The average increase in shear capacity of beams with GFRP anchors was 24% greater than similar unanchored beams. (3) The maximum strain in u-wrapped FRP sheets was increased with the presence of FRP anchors.

5.7.1 Presence of FRP anchors

Eight shear critical beams were analyzed: Four beams had no anchors and four beams had anchors. (Four beams were strengthened with Sikawrap 430G sheets and four beams were strengthened with Sikawrap 100G sheets).

The load vs. deflection response of the strengthened beams is shown in Figure 5-37. Additional strength was provided in the beams which contained FRP anchors. All eight beams failed in shear with the 1100mm wide 100G sheet recording the highest ultimate strength. The beams with FRP anchors had an enhanced ductility at failure with a much smaller drop in load compared to beams without FRP anchors.

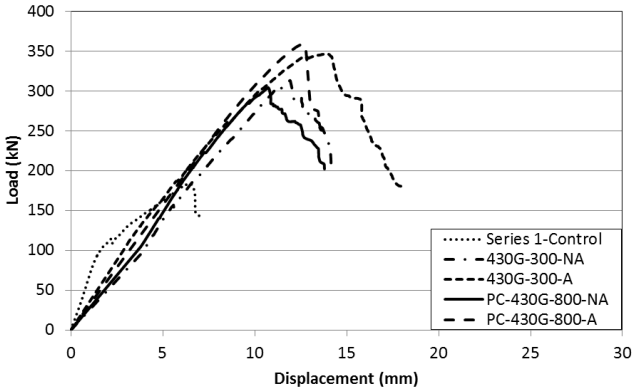

a) Sikawrap 430G strengthened beams

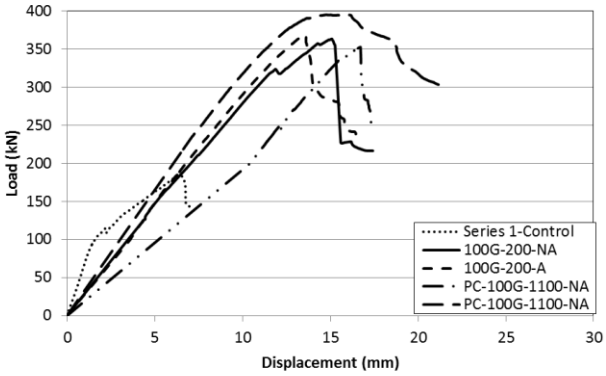

b) Sikawrap 100G strengthened beams

Figure 5-37: Load vs. deflection of GFRP strengthened beams without & with anchors

Effect on Strength

Comparison of the strength increase in beams with GFRP anchors over the companion unanchored beams is displayed in Figure 5-38. The increase in strength was 3% for 100G-200-A, 18% for 430G-300-A, 29% for PC-430G-800-A and 24% for PC-100G-1100-A.

As the amount of the u-wrapped GFRP sheets increased, the effect of FRP anchors also increased. The data suggests that there is a linear relationship between the amount of GFRP sheets and the increase in strength provided by GFRP anchors. Conversely, one can argue that a relationship exists between the debonding capacity and the amount of u-wrapped FRP sheets. Therefore, as the amount of FRP provided for strengthening is increased, the applied load to cause FRP debonding decreased. This can be attributed to the bonded area of the FRP sheet; configurations

with wider sheets have more surface area bonded to the member and thus have higher resistance. It is clear that as the width of a u-wrapped GFRP sheet increases, the efficiency of GFRP anchors to secure these sheets to avoid GFRP debonding increases. This can be attributed to the amount of GFRP provided for strengthening. With the presence of FRP anchors, debonding is no longer a concern and FRP sheets are able to resist higher forces and develop higher strain. Therefore, as the amount of FRP strengthening material is increased, the efficiency of the FRP anchors and the strength capacity is increased.

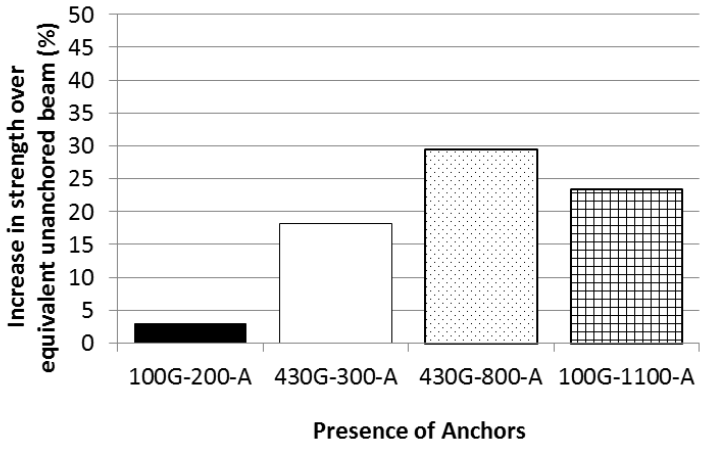

Figure 5-38: Strength increase of anchored beams over companion unanchored beams

Effect on Stiffness

The stiffness of beams with and without anchors showed that the initial stiffness was slightly higher or the same when FRP anchors were installed. The slight increase in stiffness can be attributed to the additional anchorage provided for the FRP sheets. The average stiffness for anchored beams was 27 kN/mm.

Effect on Deflection

Figure 5-39 compares the increase in maximum deflection at failure for beams strengthened with Sikawrap 430G and Sikawrap 100G sheets with anchors over companion unanchored beams. An average increase in deflection of 25% was achieved over companion unanchored beams.

The graph shows that the deflection increased in three beams when anchors were present. The increase in deflection of anchored beams over the companion unanchored beam was 17% (430G-

300-A), 29% (PC-430G-800-A) and 29% (PC-100G-1100-A). Beams PC-430G-800-A and PC-100G-1100-A with continuous GFRP sheets covering the full shear span experienced an additional 12% increase over beam 430G-300-NA with intermittent GFRP strips. One beam (100G-200-A) experienced a 10% decrease in maximum deflection over the companion unanchored beam. This can be attributed to the minimal increase in ultimate load over the companion unanchored beam and the stiffness (E=25 GPa) of the thick (t=1.01 mm) Sikawrap 100G sheet. Providing GFRP anchorage on the 100G sheet eliminated FRP debonding and increased the stiffness causing less deflection at ultimate load.

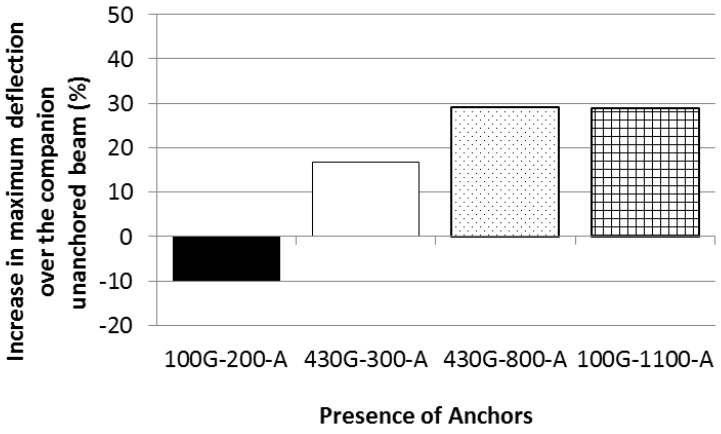

Figure 5-39: Increase in max deflection of anchored beams over companion unanchored beams

Strain Response

A bar chart comparing the maximum stirrup and GFRP strain at failure in beams with and without anchors is shown in Figure 5-40 and Figure 5-41, respectively. The strain in the internal stirrup increased with the presence of GFRP anchors in two cases and decreased in two cases. When anchors were installed the maximum strain in the stirrups at failure decreased by 27% and 26% for beams 100G-200-A and PC-430G-800-A. On the other hand, the stirrup strain increased by 82% and 98% for beams 430G-300-A and PC-100G-1100-A. The stirrups reached higher strain values at failure because of the increased shear strength of the beam and confinement provided by u-wrapped FRP sheets.

The maximum strain in the GFRP sheets at failure increased when GFRP anchors were installed. The increases were: 21% for beam 100G-200-A, 26% for beam 430G-300-A, 22% for beam PC-

430G-800-A and 6% for beam PC-100G-1100-A. The lowest strains were recorded in beams PC-430G-800-A and PC-100G-1100-A with continuous GFRP sheets covering the full shear span. Both beams experienced an average decrease in strain of 10% over beams 430G-300-NA and 100G-200-NA with intermittent GFRP strips.

Securing u-wrapped GFRP sheets with GFRP anchors enabled the GFRP sheets to withstand increased strains compared to unanchored sheets. Therefore, the use of FRP anchors enabled the FRP sheets to utilize their full capacity.

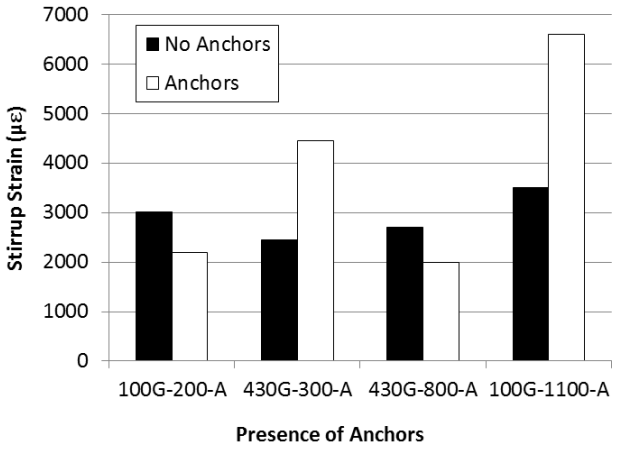

Figure 5-40: Stirrup strain at failure of unanchored & anchored beams

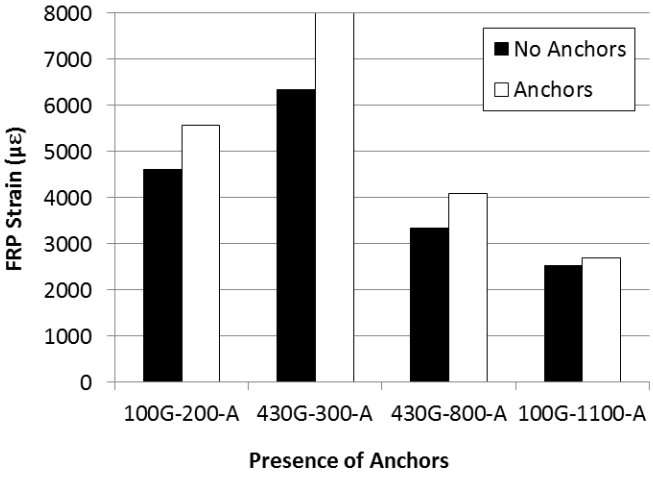

Figure 5-41: GFRP strain at failure of unanchored & anchored beams

5.7.2 FRP Anchors of U-Wrap vs. Full Wrap Beams

In this section the efficiency of FRP anchors to strengthen and repair pre-cracked shear critical beams with u-wrapped GFRP sheets vs. full wrapping is evaluated. Three shear critical beams were repaired with Sikawrap 430G sheets. One beam was repaired with u-wrapped GFRP sheets unanchored (PC-430G-800-NA), one beam was repaired with u-wrapped GFRP sheets secured with GFRP anchors (PC-430G-800-A) and the third beam was repaired with fully wrapped sheets with a 150 mm lap splice (PC-430G-800-FW). The anchored beam (PC-430G-800-A) had seven GFRP anchors spaced every 100 mm.

The efficiency of FRP anchors was established by comparing unanchored, anchored and full wrap sheets in terms of the load, stiffness, deflection and strain response of each beam. The unanchored beam (PC-430G-800-NA) failed by FRP debonding and the GFRP anchored (PC-430G-800-A) and fully wrapped beams (PC-430G-800-FW) both failed in shear by diagonal tension end anchorage failure.

The load vs. deflection curves of the strengthened beams are shown in Figure 5-42. The load deflection behaviour of PC-430G-800-NA and PC-430G-800-FW showed the differences between the unanchored and a fully wrapped beam. Additional strength was provided when the GFRP sheet was secured with GFRP anchors, achieving the same failure load as the full wrap beam.

The three beams experienced a sudden drop in load in their post peak behaviour. The fully wrapped beam had a more ductile gradual failure. This can be attributed to the confinement provided by fully wrapping the beam's cross-section. The GFRP sheet would have to rupture to replicate the sudden post peak failure experienced with the continuous u-wrapped sheets with and without anchors.

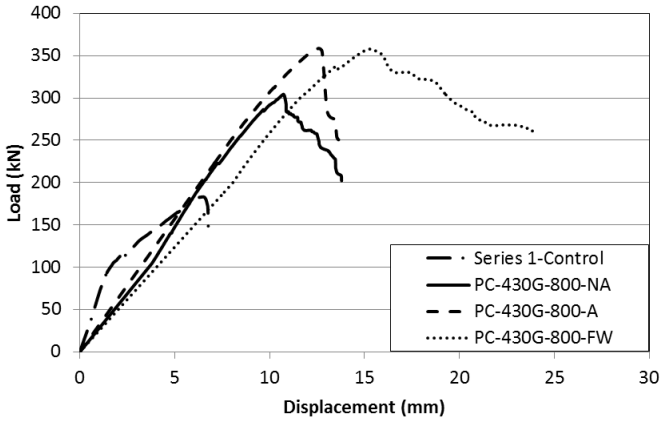

Figure 5-42: Load vs. deflection of pre-cracked beams without & with anchors

Effect on Strength

A comparison of the strength increase of the unanchored, anchored and full wrap Sikawrap 430G strengthened beams over the control is displayed in Figure 5-43. The increase in strength over the control was 66% (PC-430G-800-NA), 95% (PC-430G-800-A) and 95% (PC-430G-800-FW). It is clear that the presence of GFRP anchors to secure u-wrapped GFRP sheets provided the same increase in shear strength as a fully wrapped beam. This is an important finding for the use of GFRP anchors to secure u-wrapped GFRP sheets in situations where full-wrapping is not feasible. The main purpose of installing GFRP anchors was to eliminate GFRP sheet debonding and replicate the anchorage provided by a fully wrapped beam.

However, it should be noted that both the GFRP anchored and fully wrapped beams did not fail by rupture of the GFRP sheets. Failure occurred by propagation of the diagonal tension shear crack in the unstrengthened beam end causing end anchorage failure as is shown in Figure 5-44. Thus, the ultimate capacity of the GFRP sheets and anchors was not achieved. Therefore, FRP anchors proved to be efficient in achieving the same increase in shear strength as a fully wrapped beam. The increase in strength over an unanchored beam was 29%.

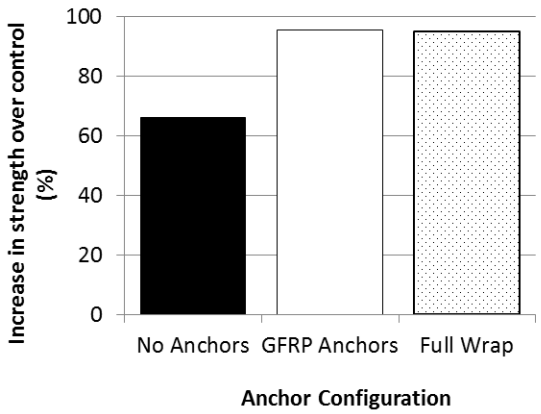

Figure 5-43: Strength increase of anchored beams over the control

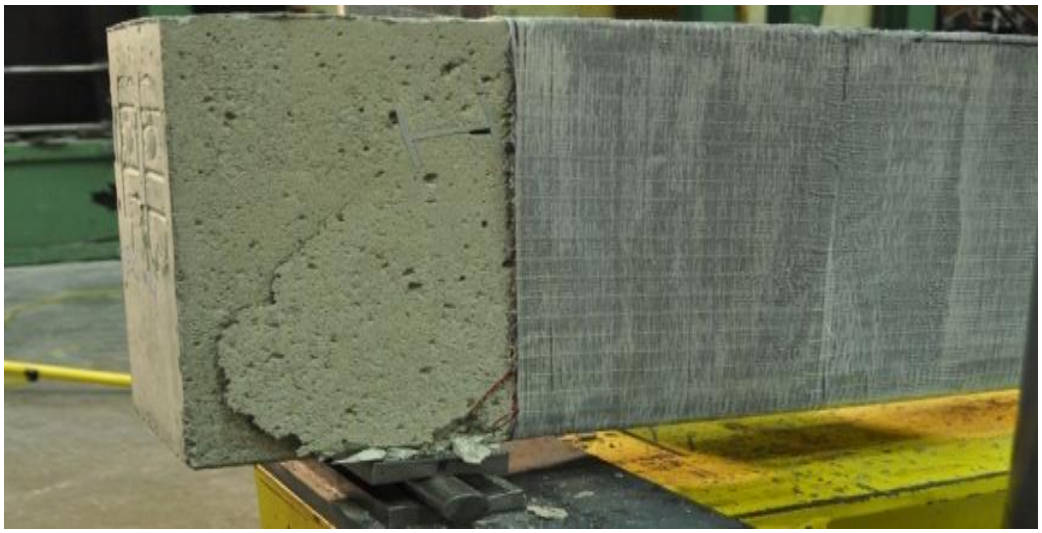

Figure 5-44: Full wrapped beam with end anchorage failure

Effect on Stiffness

The beam stiffness in the strengthened beams increased over the control with the two u-wrapped beams having a slightly stiffer behaviour (30 kN/mm) than the fully wrapped beam (27 kN/mm) as seen in Figure 5-42. The lower stiffness provided by the fully wrapped beam can be attributed to the size and width of the diagonal tension shear crack that was induced during pre-cracking the beam.

Effect on Deflection

A bar chart comparing the maximum deflection at failure is shown in Figure 5-45. The increase in maximum deflection at failure was 64% (PC-430G-800-NA), 93% (PC-430G-800-A) and 134% (PC-430G-800-FW) over the control. The fully wrapped beam had the best performance, this can be attributed to the increased stiffness of the beam provided by full confinement compared to u-wrapping.

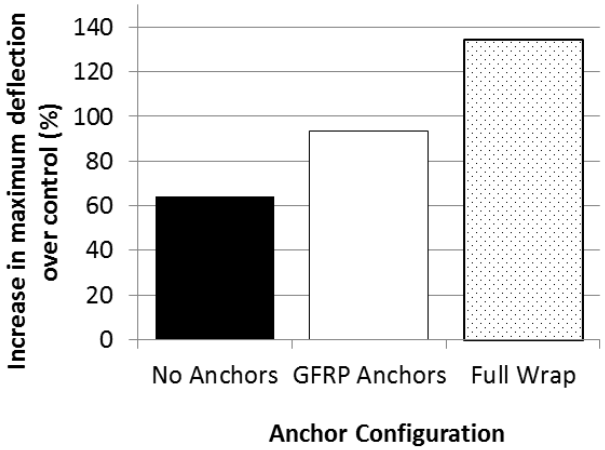

Figure 5-45: Increase in maximum deflection of anchored beams over control

Strain Response

A bar chart comparing the stirrup and GFRP strains at failure is shown in Figure 5-46 and Figure 5-47. Slight increases in the strains at failure were recorded in the GFRP sheets and internal steel stirrups between unanchored, anchored and fully wrapped beams.

The highest strain experienced in the internal steel stirrups was recorded in the unanchored beam. The anchored and fully wrapped beam recorded strains above 2000 με and the difference in stirrup strain between the anchored and fully wrapped beams was minimal. Providing GFRP anchors decreased the strain in stirrups at failure by 33% vs. the unanchored beam.

The FRP strain showed an increasing trend of GFRP strain at failure between the unanchored, anchored and fully wrapped beams. This can be attributed to the anchorage level provided by the GFRP anchors and full wrap which secured the side bonded GFRP sheet from debonding from concrete thus allowing for higher loads and increased FRP strains at failure.

The strain response of the anchored and the fully wrapped beam showed a 13% increase in the full wrap (PC-430G-800-FW) over the anchored beam (PC-430G-800-A). Considering that both beams failed at the same load, the difference in strain can be attributed to the location of the strain gauges on the FRP sheet relative to the location of the shear crack. In the fully wrapped beam, the shear crack was closer to the FRP strain gauges over the GFRP anchored beam and thus recorded higher strains.

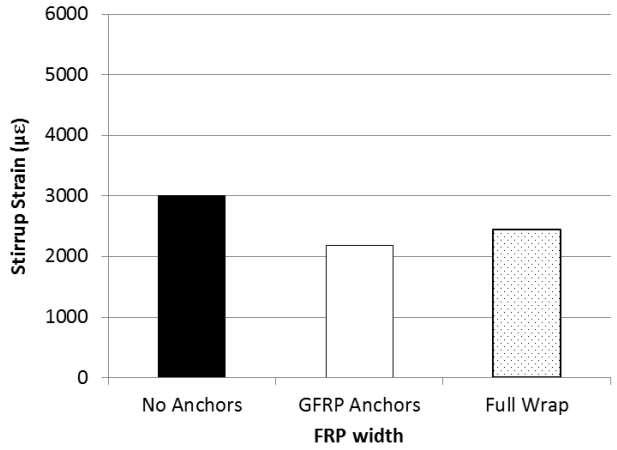

Figure 5-46: Stirrup strain at failure for different anchorage configurations

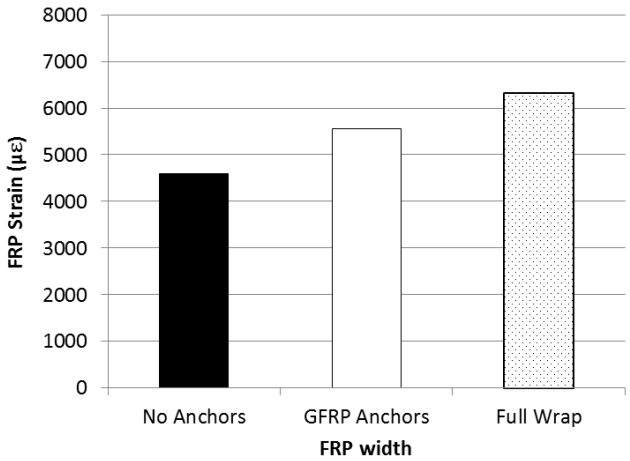

Figure 5-47: GFRP strain at failure for different anchorage configurations

Comparing all unanchored and the companion anchored beams, the strength increases provided by FRP anchors for u-wrapped FRP sheets was:

- 430G-200-A (Sikawrap 430G, 200 mm wide) - 0%
- 100G-200-A (Sikawrap 100G, 200 mm wide) – 1.65%
- 430G-300-A (Sikawrap 430G, 300 mm wide) – 18%
- PC-430G-800-A (Sikawrap 430G, 800 mm wide) – 29%
- PC-100G-1100-A (Sikawrap 100G, 1100 mm wide) – 24%

The average increase in strength provided by FRP anchorage for FRP configurations which did not experience premature loss of aggregate interlock was 24%. A trend observed in the data shows that the wider the u-wrapped FRP sheets, the higher the effect FRP anchors have on the shear strength. This can be explained by the overall increased capacity provided by wider FRP sheets which have a larger effective FRP area (A_{frp}) which allows higher strain resistance.

The two 200 mm wide intermittent u-wrap configurations had very little increase when FRP anchors were installed because loss of aggregate interlock occurred prior to the FRP sheets becoming engaged. The narrow FRP strips were not wide enough to prevent the diagonal crack from propagating and widening causing aggregate interlock to govern regardless if FRP anchors were present.

5.8 Shear Critical Beam Section Highlights

Key trends discovered with FRP strengthening of shear critical beams with and without FRP anchors are highlighted.

- Strain capacity in FRP sheets was increased with the presence of FRP anchors. FRP anchors allowed the FRP sheets to develop higher strains instead of debonding.
- The presence of FRP anchors increased the deflection at failure.
- GFRP anchors provided the same increase in shear strength as a fully wrapped beam.
- Debonding of unanchored FRP sheets by concrete substrate failure occurred at FRP strains between 3000 με to 5000 με.
- Debonding of u-wrapped GFRP sheets occurred at the same strain level regardless of GFRP thickness.
- Debonding of u-wrapped GFRP sheets was decreased as the width of the FRP sheet was increased. Wider GFRP sheets have a larger bonded area which prolongs debonding from occurring compared to narrow GFRP sheets.
- Rupture of 430G GFRP sheets occurred at a strain of 8000 με which is lower than the manufactures specifications (22,100 με).
- Maximum deflection at failure in a strengthened beam was affected by the type of FRP material used and the presence of FRP anchors.
- The shear strengthening contribution of FRP sheets was not directly proportional to the FRP thickness.
- The effect of FRP anchors on shear strength increase is proportional to the width of the u-wrapped FRP sheet.
- It is possible to achieve the rupture strength of a FRP sheet when FRP anchors are provided to eliminate premature debonding.

Chapter 6– Discussion of Flexure Critical Slab Results

6.1 Introduction

Eight flexure critical slabs were tested: one slab was the control (unstrengthened) and seven slabs were strengthened with CFRP sheets and anchors. Test variables were the number of layer of CFRP sheets (one, two) and the use of FRP anchors (no anchors, 8, 12).

The behaviour of the test specimens was monitored visually by recording the cracking patterns and failure modes. Load was measured using a load cell and mid-span deflection was recorded by a LVDT. Strain response of the CFRP sheet and steel rebar were measured using strain gauges. Three CFRP strain gauges were applied along the length of the slab. One gauge was located directly in the center of the slab (1100 mm from the end of the slab), a second gauge was located under one of the loading points (850 mm from the end of the slab) and the third gauge was located 100 mm inside the end of the CFRP sheet (350 mm from the end of the slab). One strain gauge was placed on the flexural steel bar to determine the strain the flexural steel reinforcement and one gauge was placed on the concrete compression fiber.

This chapter discusses the experimental results in terms of failure modes, load-deflection behaviour and load-strain behaviour. The analysis is divided into the following sections:

- Section 6.2 – Observed Behaviour of Flexure Critical Slabs
- Section 6.3 – Failure Modes
- Section 6.4 – Effect of amount of FRP
- Section 6.5 – Effect of FRP Anchors
- Section 6.6 – Flexure Critical Slab Highlights

6.2 Observed Behaviour of Flexure Critical Slabs

In this section, the observed behaviour of flexure critical slabs strengthened with external FRP sheets and FRP anchors are discussed. Comparisons are made based on the type and thickness of FRP sheets used and the presence of FRP anchors to secure the FRP sheets.

6.2.1 Slabs Strengthened with Sikawrap 230C Sheets

Two slabs were strengthened with Sikawrap 230C CFRP sheets. One slab was strengthened with CFRP sheets and the other slab had eight CFRP anchors installed to secure the CFRP sheets. Slabs 230C-2L-NA and 230C-2L-8A are both flexure critical slabs with three 15M steel bars. Each slab was externally strengthened with two layers of 300 mm wide Sikawrap 230C sheets. The failure load of slab 230C-2L-NA was 190 kN and the failure load of slab 230C-2L-A was 201 kN. The slab strengthened with CFRP sheets and anchors did not experience a significant increase in flexural capacity over the unanchored slab.

Slab 230C-2L-A had vertical flexural cracks appearing at mid-span starting at the bottom soffit and extending vertically towards the top face. As the load was increased the number of flexural cracks increased along the length of the slab. For the FRP strengthened beam without FRP anchors, failure was caused by debonding of the CFRP sheets (Figure 6-1). No sudden drop in load was experienced but a slow gradual drop in the post peak load deflection curve was observed. The maximum load was reached when the FRP sheet debonded from the concrete surface.

Figure 6-1: Flexural failure of slab 230C-2L-NA

Slab 230C-2L-A had a 6% increase in the failure load over slab 230C-2L-NA. The presence of FRP anchors did not provide a significant increase in flexural capacity.

Failure occurred when the concrete around the anchor cracked and separated as a cone and the CFRP anchor fibers ruptured. This was accompanied with longitudinal tension splitting of concrete at the level of steel rebar. The failure was brittle with a sudden drop in the load deflection curve. Yielding of the steel reinforcement occurred before concrete cone anchor failure. Figure 6-2 shows photos of the CFRP sheet debonding (a,b), concrete tension splitting (b), concrete cone anchor failure (c) and CFRP anchor rupture (d,e).

In summary, the presence of CFRP anchors to secure CFRP sheets provided a 6% increase in flexural capacity over the unanchored slabs. The failure mode of slab 230C-2L-NA was FRP debonding. Slab 230C-2L-8A which contained eight CFRP anchors failed by concrete cone anchor failure and concrete tension splitting followed by CFRP debonding. Concrete cone and concrete cover failure can be attributed to the low concrete strength in the slabs.

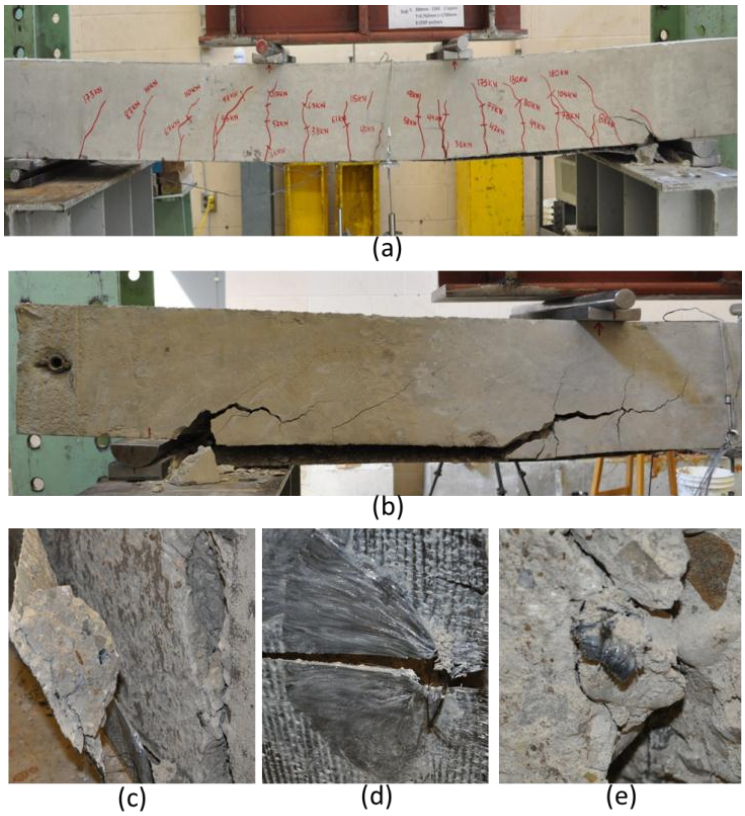

Figure 6-2: Concrete cone anchor failure (b,c) & anchor rupture (d,e) of slab 230C-2L-8A

6.2.2 Slabs with 600C CFRP Strengthening

Three slabs were strengthened with Sikawrap 600C CFRP sheets. One slab was strengthened with only CFRP sheets and two slabs had CFRP anchors installed. One slab had eight anchors and the other slab had twelve anchors used to secure the CFRP sheets. Slabs 600C-2L-NA, 600C-2L-8A and 600C-2A-12A are flexure critical slabs each with three 15M bars. All three slabs were externally strengthened with two layers of 300 mm wide Sikawrap 600C sheets. The failure load of slab 600C-2L-NA was 192 kN; slab 600C-2L-8A was 228 kN; and slab 600C-2L-12A was 219 kN.

Slab 600C-2L-NA had initial flexural cracks in the center span. The cracks originated from the bottom face and propagated vertically towards the top face of the slab. As the load was increased, the number of flexural cracks increased along the length of the slab. Failure was caused by debonding of the CFRP sheets followed by concrete cover failure (Figure 6-3). A sudden drop in load was experienced in the post peak load deflection curve.

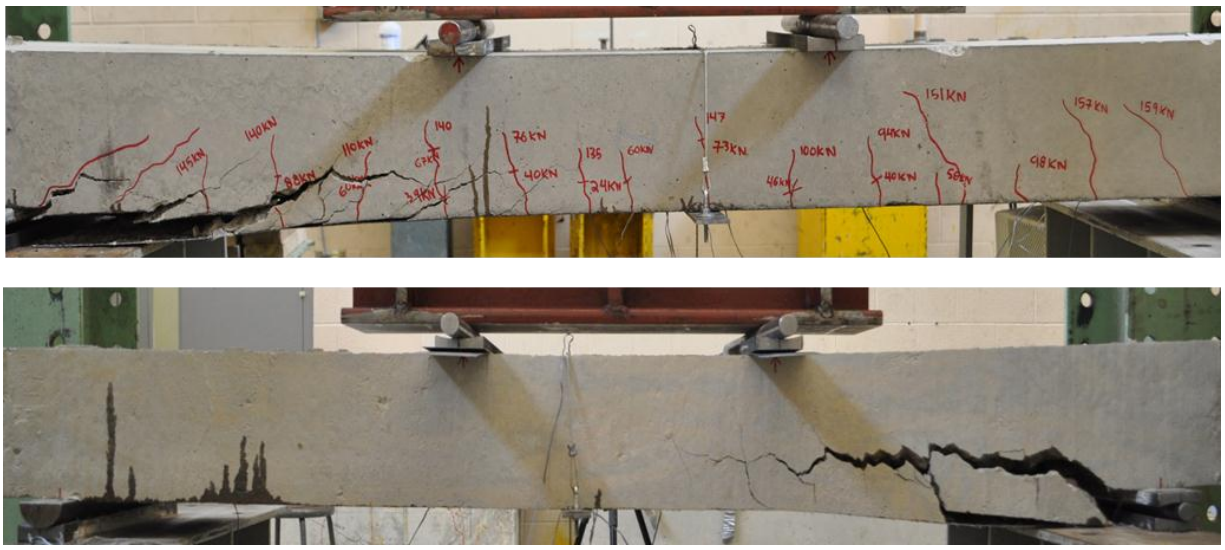

Figure 6-3: Failure of slab 600C-2L-NA

CFRP strengthening increased the flexural capacity of the slab causing simultaneous FRP debonding and concrete cover failure. Installing such a large amount of flexural reinforcement on the bottom face of the slab caused failure to occur at the concrete/steel rebar interface. Figure 6-4 shows a close up of the concrete cover failure that occurred in slab 600C-2L-NA.

Slabs 600C-2L-8A and 600C-2L-12A resulted in 19% and 14% increase in the failure load over slab 600C-2L-NA. The presence of FRP anchors offered significant benefits by delaying premature debonding and thus increasing the flexural capacity of the slab. Initially, flexural cracks appeared starting from the bottom surface extending vertically upwards. As the load was increased, additional diagonal cracks developed in the shear spans. Ultimate failure occurred by concrete cover failure at the concrete/steel rebar interface in slab 600C-2L-8A (Figure 6-5) and intermediate flexural-shear crack induced interfacial debonding in slab 600C-2L-12A (Figure 6-6). The concrete cover failure experienced at the concrete/steel rebar interface can be attributed to the low concrete strength in the slabs.

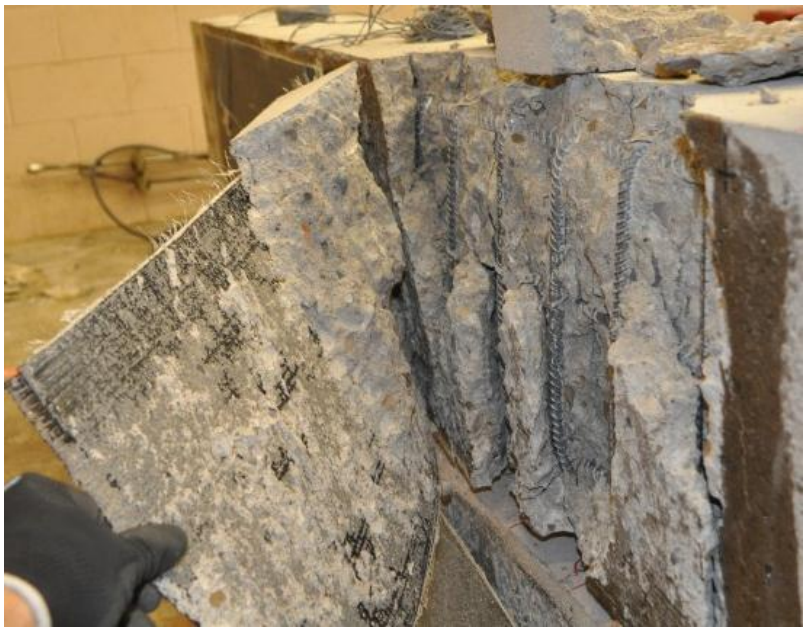

Figure 6-4: Concrete cover failure at steel rebar interface (no anchors)

In summary, the failure mode of slab 600C-2L-NA was debonding of the CFRP sheets and concrete cover failure with a 45% increase in flexural capacity over the control. Slab 600C-2L-8A experienced concrete cover failure with a 19% increase in capacity over the companion unanchored slab. Slab 600C-2L-12A experienced intermediate flexural-shear crack induced interfacial debonding failure with a 14% increase in capacity over the companion unanchored slab.

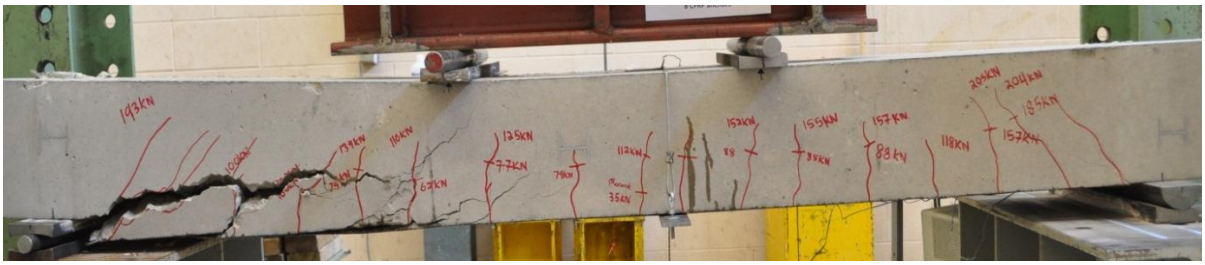

Figure 6-5: Failure of slab 600C-2L-12A

Figure 6-6: Failure of slab 600C-2L-8A

6.3 Failure Modes

Five different failure modes occurred when testing flexure critical slabs strengthened with CFRP sheets and FRP anchors. The failure modes include:

- Flexural failure - Figure 6-7a
- FRP debonding - Figure 6-7b,c
- FRP rupture - Figure 6-7d, e
- Concrete cover failure - Figure 6-7f, g
- Anchor pullout and rupture - Figure 6-7h

Flexural failure occurred in all but two slabs. Flexural failure is characterized by the formation of vertical flexural cracks beginning at the bottom of the slab (tension face) between the loading points or in the center span. Failure was gradual by yielding of the longitudinal steel followed by crushing of concrete in the compression zone.

Yielding of the internal steel rebar was delayed with the application of flexural CFRP sheets. The strength and stiffness of slabs was increased with the application of FRP strengthening. The quality of application of FRP sheets affects their strength contribution and quality of bond to the concrete substrate.

Observations of the five failure modes identified various trends based on the FRP strengthening configuration. The control slab (unstrengthened) failed in flexure by yielding of the tensile steel followed by crushing of the concrete (Figure 6-7a). Three strengthened slabs failed by FRP debonding (Figure 6-7b, c), with one slab containing FRP anchors. One slab failed by FRP rupture (Figure 6-7d, e), this slab had the least amount of FRP strengthening and did not contain any CFRP anchors. Two slabs failed by concrete cover delamination (Figure 6-7f, g), both of these slabs had high CFRP reinforcement with and without CFRP anchors. One slab failed by concrete cone anchor pullout and anchor rupture (Figure 6-7h).

CFRP anchors used to secure CFRP sheets to strengthen a slab in flexure eliminated FRP debonding but changed the mode of failure by shifting the critical strain region from the bottom soffit to the concrete/steel rebar interface. The efficiency of CFRP anchors was maximized and

no additional flexural capacity was achieved by installing twelve anchors vs. eight anchors. Optimizing the number of CFRP anchors is a significant finding.

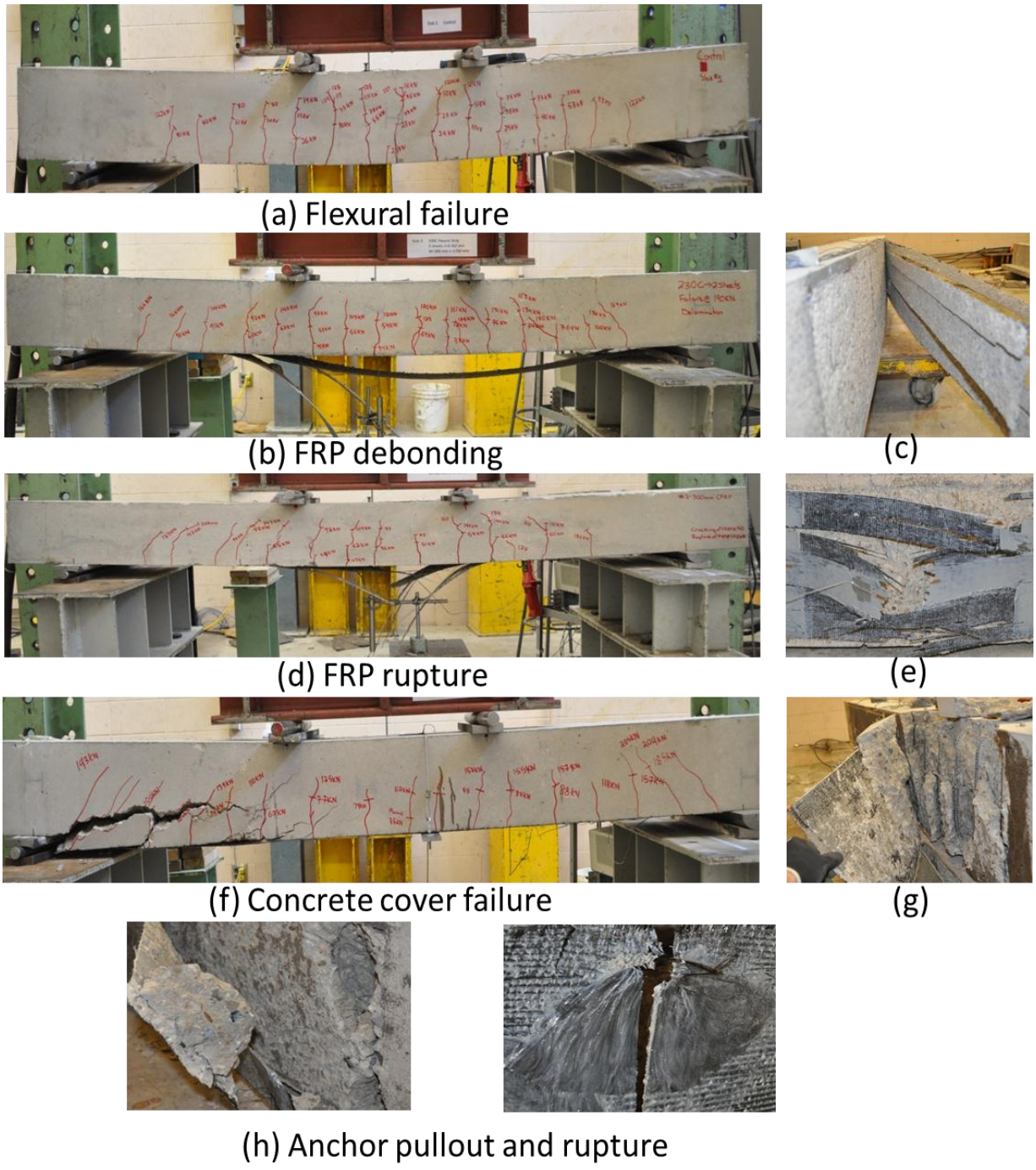

Figure 6-7: Failure modes of flexure critical slabs

6.4 Effect of Amount of FRP

In this section the effect of the amount of FRP used to strengthen or repair a flexure critical slab on the load, stiffness, deflection and the strain response is analyzed. Each comparison includes slabs with and without anchors.

Four flexure critical slabs were strengthened with two types of CFRP sheets (Table 6-1). Two slabs were strengthened with one layer of CFRP sheets: (230C-1L-NA and 600C-1L-NA) and two slabs were strengthened with two layers of CFRP: (230C-2L-NA and 600C-2L-NA).

The load vs. deflection curves of all four slabs is shown in Figure 6-9. Figure 6-9a compares the slab strengthened with one Sikawrap 230C sheet (230C-1L-NA), the slab strengthened with two layers of Sikawrap 230C sheet (230C-2L-NA) and the control slab. Figure 6-9b compares the slab strengthened with one Sikawrap 600C sheet (600C-1L-NA), the slab strengthened with two layers of Sikawrap 600C sheet (600C-2L-NA) and the control slab. The ultimate loads for the control, slabs 230C-1L-NA, 230C-2L-NA, 600C-1L-NA and 600C-2L-NA were 132 kN, 174 kN, 190 kN, 186 kN and 192 kN, respectively.

The additional flexural strength provided by the thicker Sikawrap 600C sheet over the Sikawrap 230C sheet changed the failure mode from FRP rupture to FRP debonding. The difference in failure mode was clear in the load deflection curves of slabs 230C-1L-NA and 600C-1L-NA. The post peak behaviour of the slabs strengthened with Sikawrap 230C had a ductile failure with rupture of the CFRP sheet compared to the slab strengthened with Sikawrap 600C which had a sudden failure with debonding of the CFRP sheet.

Slabs strengthened with 2 layers of Sikawrap 600C and 230C sheets had the same load at failure triggered by debonding of the CFRP sheets. This suggests that a maximum strain limit is reached with 2 layers of unanchored CFRP laminates causing debonding to occur and a plateau in capacity regardless of the amount of CFRP material. However, differences in the post peak behaviour between the two slabs showed gradual failure after debonding of the CFRP sheet in slab 230C-2L-NA compared to slab 600C-2L-NA which showed a more sudden failure with debonding of the CFRP sheet.

Significant change in the structural behaviour of slabs strengthened with two layers of Sikawrap 600C was also observed. The failure region shifted from the bottom soffit of the slab to the concrete steel rebar interface causing concrete cover failure at the concrete/steel rebar interface (Figure 6-8). The performance of beams strengthened with thicker Sikawrap 600C sheets was slightly better than the beams strengthened with Sikawrap 230C sheets.

Figure 6-8: Concrete cover failure at concrete/steel rebar interface

Table 6-1: CFRP strengthening and failure data

Nomenclature	Sheet	Thickness (mm)	Maximum strain in CFRP at Ultimate load (με)	Ultimate Load (kN)	Failure mode
Control				132	• FF
230C-1L-NA	230C	0.381	10,743	174	• FRP R
230C-2L-NA	230C	0.762	7798	190	• FRP-D
600C-1L-NA	600C	1.30	7000	186	• FRP-D
600C-1L-NA	600C	2.60	3627	192	• FRP-D & CCF

where: FF=Flexural failure with concrete crushing, FRP R=FRP rupture, FRP D=FRP debonding, CCF=Concrete cover failure

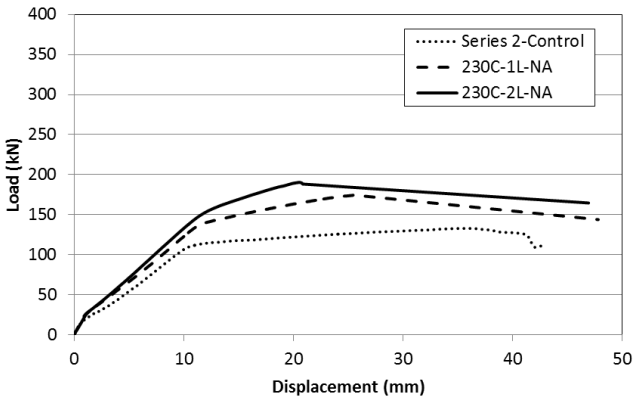

a) Sikawrap 230C strengthened slabs

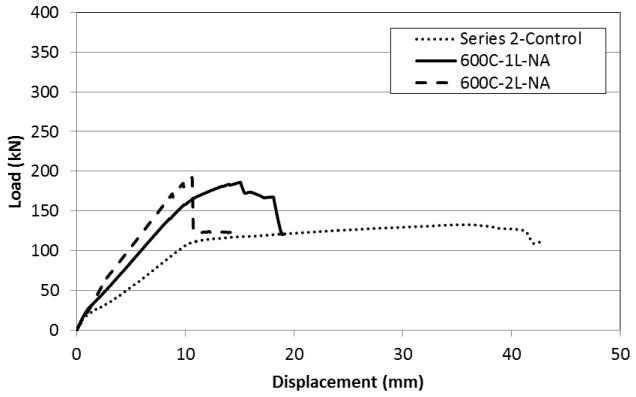

b) Sikawrap 600C strengthened slabs

Figure 6-9: Load vs. deflection of slabs strengthened with Sikawrap 230C & 600C sheets

Effect on Strength

A comparison of the strength increase of slabs strengthened with one and two layers of Sikawrap 230C and Sikawrap 600C are shown in Figure 6-10. The increase in strength over the control for the slabs strengthened with one layer of Sikawrap 230C and 600C sheet was 32% and 41%, respectively. The increase in strength over the control for the slabs strengthened with two layers of Sikawrap 230C and 600C sheets was 44% and 46%, respectively.

It was evident that two layers of Sikawrap 230C provided approximately the same increase in strength as one layer of Sikawrap 600C. This can be attributed to the increase in thickness provided by the second layer. However, two layers of Sikawrap 230C increased the strength of

the slab by 38% over one layer. This implies that the increase in strength is not linearly proportional to the amount of FRP applied. The additional strength provided by Sikawrap 600C sheets can be attributed to the thickness of the sheet. Sikawrap 600C is 3.4 times as thick as Sikawrap 230C sheet (1.30 mm vs. 0.381 mm).

Slabs 230C-2L-NA and 600C-2L-NA reached the same ultimate strength because both slabs failed by debonding. The strain limit in the concrete substrate was lower than the tensile strength of two layers of Sikawrap 230C and 600C. In theory the Sikawrap 600C sheet should provide a significant increase in the flexural capacity but premature FRP debonding occurred due to the lack of anchorage of the CFRP sheet.

The ultimate capacity of two layers of Sikawrap 230C or 600C could not be determined because debonding occurred in both slabs. FRP anchorage is required to obtain the full capacity and provide a fair comparison of Sikawrap 230C and 600C sheets.

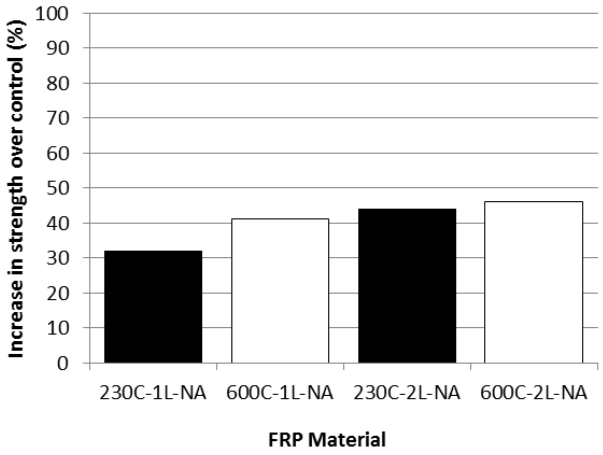

Figure 6-10: Strength increase of 230C & 600C CFRP strengthened slabs over the control

Effect on Stiffness

The slab stiffness was increased in all CFRP strengthened slabs over the control. The slab strengthened with one layer of Sikawrap 600C was stiffer (15 kN/mm) compared to the slab strengthened with one layer of Sikawrap 230C sheet (12 kN/mm).

The slab stiffness increased in both slabs when 2 layers of CFRP were applied. Slab 600C-2L-NA strengthened with two layers of Sikawrap 600C had a very high stiffness (19.2 kN/mm) compared to slab 230C-2L-NA (10.5 kN/mm). The presence of two layers of CFRP sheets led to higher stiffness increases for Sikawrap 600C sheets.

Effect on Deflection

A bar chart comparing the deflection at ultimate load is shown in Figure 6-11. Slabs strengthened with one and two layers of Sikawrap 600C sheets experienced a 58% and 71% decrease in deflection, respectively over the control. Conversely, slabs strengthened with one and two layers of the thinner Sikawrap 230C sheets recorded a 33% and 43% decrease in deflection, respectively over the control.

Comparing Sikawrap 600C and 230C sheets showed that slabs strengthened with one and two layers of Sikawrap 600C resulted in decreases of 20% and 28%, respectively over companion slabs strengthened with Sikawrap 230C. These results show that CFRP strengthening causes a reduction in ultimate deflection and that the decrease is significantly affected by the amount of CFRP strengthening applied. The reduction in deflection is occurring because the flexural steel reinforcement is not yielding (increasing the deflection) prior to failure. Since such a large amount of external flexural strengthening is being provided other components of the slab are failing before the flexural steel reinforcement had the opportunity to yield.

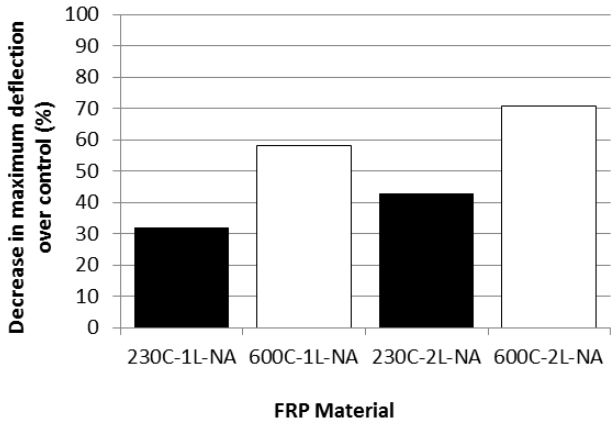

Figure 6-11: Decrease in maximum deflection of 230C & 600C CFRP slabs over the control

Strain Response

A bar chart comparing the strain at failure is shown in Figure 6-12 and Figure 6-13. The steel rebar strain at failure is shown in Figure 6-14. Slabs strengthened with Sikawrap 230C sheets experienced higher strains in the CFRP and the steel rebar compared to slabs strengthened with Sikawrap 600C sheets. This correlates with the deflection results where the maximum deflection at failure was significantly higher for the Sikawrap 230C strengthened slabs. The largest strains in the CFRP sheets was recorded at mid-span in both slabs. The ultimate strain capacity of the Sikawrap 230C sheet was 10,000 με with failure occurring by rupture of the CFRP fibers. Both slabs with two layers of CFRP failed by CFRP debonding which occurred at strains of 7,798 με (230C-2L-NA) and 3,627 με (600C-2L-NA).

34% and 53% decreases in CFRP strain was recorded with one and two layers of Sikawrap 600C over Sikawrap 230C (Figure 6-12). Slab 230C-1L-NA failed by rupture of the CFRP sheet which explains the higher strains in the CFRP material and steel. Slab 600C-1L-NA failed by CFRP debonding, lower strains were recorded in the CFRP and flexural steel.

The steel rebar strains were greater than 2000 με indicating that the flexural steel rebar yielded recorded values of 7000 με for both slabs 230C-1L-NA and 230C-2L-NA and 5000 με and 2495 με for slabs 600C-1L-NA and 600C-2L-NA. The highest strains recorded at mid-span were: 10,743 με (230C-1L-NA), 7006 με (600C-1L-NA), 7798 με (230C-2L-NA) and 2495 με (600C-2L-NA). These results indicate that the highest strain for a single Sikawrap 600C sheet can withstand prior to debonding is 7000 με and the ultimate capacity of a Sikawrap 230C sheet at rupture is 10,743 με.

Slabs strengthened with Sikawrap 230C sheets experienced much higher strains in the steel rebar and the CFRP sheet than slabs strengthened with Sikawrap 600C. This is related to the larger amount of FRP provided by the thicker Sikawrap 600C material over the Sikawrap 230C material. This can be explained by the amount of reinforcement provided (A_{frp}), therefore as the amount of material provided is increased, the strain in the FRP material decreases.

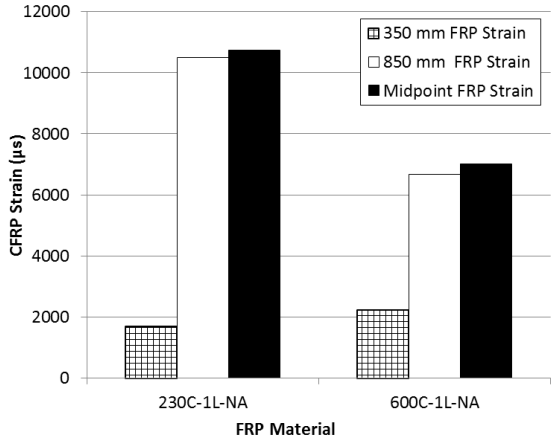

Figure 6-12: CFRP strain at failure - 1 layer of Sikawrap 230C or 600C

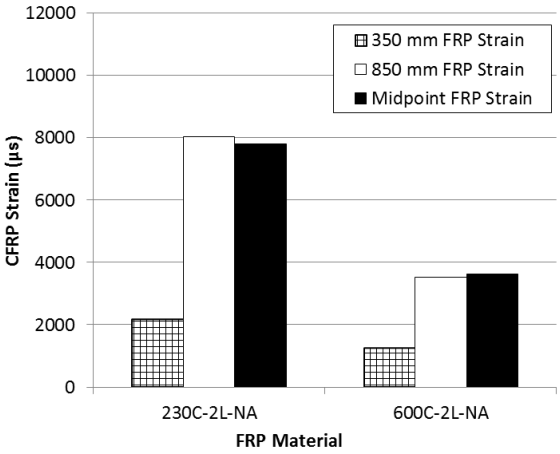

Figure 6-13: CFRP strain at failure - 2 layers of Sikawrap 230C or 600C

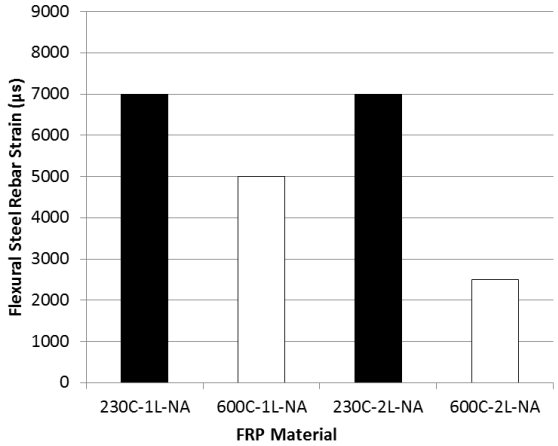

Figure 6-14: Steel rebar strain at failure of Sikawrap 230C & 600C strengthened slabs

6.5 Effect of FRP Anchors

In this section the effect of FRP anchors used to eliminate FRP debonding in CFRP strengthened flexural critical slabs on the load, stiffness, deflection and strain response is presented. Five flexural critical slabs were analyzed in two separate groups. Each group consisted of an unanchored and anchored CFRP strengthened slabs with two layers of Sikawrap 230C or Sikawrap 600C CFRP sheets. The CFRP anchors have a diameter of 10 mm, E=70GPa and $\varepsilon_{rupture}$=3.99% and were installed at 280 mm and 850 mm from both ends of each slab.

Three trends were discovered with CFRP strengthened slabs with CFRP anchors: Slabs had a smaller drop in load in the post peak behaviour compared to unanchored slabs. The average increase in flexural capacity of slabs with anchors was 17% over companion unanchored slabs. The maximum strain in flexural CFRP sheets was increased with the presence of FRP anchors.

6.5.1 Presence of FRP Anchors – 2 Layers of Sikawrap 230C

The load vs. deflection response of two slabs strengthened with two layers of Sikawrap 230C is shown in Figure 6-15. One slab strengthened without anchors (230C-2L-NA) and one slab strengthened with eight CFRP anchors (230C-2L-8A) are plotted with the control. The ultimate strength of the control, slab 230C-2L-NA and slab 230C-2L-8A was 132 kN, 190 kN and 201 kN, respectively.

The behaviour CFRP strengthened slabs exhibited typical flexural failure with vertical flexural cracking. Providing CFRP anchors changed the failure from FRP debonding in the unanchored slab to anchor pullout and rupture. The anchored slab experienced an 18% higher ultimate load over the unanchored slab. Both strengthened slabs had significant strength increases over the control.

The post peak behaviour of the unanchored slab (230C-2L-NA) showed a gradual failure past the peak load while the anchored slab experienced a sudden drop in load.

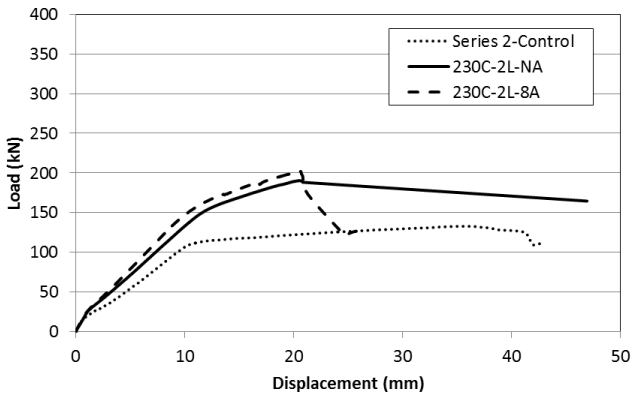

Figure 6-15: Load vs. deflection of unanchored and anchored 230C strengthened slabs

Effect on Strength

Figure 6-17shows the strength increase in slabs with CFRP anchors over the companion unanchored slab is shown in. The increase in strength of the strengthened slab without CFRP anchors was 44% (230C-2L-NA) and the slab with eight CFRP anchors was 52% (230C-2L-8A). The additional increase in strength can be attributed to the eight CFRP anchors. The presence of CFRP anchors eliminated the CFRP debonding observed in 230C-2L-NA which caused the slab to fail prematurely by CFRP anchor rupture and concrete cone anchor failure (Figure 6-16).

Figure 6-16: Concrete cone anchor failure and anchor rupture

In theory, CFRP flexural strengthening should reach the rupture capacity of the CFRP sheets when adequate anchorage is provided. However, the full capacity of a CFRP strengthened slab with CFRP anchors and the full contribution of CFRP anchors could not be determined because of the two types of premature anchor failure that occurrs.

The critical stress region was transferred from the CFRP sheet in the unanchored slab to the CFRP anchors in the anchored slab. This resulted in a change in the mode of failure due to the presence of CFRP anchors and the quality of the CFRP anchor installation.

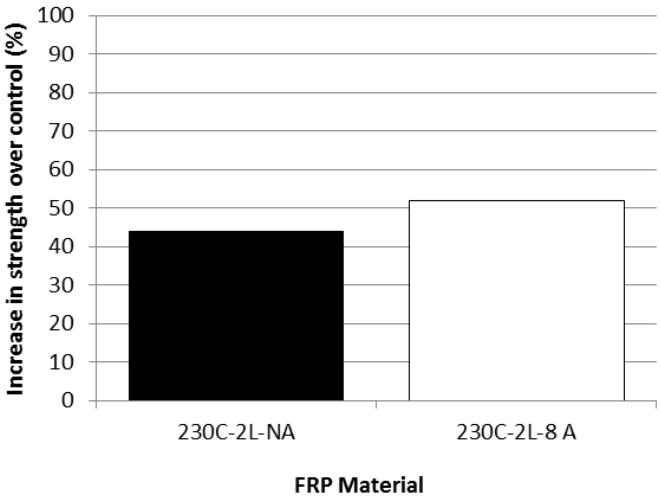

Figure 6-17: Strength increase of unanchored and anchored 230C slabs over the control

Effect on Stiffness

The stiffness of the anchored and unanchored slabs was 12.5 kN/mm and was not affected by the addition of CFRP anchors. Both slabs (unanchored and anchored) had the same behaviour experiencing increased stiffness over the control.

Effect on Deflection

A bar chart comparing the deflection at ultimate load is shown in Figure 6-18. The deflection at ultimate load for both slabs resulted in an average decrease of 44% over the control. The unanchored (230C-2L-NA) and anchored (230C-2L-8A) slabs experienced a 43% and 44% decrease in deflection over the control. It is evident that the presence of eight CFRP anchors did not cause any additional decrease in deflection over the unanchored slab. However, the primary mode of failure of the anchored slab was failure of the CFRP anchors and thus, no conclusion can be made on the effectiveness of the CFRP anchors without further research.

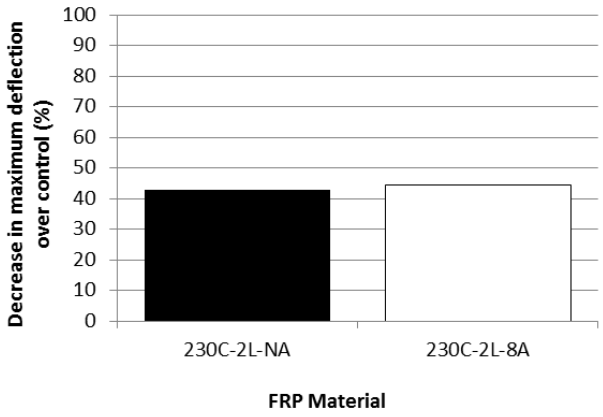

Figure 6-18: Decrease in maximum deflection of 1 & 2 layers of 230C sheets over control

Strain Response

The largest strain in the CFRP material was recorded at mid-span in both slabs with the anchored slab recording an additional 1000 με over the unanchored slab. The maximum strain recorded at mid-span was 8018 με (230C-2L-NA) and 8978 με (230C-2L-8A).

The CFRP strain in the anchored slab over the unanchored slab at the end (350 mm from the end of the slab) and under the loading point (850 mm from the end of the slab) exhibited decreases of 70% and 35%, respectively. At mid-span, the CFRP strain of the anchored slab (230C-2L-8A) exhibited a 15% increase over the unanchored slab (230C-2L-NA). These increases correspond with the flexural strength increases obtained.

Providing CFRP anchors decreased the strain at failure in the CFRP along the flexural sheet at two locations close to where anchors were applied. The maximum strain in the CFRP was 9000 με in the anchored slab when concrete cone anchor failure occurred. In the unanchored slab, failure occurred by CFRP debonding in the concrete substrate. It can be concluded that CFRP debonding on a multi-layered Sikawrap 230C strengthened slab will occur when FRP strain reaches 8000 με. This is slightly higher than the theoretical debonding strain limit of 7000 με specified by ISIS-M04. The flexural steel strain response showed both slabs yielded recording strains greater than 2000 με (Figure 6-20). Figure 6-19 compares the CFRP strain at failure of unanchored and anchored slabs.

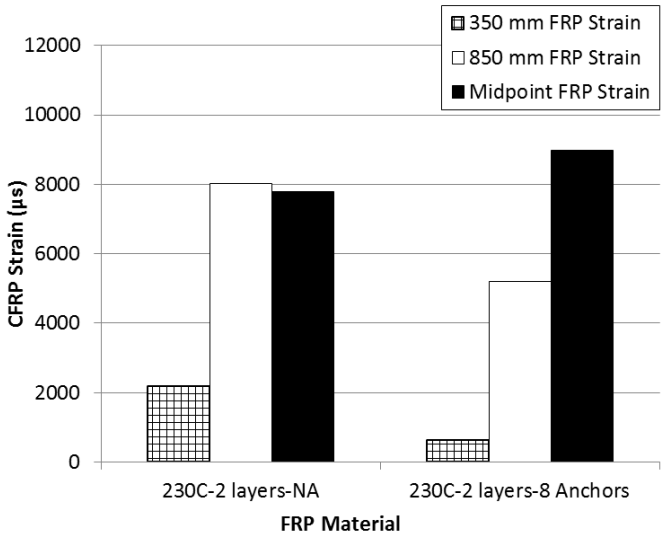

Figure 6-19: CFRP strain at failure of unanchored and anchored Sikawrap 230C strengthened slabs

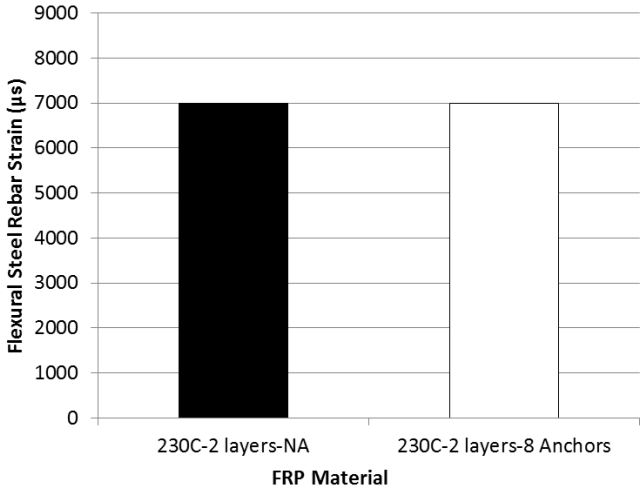

Figure 6-20: Flexural steel rebar strain at failure of unanchored and anchored Sikawrap 230C strengthened slabs

6.5.2 Presence of FRP Anchors – 2 Layers of 600C CFRP

The load vs. deflection response of three slabs strengthened with two layers of Sikawrap 600C are shown in Figure 6-22. One slab without CFRP anchors (600C-2L-NA), one slab with eight CFRP anchors (600C-2L-8A) and one slab with twelve CFRP anchors (600C-2L-12A) are plotted with the control. The ultimate strength of the control, slab 600C-2L-NA, slab 600C-2L-8A and slab 600C-2L-12A was 132 kN, 192 kN, 228 kN and 219 kN, respectively.

Slab 600C-2L-12A had an additional two anchors placed at 570 mm from each end (Figure 6-21). Each slab with CFRP anchors obtained additional increases in strength over companion unanchored slabs. The three slabs experienced three different failure modes: FRP debonding and concrete cover failure (600C-2L-NA), concrete cover failure (600C-2L-8A) and intermediate flexural shear crack induced interfacial debonding (600C-2L-12A) The two slabs with CFRP anchors recorded a 23% increase in flexural strength over the companion unanchored slab and a 70% increase in flexural strength over the control.

The post peak behaviour of the strengthened slabs showed that each slab with two layers of CFRP strengthening failed with a sudden drop in load. The two anchored slabs exhibited a smaller drop in load maintaining a reserve capacity compared to the unanchored slab.

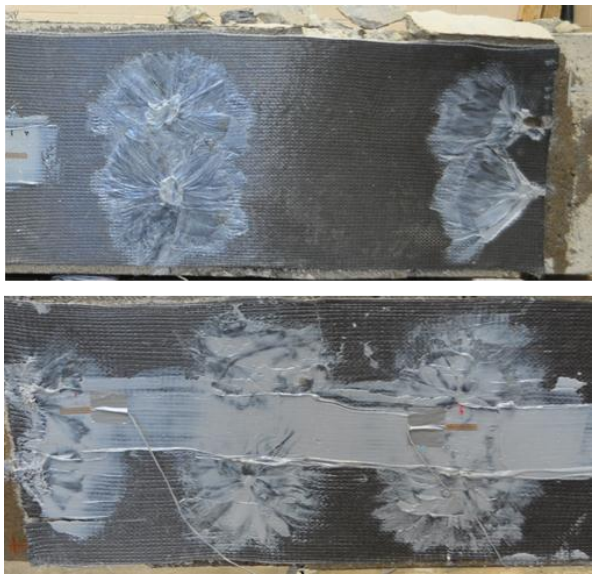

Figure 6-21: Eight and twelve anchor configuration

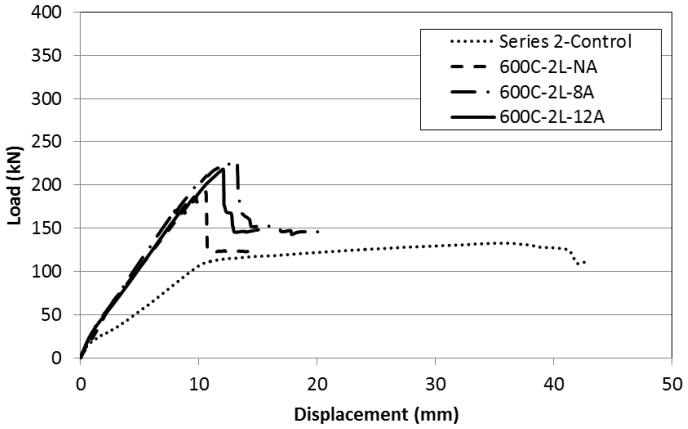

Figure 6-22: Load vs. deflection of unanchored and anchored 230C strengthened slabs

Effect on Strength

Figure 6-23compars the strength increase in slabs with CFRP anchors over the companion unanchored slab. The increase in strength of the strengthened slab without CFRP anchors was 46% (600C-2L-NA), for the slab with eight CFRP anchors was 73% (600C-2L-8A) and for the slab with twelve CFRP anchors was 66% (600C-2L-12A). The strengthened slab with twelve anchors exhibited a 10% reduction in strength and different failure mode compared to the slab with eight CFRP anchors.

Comparing the increase in strength capacity between the slabs with eight and twelve anchors revealed that the optimum amount of anchors was reached in such a way that the additional four anchors installed did not provide any additional increase in flexural strength but rather changed the mode of failure which led to a reduction in strength.

The average increase in strength of both slabs with anchors was 24% over the unanchored slab. Applying eight CFRP anchors eliminated any CFRP sheet debonding but the critical failure region moved from the bottom soffit of the slab to the concrete/steel rebar interface.

Twelve CFRP anchors did not provide any increase in strength over the strengthened slab with eight CFRP anchors and did not prevent concrete cover failure from occurring. Instead, wide horizontal cracks along the concrete and flexural steel interface were the primary mode of failure similar to what was experienced in the slab with eight anchors.

In theory, CFRP flexural strengthening should reach the rupture capacity of the CFRP sheets when adequate anchorage is provided. However, the full capacity of a CFRP strengthened slab with CFRP anchors and the full contribution of CFRP anchors could not be determined because failure occurred at the concrete/steel rebar interface.

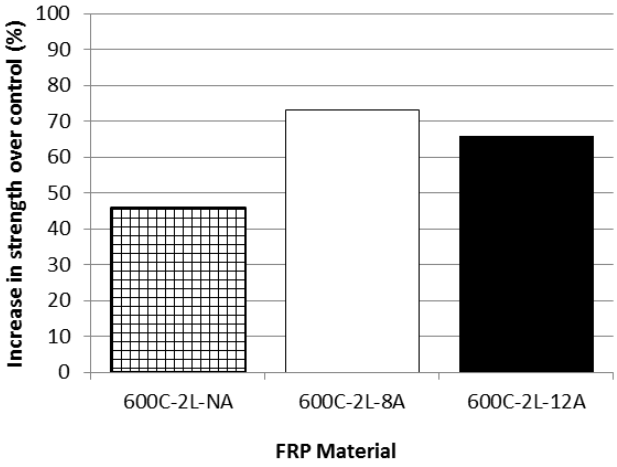

Figure 6-23: Strength increase of unanchored and anchored 230C slabs over the control

Effect on Stiffness

The stiffness of unanchored and anchored slabs was 17.5 kN/mm and was not affected by the addition of CFRP anchors. Both slabs (unanchored and anchored) had the same behaviour increasing the stiffness over the control.

Effect on Deflection

A bar chart comparing the deflection at ultimate load is shown in Figure 6-18. The deflection at ultimate load for both slabs had an average decrease in deflection of 65% over the control. The unanchored slab (600C-2L-NA) experienced a 71% decrease in deflection over the control and the anchored slabs (600C-2L-8A) and (600C-2L-12A) experienced 63% and 67% decreases in deflection over the control. The presence of CFRP anchors caused an additional 10% decrease in deflection at ultimate load over the unanchored slab. No increase was obtained between the slabs with eight and twelve anchors.

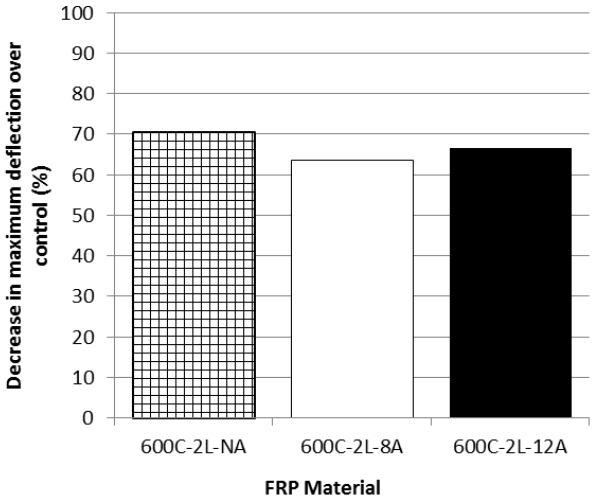

Figure 6-24: Decrease in maximum deflection of slabs without and with anchors

Strain Response

Figure 6-25 compares the CFRP and flexural strain at failure of unanchored and anchored slabs. The unanchored slab (600C-2L-NA) experienced the lowest strains in the CFRP and steel rebar relative to the anchored slabs. This can be attributed to the higher loads reached by the anchored slabs compared the unanchored slab. The highest strain in the CFRP sheet was 4666 με at mid-span of slab 600C-2L-8A with eight anchors. The average increase in CFRP strain in the anchored slab over the unanchored slab was: 20% (350 mm from the beam end), 14% (850 mm from the beam end) and 27% (mid-span).

The CFRP strain in the slabs with eight and twelve anchors showed no difference between the two strengthening configurations. This means that eight CFRP anchors provided the optimum anchorage for this slab strengthening configuration. The flexural steel strain response showed both slabs yielded recording strains greater than 2000 με.

The highest CFRP strains were recorded at mid-span as 3627 με, 4666 με and 4579 με for slabs 600C-2L-NA, 600C-2L-8A and 600C-2L-12A, respectively. Comparison of the strain results in 600C series with those of the 230C series show that strains in the Sikawrap 600C strengthened slabs were much less than those recorded for the slabs strengthened with 230C sheets.

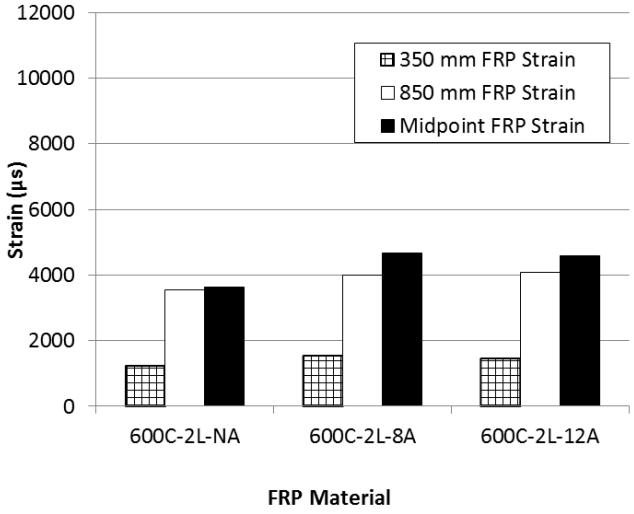

Figure 6-25: CFRP strain at failure of Sikawrap 600C strengthened slabs

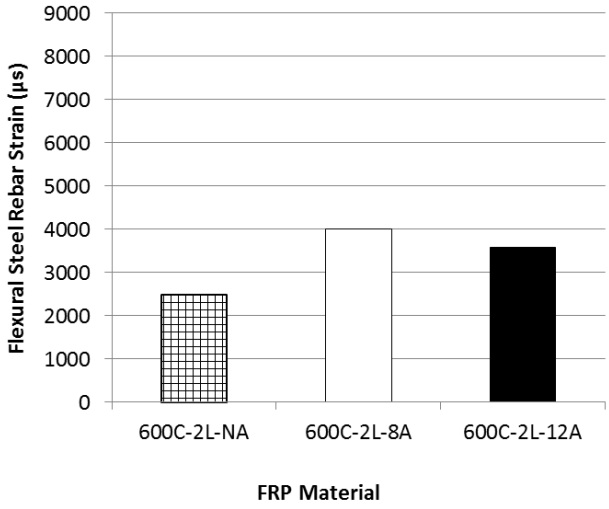

Figure 6-26: Steel rebar strain at failure of Sikawrap 600C strengthened slabs

6.6 Flexure Critical Slab Section Highlights

In this section, key findings with flexural strengthening of RC slabs with CFRP sheets and CFRP anchors are highlighted.

- Strain in FRP sheets were increased with the presence of CFRP anchors. CFRP anchorage enables CFRP sheets to develop larger strains instead of debonding.
- The presence of FRP anchors decreased the sudden drop in load experienced with FRP debonding failures. FRP anchors provide a residual strengthening capacity over an unanchored slab by securing the CFRP material.
- Debonding of unanchored flexural FRP sheets occurred in the concrete substrate at a strain of 7000 με which was consistent with the theoretical limit from ISIS-M04.
- Rupture of the Sikawrap 230C CFRP sheets occurred at a strain of 10,000 με which was in agreement with the reported manufacturer's data.
- Maximum deflection in a strengthened beam was affected by the type of CFRP and the presence of CFRP anchors. Heavily strengthened slabs have a lower deflection at failure because the flexural steel reinforcement is not yielding (increasing the deflection) prior to failure. Since such a large amount of external flexural strengthening is being provided other components of the slab are failing before the flexural steel reinforcement begins to yield.
- Flexural strength gain of CFRP strengthened slabs was not directly proportional to the FRP thickness.
- Concrete cover failure occurred when additional flexural strengthening was provided from thicker CFRP sheets with CFRP anchors. The mode of failure shifted the critical strain region from the bottom soffit to the concrete/steel rebar interface.

Chapter 7 – Efficiency of FRP Anchors

7.1 Introduction

The procedure to install FRP anchors to secure external FRP sheets is explained herein. The efficiency of FRP anchors is calculated using models for shear critical beams and flexure critical slabs.

7.2 FRP Anchor Installation Procedure

To the best of the author's knowledge, currently there are no detailed procedures or specifications that describe the installation of FRP anchors used to secure external FRP sheets. The proposed FRP anchor installation procedure was developed through trial and error, expert advice and manufacturers recommendations. A flow chart describing the procedure is outlined in Figure 7-1. The procedure has several steps and is as follows:

1. Determine the number of anchors required and the anchor hole locations.
2. Drill holes into the concrete member and prepare the hole and surface for installation.
3. Prepare and impregnate FRP anchors with epoxy.
4. Install FRP sheets and anchors.

7.3 Efficiency of FRP Anchors in Shear Critical Beams

The efficiency of FRP anchors in securing FRP u-wraps used for strengthening shear critical beams is examined. The efficiency of the anchor configuration is determined by calculating the effective strain experienced in the FRP sheet using CSA A23.3-04 and ISIS-M04 design codes.

7.3.1 Shear Prediction Model

The design of the shear critical RC beams for the pilot study and main study were calculated based on the general method given in the Canadian design code CSA A23.3-04 (Clause 11.3). An iterative procedure of the general method is presented in Figure 7-2. The equations and nomenclature is explained in table 2.5.This method was used to calculate the predicted failure load of the control unstrengthened beams in this study. All resistance factors were assumed as unity.

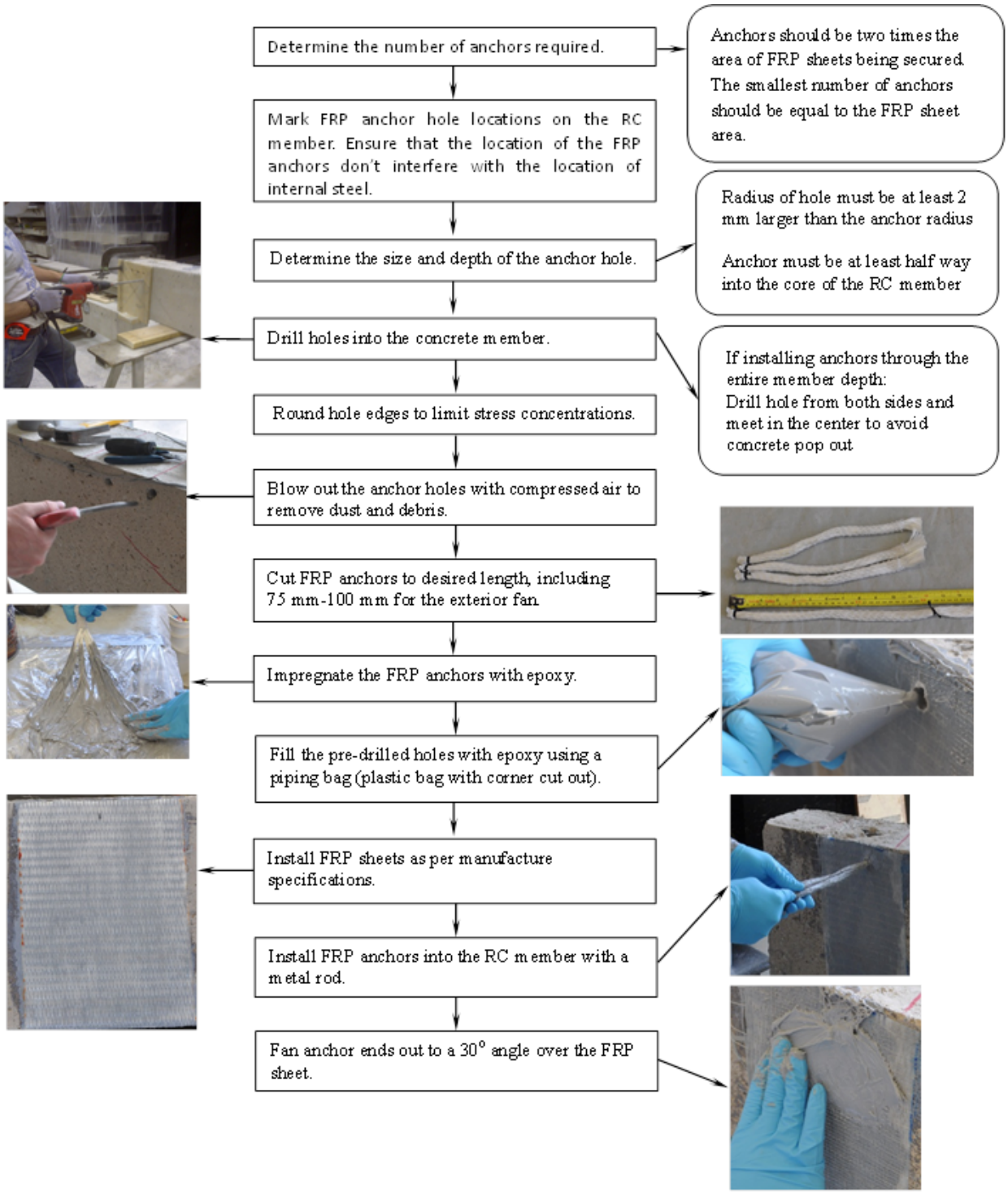

Figure 7-1: FRP anchor installation procedure

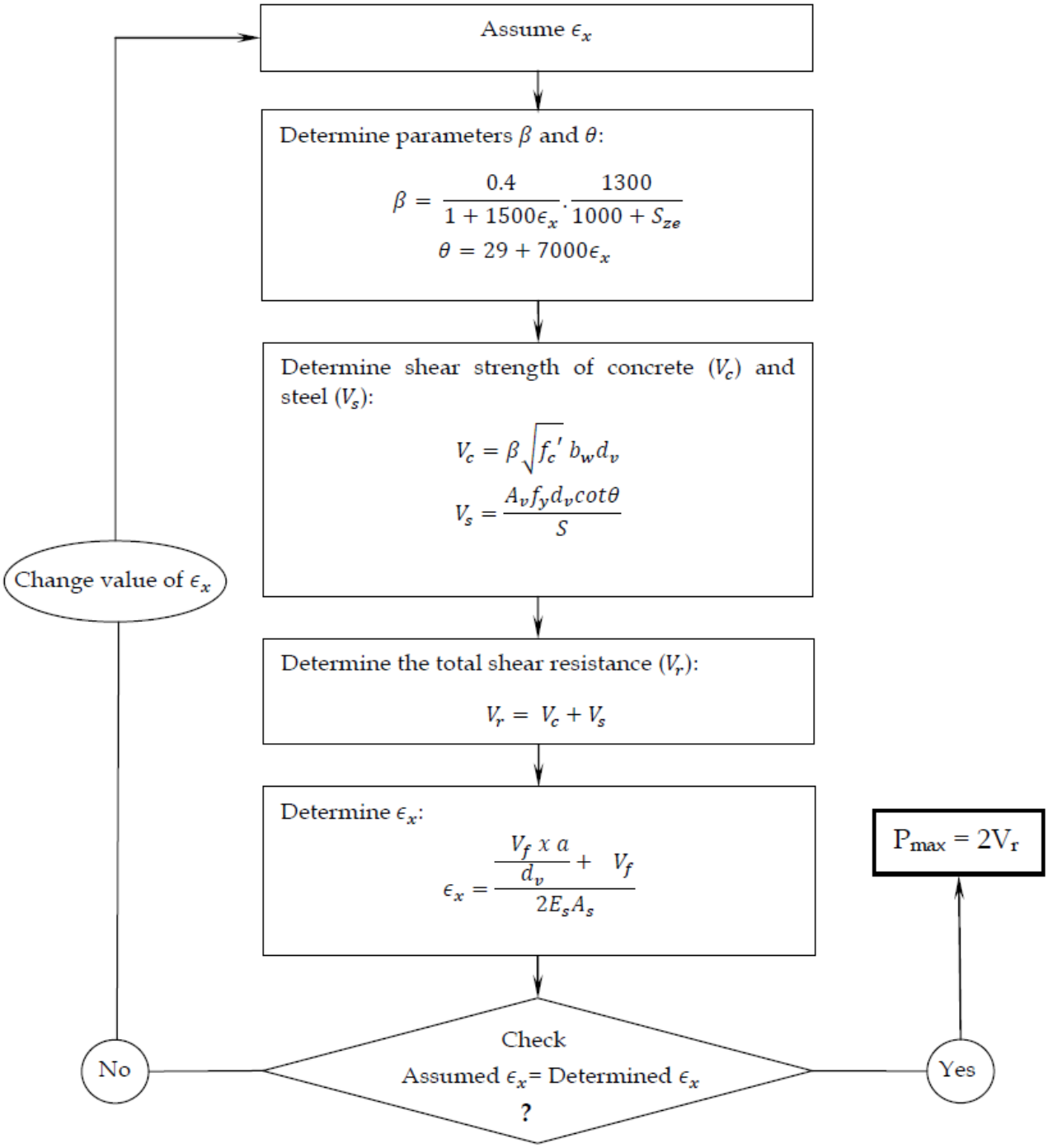

Figure 7-2: Shear design iterative procedure for unstrengthened beams using the general method (CSA A23.3-04) (Azam, 2010)

A comparison of the predicted and experimental results of the control unstrengthened beams in the pilot study and series I is presented in Table 7-1.

Table 7-1: Experimental and predicted ultimate loads for control beams

Beam	Experimental Ultimate Load (kN)	Predicted Ultimate Load (kN)	Experimental/ Predicted
Control (Pilot Study)	223	214	1.04
Control (Series I)	182	217	0.84

The beam design and predicted failure load of the control beam in the pilot study was conservative to within 4% of the observed failure load. The beam design and predicted failure load of the control beam in series I had an un-conservative prediction with a percent error of 16%. In series I, the unstrengthened design load was higher than the observed failure load because the stirrups were not as effective in controlling the crack width and crack propagation and thus caused the beam to fail at a lower load.

For beams which contained FRP strengthening, the total shear capacity of a FRP strengthened beam was calculated by adding individual contributions from the concrete, steel stirrups and external FRP sheets. The shear resistance contributions of the concrete and steel were calculated using equations provided in CSA A23.3-04 while the shear resistance contribution of the FRP sheets was calculated using equations provided from the ISIS-M04 design manual. These equations are listed in Table 7-2.

Table 7-2: Shear resistance of FRP strengthened members (CSA A23.3-04 & ISIS-M04)

Expression	Notation
$V_r = V_c + V_s + V_{frp}$	V_r= factored shear resistance V_c= shear resistance from concrete V_s= shear resistance from steel V_{frp}= shear resistance from FRP V_p= shear resistance from prestressing
$V_c = \phi_c \lambda \beta \sqrt{f_c'} b_w d_v$	Φ_c=resistance factor for concrete λ= factor to account for low density concrete β= factor accounting for shear resistance of cracked concrete f'$_c$=specified compressive strength of concrete b_{wt}= beam web width d_v= effective shear depth (greater of 0.9d or 0.72h)
$V_s = \frac{\phi_s A_v f_y d_v cot\theta}{s}$	Φ_c= resistance factor for concrete A_v= area of shear reinforcement with a distance s f_y= specified yield strength of non-prestressed reinforcement θ= angle of inclination of the diagonal compressive stresses s= spacing of shear reinforcement
$V_{frp} = \frac{\phi_{frp} E_{frp} \varepsilon_{frp} A_{frp} d_{frp} (cot\theta + cot\beta) sin\beta}{s_{frp}}$	Φ_{frp}= resistance factor of FRP material E_{frp}= modulus of elasticity of FRP material ε_{frp}= effective strain of FRP material A_{frp} = cross-section area of FRP material d_{frp}= effective depth θ= angle of inclination of diagonal cracks in the concrete β= angle of the FRP stirrups s_{frp}= spacing of the FRP stirrups

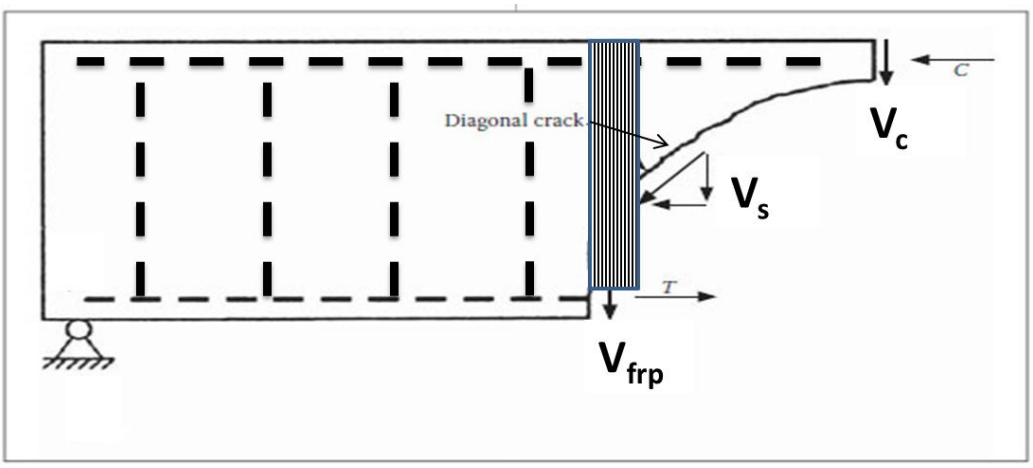

Figure 7-3: Free body diagram of internal forces

Several variables affect the shear resistance contribution of an FRP sheet are:

- The width and thickness of the FRP sheets.
- The spacing of FRP sheets.
- The elastic modulus of the FRP material.
- The effective strain in the FRP material.

When designing or calculating the FRP shear contribution, the first three variables are determined based on design restrictions, beam dimension limitations, strengthening requirements and cost requirements. The fourth variable, (ε_{frp}, effective strain in the FRP sheet) is selected as the smallest of three strain limits to ensure that the strength of the FRP sheet is not exceeded (Equation 7-1), loss of concrete aggregate interlock is prevented (Equation 7-2) and the debonding of FRP sheet does not occur (Equation 7-3).

$$\varepsilon_{frpe} \leq 0.75\varepsilon_{FRPu} \qquad \textbf{Equation 7-1}$$

$$\varepsilon_{frpe} \leq 0.004 \qquad \textbf{Equation 7-2}$$

$$\varepsilon_{frpe} \leq K_v\varepsilon_{FRPu} \qquad \textbf{Equation 7-3}$$

where

$$K_v = \frac{k_1 k_2 L_e}{11900\varepsilon_{FRPu}} \leq 0.75$$

$$k_1 = \left(\frac{f_c'}{27}\right)^{2/3}$$

$$\mathrm{k_2} = \frac{d_{FRP} - L_e}{d_{FRP}}$$

$$\mathrm{L}_e = \frac{23300}{(t_{FRP}E_{FRP})^{0.58}}$$

In this study the effective FRP strain (ε_{frpe}) is back calculated using the FRP shear strength contribution (V_{frp}) which is based on the experimental failure load.

The procedure to determine the experimentally estimated effective FRP strain is as follows:

1. Determine the shear contribution from concrete and steel using the CSA A23.3-04 (Table 7-2). Assume the same θ and β determined for a companion unstrengthened beam.
2. Determine the FRP shear strength contribution by subtracting the shear contributions from concrete and steel from the experimental shear resistance (V_{exp}) (Equation 7-4).

$$V_{frp} = V_{exp} - (V_c + V_s) \qquad \textbf{Equation 7-4}$$

3. Calculate the effective FRP strain in the FRP using the FRP shear strength contribution from step 2 (Table 7-3) and the FRP material properties (Equation 7-5). Set Φ_{frp}=1.0

$$\varepsilon_{frp} = \frac{V_{frp} s_{frp}}{\phi_{frp} E_{frp} A_{frp} d_{frp} (cot\theta + cot\beta) sin\beta} \qquad \textbf{Equation 7-5}$$

4. Calculate the accuracy of the experimentally estimated effective FRP strain (Equation 7-6).

$$\text{Percent Error} = \frac{|\text{Measured Strain} - \text{Predicted Strain}|}{\text{Measured Strain}} \cdot 100 \qquad \textbf{Equation 7-6}$$

5. Calculate the experimentally estimated efficiency of FRP anchors as the ratio of the experimentally estimated FRP strain in a beam with anchors by the experimentally estimated strain in a beam without anchors.
6. Calculate the measured efficiency of FRP anchors as the ratio of the measured FRP strain in a beam with anchors divided by the measured strain in a beam without anchors.

The measured effective strain recorded during testing, the experimentally estimated effective strain calculated using Equation 7-5, the percent error and the efficiency of FRP anchors for the different FRP sheet and anchor configurations are lsited in (Table 7-4)

.

Table 7-3: Calculated Shear Forces of RC FRP Strengthened Beams

Nomenclature	Load at failure (kN)	Shear force (V_{exp})	FRP force (V_{frp})	Experimentally Estimated Effective Strain (ε)
Control	182	81.9	-	-
430G-200-NA	332	166	57	0.0061
430G-200-A	332	166	57	0.0061
100G-200-NA	363	181	72	0.0040
100G-200-A	369	184	75	0.0042
430G-300-NA	313	156	47	0.0046
430G-300-A	346	173	64	0.0062
PC-430G-800-NA	304	152	43	0.0033
PC-430G-800-A	358	179	70	0.0054
PC-430G-800-FW	357	178	69	0.0059
PC-100G-1100-NA	352	176	67	0.0027
PC-100G-1100-A	395	197	88	0.0035

*As per prediction: V_c+V_s=109 kN

Table 7-4: Effective Strain Comparisons of RC Beams

Nomenclature	Measured Effective Strain (ε)	Experimentally Estimated Effective Strain (ε)	Percent Error (%)	Measured Efficiency of FRP Anchors (%)	Experimentally Estimated Efficiency of FRP Anchors (%)
Series I					
Control	-	-	-	-	-
430G-200-NA	0.0051	0.0061	-20		
430G-200-A	0.0084	0.0061	27	65	0
100G-200-NA	0.0046	0.0040	12		
100G-200-A	0.0055	0.0042	16	9	4
430G-300-NA	0.0046	0.0046	0		
430G-300-A	0.0098	0.0062	37	113	34
PC-430G-800-NA	0.0033	0.0033	0		
PC-430G-800-A	0.0046	0.0054	-18	53	63
PC-430G-800-FW	0.0069	0.0059	22	130	61
PC-100G-1100-NA	0.0033	0.0027	18		
PC-100G-1100-A	0.0065	0.0035	45	97	32

Evaluation of the percent error between the measured and experimentally estimated effective strain showed that the results varied between conservative and un-conservative predictions. As was reported in Chapter 4, the presence of external FRP reinforcement and FRP anchorage affects the diagonal tension shear crack inclination (i.e. angle of inclination of diagonal compressive stresses, θ), the strains in the stirrups and the shear crack width (i.e. loss of aggregate interlock as a shear transfer mechanism).

The experimentally estimated FRP strain calculation is limited because providing external FRP reinforcement affects the longitudinal strain at mid-depth (ε_x), angle of inclination of diagonal compressive stresses (θ) and factor accounting for the shear resistance of concrete (β) in a RC beam. In addition, when calculating the experimentally estimated FRP strain, the calculations to determine the shear resistance provided by the concrete (V_c) and the shear resistance provided by the steel reinforcement (V_s) were completed with using ε_x, θ, β of an unstrengthened beam.

A second limitation with the experimental estimation calculation is the failure modes which exist for FRP strengthened beams are not considered when using the modified compression field theory. Therefore, some of the premature failure modes experienced are not considered and can increase the error in the experimentally estimated calculations.

In general, the high variability and unpredictability of shear failures combined with the limits mentioned above can explain the higher percent error for the experimentally estimated shear critical beam calculations compared to the experimentally estimated flexure calculations.

Analysis shows that the effective strain in FRP sheets was increased when anchors were used to secure FRP sheets. The anchor efficiency was determined by analyzing the increase in effective strain in the FRP sheet when FRP anchors were installed. The efficiency of FRP anchors based on the measured effective FRP strains ranged from 9 to 130% with an average increase of 78%. The corresponding increase in shear strength when FRP anchors were used ranged from 10% to 20%. The FRP anchored beam behaved similarly to the fully wrapped beam attaining increases in effective FRP strain of 63%.

Analysis of the experimentally estimated versus measured efficiency of FRP anchors showed a linear trend with R^2= 0.18. The experimentally estimated and measured anchor efficiencies had no correlation; this can be attributed to premature failure (loss of aggregate interlock and end

anchorage failure) which occurred with the GFRP strengthened beams. The experimentally estimated calculations were based on an unstrengthened beam which has a different failure mechanism than a FRP strengthened beam. To improve the anchor prediction efficiency, the beam design should be changed to ensure that FRP debonding is the limiting strain to cause failure and sufficient tensile and compression reinforcement is provided.

Comparison of the effective strain in beams with and without GFRP anchors showed that the largest increase in the experimentally estimated effective FRP strain occurred in the beam strengthened with 800 mm wide u-wrapped GFRP sheets with GFRP anchors. Conversely, the largest increase in the measured effective strain occurred in the beam strengthened with 300 mm wide u-wrapped GFRP sheets with GFRP anchors.

No increase in effective strain was experimentally estimated and measured for all beams strengthened with 200 mm wide Sikawrap 100G sheets. The measured effective strain shows that all but two beams recorded effective strain above aggregate interlock capacity. The same four beams reached effective strains above the debonding strain.

A plot comparing the experimentally estimated and experimental efficiency is shown in Figure 7-4. Graphs comparing the experimentally estimated and measured effective strain of unanchored and anchored beams with and without anchors are presented in Figure 7-5 and Figure 7-6.

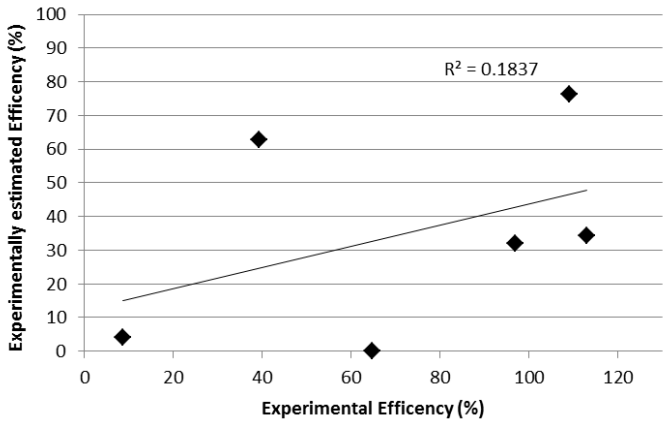

Figure 7-4: Comparison of experimentally estimated & measured efficiency of FRP anchors

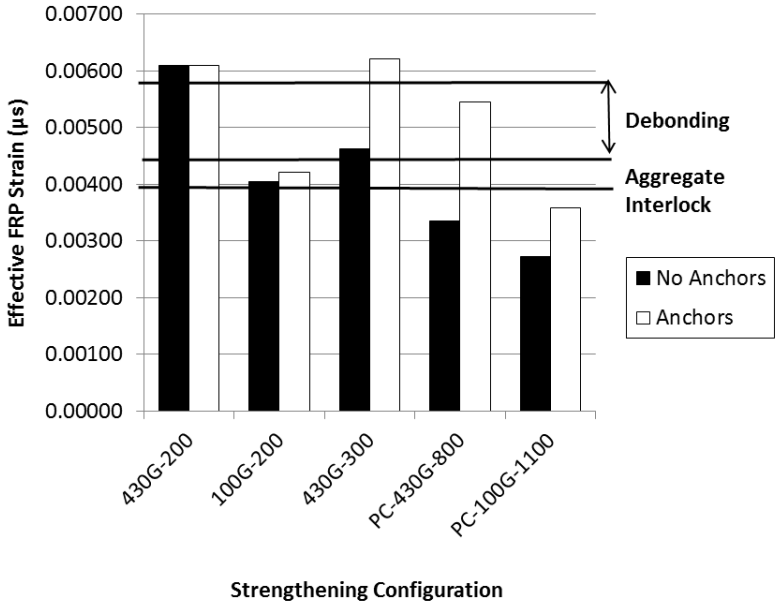

Figure 7-5: Comparison of experimentally estimated FRP strain in unanchored & anchored beams

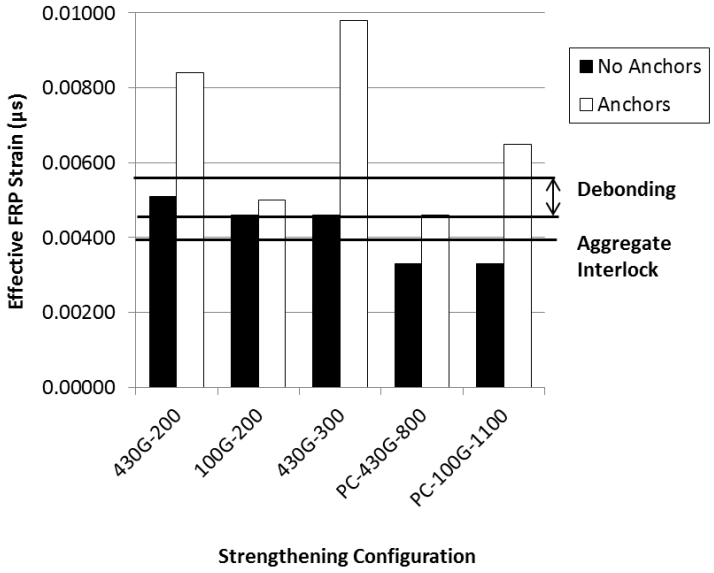

Figure 7-6: Comparison of measured FRP strain in unanchored & anchored beams

The increase in strength between anchored and unanchored FRP strengthened beams was compared with the experimentally estimated and measured anchor efficiency to determine the benefit of providing FRP anchors (Table 7-5). Figure 7-7 illustrates the anchor efficiency vs. the increase in shear strength of anchored vs. unanchored beams. This plot shows that the experimentally estimated anchor efficiency varied linearly with the strength increases with a slope of 2.4. The linear trend R^2= 0.71 indicates that the data is reasonably correlated.

Table 7-5: Strength increase and anchor efficiency of Sikawrap 430G strengthened beams

FRP Strengthening Configuration	Increase in Shear Strength (%)	Measured Anchor Efficiency (%)	Experimentally Estimated Anchor Efficiency (%)
430G-300	18	113	34
PC-430G-800	30	39	63
PC-430G-1100	24	97	32

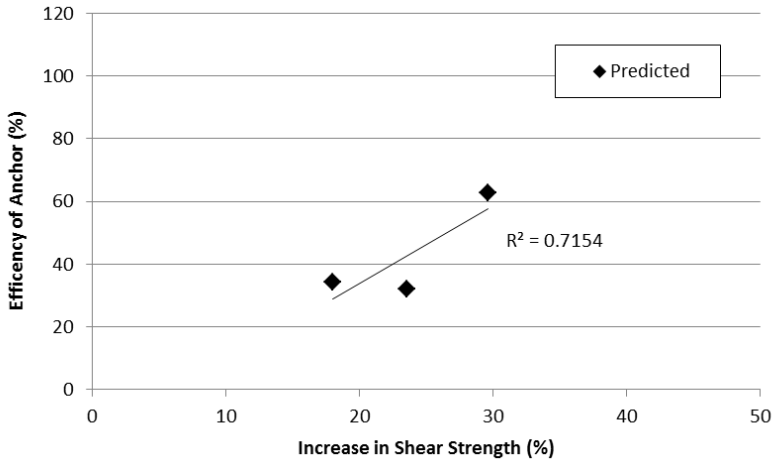

Figure 7-7: Relationship between strength increase and anchor efficiency of Sikawrap 430G strengthened beams

7.4 Efficiency of FRP Anchors in Flexure Critical Slabs

In this section, the efficiency of anchors to secure externally bonded CFRP sheets used to strengthen flexure critical slabs is examined. Current flexure prediction equations are applied to each configuration and analyzed. The efficiency of the anchor configuration is determined by calculating the effective FRP strain experienced in the FRP sheet using experimental results and the ISIS-M04 design code.

7.4.1 Flexure Prediction Model

The existing model to predict the flexural strength of FRP strengthened slabs uses equilibrium of forces and strain compatibility (Figure 7-8). Equation 7-7 defines the equilibrium forces for concrete, steel reinforcement and FRP sheets. Equation 7-8 defines the flexural capacity of a FRP strengthened RC member. This method was used to predict the failure load of the control slab in series II. All resistance factors were taken as unity.

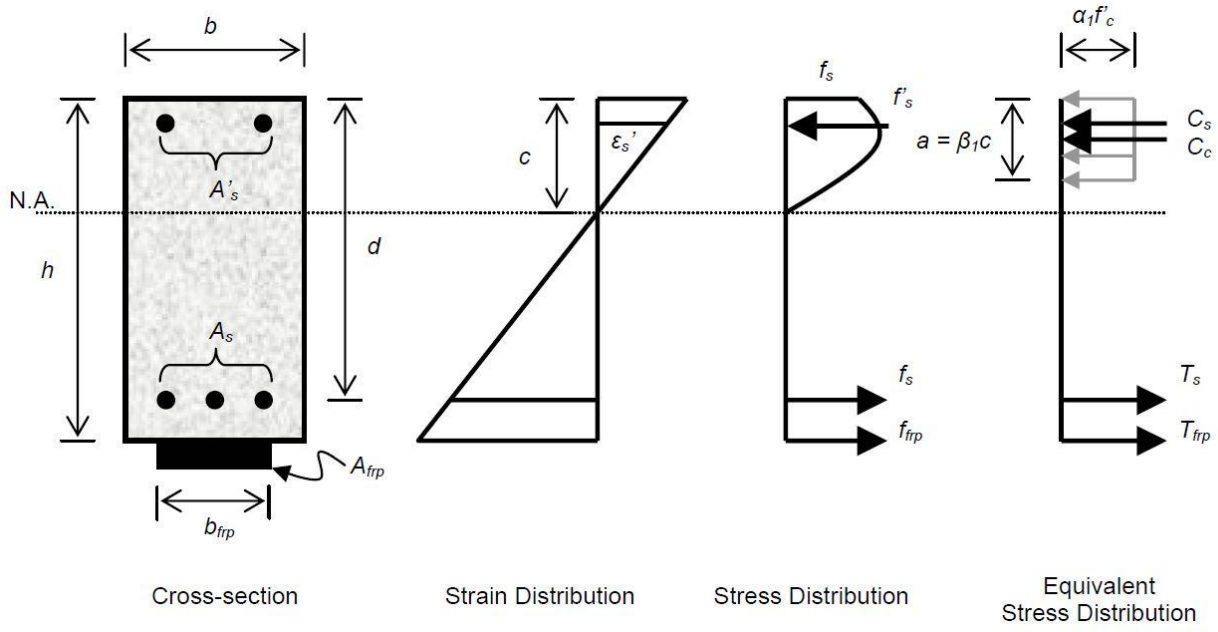

Figure 7-8: Stress strain profile of a flexure critical slab (ISIS Canada, 2004)

$$C_c + C_s = T_s + T_{FRP} \quad \textbf{Equation 7-7}$$

where

$$C_c = \alpha_1 \phi_c f_c' \beta_1 c b$$

$$C_s = \phi_s E_s \varepsilon_s' A_s'$$

$$T_s = \phi_s E_s \varepsilon_s A_s$$

$$T_{FRP} = \phi_{FRP} E_{FRP} \varepsilon_{FRP} A_{FRP}$$

$$M_r = C_s \left(\frac{a}{2} - d'\right) + T_s \left(d - \frac{a}{2}\right) + T_{FRP} \left(h - \frac{a}{2}\right) \quad \textbf{Equation 7-8}$$

Table 7-6: Experimental and predicted ultimate load for control slab

Beam	Experimental Ultimate Load (kN)	Predicted Ultimate Load (kN)	Experimental/ Predicted
Series II: Control	132	126	1.04

The predicted failure load of series II: control slab was conservative to within 4% of the measured failure load (Table 7-6). Several variables which affect the flexural resistance contribution of a FRP sheet are:

- The width and thickness of the FRP sheets ($t_{frp,}$ w_{frp}).
- Distance from the neutral axis (c).
- The elastic modulus of the FRP material (E_{frp}).
- The effective strain in the FRP material (ε_{frp}).

When designing or calculating the FRP shear contribution, the first three variables are determined based on: design restrictions, slab dimension limitations, strength requirements and cost requirements. The fourth variable ($\varepsilon_{frp,}$ effective strain in the FRP sheet) is selected as the smaller of two strain limits (Equation 7-9): the ultimate strain of the FRP material (ε_{frpu}, Equation 7-11) or the maximum strain value of externally-bonded FRP strengthening system otherwise known as the debonding stain ($\varepsilon_{frpt,}$ Equation 7-10).

$$\varepsilon_{frp} = \text{lesser of } (\varepsilon_{FRPu} \; or \; \varepsilon_{frpt}) \qquad \textbf{Equation 7-9}$$

where

$$\varepsilon_{frpt} = 0.007 \qquad \textbf{Equation 7-10}$$

$$\varepsilon_{frpu} = \text{ultimate FRP strain} \qquad \textbf{Equation 7-11}$$

The effective FRP strain was back calculated using the experimental failure load. In all tested slabs, the concrete never reached the crushing strain ($\varepsilon_{cu=}$ 0.0035) therefore, α_1 and β_1 cannot be applied and the compressive force in the concrete could not be modeled using the rectangular stress block. The slab was modeled using layer-by-layer strain compatibility analysis (West, 2011) as shown in Figure 7-9. None of the strain values across the slab section were known in the four materials. The strain in the concrete was unknown, the compressive and tension steel strain were unknown and the effective strain in the FRP was unknown.

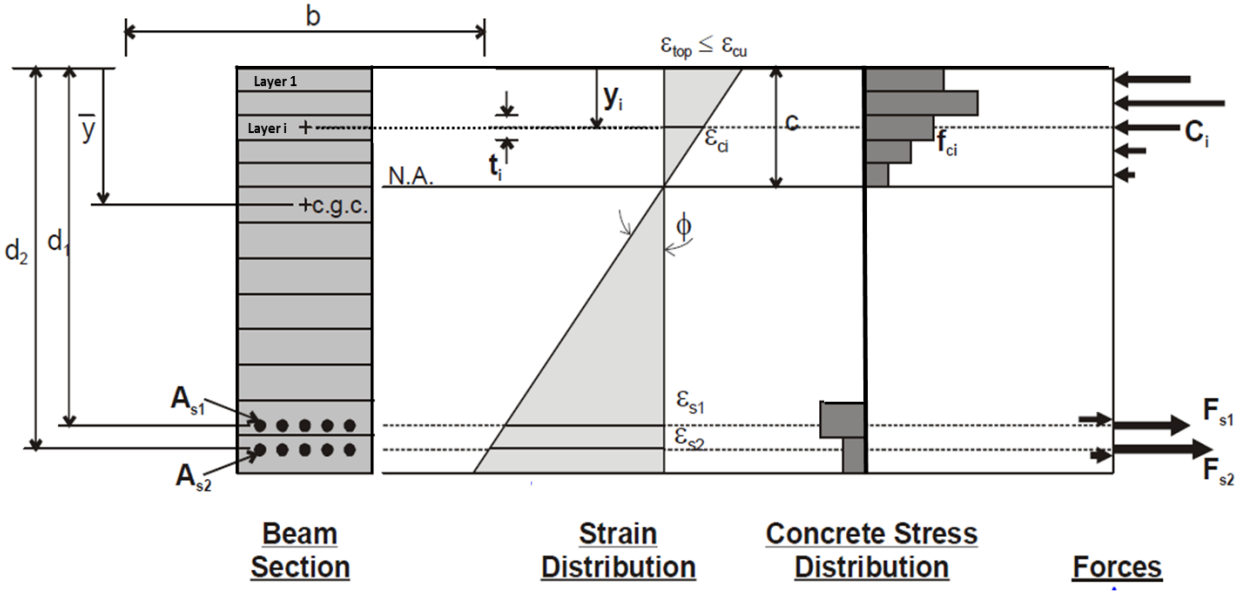

Figure 7-9: Layer-by-layer strain compatibility of a flexure critical slab (West, 2011)

The layered approach utilizes the concrete section forces with strain compatibility. Two equilibrium equations are utilized:

1. Internal Equilibrium: The summation of the forces in the section must equal zero (Equation 7-7)
2. The sum of the moments in the section must be equal: The internal resultant moment must equal the external applied moment. (Equation 7-8)

To solve this problem, all strains were written in terms of two unknown variables:

1. The depth of the neutral axis "c"
2. The strain in the top fibre "$\varepsilon_{c\text{-top fibre}}$"

The strain equations for each material and the rectangular layer are outlined below.

$$\varepsilon_{ci} = \left(\frac{c - y_i}{c}\right)\varepsilon_{cmax} \qquad \textbf{Equation 7-12}$$

$$\varepsilon_s' = \left(\frac{d_j - c}{c}\right)\varepsilon_{cmax} \qquad \textbf{Equation 7-13}$$

$$\varepsilon_s = \left(\frac{c - d_j}{c}\right)\varepsilon_{cmax} \qquad \textbf{Equation 7-14}$$

$$\varepsilon_{frp} = \left(\frac{d_{frp} - c}{c}\right)\varepsilon_{cmax} \qquad \textbf{Equation 7-15}$$

where

y_i=distance from the top to the centroid of concrete layer i
d_j=distance from the top to the centroid of the reinforcement
ε_{ci}=strain in concrete layer i
ε_s'=strain in the compression steel
ε_s=strain in the tension steel
ε_{frp}=strain in the FRP sheet
d_{frp}=distance from the top of the member to the FRP reinforcement

The procedure to calculate the effective strain in the FRP was as follows:

1. Assume initial values for c and $\varepsilon_{c\text{-top fibre.}}$
2. The concrete compression zone was divided into 40 equal rectangular layers.
3. Strains in each concrete layer, steel layer and FRP layer were expressed in terms of c and $\varepsilon_{c\text{-top fibre}}$ using Equation 7-12 to Equation 7-15.
4. The resultant force for each non-concrete element (compression steel rebar, tension steel rebar and FRP sheets) and the force in each concrete layer were calculated.
5. Equilibrium was calculated by summing all the forces in each layer (tension + compression).
6. The internal moment about the center of gravity of the section was calculated and compared to the externally applied moment.
7. By varying c and $\varepsilon_{c\text{-top fibre,}}$ equilibrium force balance of zero is achieved.
8. Prior to solving, a constraint that the internal moment must be equal to the external experimental moment was applied.
9. Using the MS Excel solver, the two equations to determine the depth of the neutral axis and strain in each rectangular stress block such that equilibrium is satisfied.
10. Using the values calculated from step 9, the effective strain in the FRP (ε_{frp}) were calculated using c and $\varepsilon_{c\text{-top fibre.}}$
11. The accuracy of the experimentally estimated effective FRP strain was calculated using Equation 7-6.
12. The experimentally estimated efficiency of FRP anchors was calculated as the ratio of the experimentally estimated FRP strain in a beam with anchors by the experimentally estimated strain in a beam without anchors.
13. The measured efficiency of FRP anchors was calculated as the ratio of the measured FRP strain in a beam with anchors by the measured strain in a beam without anchors.

The procedure was applied for each FRP strengthened slab. The results of the experimentally estimated effective FRP strain, the measured effective FRP strain recorded during testing, the percent error and the efficiency of FRP anchors are listed in Table 7-7.

Table 7-7: Calculated Shear Forces of RC FRP Strengthened Beams

Nomenclature	Load at Failure (kN)	Experimentally Estimated Concrete Strain (ε)	Experimentally Estimated Compression Steel Strain (ε)	Experimentally Estimated Tension Steel Strain (ε)	Experimentally Estimated FRP Strain (ε)
Control	132	-	-	-	-
230C-1L-NA	174	-0.002904	-0.000987	0.011579	0.013922
230C-2L-NA	190	-0.002336	-0.001037	0.007482	0.009070
230C-2L-8A	201	-0.002687	-0.001037	0.007482	0.009070
600C-1L-NA	186	-0.001908	-0.000937	0.005427	0.006613
600C-2L-NA	192	-0.001466	-0.000872	0.003020	0.003745
600C-2L-8A	228	-0.001772	-0.001087	0.003406	0.004244
600C-2L-12A	219	-0.001866	-0.001083	0.004052	0.005009

Table 7-8: Effective Strain Comparisons of RC Slabs

Nomenclature	Measured Effective Strain (ε)	Experimentally Estimated Effective Strain (ε)	Percent Error (%)	Measured Efficiency of FRP Anchors (%)	Experimentally Estimated Efficiency of FRP Anchors (%)
Series II					
Control	-	-	-	-	-
230C-1L-NA	0.01070	0.01392	-30	-	-
230C-2L-NA	0.00780	0.00907	-16		
230C-2L-8A	0.00898	0.01045	-16	15	15
600C-1L-NA	0.00700	0.00661	5	-	
600C-2L-NA	0.00362	0.00374	-3		
600C-2L-8A	0.00466	0.00424	8	28	13
600C-2L-12A	0.00457	0.00500	-9	26	33

Analysis of the percent error between the measured and experimentally estimated effective strain showed that the results varied between conservative and un-conservative predictions. In general, flexural prediction formulas are very accurate. Predictions with a percent error below 10% are desired results.

Five slabs had un-conservative effective strain predictions: slab 230C-1L-NA (-30%), slab 230C-2L-NA (-16%), slab 230C-2L-8A (-16%), slab 600C-2L-NA (-3%) and slab 600C-2L-12A (-9%). Three slabs strengthened with Sikawrap 230C had high un-conservative predictions. The percent errors for slabs 230C-1L-NA (-30%), 230C-2L-8A (-16%) and 230C-2L-12A (-9%) can be

attributed to the observed premature failure mode in these slabs. Slab 230C-1L-NA failed by FRP rupture but the FRP strain measured during testing was only 0.0107. The FRP rupture strain provided by the manufacturer is 0.0133 and the experimentally estimated FRP strain was 0.0139. The experimentally estimated and manufacturer strain were within 5% error and FRP rupture was the mode of failure. The measured FRP strain in the slab did not accurately measure the effective strain at failure. Slab 230C-2L-NA and slab 230C-2L-8A failed prematurely by FRP debonding and concrete cone anchor failure respectively. The prediction formulas do not take into account FRP debonding or concrete cone anchor failures which are both premature failure modes. Thus, the measured FRP strain was lower than the experimentally estimated FRP strain.

Two slabs had low conservative predictions: slab 230C-1L-NA (5%) and slab 230C-2L-8A (8%). The presence of CFRP anchors eliminated the premature debonding from occurring in slab 230C-2L-8A. This allowed the CFRP sheets to resist higher strains than predicted in the model.

Four slabs strengthened with Sikawrap 600C had effective FRP strain predictions with percent errors between 0 and 9% compared to laboratory observations. The variation in the experimental estimation vs. measured values of these two slabs can be attributed to the thicker CFRP material (Sikawrap 600C) used to strengthen both slabs. Furthermore, the accuracy of the effective FRP strain predictions validates the prediction model when flexure failure governed.

Analysis of the data shows that the effective strain in the FRP sheets was increased when anchors were used to secure FRP sheets. Anchor efficiency was determined by analyzing the increase in effective strain in the FRP sheet when FRP anchors were installed. The efficiency of FRP anchors based on effective FRP strain ranged from 15% to 26% with an average increase of 18%. The FRP anchor efficiencies based on the experimentally estimated effective FRP strain ranged from 15% to 33% with an average increase of 23%. The corresponding increase in flexural strength ranged from 5.5% to 19% (average).

A plot comparing the experimentally estimated and experimental efficiency of FRP anchors is shown in Figure 7-10. Analysis of the experimentally estimated and experimental efficiencies of FRP anchors shows a no linear trend with an R^2=0.06. The experimentally estimated and actual anchor efficiencies had a no correlation. Such a low R^2 value can be attributed to the undesirable failure modes (concrete cone anchor failure, concrete cover failure and intermediate flexural

shear crack induced interfacial debonding) which occurred with the CFRP strengthened slabs with anchors. To improve the prediction, the slab design should be modified to ensure that the concrete strength is sufficient to withstand the high strains imposed by adding significant flexural strengthening.

Graphs for the experimentally estimated and measured effective strains of unanchored and anchored slabs are provided in Figure 7-11and Figure 7-12. The largest increase in the experimentally estimated effective FRP strain occurred in the slab strengthened with two layers of Sikawrap 600C sheets with twelve CFRP anchors. The largest increase in the measured effective strain occurred in the slab strengthened with two layers of Sikawrap 600C sheets with eight CFRP anchors.

Minimal increase (15%) in the effective strain was experimentally estimated for both slabs strengthened with two layers of the thinner Sikawrap 230C sheets. The experimentally estimated effective FRP strain showed that all slabs strengthened with Sikawrap 230C sheets had effective strains above the debonding strain limit (ε_{frpt}= 0.007) and all slabs strengthened with Sikawrap 600C sheets had effective strains below the debonding strain limit.

Two layers of Sikawrap 600C increased the tensile strain on the bottom soffit of the slab such that the imposed tension strain was greater than the concrete/steel interface tensile strength. This caused concrete cover failure and thus the full potential of the CFRP sheets and anchors was not utilized. Providing FRP anchorage increased the FRP strain from 6% to 20%.

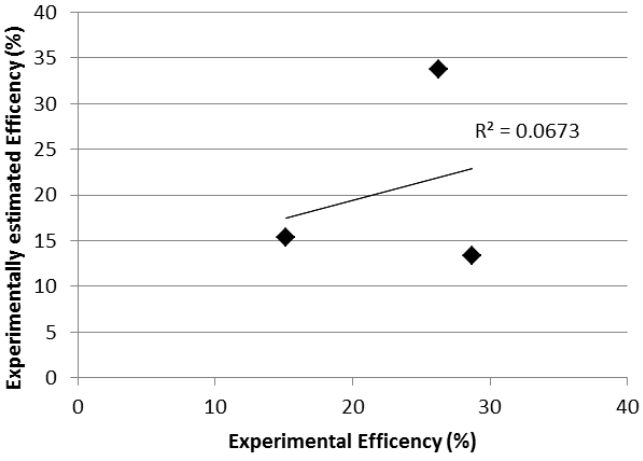

Figure 7-10: Comparison of effective FRP strain in unanchored and anchored slabs

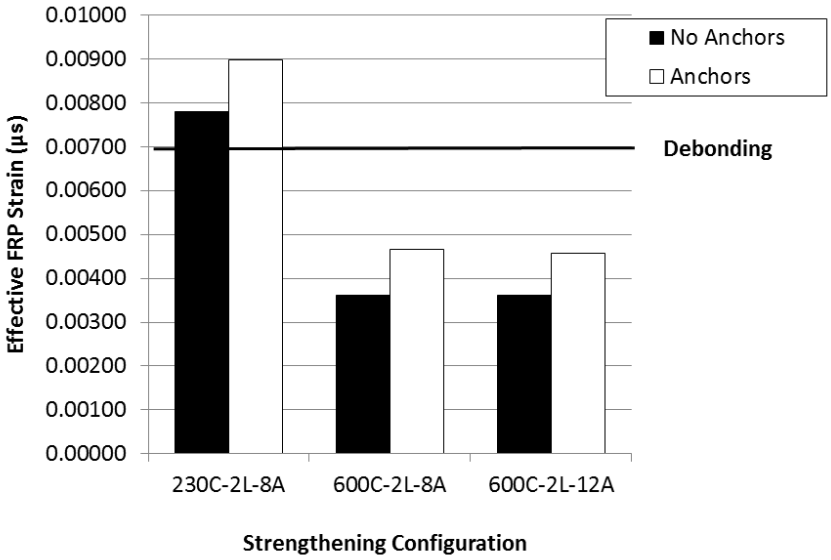

Figure 7-11: Comparison of experimentally estimated FRP strain in unanchored & anchored slabs

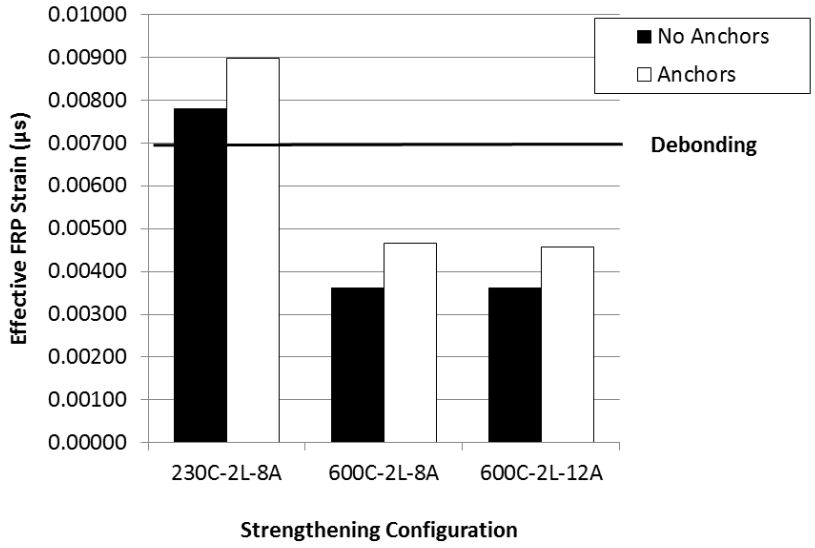

Figure 7-12: Comparison of measured FRP strain in unanchored & anchored slabs

The increase in strength between unanchored and anchored slabs strengthened with CFRP sheets was correlated with the anchor efficiency (Table 7-9). Analysis of the anchor efficiency vs. the increase in shear strength plot shows that the experimentally estimated anchor efficiency had a linear trend with a slope of 0.7, R^2=0.96 (Figure 7-13). The results are presented in Table 7-9 and Figure 7-13.

Table 7-9: Strength increase and anchor efficiency of CFRP strengthened slabs

FRP Strengthening Configuration	Increase in Shear Strength (%)	Measured Anchor Efficiency (%)	Experimentally Estimated Anchor Efficiency (%)
230C-2L-8A	8	15	15
600C-2L-8A	27	29	13
600C-2L-12A	20	26	34

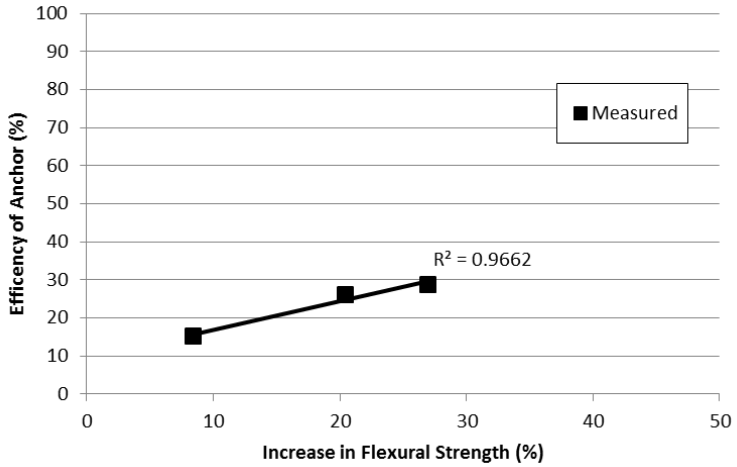

Figure 7-13: Relationship between strength increase and anchor efficiency of CFRP strengthened slabs

7.5 Design Procedure: FRP Strengthening with FRP anchors

In this section, the Baggio FRP anchor design procedure is outlined. This design approach will allow a designer to determine the number of anchors required to secure a FRP sheet to eliminate a premature failure mode caused by FRP debonding. It is assumed that FRP sheets are designed and applied according to ISIS-M04 design guidelines and that sufficient concrete and steel reinforcement capacity is available such that providing FRP anchorage will not cause premature yielding of steel or crushing of concrete.

The proposed design is based on the equivalent area approach. Kobayashi, et al. (2001) proposed that the material in the anchor to be at least twice the amount of material contained within the main FRP sheet. In the Baggio FRP anchor design approach, the total tension force per FRP sheet 'T_{frp}' is matched with tension force in the anchors 'F_{frpa}' ensuring that there is double the amount of anchorage area to develop the full tensile strain in the FRP sheet.

The proposed design procedure has the following steps:

1. Design the FRP shear or flexural strengthening configuration based on the FRP rehabilitation ISIS-M04 design manual.
2. Calculate the maximum tension force per FRP sheet (T_{frp}) from the design in step 1.

$$T_{frp} = A_{frp} E_{frp} \varepsilon_{frpe}$$ **Equation 7-16**

where $A_{frp} = w_{frp} t_{frp}$

E_{frp}= modulus of elasticity of FRP material
ε_{frpe}= effective strain of FRP material
A_{frp} = cross-section area of FRP material
w_{frp}= width of the FRP sheet
t_{frp}= FRP material thickness

3. Calculate the tension force in FRP anchors (F_{frpa}).

$$F_{frpa} = \frac{1}{2} n A_{frpa} E_{frpa} \varepsilon_{frpau}$$ **Equation 7-17**

where $A_{frpa} = \pi r_{frpa}^2$

n=number of FRP anchors per FRP sheet
A_{frpa} = cross-section area of FRP anchor
E_{frpa}= modulus of elasticity of FRP anchor
ε_{frpau}= ultimate strain of FRP anchor
r_{frpa}= radius of FRP anchor

4. Set the tension force of FRP anchors (T_{frp}) equal to the tension force per FRP sheet (F_{frpa}) and solve for the unknown variable "n" the number of FRP anchors required per sheet.

$$T_{frp} = F_{frpa} \qquad \textbf{Equation 7-18}$$

$$n = \frac{A_{frp} E_{frp} \varepsilon_{frpe}}{{}^{1}/_{2}\, A_{frpa} E_{frpa} \varepsilon_{frpau}}$$

T_{frp}= tension force per FRP sheet
F_{frpa}= tension force of FRP anchors

It should be noted that when calculating the total strength capacity of a FRP strengthened beam or slab, calculations and capacity predictions are to be determined as per the FRP rehabilitation ISIS-M04 design manual. If an additional factor of safety is desired, providing FRP anchors with the Baggio design procedure will offer additional capacity over and above the unstrengthened ISIS-M04 design manual calculation.

7.5.1 Sample Calculation for Proposed Design Procedure

The properties of a reinforced concrete beam which require u-wrap FRP shear strengthening are listed in Table 7-10. It was determined that the entire shear span (800 mm) of the beam will be strengthened with a continuous sheet of Sikawrap 100G.

Table 7-10: FRP Material Properties

Sikawrap 100G Material Properties	Width of the FRP sheet	w_{frp}	800 mm
	Thickness of the FRP sheet	t_{frp}	1.016 mm
	Elastic modulus of the FRP sheet	E_{frp}	25 GPa
	Ultimate strain of the FRP sheet	ε_{frpu}	0.0231
GFRP - Anchor G Material Properties	Radius of the FRP anchor	r_{frpa}	5 mm
	Elastic modulus of the FRP anchor	E_{frpa}	70 GPa
	Ultimate strain of the FRP anchor	ε_{frpau}	0.0399

Sample Calculations

Calculate the maximum tension force per FRP sheet	T_{frp}	$= A_{frp} \times E_{frp} \times \varepsilon_{frpu}$
	A_{frp}	$= w_{frp} \times t_{frp}$
		$= 800 \text{ mm} \times 1.016 \text{ mm}$
		$= 812.8 \text{ mm}^2$
	T_{frp}	$= 2 \times 812.8 \text{ mm}^2 \times 25 \text{ GPa} \times 0.0231$
		$= 938 \text{ kN}$
Calculate the maximum tension force per FRP anchor	F_{frpa}	$= ½ \times n \times A_{frpa} \times E_{frpa} \times \varepsilon_{frpau}$
	A_{frpa}	$= \prod \times r^2_{frpa}$
		$= 3.14159 \times 5 \text{ mm}^2$
		$= 78.5 \text{ mm}^2$
	F_{frpa}	$= ½ \times n \times 78.5 \text{ mm}^2 \times 70 \text{ GPa} \times 0.0399$
		$= 109.7n \text{ kN}$
Set the tension force of FRP anchors equal to the tension force per FRP sheet	T_{frp}	$= F_{frpa}$
Solve for the number of anchor required (n)	938	$= 109.7n$
	n	$= 8.55$
Therefore each 800 mm wide GFRP sheet requires a minimum of 9 GFRP anchors.	$\therefore n$	$= 9$
Space each anchor equally.	S	$= 800 \text{ mm} / (n+1)$
		$= 800 \text{ mm} / 10$
		$= 80 \text{ mm}$
Therefore, the complete design will consist of 9 GFRP anchors spaced every 80 mm along the width of the FRP sheet.	$\therefore S$	$= 80 \text{ mm o/c}$

Chapter 8 – Conclusions and Recommendations

8.1 Introduction

Experimental and analytical studies were conducted to investigate the effect of FRP anchors on the FRP rehabilitation of shear critical RC beams and flexure critical RC slabs. The variables included: the type of FRP sheets (CFRP, GFRP, FRCM), the presence and type of anchor (CFRP or GFRP), the number of FRP layers (one or two layers) and u-wrapping schemes (full depth vs. partial depth).

The results showed that installing FRP anchors to secure FRP sheets used to strengthen shear critical beams delayed or eliminated the FRP from debonding and improved the shear capacity of the beams. Installing FRP anchors in FRP strengthened flexure critical slabs prevented the FRP from debonding and changed the mode of failure with modest enhancements in flexural capacity.

The effective strain in a FRP sheet was experimentally estimated with a model based on the Canadian design code CSA A23.3-04 – Design of concrete structures and ISIS-M04 design manual - Reinforcing RC structures with FRP. The experimentally estimated results were compared with the experimental data which calculated to acceptable accuracy. A model to predict the number of FRP anchors required to secure a FRP sheet was proposed and a step-by-step FRP anchor installation procedure was developed.

8.2 Experimental Conclusions

8.2.1 Effect of FRP Anchors

- The installation of FRP anchors to secure u-wrap FRP sheets changed the overall behaviour of FRP strengthened shear critical RC beams and flexure critical slabs. The presence of FRP anchors increased the deflection at failure of shear critical beams and flexural critical slabs.
- The installation of FRP anchors to secure u-wrapped FRP sheets in shear critical beams provided an average 15% increase in shear strength over companion unanchored beams. FRP anchors installed to secure flexural FRP sheets provided an average 17% increase in flexural strength over companion unanchored slabs. Additionally, as the width of FRP sheets increased, larger increases in the strength are obtained by FRP anchors.
- FRP anchors provided the same increase in shear strength as fully wrapping the beam's cross-section. Therefore, when FRP sheets cannot be fully wrapped around the section of a RC beam and anchorage is required; FRP anchors can be installed to provide equivalent anchorage as a full wrap member.
- Providing FRP anchors aids in the development of the ultimate tensile capacity of shear and flexural FRP sheets leading to increases in the maximum strains measured in FRP sheets at failure. Average increases in FRP strain at failure were 20% to 30% when FRP anchors were provided. Flexural and shear strength was significantly increased when FRP anchors were installed on beams with sufficient flexural reinforcement and concrete strength.
- The presence of FRP anchors to secure FRP sheets increased the stiffness over unanchored shear strengthened beams. Also, beams with FRP anchors experienced a 10% increase in maximum deflection over companion unanchored beams.
- Ancillary testing on FRP anchor installation was conducted and revealed that anchors with the following provisions had the best performance:
    - FRP anchors should be installed into a RC members at a distance equivalent to 75% of the width for beams or 75% of the depth for slabs.
    - The optimum length for the anchor fan is 75 mm to 100 mm.
    - The FRP anchor fan should be fanned out 30^{o} over the FRP sheet.

- FRP anchors which are installed through the entire width of a member are to be drilled into half of the depth from either side to avoid concrete pop-out.
- The diameter of the anchor hole must be 40% larger than the diameter of the FRP anchor.

8.2.2 Effect of FRP Repair

- The shear capacity of beams and flexural capacity of slabs was increased when FRP strengthening was provided (u-wraps, flexural sheets). Larger strength increases were obtained when the thickness of the FRP material was increased. However, the strength increase was not linearly proportional to the increase in thickness.
- Providing shear strengthening can change the mode of failure in shear critical beams from a brittle shear failure to flexural failure. In addition, FRP strengthening improved the ductility of failure. Providing flexural strengthening changed the mode of failure in flexural critical slabs from flexural failure to concrete cover failure by increasing the tensile resistance in the bottom soffit over that of the concrete/steel interface.
- The presence of FRP sheets and anchors on a beam eliminated the initial cracking phase in the load deflection response of beams and slabs. In addition, the deflection at ultimate load was increased in shear strengthened beams and decreased in flexural strengthened slabs when FRP strengthening was provided.
- Debonding failure occurred in the concrete substrate and not in the FRP epoxy interface for all beams and slabs. Debonding of unanchored FRP sheets in the concrete substrate occurred at GFRP strains between 4000 με to 5000 με, in the u-wrapped GFRP sheets and CFRP strains between 7000 με to 8000 με, in flexural strengthened CFRP sheets. FRP debonding in the concrete substrate can be resolved by using higher concrete strength. The strength of the system was more dependent on the tensile strength of the concrete, not the FRP/epoxy interface.
- U-wrapped continuous FRP sheets provided larger strength increases compared to intermittent strips in shear strengthening. In addition to the increases in strength, continuous sheets were easier to install as they did not need to be cut into strips.

8.3 Analytical Conclusions

- The experimentally estimated effective strain experienced in a shear critical RC beam with u-wrapped FRP sheets was determined using equations from the Canadian design code CSA A23.3-04 and FRP rehabilitation ISIS-M04 design manual. The model predicted un-conservative results when secondary premature failure by FRP debonding, concrete cover failure and loss of aggregate interlock occurred which the model did not consider. Poor correlation existed between the predicted vs. measured anchor efficiencies.
- The effective strain experienced in a RC slab strengthened with flexural FRP sheets can be effectively predicted using the layered approach. However, the model predicted un-conservative results because secondary premature failure modes were not considered.
- The increase in effective strain of RC members with installed FRP anchors was predicted for both shear strengthened beams and flexural strengthened slabs. The average increase in effective strain for shear critical beams with FRP anchors was 23% (experimentally estimated) vs. 18% (measured). For flexural strengthened RC slabs, the average increase in effective strain was 48% (experimentally estimated) vs. 78% (measured). No trend (R^2<0.5) existed between the experimentally estimated and measured anchor efficiency because the modified compression field theory does not consider premature failures which occur in FRP reinforced members and the experimental estimation was based on calculated values (ε_x, θ, β) of an unstrengthened beam.
- A strong relationship (R^2>0.7) existed between the increase in strength and anchor efficiency of beams and slabs when FRP anchors were provided. Both beams and slabs had strong linear correlations for shear strengthened beams and flexure strengthened slabs.
- In the FRP strengthened slabs without anchors, the maximum CFRP strain measured was consistent with the debonding FRP strain limit 0.007 in ISIS-M04.

8.4 Recommendations for Future work

- RC shear critical beams strengthening with FRP u-wrap strips failed from a loss of aggregate interlock due to the size of the beam cross-section.
  Therefore, it is recommended that future testing be conducted on beams where failure by aggregate interlock does not govern. Rather, FRP debonding and FRP rupture should be the limiting factors.
  Future tests should be conducted on T-beams. The compression resistance provided by the flange and the short depth of the T-beam would create the preferred conditions to ensure failure is governed by FRP debonding.
- End anchorage failure occurred in beams with complete shear span strengthening with continuous u-wrapped FRP sheets. Therefore, it is recommended that future beams be designed with additional internal steel stirrups and hooked or headed longitudinal steel reinforcement to ensure end anchorage failure does not occur even after FRP strengthening. This will allow for the full determination of the FRP contribution of FRP anchors to secure FRP sheets.
- In this study, a bell-shape strain profile was observed when a u-wrapped FRP sheet intercepted a diagonal tension shear crack at mid-depth. However, very little research has been conducted on the strain distribution in FRP laminates with and without anchors. It is recommended that future research be conducted using finite element modeling to gain a better understand of the following areas:
  - The strain distribution within a FRP sheet.
  - Bond transfer mechanism between the FRP sheet/concrete interface.
  - The strain transfer mechanism between FRP anchors and FRP sheets.
- Providing significant flexural strengthening with FRP laminates changed the failure zone from the bottom soffit of the slab to the concrete/steel interface. In future research, it is recommended to use higher concrete strength to avoid premature failure at the concrete/steel rebar interface. By doing so, the tensile strength at the concrete/steel interface is increased such that it is not the critical zone.
- The FRP anchor prediction model was presented in this thesis to determine the number of FRP anchors required to secure a single FRP sheet. It is recommended that further testing be conducted to validate this approach.

References

ACI, 2007. *Report on Fiber-Reinforced Polymer (FRP) Reinforcement for Concrete Structures,* Farmington Hills, MI: American Concrete Institute (ACI).

Adhikary, B. B., Mutsuyoshi, H. & Sano, M., 2000. Shear Strengthening of Reinforced Concrete Beams using Steel Plates Bonded on Beam Web: Experiments and Analysis. *Construction and Building Materials,* Volume 14, pp. 237-244.

Al-Amery, R. & Al-Mahaidi, R., 2006. Coupled Flexural-Shear Retrofitting of RC Beams using CFRP straps. *Thirteenth International Conference on Composite Structures,* 75(1-4), pp. 457-464.

Ali, M., Oehlers, D. & Seracino, R., 2006. Vertical Shear Interaction Model between External FRP Transverse Plates and Internal Steel Stirrup. *Engineering Structures,* 28(3), pp. 381-389.

American Concrete Institute, 2008. *ACI 440.2R-08.* Farmington Hills(MI): s.n.

Au, C. & Buyukozturk, O., 2006. Peel and Sher Fracture Characterization of Debonding in FRP Plated Concrete Affected by Moisture. *Journal of Composites for Construction* , 10(1), pp. 35-47.

Azam, R., 2010. Behaviour of Shear Critical RC Beams with Corroded Longitudinal Steel Reinforcement. *M.A.Sc. Thesis.*

Bank, L. C., 2006. *Composites in Construction: Structural Design with FRP Materials.* Hoboken, NJ: John Wiley & Sons.

Bousselham, A. & Chaallal, O., 2008. Mechanisms of Shear Resistance of Concrete Beams Strengthened in Shear with Externally Bonded FRP. *Journal of Composites for Construction,* 12(5), pp. 499-512.

Burgoyne, C. J., 1993. *Should FRP be Bonded to Concrete.* Vancouver, s.n.

Cao, S. Y. et al., 2005. Debonding in RC Beams Sher Strengthened with Complete FRP Wraps. *Journal of Composites for Construction,* 9(5), pp. 417-428.

Cement Association of Canada, 2008. *Concrete Design Handbook Third Edition.* Ottawa: CAC.

Chaallal, O., Noellet, M. & Perraton, D., 1998. Strengthening of Reinforced Concrete Beams with Externally Bonded FRP Plates: Design Guidelines for Shear and Flexure. *Canadian Journal in Civil Engineering,* Volume 25, pp. 692-704.

Chaallal, O., Shahawy, M. & Hassan, M., 2002. Performance of Reinforced Concrete T-Girders Strengthened in Shear with Carbon Fiber-Reinforced Polymer Fabric. *ACI Structural Journal,* 99(3), pp. 335-343.

Chen, G. M., 2010. *Shear Behaviour and Strength of RC Beams Shear-Strengthened with Externally Bonded FRP Reinforcement.* Hong Kong: The Hong Kong Polytechnic University.

Chen, G. M., Teng, J. G. & Chen, J. F., 2012. Shear Strength Model for FRP-Strengthened RC Beams with Adverse FRP-Steel Interaction. *Journal of Composites for Construction.*

Chen, G. M., Teng, J. G., Chen, J. F. & Rosenboom, O. A., 2010. Interaction between Steel Stirrups and Shear-Strengthening FRP Strips in RC Beams. *Journal of Composites for Construction,* 14(5), pp. 498-509.

Chen, J. F. & Teng, J. G., 2003. Shear Capacity of FRP Strengthened RC Beams: FRP Rupture. *Journal of Structural Engineering,* 129(5), pp. 615-625.

Chen, J. F. & Teng, J. G., 2003. Shear Capacity of FRP Strengthened Reinforced Concrete Beams: Fiber Reinforced Polymer Debonding. *Journal of Construction and Building Materials,* 17(1), pp. 27-41.

Deifalla, A. & Ghobarah, A., 2006. *Calculating the Thickness of FRP Jacket for Shear and Torsion Strengthening of RC Girders T-Girders.* Miami, FL, CICE.

Deniaud, C. & Cheng, J., 2003. Reinforced Concrete T-Beams Strengthened in Shear with Fiber Reinforced Polymer Sheets. *Journal of Composites for Construction,* pp. 302-310.

DeWolf, J. T., Beer, F. P. & Johnston, R., 2006. *Mechanics of Materials 4th Edition.* s.l.:McGraw Hill.

El-Sayed, A. K., 2006. Concrete Contribution To Shear Resistance of FRP-Reinforced Concrete Beams. *PhD Thesis.*

Fang, T. Q., 2002. *Study on U-shaped sheet behaviour of anti-debonding in the concrete beam reinforced flexurally with FRP.* s.l.:Tsinghua University.

Grande, E., Imbimbo, M. & Rasulo, A., 2009. Effect of Transverse Steel on the Response of RC Beams Strengthened in Shear by FRP: Experimental Study. *Journal of Composites for Construction,* 13(5), pp. 405-414.

ISIS Canada, 2004. *ISIS Education Module 4: An Introduction to FRP Strengthening of Concrete Structures.* s.l.:ISIS Canada.

ISIS-M04, 2009. *FRP Rehabilitation of Reinforced Concrete Structures Design Manual 4.* Winnipeg: ISIS Canada.

Jayaprakash, J., Abdul Samad, A. A., Abbasovich, A. A. & Abang Ali, A. A., 2008. Shear capacity of pre-cracked and non pre-cracked reinforced concrete shear beams with externally bonded bi-directional CFRP strips. *Journal of Construction and Building Materials,* Volume 22, pp. 1148-1165.

Jinno , Y. & Tsukagishi, H., 1998. *Structural Properties of RC Walls Strengthened by Carbon Fiber Sheets.* Fukuoda, Japan, s.n., pp. 209-210.

Kalfat, R., Al-Mahaidi, R. & Smith, S. T., 2011. Anchorage Devises Used to Improve the Performance of Reinforced Concrete Beams Retrofitted with FRP Composites: A-State-of-the-Art-Review. *Journal of Composites for Construction* .

Khalifa, A., Alkhrdaji, T., Nanni, A. & Lansburg, S., 1999. Anchorage of Surface Mounted FRP Reinforcement. *Concrete International: Design and Construction,* 21(10), pp. 49-54.

Khalifa, A., Gold, W. J., Nanni, A. & Aziz, A., 1998. Contribution of Externally Bonded FRP to Shear Capacity of RC Flexural Members. *Journal of Composites for Construction,* 2(4), pp. 195-202.

Khalifa, A. & Nanni, A., 2000. Improving Shear Capacity of Existing RC T-Section Beams Using CFRP Composites. *Journal of Cement and Concrete Composites,* Volume 22, pp. 164-174.

Kim, S. J. & Smith, S. T., 2009. Behaviour of Handmade FRP Anchors under Tensile Load in Un-cracked Concrete. *Advances in Structural Engineering,* 12(6), pp. 845-865.

Kim, S. J. & Smith, S. T., 2009. *Shear strength and behaviour of FRP spike anchors in cracked concrete.* Sydney, Australia, FRPRCS-9, pp. 1-4.

Kit Ng, S. T., 2005. Shear Behaviour of RC Beams Externally Prestressed with CFRP Rods. *PhD Thesis.*

Kobayashi, K. et al., 2001. *Advanced Wrapping System with CF Anchor-Stress Transfer mechanism of CF Anchor.* Cambridge, U.K. , s.n., pp. 379-388.

Kobayashi, K., Kanakubo, T. & Jinno, Y., 2004. *Seismic Retrofit of Structures Using Carbon Fibres.* s.l., s.n., pp. 1-21.

Lu, X. Z., Teng, J. G., Ye, L. P. & Jiang, J. J., 2007. Intermediate Crack Debonding in FRP-Strengthened RC Beams: FE Analysis and Strength Model. *Journal of Composites for Construction,* 11(2), pp. 161-174.

Mabsout, M., Tarhini, K., Jabakhanji, R. & Awwad, E., 2004. Wheel load distribution in simply supported concrete slab bridges. *Journal of Bridge Engineering,* 9(2), pp. 147-155.

MacGregor, J. G. & Bartlett, M. F., 2000. *Reinforced Concrete Mechanics and Design.* Toronto: Prentice Hall.

Maeda, T. et al., 1997. *A Study on Bond Mechanism of Carbon Fiber Sheets.* s.l., Proceedings of the 3rd International Symposium, pp. 279-286.

Mofidi, A., Chaallal, O., Benmokrane, B. & Neale, K., 2012. Performance of End-Anchorage Systems for RC Beams Strengthened in Shear with Epoxy-Bonded FRP. *Journal of Composites for Construction,* 16(3), pp. 322-331.

Noel, M. & Soudki, K., 2011. Evaluation of FRP posttensioned slab bridge strips using AASHTO-LRFD Bridge design specifications. *Journal of Bridge Engineering,* Volume 16, pp. 839-846.

Oehlers, D. & Seracino, R., 2004. *Design of FRP and steel plated RC structures: retrofitting beams and slabs for strength, stiffness and ductility.* U.K.: Elsevier.

Ortega, C. A., Belarbi, A. & Bae, S. W., 2009. *End Anchorage of Externally Bonded FRP Sheets for the Case of Shear Strengthening of Concrete Girders.* Sydney, Australia, FRPRCS-9, pp. 1-4.

Orton, S. L., 2007. *Development of a CFRP System to Provide Continuity in Existing Reinforced Concrete Structures Vulnerable to Progressive Collapse.* Austin, Texas: The University of Texas at Austin, Department of Civil, Environmental and Architectural Engineering.

Orton, S. L., Jirsa, J. O. & Bayrak, O., 2008. Design considerations of carbon fiber anchors. *Journal of Composites for Construction ,* 12(6), pp. 608-616.

Ozbakkaloglu, T. & Saatcioglu, M., 2009. Tensile Behaviour of FRP Anchors in Concrete. *Journal of Composites for Construction ,* 12(6), pp. 608-616.

Ozdemir, G., 2005. *Mechanical Properties of CFRP Anchorages.* Istanbul, Turkey: Middle East Technical University.

Pellegrino, C. & Modena, C., 2002. Fiber Reinforced Polymer Shear Strengthening of Reinforced Concrete Beams with Transverse Steel Reinforcement. *Journal of Composites for Construction,* 6(2), pp. 104-111.

Quinn, K. T., 2009. *Shear Strength of Reinforced Concrete Beams with Carbon Fiber Reinforced Polymer (CFRP) and Improved Anchor Details.* Texas(Austin): University of Texas at Austin.

Rahimi, H. & Hutchinson, A., 2001. Concrete Beams Strengthened with Externally Bonded FRP Plates. *Journal of Composites for Construction ,* 5(1), pp. 44-56.

Robert Park, T. P., 2006. *Reinforced Concrete Structures.* s.l.:John Wiley and Sons.

Sharif, A. et al., 1994. Strengthening of Initally Loaded Reinforced Concrete Beams using FRP plates. *ACI Structural Journal,* 91(2), pp. 160-168.

Sherwood, E. G., 2008. *One-Way Shear Behaviour of Large, Lightly-Reinforced Concrete Beams and Slabs,* Toronto, ON: University of Toronto.

Siddiqui, N. A., 2009. Experimental investigation of RC beams strengthened with externally bonded FRP composites. *Latin American Journal of Solids and Structures,* 6(4), pp. 343-362.

Sika Canada Inc., 2011. *SikaWrap Product Data Sheet,* Mississauga, ON: Sika Canada Inc..

Smith , S. T., Hu, S., Kim, S. J. & Seracino, R., 2011. FRP-strengthened RC slabs anchored with FRP anchors. *Engineering Structures,* pp. 33: 1075-1087.

Smith, S., 2010. *Strengthening of Concrete, Metallic and Timber Construction Materials with FRP Composites.* s.l., CICE 2010, pp. 13-9.

Smith, S. T. & Kim, S. J., 2008. *Sher strength and behaviour of FRP spike anchors in FRP-to-concrete joint assemblies.* Winnipeg, Canada, ACMBS-V.

Stanley, T. & Ng, K., 2005. Shear Behaviour of RC Beams Externally Prestressed with CFRP Rods. *PhD Thesis.*

Swaddiwudhipong, S., Lu, H.-R. & Wee, T.-H., 2003. Direct Tension Test and Tensile Strain Capacity of Concrete at Early Age. *Cement and Concrete Research,* July, Issue 33, pp. 2077-2084.

Teng, J. G., Lam, L. & Chen, J. F., 2004. Shear strengthening of RC beams using FRP composites. *Progress in Structural Engineering and Materials,* 6(3), pp. 173-184.

Teng, J. G., Smith, S. T., Yao, J. & Chen, J. F., 2003. Intermediate Crack Induced Debonding in RC Beams and Slabs. *Construction and Building Materials,* 17(6-7), pp. 447-462.

Triantfillou, T. C. & Antonopoulos, C. P., 2000. Design of Concrete Flexural Members strengthened in shear with FRP. *Journal of Composites for Construction,* pp. 198-205.

Triantifillou, T. C., 1998. Shear Strengthening of Reinforced Concrete Beams Using Epoxy-Bonded FRP Composites. *ACI Structural Journal,* pp. 95 (2): 107-115.

Uji, K., 1992. *Improving Shear Capacity of Existing RC Concrete Members by Applying Carbon Fiber Sheets.* s.l., s.n., pp. 253-256.

West, J., 2011. *Part 2: Behaviour of Structural Concrete.* Waterloo, ON: University of Waterloo.

Williams, A., 2000. *Design of Reinforced Concrete Structures 2nd Edition.* Austin, Texas: Engineering Press.

Wu, Y.-F. & Huang, Y., 2008. Hybrid Bonding of FRP to Reinforced Concrete Structures. *Journal of Composites for Construction ,* 12(3), pp. 266-273.

Yao, J., Teng, J. G. & Lam, L., 2002. *Debonding in RC Cantilever Slabs Strengthened with FRP strips'.* Southampton University, U.K., s.n., pp. 125-133.

Zhang, H. W., Smith, S. T. & Kim, S. J., 2011. Optimisation of Carbon and Glass FRP Anchor Design. *Construction and Building Materials,* Volume 32, pp. 1-12.

Zhang, Z. & Hsu, C. T., 2005. Shear Strengthening of Reinforced Concrete Beams Using Carbon Fiber Reinforced Polymer Laminates. *Journal of Composites for Construction,* Volume 9, pp. 158-169.

Appendix A : Pilot Study – Test Results and Discussion

A.1 Introduction

This appendix presents the experimental results of a pilot study designed to investigate the feasibility of using commercial manufactured FRP anchors to secure FRP sheets installed to strengthen RC beams in shear. The data is presented as one section containing shear strengthened slender beams (a/d ratio = 3.0). The primary goal of the pilot study was to determine:

- The feasibility of the shear critical RC beam design
- The effect of various FRP strengthening systems
- The effect of FRP anchors applied to external u-wrapped FRP sheets
- The effect of various FRP strengthening configurations

The test results presented include:

- Load-displacement behaviour
- Steel and concrete strain response
- FRP strain response

A.2 Pilot Study – Shear Critical Beams

Nine shear critical beams were strengthened with three types of FRP sheets. One beam was tested as control (unstrengthened), five beams were strengthened with intermittent u-wrapped FRP sheets applied the full depth of the beam and three beams were strengthened with intermittent u-wrapped FRP sheets applied the partial depth of the beam. The test variables were:

1. Condition of the beam: Full depth vs. Partial depth
2. Type of FRP sheet: Sikawrap 230C, 350G and 430G
3. FRP shear span configuration: Intermittent strips (200 mm vs. 100 mm wide)
4. Use of FRP anchors: No anchors vs. GFRP anchors
CFRP vs. GFRP

A summary of the test results, ultimate load, deflection at ultimate load, percent increase over the control and mode of failure for all beams is provided in Table A-1.

Debonding and peeling of the FRP sheet occurred in four out of the eight FRP strengthened beams (430G-100-NA, PD-430G-100-NA, PD-430G-100-CA, PD-430G-100-GA). All nine experienced the same initial behaviour during testing. Cracking initiated as flexural cracks between the two loading points. As the load increased, diagonal tension shear cracks began to develop in the shear span and propagated to the support and loading points.

Table A-1: Pilot Study - Summary of test results

Nomenclature	Specimen Description	Ultimate Load (kN)	Deflection at ultimate load (mm)	Percent increase over the control (%)	Failure mode
Control	Control	232	8.80	-	• DT-SF
230C-200-NA	230C-200 mm-No anchors	373	11.4	67.5	• FF
230C-200-A	230C-200 mm-Anchors	390	16.9	75.1	• FF
350G-200-NA	350G-200 mm- No anchors	294	12.0	32.0	• DT-SF
350G-200-A	350G-200mm-Anchors	300	10.7	34.7	• DT-SF
430G-100-NA	430G-100 mm-No anchors	334	13.7	50.1	• FRP Debond
PD-430G-100-NA	PD-430G-100mm-No anchors	305	12.0	36.8	• FRP Debond
PD-430G-100-CA	PD-430G-100mm-C Anchors	310	14.2	39.2	• DT-SF
PD-430G-100-GA	PD-430G-100 mm-G Anchors	339	13.7	52.2	• DT-SF

where: DT=Diagonal tension, SF=Shear failure, FF=Flexural failure, AF=Anchor failure

A.2.1 Control Beam

The failure mode of the control beam was diagonal tension shear failure by loss of aggregate interlock. The diagonal tension shear crack propagated in the shear span between the loading point and the support. Failure by loss of aggregate interlock from two diagonal tension shear cracks is shown in Figure A-1.

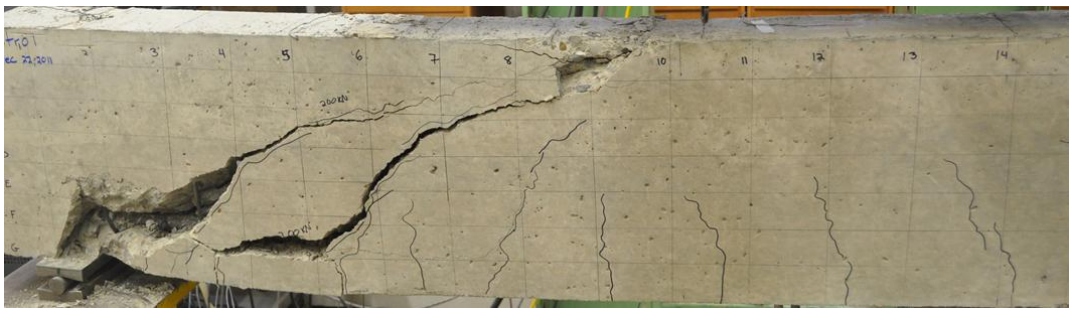

Figure A-1: Failure mode of control beam (pilot study)

The load deflection response of the control beam is shown in Figure A-2. The load deflection curve shows a linear response up to cracking. Diagonal tension shear failure occurred suddenly after the peak load of 223 kN. The maximum deflection recorded was 8.8 mm. After failure a gradual drop in load with deflection was exhibited indicating the brittle nature of this type of failure.

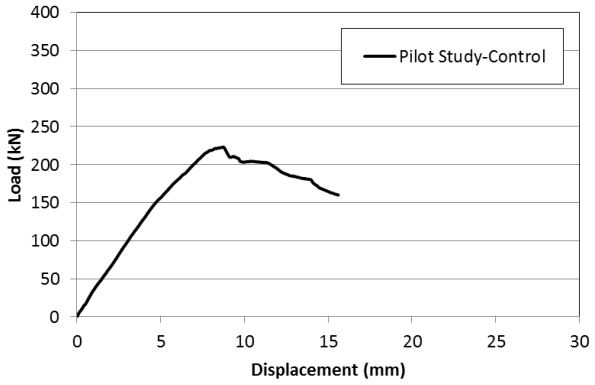

Figure A-2: Load vs. deflection curve of control beam (pilot study)

The strain response for the concrete at the top fiber, longitudinal steel reinforcement at mid-span and stirrup strain response is presented in Figure A-3 and Figure A-4. At failure, the strain in the concrete was below the strain to cause concrete crushing and the strain in the longitudinal steel bars was below the yield strain. The strain response in the stirrups shows the 2nd stirrup (380 mm from the support) yielded reaching a maximum strain of 2000 με and the 4th stirrup (450 mm from the support) did not yield, recording a maximum strain of 1600 με.

In both cases, the load vs. strain in the stirrups had a bi-linear shape. Almost no strain was recorded up to a load of 100 kN at which time a steady gradual increase in strain occurred as the load was increased. The strain response indicated that the internal steel stirrups did not carry any load until the tensile capacity of the concrete was reached and cracking occured close to the stirrup location.

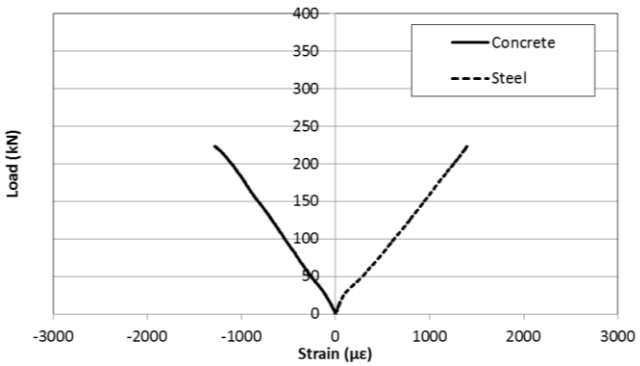

Figure A-3: Concrete and steel rebar strain response of control beam (pilot study)

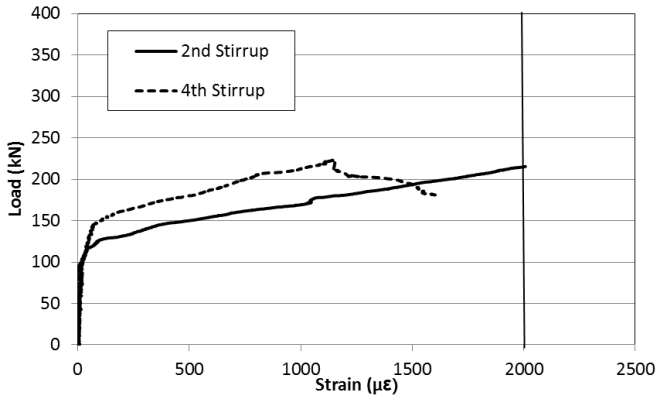

Figure A-4: Stirrup strain response of control beam (pilot study)

A.2.2 CFRP Strengthened Beams

Two beams were strengthened with CFRP sheets installed as u-wraps (200 mm wide at 275 mm spacing) with and without CFRP anchors. The beams were strengthened with Sikawrap 230C sheets (0.381 mm thick) and were applied with Sikadur 330 epoxy. The failure mode for both beams was flexural failure with crushing of the concrete (Figure A-5).

The load deflection response of the two CFRP strengthened beams is shown in Figure A-6. The load deflection curve shows linear behaviour with a slow gradual decrease in the post peak response. Cracking initiated as flexural cracks on the bottom of the beam under the loading points at a load of 128 kN for 230C-200-NA and 87 kN for 230C-200-A. Hairline shear cracks began to appear in the shear span between the CFRP sheets at loads of 140 kN and 150 kN and did not widen due to the presence of the CFRP u-wraps. As the flexural cracks propagated, the longitudinal tension steel bars and the compression steel bars yielded.

Cracking and popping of the CFRP sheets and epoxy was heard during loading up to failure. Debonding of the CFRP sheets did not occur for the unanchored beam. Complete failure of both beams occurred by crushing of the concrete in the compression zone. The failure load recorded for 230C-200-NA was 373 kN with a maximum deflection of 11.4 mm. The failure load for 230C-200-A was 390 kN with a maximum deflection of 16.9 mm. Figure A-5b shows an image of the failed beam (230C-200-A) with anchors.

The benefits of using CFRP anchors could not be fully assessed because both beams failed in flexure. The difference between the FRP strengthened beams with and without anchors was 17 kN. The 4.5% difference is within experimental error and cannot be attributed to the presence of FRP anchors.

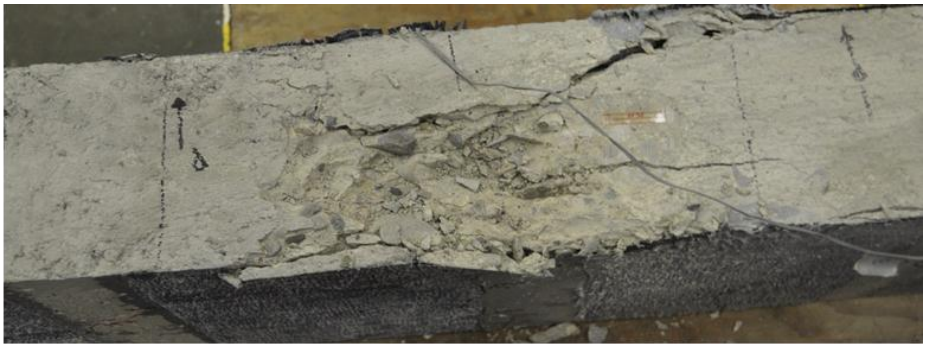

(a)

(b)

Figure A-5: Failure mode of CFRP strengthened beams (pilot study)

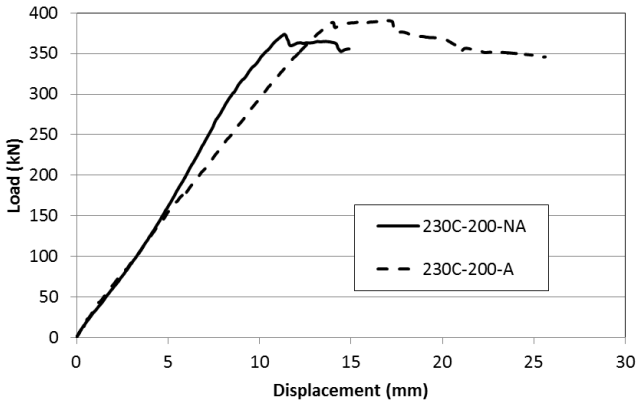

Figure A-6: Load vs. deflection of CFRP strengthened beams (pilot study)

At failure, the concrete strain in beam 230C-200-A exceeded the crushing strain of the concrete. The strain in the longitudinal steel was above the yielding strain for both beams. The strain response in the stirrups showed that the 2nd stirrup (380 mm from the support) of beam 230C-200-A was the only stirrup that reached a strain above yield (2000 με). All other stirrups recorded maximum strain values of 1500 με which indicate that the beam had substantial shear strength reserve. The strain gauge readings for the concrete, longitudinal reinforcement, stirrup and CFRP strain response are presented in Figure A-7 - Figure A-10.

The CFRP strain response varied depending on the presence of anchors. Beams 230C-200-NA and 230C-200-A recorded maximum strains of 4000 με and 5400 με respectively at mid-depth on the CFRP sheet. Beam 230C-200-A experienced higher CFRP strains because the presence of CFRP anchors did not allow for any debonding or slippage. The highest strains were recorded at mid-depth between 100-150 mm for the unanchored beam and 150-200 mm for the anchored beam.

These strain results correlated with the load vs. displacement curve and the visual observations and confirmed that the mode of failure was flexure failure with yielding of the longitudinal steel followed by crushing of concrete in the compression zone. Shear failure by concrete crushing can be ruled out as a possible failure mode because most of the stirrups did not yield and the load vs. deflection curves exhibited flexural behaviour.

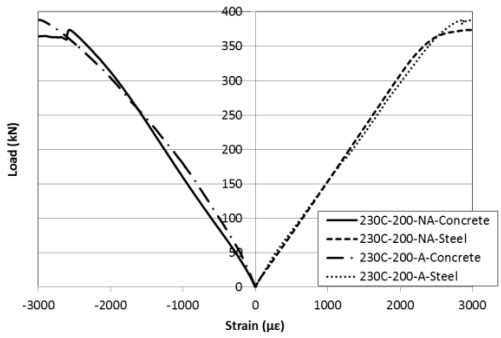

Figure A-7: Concrete and steel rebar strain response of CFRP beams (pilot study)

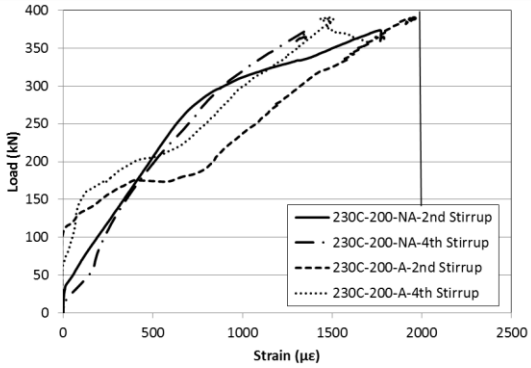

Figure A-8: Stirrup strain response of CFRP strengthened beams (pilot study)

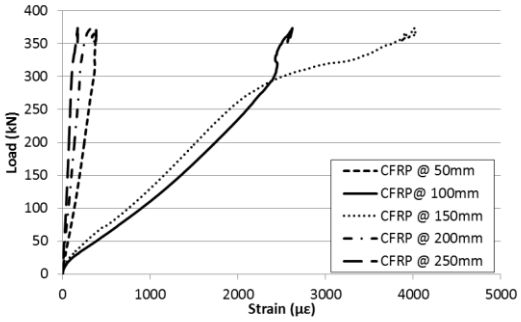

Figure A-9: CFRP strain response of 230C-200-NA (pilot study)

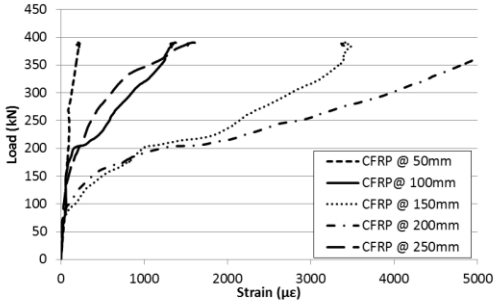

Figure A-10: CFRP strain response of 230C-200-A (pilot study)

A.2.3 FRCM Strengthened Beams

Two beams were strengthened with FRCM u-wrap 200 mm wide at a spacing of 275 mm o/c with and without CFRP anchors. The Sikawrap 350G sheet is 1.170 mm thick and was applied with Sika MonoTop-623 cementitious grout.

The mode of failure for both beams was diagonal tension shear failure. Debonding did not occur in either beam (Figure A-11). The load deflection response of the two CFRP strengthened beams is shown in Figure A-12.

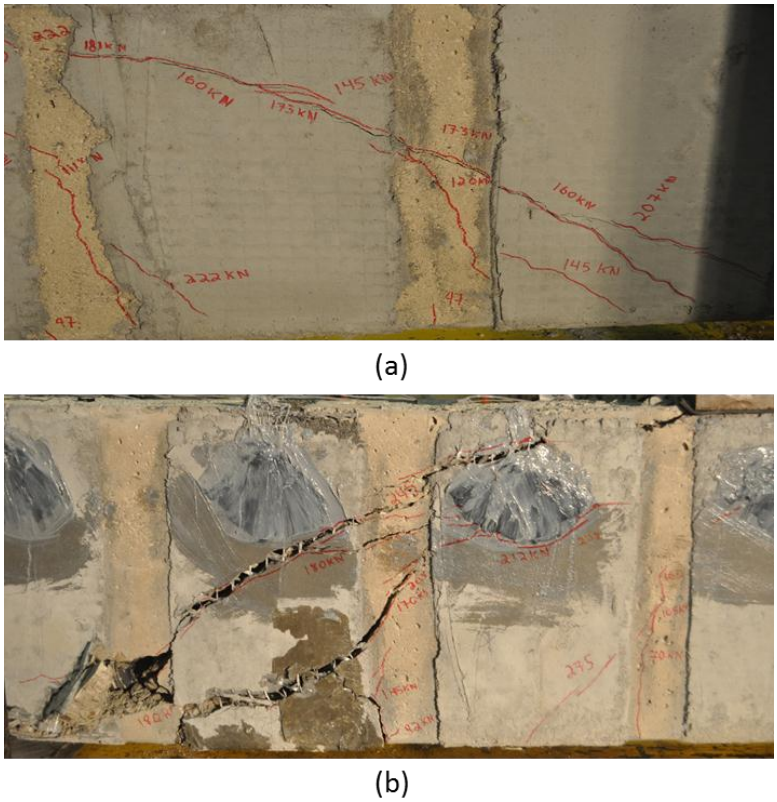

(a)

(b)

Figure A-11: Failure mode of FRCM strengthened beams

The load deflection curves had a linear response with two plateaus. The first flexural cracks were observed at a load of 63 kN and 70 kN for beams 350G-200-NA and 350G-200-A, respectively. As the load was increased, diagonal tension shear cracks began to develop in the shear span at loads of 150 kN for 350G-200-NA and 155 kN for 350G-200-A. The cracks propagated and widened until they reached the support and loading point at which point failure occurred.

The failure load for beam 350G-200-NA was 294 kN at a maximum deflection of 12.0 mm and the failure load for 350G-200-A was 300 kN with at a maximum deflection of 10.7 mm. It was

observed that in the case of the FRCM strengthened beam with CFRP anchors, the diagonal shear crack took the path of least resistance travelling above the anchor fan propagating to the loading point (Figure A-11b). The difference in capacity between beams 350G-200-NA and 350G-200-A (6 kN) was within experimental error and the benefits of using CFRP anchors could not be full assessed.

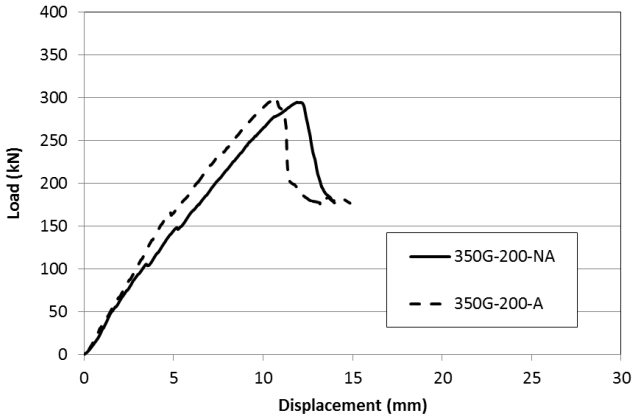

Figure A-12: Load vs. deflection of FRCM strengthened beams (pilot study)

The strain response for the concrete top fiber and longitudinal steel reinforcement at mid-span is shown in Figure A-13 and the strain response of the stirrups is shown in Figure A-14.

For both FRCM strengthened beams, the concrete strain was below the crushing strain of concrete and the longitudinal steel strain was below the yielding strain of steel when failure occured. The strain response in the stirrups show that the recorded strains in the 2nd stirrup of beams 350G-200-NA and 350G-200-A were higher than the yield strain with maximum strain values of 2600 με and 5000 με respectively. Strain in the 4th stirrup was below the yield strain for both beams. The FRCM strain response showed very little to no strain response for the FRCM sheets with and without anchors. Low strain values are possible because cementitious mortar was used to secure the fiber grid. The mortar cracked instead of stretching the fibers and the strain gauges did not work well in measuring tension strains of cracked cementitious mortar. The strain in the longitudinal steel and stirrups correlated with the load deflection curves and observed failure mode.

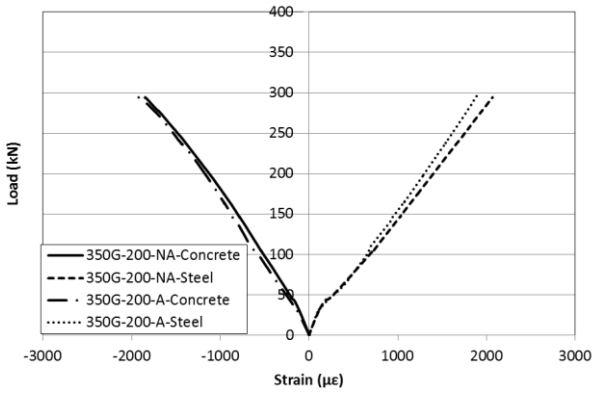

Figure A-13: Concrete and longitudinal steel strain response of FRCM beams (pilot study)

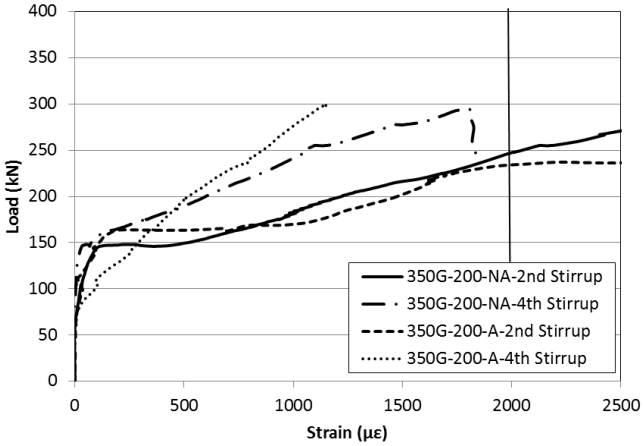

Figure A-14: Stirrup strain response of FRCM strengthened beams (pilot study)

A.2.4 GFRP Strengthened Beams

Four beams were strengthened with u-wrap Sikawrap 430G sheets 100 mm wide at a spacing of 200 mm o/c. Sikawrap 430G sheets are 0.508 mm thick and were applied with Sikadur 330 epoxy. One beam had GFRP sheets installed the full depth of the beam and three beams had GFRP sheets with partial depth installation (50 mm below the top of the beam).

Beam with full depth GFRP sheets:

The failure mode of the beam with full depth installation (430G-100-NA) was debonding of the GFRP sheet and simultaneous shear diagonal tension failure (Figure A-15). The load deflection response of beam 430G-100-NA is shown in Figure A-16.

The load deflection cruve had a bi-linear response with two slopes. The first flexural cracks appeared at a load of 58 kN. As the load was increased, inclined cracks began to develop in the shear span at a load of 160 kN. Crack development occurred in both shear spans with the GFRP

sheets debonding at the top of the sheet at a load of 270 kN. Diagonal tension shear failure occurred at 334 kN with a maximum deflection of 13.7 mm. The post peak behaviour exhibited brittle shear failure. The strain gauge readings for the concrete top fiber and longitudinal steel reinforcement are shown in Figure A-17 and Figure A-18.

At failure, the concrete strain was below the concrete crushing strain and the longitudinal steel strain was below the yielding strain of steel. The strain response in the stirrups showed that both stirrups surpassed the yield strain, recording maximum strains of 2000 με and 2300 με respectively.

Figure A-15: Failure mode of full depth GFRP strengthened beam (pilot study)

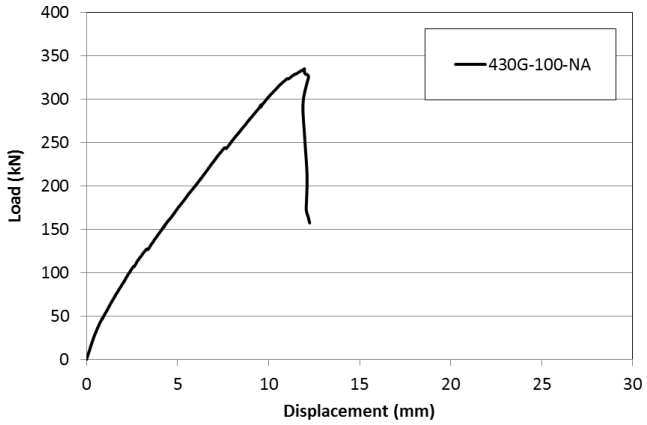

Figure A-16: Load vs. deflection of GFRP strengthened full depth beam (pilot study)

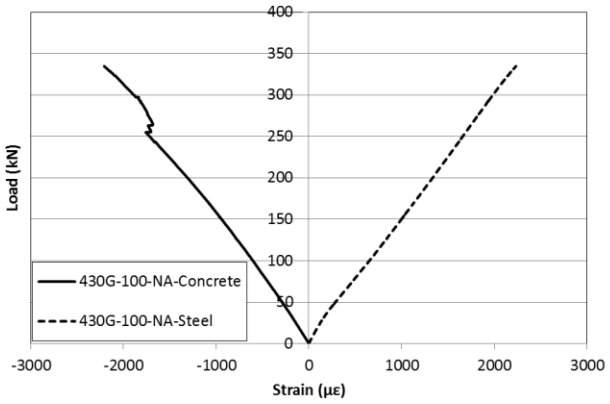

Figure A-17: Concrete & steel strain response of full depth GFRP strengthened beam

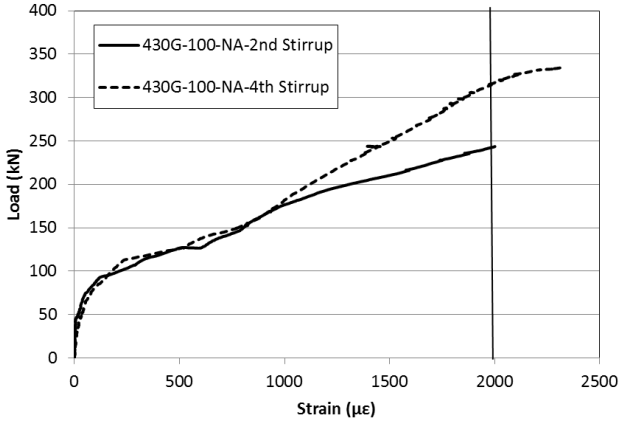

Figure A-18: Stirrup strain response of full depth GFRP strengthened beam (pilot study)

Beams with partial depth GFRP sheets:

The mode of failure for beams with partial depth strengthening without anchors (PD-430G-100-NA) was FRP debonding and the failure mode observed for the two beams strengthened with partial depth GFRP sheets and FRP anchors (PD-430G-100-CA, PD-430G-100-GA) was diagonal tension shear failure with crushing of the concrete. No debonding was observed in the anchored beams.

The load deflection response for partial depth GFRP strengthened beams is shown in Figure A-19. All three curves show a linear response. The first flexural cracks were observed at loads of 65 kN, 50 kN and 55 kN for beams PD-430G-100-NA, PD-430G-100-CA and PD-430G-100-GA, respectively. Diagonal shear cracks began to appear in the shear span between the support and loading point at loads of 130 kN, 133 kN and 140kN for beams PD-430G-100-NA, PD-430G-100-CA and PD-430G-100-GA, respectively. Cracking and popping was heard from the GFRP sheets as the load increased. Debonding occurred at the ends of the GFRP sheets at loads

of 230 kN, 260 kN and 264 kN (75% of the ultimate load) for beams PD-430G-100-NA, PD-430G-100-CA and PD-430G-100-GA, respectively.

Full debonding was prevented in PD-430G-100-CA and PD-430G-100-GA because of the presence of FRP anchors. As the load was increased, the diagonal tension shear cracks began to propagate towards the support and loading point taking the path of least resistance. Failure occurred, when the shear cracks reached the loading point and the support. The ultimate load for beams PD-430G-100-NA, PD-430G-100-CA and PD-430G-100-GA was 305 kN, 340 kN and 310 kN and the maximum deflection at ultimate load was 12.0 mm, 14.2 mm and 13.7 mm, respectively.

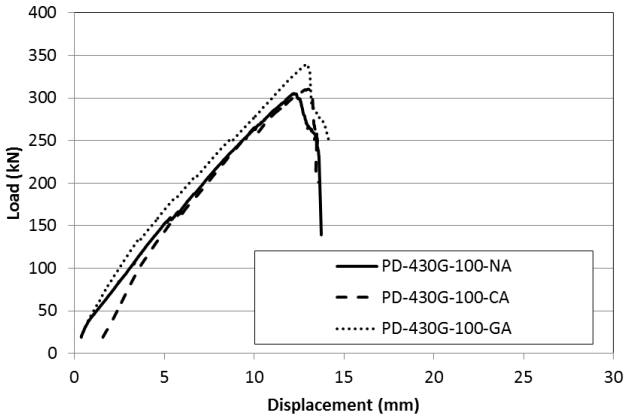

Figure A-19: Load vs. deflection of GFRP strengthened partial depth beams (pilot)

Anchors in PD-430G-100-CA and PD-430G-100-GA prevented complete debonding of the FRP sheet from the concrete. The top section above the FRP anchor was the only portion of the FRP sheet to debond. The shear crack was observed propagating around the anchors of two separate sheets towards the compression zone of the beam. The crack bypassed the GFRP sheet at the loading point as shown in Figure A-20.

Figure A-20: Crack propagation around FRP anchor

The strain response for the concrete top fiber and longitudinal steel reinforcement at mid-span is shown in Figure A-21. At failure, the concrete strain was below the crushing strain of concrete and the longitudinal steel strain was below the yielding strain for all beams. The strain gauge on the longitudinal steel rebar of beam PD-430G-100-CA was not functioning. Strain response in the stirrups is presented in Figure A-22. The strain response in the stirrups showed that the 2nd stirrup yielded in beam PD-430G-100-NA recording a maximum strain of 3000 με.

In all three partial depth beams, beam PD-430G-100-NA was the only beam to record strains larger than 500 με. Figure A-23 shows the tensile strain response in the GFRP at various depths from the top of the beam.

Two strain gauges located 100 mm and 150 mm from the top of the beam had the highest strain response recording maximum strains of 7500 με. Cross-referencing the GFRP sheet strain data with the shear crack location, it is clear that the diagonal tension shear crack passed directly behind the GFRP sheet at mid-depth causing high tensile strain 100-150 mm from the top of the beam.

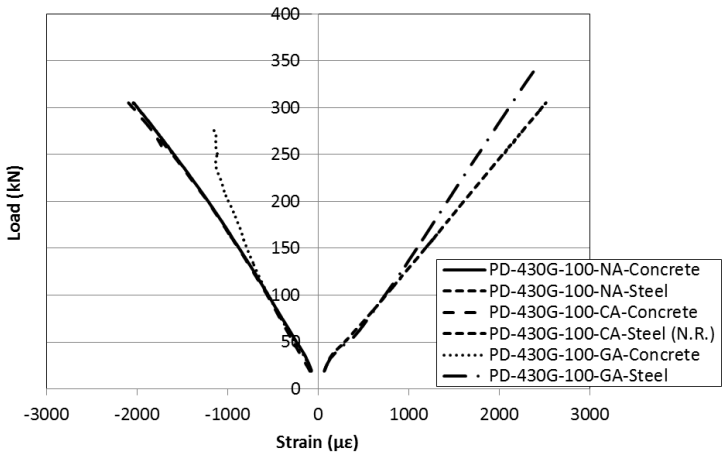

Figure A-21: Concrete & steel strain response of PD-GFRP strengthened beams

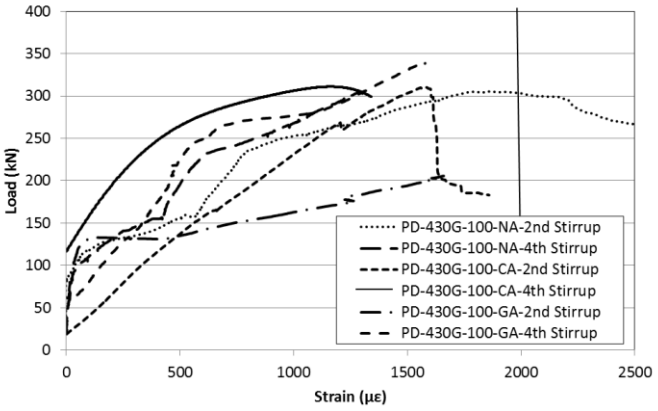

Figure A-22: Stirrup strain response of PD-GFRP strengthened beams (pilot study)

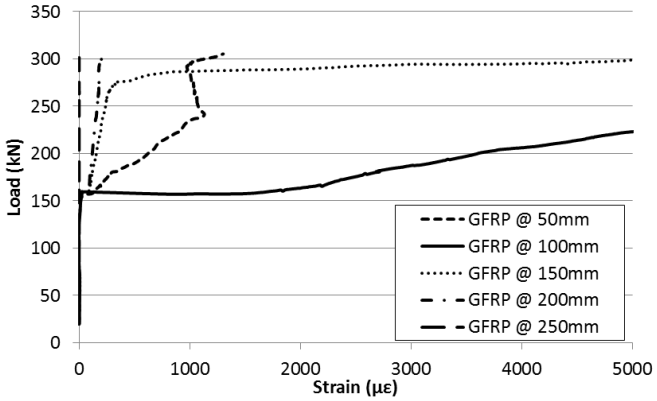

Figure A-23: FRP strain response of PD-430G-100-NA (pilot study)

A.3 Discussion of Shear Critical Beam Results

A.3.1 Observed Behaviour

Three modes of failure were observed: shear failure (control unstrengthened beam - Figure A-24a), shear failure with debonding of the FRP sheet (Figure A-24b) and flexural failure with crushing of the concrete (Figure A-24c). The beams that experienced flexural failure (Figure A-24c), both beams were strengthened with Sikawrap 230C sheets and were designed to fail in shear after strengthening. Figure A-24 shows photos of each of these failure modes.

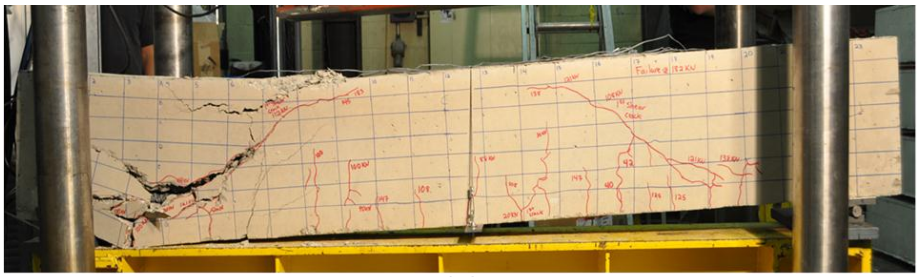

(a)

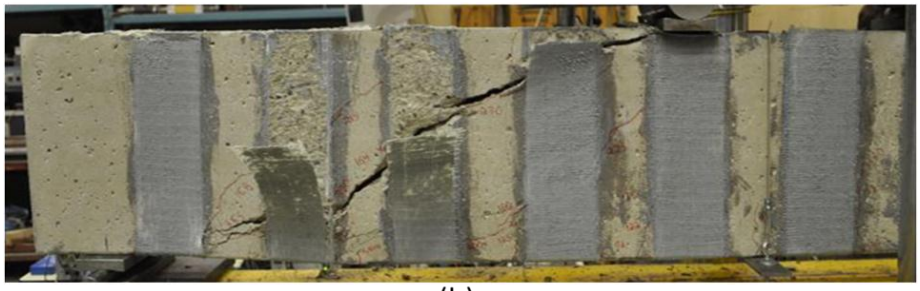

(b)

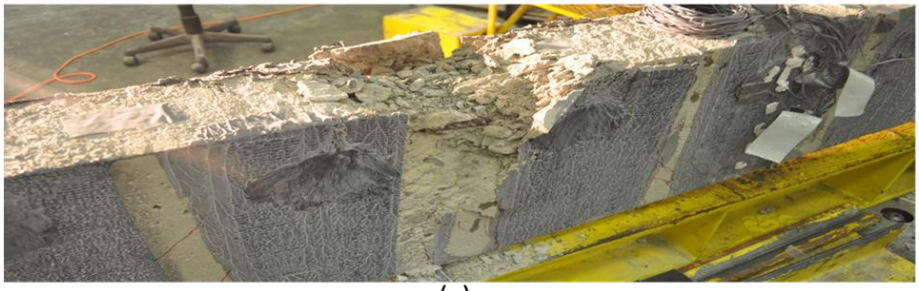

(c)

Figure A-24: Failure modes in pilot phase

A.3.2 Effect of FRP Type

In this section, the effect of the type of FRP used to strengthen or repair a shear critical beam on the load, stiffness, deflection and the strain response is analyzed and compared. The comparison includes beams with and without anchors.

In all beams, yielding of internal steel rebar was delayed or did not occur with the application of u-wrapped FRPs and the stiffness of the beams was increased with FRP strengthening

A.3.2.1Carbon FRP vs. Glass FRCM

GFRCM strengthened beams 350G-200-NA and 350G-200-A were strengthened with Sikawrap 350G sheets with and without GFRP anchors. The GFRCM strengthened beams failed in shear as designed. However, the CFRP strengthened beams failed in flexure. The load deflection curves of the four strengthened beams vs. control are shown in Figure A-25.

The CFRP strengthened beams exhibited flexural load deflection behaviour with ductile performance beyond the yield load. The GFRCM strengthened beam displayed typical load deflection behaviour with a sudden drop in the load at failure.

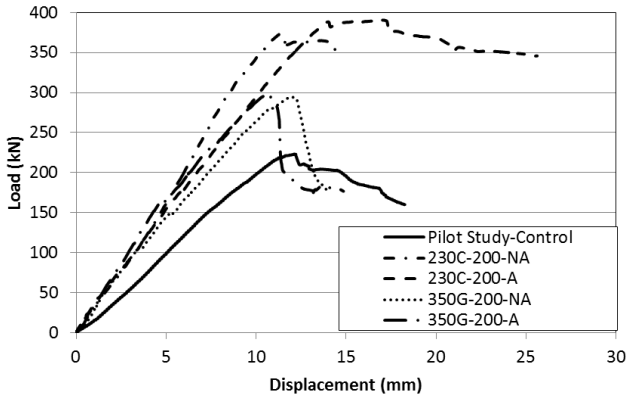

Figure A-25: Load vs. deflection of CFRP & GFRCM strengthened beams

Effect on Strength

A comparison of strength increase in CFRP and GFRCM strengthened beams over the control is shown in Figure A-26. The increase in strength over the control for CFRP and GFRCM strengthened beams without anchors was 67.5% and 32.0% and beams with anchors was 75.1%

and 34.7%. Analysis of the GFRCM beams shows that both beams failed in shear. However, this is not a fair assessment because the beams with CFRP strengthening failed in flexure.

The difference in strength between each beam can be attributed to the material properties of the strengthening material. Sikawrap 230C has a $\varepsilon_{rupture}$=1.33% with an elastic modulus of 65 GPa and Sikawrap 350G has a $\varepsilon_{rupture}$=2.80% with an elastic modulus of 75 GPa. The Sikawrap 350G GFRCM is a bi-directional grid applied with a cementitious mortar. During testing and at failure, the strengthening system never debonded as was observed for FRP epoxied sheets. Failure in the GFRCM system occurred by slippage of the GFRCM grid through the cementitious mortar and rupture of individual GFRCM nodes. GFRCM slippage can be attributed to the premature failure even though GFRCM has higher elongation at rupture and elastic modulus over Sikawrap 230C. The CFRP material was able to resist much higher loads such that the flexural capacity of the member was attained before the shear capacity reached

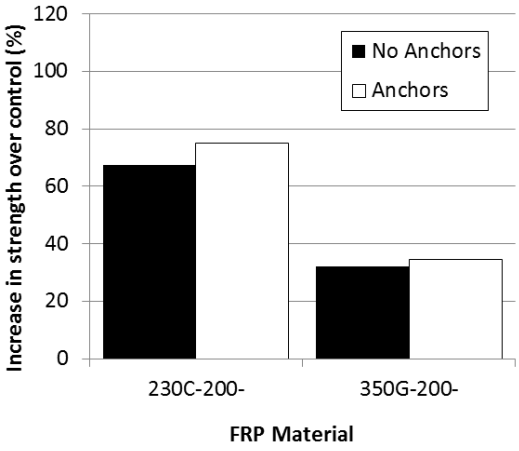

Figure A-26: Strength increase of CFRP & GFRCM strengthened beams over control

Effect on Stiffness

The beam stiffness was increased in all CFRP and GFRCM strengthened beams. The CFRP and GFRCM strengthened beams exhibited significant increases in the stiffness compared to the control beam. The two CFRP strengthened beams had the highest increase in stiffness with an average slope of 35 kN/mm compared to an average slop of 27 kN/mm for the GFRCM strengthened beams. Taking into consideration the differences in material properties, FRCM (E=75GPa) is stiffer compared to CFRP (E=65GPa) with a higher elastic modulus and

elongation at rupture. A correlation between the type of FRP material and its effect on the stiffness in the load deflection response was obvious.

Effect on Deflection

A bar chart comparing the maximum deflection at failure for the CFRP and GFRCM strengthened beams is shown in Figure A-27. Three beams exhibited on average a 29% increase in maximum deflection over the control beam. The fourth, CFRP strengthened beam with CFRP anchors, experienced a 92% increase in deflection over the control. This suggests that the presence of CFRP anchors significantly improves the maximum deflection at failure. However, it is recommended that further tests be conducted to confirm this finding. Beams strengthened with CFRP or GFRCM exhibited similar increases in deflection at failure over the control beam.

No consistent tend was observed when comparing the deflection at failure of unanchored and anchored CFRP and GFRCM strengthened beams. The CFRP beam with anchors had a significant increase in deflection while the GFRCM beam with anchors had a slight reduction in deflection versus the companion strengthened beams without anchors.

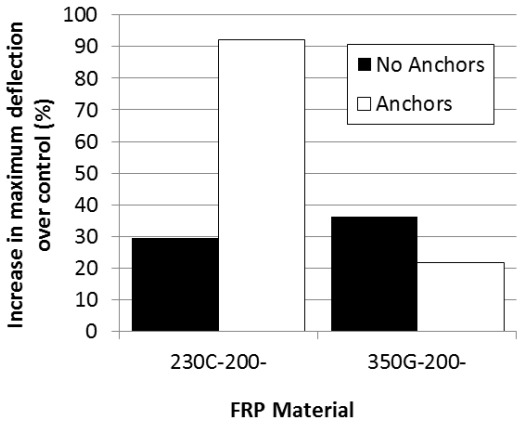

Figure A-27: Increase in maximum deflection of CFRP & GFRCM beams over the control

Strain Response

The maximum strain at failure shows a large difference in the strain recorded in the FRP sheet and internal steel stirrup between CFRP and GFRCM strengthened beams. The largest increase in stirrup strain was recorded in the GFRCM beam with anchors. The high strains recorded in the stirrups correlate with the shear failure mode observed for both GFRCM strengthened beams.

Lower stirrups strains were recorded in CFRP strengthened beams and can be attributed to the Sikawrap 230C material properties. The largest strain in the CFRP strengthened beams was recorded in the CFRP sheet with anchors. The ultimate CFRP sheet strain capacity is unknown because both beams failed in flexure and thus the limit was not reached.

A bar chart comparing stirrup and CFRP strain at failure is shown in Figure A-28 and Figure A-29. The CFRP strain response varied depending on the presence of anchors. Beams 230C-200-NA and 230C-200-A recorded maximum strains of 767 με and 5400 με, respectively at mid-depth on the CFRP sheet. Shear failure by concrete crushing can be ruled out as a possible failure mode because most of the stirrups did not yield and the load vs. deflection curves exhibited a flexural response.

Figure A-30 and Figure A-31show the CFRP and GFRCM strain profile at failure for each beam. The FRCM strain profile across the depth of the beam shows very little to no strain response in the FRCM sheets with and without anchors. The highest strain was 1000 με at mid-depth of beam 350G-200-A. CFRP strain was four times higher in the CFRP strengthened beam with anchors over GFRCM strengthened beam with anchors. Stirrup strains above 2000 με were recorded in both FRCM beams which failed by diagonal tension shear failure and the stirrup strains were below 2000 με for the two CFRP strengthened beams which failed in flexure.

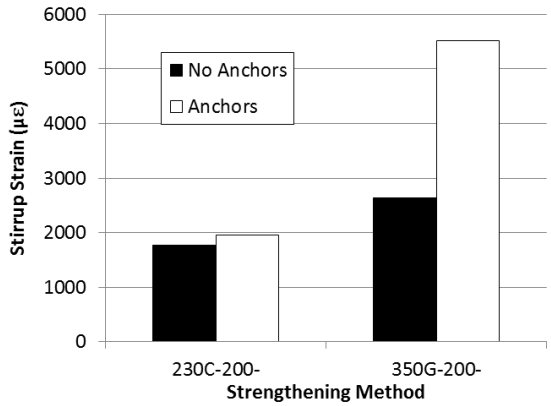

Figure A-28: Comparison of CFRP & GFRCM stirrup strain at failure

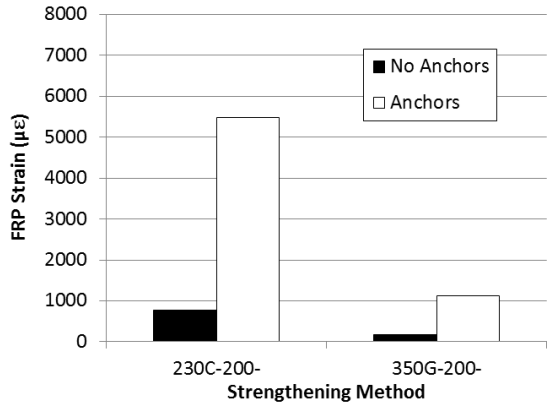

Figure A-29: Comparison of CFRP & GFRCM FRP strain at failure

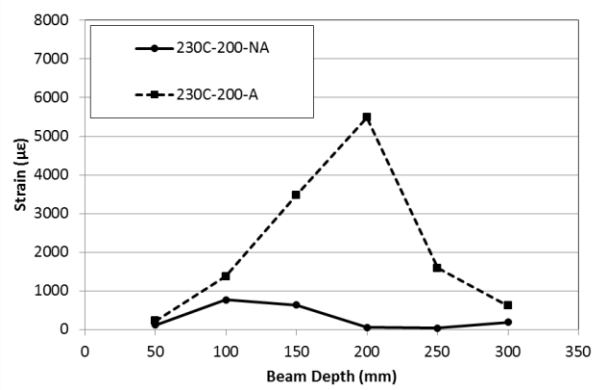

Figure A-30: FRP strain profile of CFRP strengthened beams

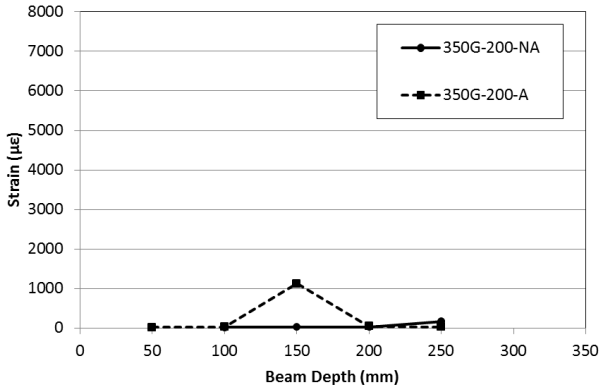

Figure A-31: FRP strain response of FRCM strengthened beams

A.3.3 Effect of FRP Configuration

In this section the effect of the FRP configuration (full depth vs. partial depth) used to strengthen or repair a shear critical beam on the load, stiffness, deflection and the strain response is analyzed and compared. The comparison includes beams without anchors.

A.3.3.1 Full Depth GFRP vs. Partial Depth GFRP

Beam 430G-100-NA was strengthened with Sikawrap 430G u-wraps installed the full depth of the beam and beam PD-430G-100-NA was strengthened with Sikawrap 430G u-wraps installed at a partial depth 50 mm below the top of the beam.

Full depth strengthening consists of u-wrapped sheets extending the entire depth of the beam (Figure A-32a) and partial depth strengthening consists of u-wrapped sheets applied 50 mm below the top of the beam (Figure A-32b). Both GFRP strengthened beams failed in shear as designed. The full depth sheets performed slightly better obtaining a higher load than the partial depth sheets.

The load vs. deflection curve of the two strengthened beams vs. control is shown in Figure A-33. The Sikawrap 430G sheet is 0.508 mm thick with an elongation at rupture of 2.21%. The GFRP strengthened beams exhibited typical shear load deflection behaviour with a sudden drop in load in the post peak phase of testing.

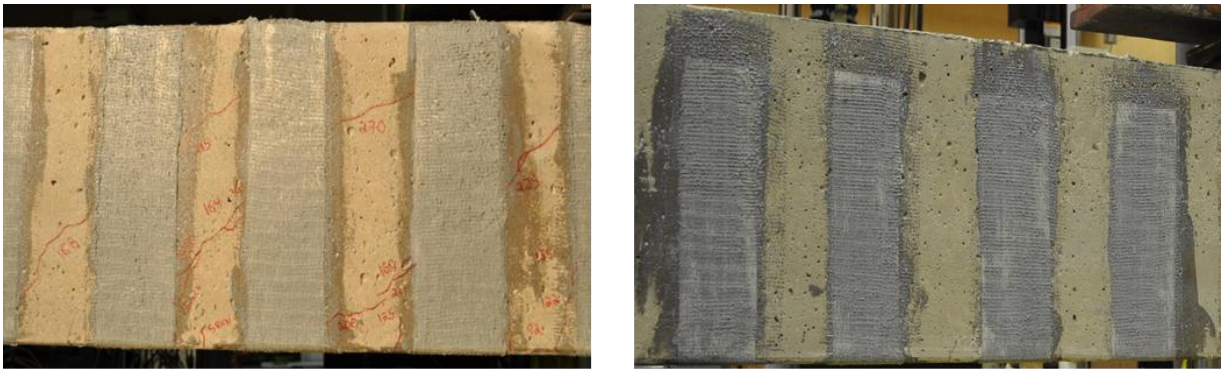

Figure A-32: Full and partial depth GFRP strengthening

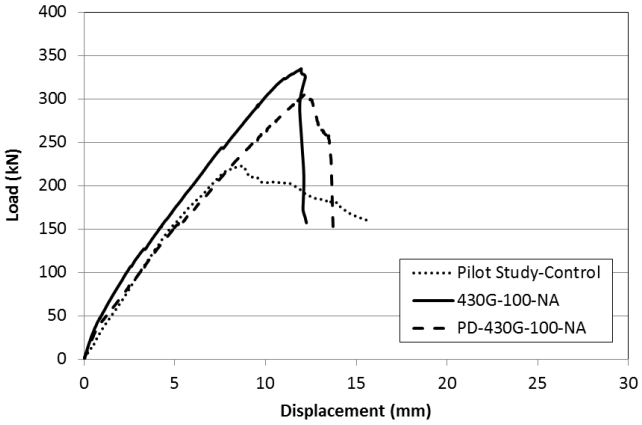

Figure A-33: Load vs. deflection of full & partial depth strengthened beams

Effect on Strength

A comparison of the strength increase in full depth and partial depth GFRP strengthened beams over the control is shown in Figure A-34.The increase in strength over the control for full and partial depth strengthened beams was 50% (430G-100-NA) and 37% (PD-430G-100-NA). Analysis of both GFRP strengthened beams showed that both beams failed in shear. The full depth beam provided a 13% increase in strength over the partial depth beam. The partial depth GFRP sheet measures 300 mm long compared to a full depth sheet which measures 350 mm long. Therefore, 30% less material is provided in a partial depth sheet compared a full depth sheet. The 13% difference in strength between the full depth beam to the partial depth beam can be attributed to 30% less strengthening material provided on the beam.

The ultimate shear capacity of both beams could not be determined because each failed by FRP debonding.

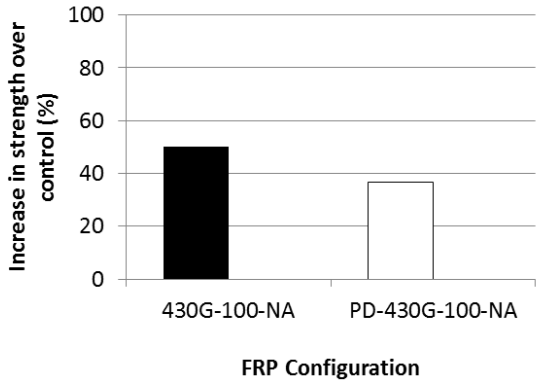

Figure A-34: Strength increase of full & partial depth configurations over the control

Effect on Stiffness

The beam stiffness was increased in the full depth GFRP strengthened beam and no increase in stiffness was achieved in the partial depth GFRP strengthened beam over the control.

The beam with full depth installation recorded a stiffness of 24.5 kN/mm and the partial depth installation recorded a stiffness of 25.5 kN/mm. Both beams were strengthened with Sikawrap 430G sheets with an elastic modulus of E=26 MPa. Applying full or partial depth u-wrapped GFRP sheets created a linear response removing the initial cracking phase.

Effect on Deflection

A bar chart comparing full and partial depth deflections at failure for the full and partial depth configurations is shown in Figure A-35. Both beams exhibited on average a 46% increase in maximum deflection of over the control beam. The full depth strengthened beam experienced a 55% increase in maximum deflection of over the control and the partial depth strengthened beam experienced a 19% increase in maximum deflection over the control. Full depth u-wrapped FRP sheets experienced larger increases in maximum deflection over partial depth u-wrapped FRP sheets.

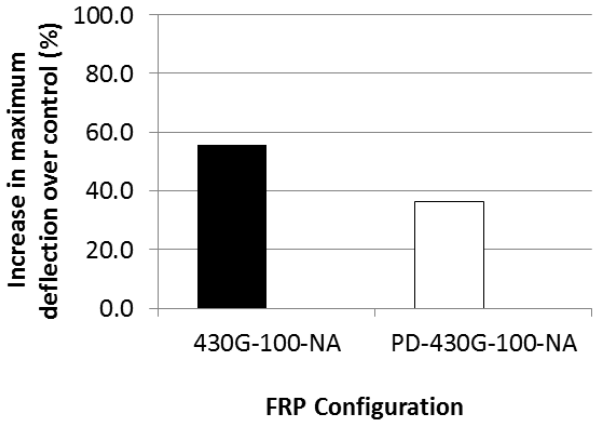

Figure A-35: Increase in max deflection of full & partial depth configurations over control

Strain Response

The largest increase in the internal steel stirrup strain at failure over the control was 16% (430G-100-NA) for the beam with full depth strengthening and 47% (PD-430G-100-NA) for the beam with partial depth strengthening. Therefore, full depth strengthening decreased the strain experienced in the internal steel stirrups compared to partial depth strengthening. Lower strains in the internal steel stirrups of the full depth beam can be attributed to the increased assistance provided by the GFRP sheet extending to the top of the beam.

The highest strains in the GFRP material were recorded in the beam with partial depth GFRP strengthening. Cross-referencing the GFRP strain data with the failure mode observed during testing showed the strain to cause FRP rupture of partial depth unanchored Sikawrap 430G sheets was 7559 με. Both beams experienced FRP debonding at failure; the strain to cause debonding of the partial depth unanchored Sikawrap 430G sheets was 5500 με. This is consistent with the strain data from beams 430G-200-NA and 100G-200-NA which recorded debonding at strains of 5000 με and rupture at strains of 8000 με. The strain data recorded for the full depth configuration did not respond properly and cannot be used.

Previous research suggests that partial depth configuration induces debonding. Debonding occurred at the same strain level as the beam with the full depth configuration. However, the load at which the strain value occurred at was much lower for the partial depth configuration: 230 kN for partial depth sheets and 270 kN for full depth sheets.

Both beams recorded strains greater than 2000 με indicating stirrups yielded in each beam. This confirms the load response behaviour which suggest that each beam failed by shear. A bar chart comparing full and partial depth internal stirrup and GFRP strain at failure is shown in Figure A-36 and Figure A-37.

The GFRP strain response had a large variation along the depth of the GFRP sheet. The beam with full depth GFRP strengthening did not have properly function strain gauges and thus did not record any data. Beam PD-430G-100-NA recorded a maximum strain of 5400 με at 100 mm from the top of the GFRP sheet. The bell curve strain response confirms the diagonal tension shear crack crossed the partial depth GFRP sheet 50 mm below the top of the GFRP sheet or 100 mm from the top of the beam as it propagated towards the loading point.

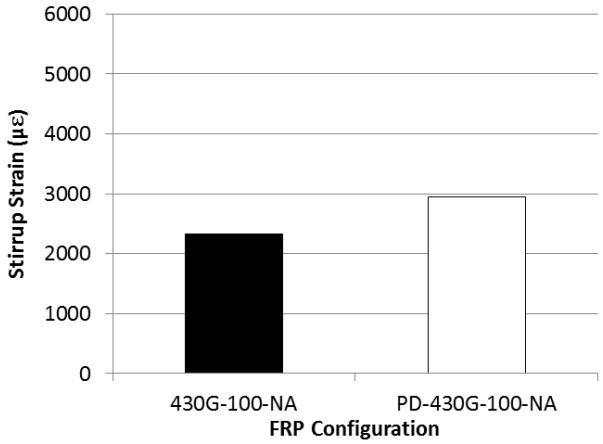

Figure A-36: Comparison of full & partial depth stirrup strain at failure

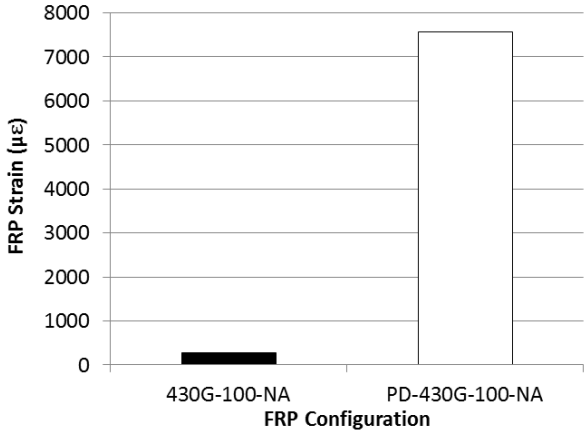

Figure A-37: Comparison of full & partial depth GFRP strain at failure

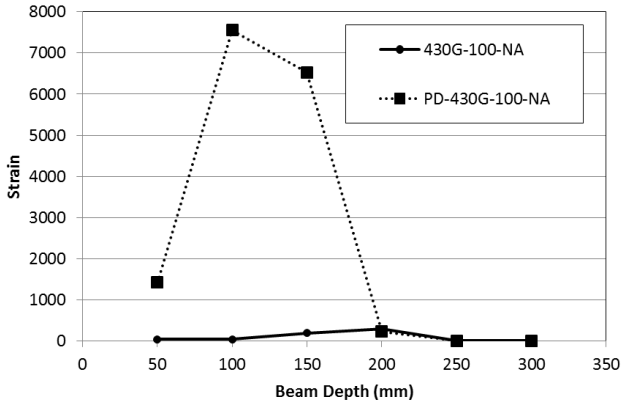

Figure A-38: FRP strain response of full and partial depth strengthened beams

A.3.4 Effect of FRP Anchors

In this section the effect of the presence and type of FRP anchors used to secure u-wrapped GFRP sheets from debonding on the load, stiffness, deflection and strain response is analyzed and compared.

Three trends were discovered with beams which contained FRP anchors: anchored beams do not have a large drop in load in the post peak behaviour compared to unanchored beams. The presence of FRP anchors increased the shear capacity in a u-wrapped FRP strengthened beams. The average increase in shear capacity of beams with FRP anchors was 9% greater than companion unanchored beams.

A.3.4.1 Presence of FRP Anchors

Five shear critical reinforced concrete beams were strengthened with GFRP and CFRP sheets. Two beams were strengthened with Sikawrap 230C sheets (0.381 mm thick with $\varepsilon_{rupture}$=1.33%): beams 230C-200-NA (no anchors) and 230C-200-A (with anchors) and three beams were strengthened with Sikawrap 430G sheets (0.508 mm thick with $\varepsilon_{rupture}$=2.21%): beams PD-100-430G-NA (no anchors), PD-100-430G-CA (with carbon anchors) and PD-100-430G-GA (with glass anchors).

The three GFRP strengthened beams failed in shear as designed and two CFRP strengthened beams failed in flexure. The beams with anchors performed slightly better failing at loads than the beams without anchors.

The load vs. deflection curves of the strengthened beams is shown in Figure A-39. The additional strength provided by the beams with anchors recorded the highest ultimate load of all the strengthened beams in this comparison. An analysis of the post peak behaviour shows the three beams with anchors all experienced higher loads over the equivalent unanchored beam.

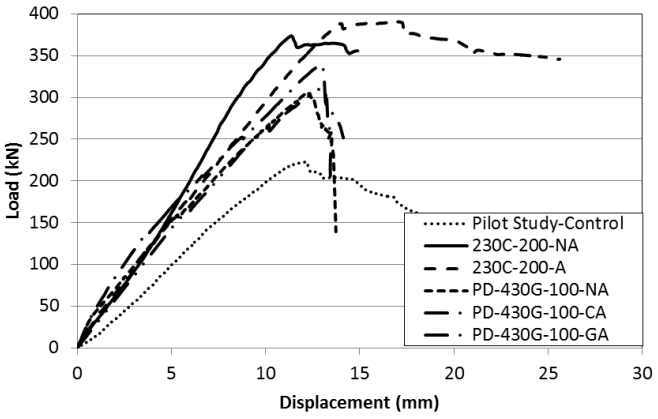

Figure A-39: Load vs. deflection of anchored and unanchored beams (series 1)

Effect on Strength

A comparison of the strength increase in Sikawrap 230C and 430G strengthened beams with and without anchors is displayed in Figure A-40. The average increase in strength over the control of beams with and without anchors was 56% and 52%, respectively. The increase in shear capacity of CFRP strengthened beams with anchors was 7.6% and GFRP strengthened beams with anchors was 15% over companion unanchored beams.

Both CFRP strengthened beams failed in flexure and the full benefit of providing CFRP anchors could not be assessed. Beams with partial depth Sikawrap 430G strengthening with anchors changed the mode of failure from FRP debonding (beam without anchors) to diagonal tension shear failure.

A limitation with the application of partial depth GFRP sheets on rectangular beams is the diagonal tension shear crack will take the path of least resistance avoiding the u-wrap FRP sheet. The crack will propagate above the FRP sheet in the top unstrengthened area as shown in Figure A-41. Regardless of the presence of FRP anchors, it is recommended that u-wrap FRP sheets be installed the full depth of the beam to have the largest increase in shear capacity.

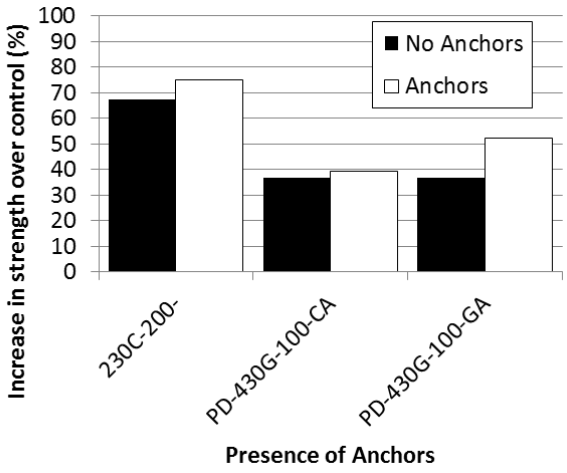

Figure A-40: Strength increase of unanchored & anchored beams over the control

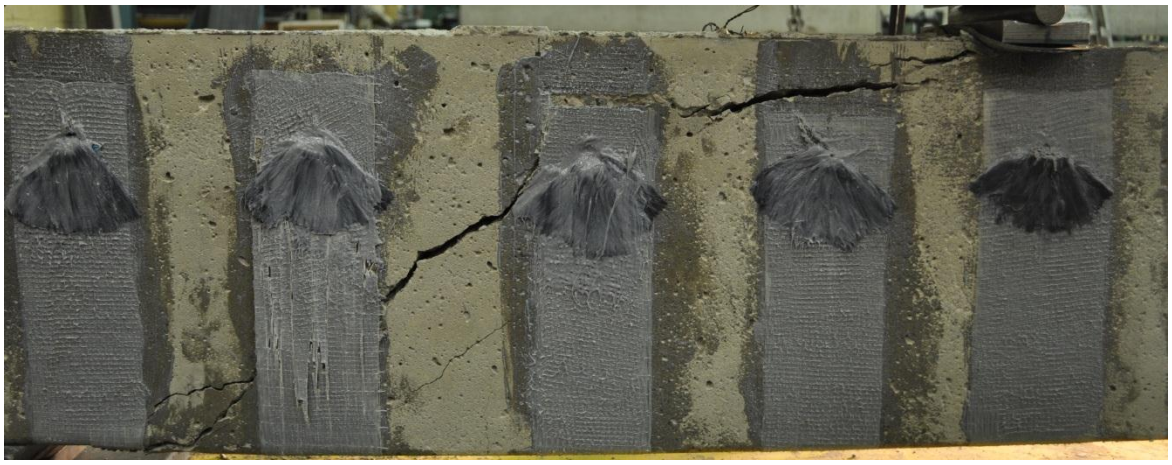

Figure A-41: Shear crack failure with partial depth GFRP sheets

Effect on Stiffness

The beam stiffness was increased in all Sikawrap 230C and 430G strengthened beams (23 kN/mm). No difference in stiffness was obtained between beams with and without anchors. The highest initial stiffness was recorded in beams 230C-200-NA and PD-430G-100-GA.

Effect on Deflection

A bar chart comparing the maximum deflection at failure of anchored and unanchored beams is shown in Figure A-42. All five beams experienced a 55% average increase in deflection over the control.

Despite improved stiffness, increases in the maximum deflection at failure can be attributed to the higher loads endured in the beams. Increased deflection was experienced in the beams with anchors with CFRP strengthening (62%) and GFRP strengthening (22%). This correlates with the increases in strength which show a connection between the ultimate load and the maximum deflection. A positive linear relationship exists between the ultimate shear capacity of a beam and the maximum deflection when FRP anchors were installed to eliminate FRP debonding,

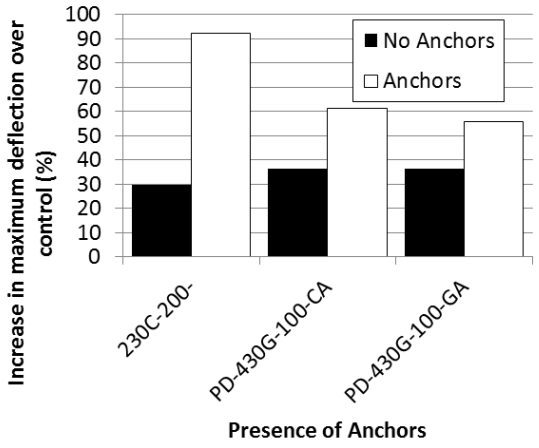

Figure A-42: Increase in max deflection of unanchored & anchored beams over control

Strain Response

A bar chart comparing the internal steel stirrup and FRP strains at failure for unanchored and anchored beams is shown in Figure A-43 and Figure A-44. Strain in the FRP of the partial depth anchored beams was unresponsive and a fair comparison could not be made. The strain in stirrups remained relatively consistent regardless of the presence of FRP anchors for Sikawrap 230C strengthened beams. This was expected as both Sikawrap 230C strengthened beams failed in flexure. A closer look at the strain in the FRP sheet of anchored vs. unanchored beams showed a significant increase in the strain response.

The strain in the stirrups decreased with the presence of FRP anchors to secure partial depth GFRP strengthened beams. This trend is consistent with the results from 200 mm and 300 mm wide full depth Sikawrap 430G and 100G strengthened beams with anchors. The presence of FRP anchors allows u-wrap FRP sheets to resist higher loads and thus relieve some of the strain on the internal steel stirrups.

The strain recorded in the FRP sheets of the anchored partial depth GFRP strengthened beams experienced a combination of two problems. First strain gauges were not functioning properly and second, the diagonal tension shear crack travelled around the FRP sheet and anchors. Since a majority of the u-wrapped FRP sheets did not intercept the diagonal tension shear crack, the FRP sheet shear strength contribution was minimal.

The highest strains in the GFRP strengthened beams were recorded in the partial depth unanchored beam. When anchors were installed the maximum strain in the stirrups at failure in the GFRP strengthened beams decreased by 78% and the maximum strain the CFRP strengthened beams increased by 600%.

Figure A-45 and Figure A-46 show the CFRP and GFRP strain profile at failure for each beam. The CFRP strain response varied depending on the presence of anchors. Beams 230C-200-NA and 230C-200-A recorded maximum strains of 767 με and 5400 με respectively at mid-depth of the CFRP strip. The partial depth GFRP strain profile across the depth of the beam shows very little to no strain response in the GFRP strengthened beams with anchors. The highest strain was 7559 με experienced 100 mm from the top of the beam. The low strain values in the two anchored beams are possible because the shear cracks travelled above the FRP sheets in the unstrengthened area.

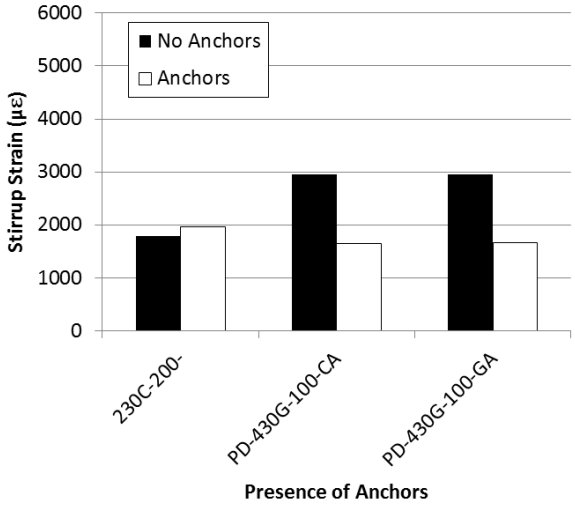

Figure A-43: Comparison of unanchored & anchored FRP strain at failure

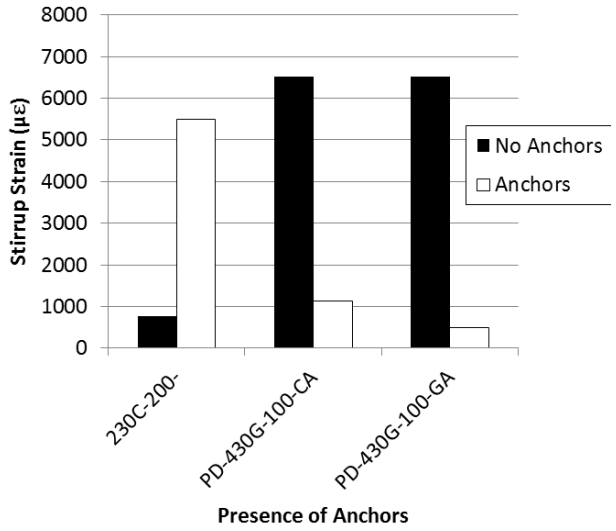

Figure A-44: Comparison of unanchored & anchored stirrup strain at failure

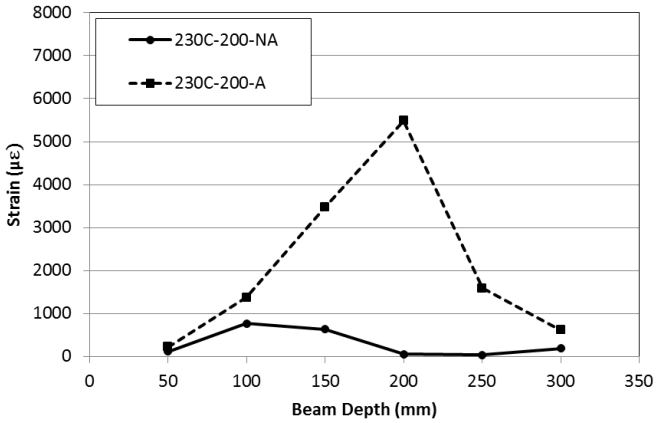

Figure A-45: FRP strain response of full depth Sikawrap 230C strengthened beams

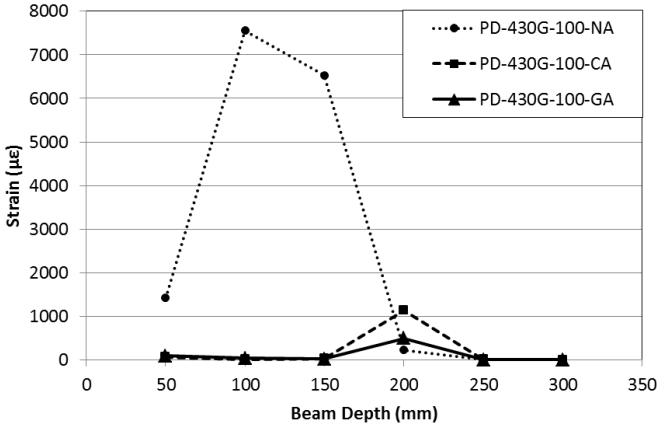

Figure A-46: FRP strain response of partial depth Sikawrap 430G strengthened beams

A.3.4.2 Type of FRP Anchors: Carbon & Glass

Three partial depth GFRP strengthened shear critical reinforced concrete beams were designed to fail in shear. Beam PD-430G-100-NA did not contain any anchors, PD-430G-100-CA contained CFRP anchors (ϕ=10 mm, E=215 GPa and $\varepsilon_{rupture}$=0.74%) and beam PD-430G-100-GA contained GFRP anchors (ϕ=10 mm, E=70 GPa and $\varepsilon_{rupture}$=3.99%). The load vs. deflection curves of all four beams is shown in Figure A-47.

The GFRP anchored beam provided increased strength over the CFRP anchored beam recording the highest ultimate load in this comparison. The post peak behaviour shows all beams had a post peak sudden drop failure. The two anchored beams had a smaller sudden drop in load compared to the unanchored beam; Beam PD-430G-100-GA recorded the smallest initial drop in the load.

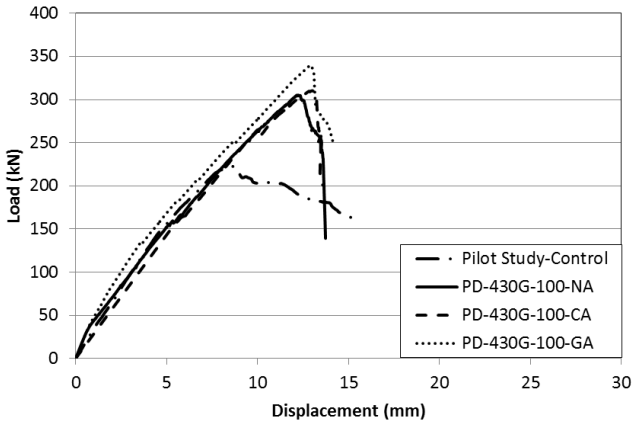

Figure A-47: Load vs. deflection of CFRP and GFRP anchored beams

Effect on Strength

A comparison of the strength increase is displayed in Figure A-48. The increase in strength over the control for CFRP and GFRP anchored beams was calculated to be 39% and 52%, respectively. GFRP anchors performed better than the stiffer CFRP anchors. Both GFRP and CFRP anchored beams did not experience GFRP sheet rupture, thus the capacity of each anchor could not be determined. Failure occurred by propagation of the diagonal tension shear crack above the u-wrapped GFRP sheets causing premature failure. This can be attributed to the partial depth installation of the FRP sheets.

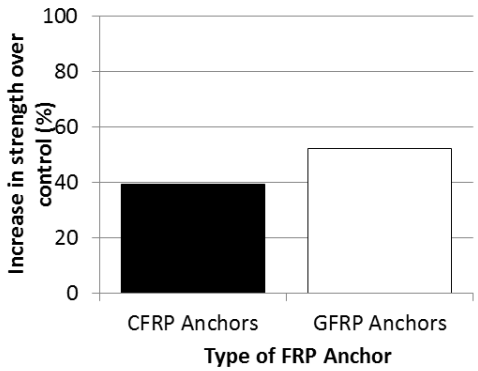

Figure A-48: Strength increase of CFRP& GFRP anchored beams over the control

Effect on Stiffness

The beam stiffness was increased in all GFRP strengthened beams. The beam with GFRP anchors had a slightly stiffer behaviour (25 kN/mm) over the beam with CFRP anchors (23 kN/mm). A second observation made irrespective of the type of FRP anchor used is the bi-linear response was not as prevalent if not at all present with the addition of the FRP sheets and anchors.

Effect on Deflection

A bar chart comparing the maximum deflection at failure of CFRP and GFRP anchored beams is shown in Figure A-49. Two beams exhibited an average 59% increase in maximum deflection over the control. The beam with GFRP anchors performed the best with the lowest deflection at failure (5.7%). This is significant because the beam with GFRP anchors sustained an additional 29 kN of load and still had a lower deflection at failure compared to the beam with CFRP anchors.

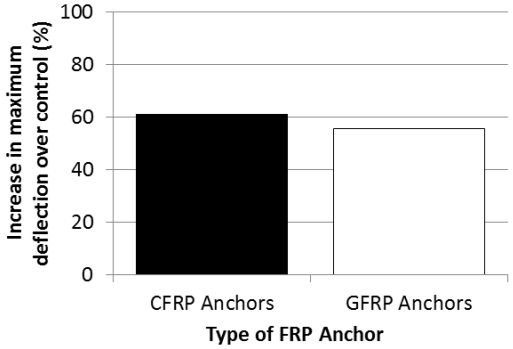

Figure A-49: Increase in maximum deflection of FRP anchored beams over the control

Strain Response

A bar chart showing the internal steel stirrup and FRP strains at failure for beams with CFRP and GFRP anchors is shown in Figure A-51 and Figure A-52.The maximum strain at failure shows a small degree of strain experienced in the internal steel stirrups and FRP sheets. Strain in the FRP of the partial depth anchored beams was unresponsive and inconsistent. Based on these results, a fair comparison cannot be made.

Analysis of the beams with CFRP and GFRP anchors shows the strain in stirrups remaining relatively consistent regardless of the type of FRP anchorage. The internal stirrup strain recorded in both beams was 1600 με at failure. This is unusual because it was clear that diagonal tension shear failure occurred in both beams (Figure A-50a,b). The failure mode suggests that the internal stirrups yielded causing the strain to be greater than 2000 με but the strain data suggests otherwise.

A closer look at the strain in the FRP sheet of the CFRP and GFRP anchored beams shows a significant decrease in the strain response in the beams with anchors over companion unanchored beams. As was mentioned above, this is unconventional because the beam with GFRP anchors sustained a higher load (29 kN) compared to the companion unanchored beam. The strain profile at failure for each beam is shown in Figure A-53.

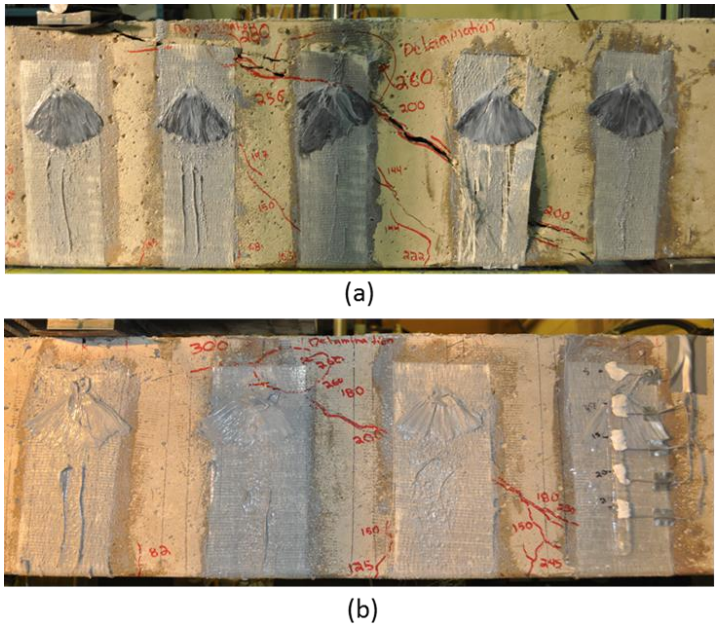

(a)

(b)

Figure A-50: CFRP & GFRP anchored beam failure modes

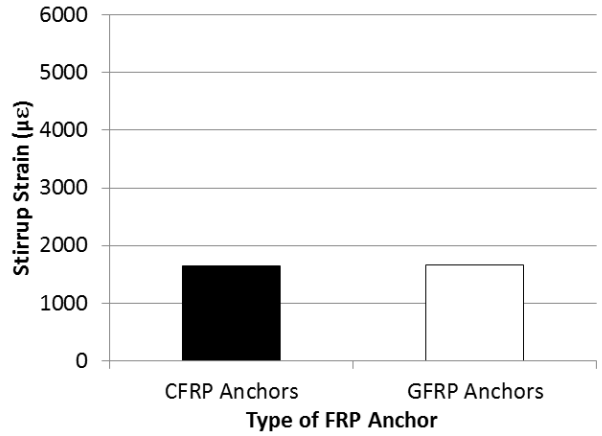

Figure A-51: Comparison of CFRP & GFRP anchor stirrup strain at failure

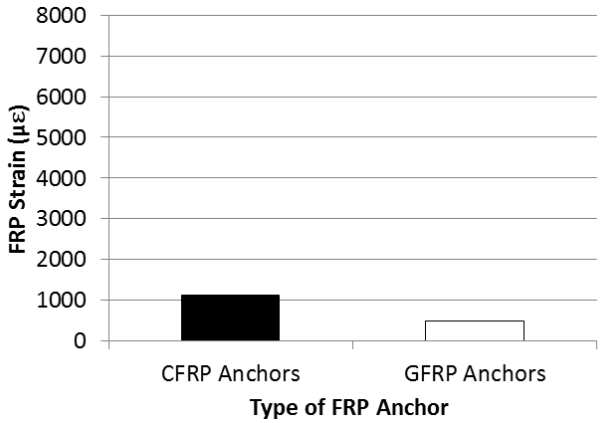

Figure A-52: Comparison of CFRP & GFRP anchor FRP strain at failure

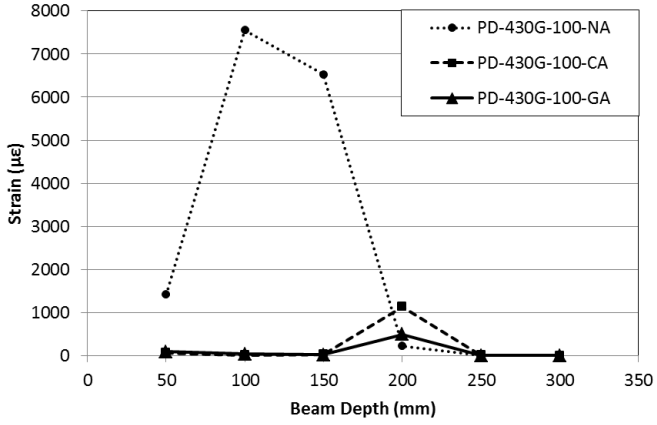

Figure A-53: FRP strain response of partial depth Sikawrap 430G strengthened beams

In summary, providing FRP anchors allowed the FRP sheets to develop strains 10% higher over companion unanchored beam. Comparing all unanchored and the equivalent anchored beams showed the greatest increase in strength provided by FRP anchors was:

- 200 mm wide, full depth - 8%
- 100 mm wide, partial depth - 15%

The average increase in strength provided by FRP anchorage for u-wrapped FRP sheets was 19%. A trend observed in the data shows the wider the u-wrapped FRP sheets the greater effect the presence FRP anchors have. This can be explained by the overall increased capacity provided by a larger sheet. A wider FRP sheet has a larger bonded area (A_{frp}) and thus will provide a higher increase in strength compared to a narrow FRP sheet with a smaller bonded area (A_{frp}). Providing FRP anchors allowed each sheet to develop higher strains and thus increased the overall strength capacity of the beam. FRP anchors proved to be more efficient with wider FRP sheet configurations over narrower configurations. This was validated in the comparisons conducted in this research study.

Appendix B
Series I: Control Beam

Dimensions	
L (mm)	2400
h (mm)	350
b (mm)	150
a (mm)	900
d (mm)	301.2
dv (mm)	271.0
jd (mm)	234.9
a/d ratio	2.989

Cover	
top (mm)	30
bottom (mm)	30
left side (mm)	30
right side (mm)	30

Beam Calculations		
β	0.895	≥ 0.67
α	0.805	≥ 0.67

Flexure Calculations	
Equilibrium	
Cc (Mpa)	480000
Cs' (Mpa)	480000
T (Mpa)	960000

a (mm)	132.51
Recalculate using quadratic	
c (mm)	148.05
Recalculate using quadratic	

Steel Properities

Bottom Steel	
As(req) (mm)2	1000
Bar dia (mm)	25
Number of bars	4
As of bar	500
As (mm)2	2000

Concrete Properities	
f'c (Mpa)	30
εc	0.0035
λ	1
Ag (mm)	19
fcr'	2.19089023

a quadratic (mm)	134.56
c quadratic (mm)	150.35

Quadratic Values	
a	3242.1
b	-260000
c	-34195000
x1=	**150.35**
x1=	**-70.15**

Top Steel	
d'	48.85
Bar dia (mm)	25
Number of bars	2
As' of bar	500
As' (mm)2	1000

Steel Ratios	
ρ/ρb	0.84
ρb (%)	2.63
ρ	2.21

fc'	ρbal (%)
20	1.83
25	2.24
30	2.63
35	3
40	3.34
45	3.67
50	3.98

εs'	0.00236
εy	0.00240
fy	480
Es	200000

FRP Properities		
tfrp (mm)	0.508	
Efrp (Gpa)	26.4	
wfrp (mm)	200	
Afrp (mm2)	101.6	
εfrpu (%)	2.21	
εfrpe		
dfrp 1 (mm)	252	
dfrp 2 (mm)	315.0	
	Estimate	Actual
sfrp (mm)	287.5	275
hfrp	350	

Stirrup Calculations	
Cover (mm)	
Number of bars	1
dia of bar (mm)	6.35
Av of bar (1/4") = mm	31.67
Av total (mm)2	63.34
fy (Mpa)	450
V(@ Max spacing) (kN)	135.52
S (max spacing) (mm)	189.72
Actual spacing (s)	180

	CFRP 230C	CFRP 103C	GFRP 430G	GFRP 100 G
tfrp (mm)	0.381	1.016	0.508	1.016
Efrp (Gpa)	65.4	70.55	26.4	25.3
εfrpu (%)	1.33	1.12	2.21	2.31

Series I: Control Beam

Checks	
c/d ≤ 700/(700+fy)	
c/d	0.492
700/(700+fy)	0.593
Tension Steel Yeilds	

Tension Steel Yields	
a/d	0.440
a/d (limit)	0.531
Tension steel yeilds	

Compression Steel Yields	
d'/a	0.369
d'/a (limit)	0.351
Compresion steel does not yeild	

FRP Strip Calculations		
Le	94.06	
k1	1.073	
k2	0.7014	
kv	0.2691	
εfrpe1	0.0059	Bond capacity
εfrpe2	0.0040	Aggregate interlock
εfrpe3	0.0166	FRP Strength
Vfrp (kN)	27.80	

Flexure Calculations	
Calculation of Moment	
Cc (kN)	487.4
Cs' (kN)	472.6
T (kN)	960.0
εs'	0.00236
Mr (kN.m) estimate	230.1
Mr (kN.m) actual	233.7
Pflexure (kN)	519.4
Vr (KN)	259.7

Shear Calculations				
% of flexure	44		β	0.2111
Pshear (KN)	228.5		εx	0.000617
Vf @ dv	114.27		sze (mm)	279.0
Vr(max) (KN)	304.9		Θ (degrees)	33.32
Cross section is large enough			Vc (kN)	47.0
Mf (KN.m)	102.84		Vstirrups (kN)	65.3
			P (actual)	224.6

Total Shear Capacity	
Vc (kN)	47.0
Vstirrups (kN)	65.3
Total Vr (kN)	112.3
Pshear (kN)	224.6

Shear Capacity General Method	
Vc	40.1
Vs	61.3
Total Vr (kN)	101.4
Pshear (kN)	202.7

Final Capacity	
Pflexure (kN)	519.4
Pshear (kN)	224.6

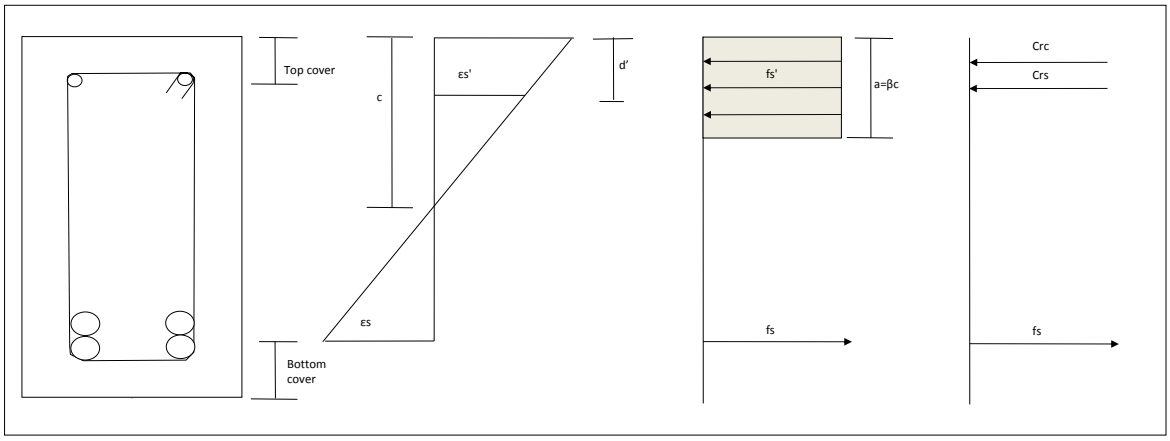

Series II: Control Slab

Dimensions	
L (mm)	2400
h (mm)	200
b (mm)	350
a (mm)	650
d (mm)	162.5
dv (mm)	146.3
a/d ratio	4.000
L (mm)	1800

Cover	
top (mm)	20
bottom (mm)	20
left side (mm)	20
right side (mm)	20

Beam Calculations		
β	0.885	≥ 0.67
α	0.799	≥ 0.67

Steel Properities

Bottom Steel	
Bar dia (mm)	15
Number of bars	3
As of bar	200
As (mm)2	600
εs	0.0024

Concrete Properities	
f'c (Mpa)	34
εc	0.0035
λ	1
Ag (mm)	19
fcr'	2.33
E (Mpa)	26239

Top Steel	
d'	35
Bar dia (mm)	10
Number of bars	2
As' of bar	100
As' (mm)2	200

Steel Ratios	
ρ/ρb	0.267413195
ρb (%)	2.63
ρ	0.703296703

εs'	
εy	0.00240
fy	480
Es	200000

FRP Properities		
GFRP		
tfrp (mm)	0.381	
Efrp (Gpa)	65.4	
wfrp (mm)	300	
Afrp (mm2)	114.3	
εfrpu (%)	1.33	
εfrpu	0.0133	Ultimate strain
εfrpt (bridge)	0.006	Bond strain
εfrpt (building)	0.007	
Tfrp (kN)	52.33	

Stirrup Calculations	
Cover (mm)	20
Number of bars	1
dia of bar (mm)	10
Av of bar	100
Av total (mm)2	200.0
fy (Mpa)	460
V(@ Max spacing) (kN)	193.38
S (max spacing) (mm)	751.33
Actual spacing (s)	100

	CFRP 230C	CFRP 103C	GFRP 430G	GFRP 100 G
tfrp (mm)	0.381	1.016	0.508	1.016
Efrp (Gpa)	65.4	70.55	26.4	25.3
εfrpu (%)	1.33	1.12	2.21	2.31

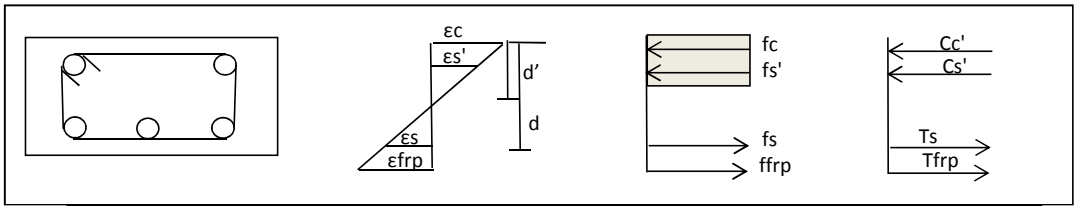

Series II: Control Slab

c	34.23
a	30.29
Recalculate using quadratic	

c (quadratic)	45.73
a (quadratic)	40.47
Use quadratic	

Quadratic Values	
ax2	45457.8
bx	1120052.3
c	-146300000
x1=	**45.73**
x2=	**-70.37**

fc'	pbal (%)
20	1.83
25	2.24
30	2.63
35	3
40	3.34
45	3.67
50	3.98

Checks	
c/d ≤ 700/(700+fy)	
c/d	0.281435472
700/(700+fy)	0.593220339
Tension Steel Yeilds	

Tension Steel Yields	
a/d	0.249070392
a/d (limit)	0.525
Tension steel yeilds	

Compression Steel Yields	
d'/a	0.864753989
d'/a (limit)	0.484261501
Compresion steel does not yeild	

Strain from equilibrium		
εc'	0.0021	
εs'	0.0005	
εfrp	0.0070	
εs	0.0053	≥ 0.002

Shear Calculations				
% of flexure	100		β	0.1437
Pshear (KN)	126.07		εx	0.001429926
Vf @ dv	63.03		sze (mm)	150.6
Vr(max) (KN)	435.1		Θ (degrees)	39.01
Cross section is large enough			Vc (kN)	42.9
Mf (KN.m)	40.972		Vstirrups (kN)	166.1
			P (actual)	418.0

Total Shear Capacity	
Vc (kN)	42.9
Vstirrups (kN)	166.1
Total Vr (kN)	209.0
Pshear (kN)	418.0

Flexure Calculations	
Calculation of Moment	
Cc' (kN)	616.31
Cs' (kN)	19.48
Ts (kN)	288.00
Tfrp (kN)	52.33

Mr (kN.m) actual	40.97
Pflexure (kN)	126.07

Final Capacity	
Pflexure (kN)	126.07
Pshear (kN)	417.99